Fall 12-2021

Synthesis and Characterization of 4,6-protected Glucosamine Derivatives and Branched Glycoconjugates

Jonathan Bietsch
Old Dominion University, jbiet001@odu.edu

SYNTHESIS AND CHARACTERIZATION OF 4,6-PROTECTED GLUCOSAMINE DERIVATIVES AND BRANCHED GLYCOCONJUGATES

by

Jonathan Bietsch
B.S. Chemistry, May 2015, Longwood University

A Dissertation Submitted to the Faculty of
Old Dominion University in Partial Fulfillment of the
Requirements for the Degree of

DOCTOR OF PHILOSOPHY

CHEMISTRY

OLD DOMINION UNIVERSITY
December 2021

Approved by:

Guijun Wang (Director)

John Cooper (Member)

Richard Gregory (Member)

Jingdong Mao (Member)

Yuan Zhang (Member)

ABSTRACT

SYNTHESIS AND CHARACTERIZATION OF 4,6-PROTECTED GLUCOSAMINE DERIVATIVES AND BRANCHED GLYCOCONJUGATES

Jonathan Bietsch
Old Dominion University, 2021
Director: Dr. Guijun Wang

Low molecular weight gelators (LMWGs) are small molecules that self-assemble in appropriate solvents to form three dimensional networks that immobilize the solvent, creating a supramolecular gel. The self-assembly of LMWGs occurs through non-covalent interactions such as hydrogen bonding, aromatic interactions, donor-acceptor interactions, Van der Waals interactions, hydrophobic forces, halogen bonding, etc. Due to self-assembly occurring through reversible non-covalent interactions, supramolecular gels can undergo a gel to solution transformation. Because of this, these materials can be sensitive to external stimuli such as temperature changes, pH changes, and other stimuli that effect non-covalent interactions. This makes the synthesis of LMWG's an appealing target for the synthesis of smart materials.

Carbohydrates are an appealing feedstock for the synthesis of LMWGs because of their natural abundance, renewability, biocompatibility, biological activity, biodegradability, structural diversity, and a capacity for chiral self-assembly. The biocompatibility and bioactivity of carbohydrate based LMWGs make them enticing materials for biomedical applications such as drug delivery and tissue engineering. The abundance and renewability make them attractive materials for larger uses, such as environmental remediation. Carbohydrates are an optimal starting material for exploring the gelation-structure relationship because of their structural diversity. Previously, we have had great success in designing carbohydrate based LMWGs via tuning the

gelation properties through changing functional groups at various positions on various carbohydrates.

In this research, the structure to gelation properties relationship was explored through the synthesis and characterization of various 4,6-protected glucosamine derivatives and branched glycoclusters. These include 4,6-(1-naphthylidene) protected glucosamine (amide, urea and carbamate) derivatives, 4,6-(4-chlorobenzylidene) protected glucosamine amide derivatives and triazole linked Janus glycoclusters. Preparation of the glucosamine derivatives were carried out using readily available N-acetyl-D-glucosamine and the preparation of the branched glycoconjugates were carried out using both D-glucose and N-acetyl-D-glucosamine, using commercially available pentaerythritol as central scaffold. The design, synthesis, and analysis of the self-assembling properties of the 4,6-protected glucosamine derivatives and Janus glycoclusters will be discussed in Chapters 2, 3, and Chapter 4. A final conclusion and future perspectives are given in Chapter 5.

This dissertation is dedicated to my family for their continuous support throughout my life and education. I am fortunate to have a close network of strong and remarkable people who have inspired me in various ways and molded me into the person that I am today.

ACKNOWLEDGEMENTS

First and foremost, I would like to express my sincere gratitude to my research advisor, Dr. Guijun Wang. Her advice and guidance have been invaluable over the past six years in designing and carrying out research, constructing career plans and as well in overall personal growth. Additionally, her hard work and dedication in synthetic chemistry is ultimately why I have had the opportunity to carry out this research and it has been my privilege to study under her mentorship.

I would like to express a special thanks to Dr. Chris Senanayake and Dr. Carl Busacca who supervised me during my fall semester internship at Boehringer Ingelheim in 2017. The internship was an amazing experience, and I learned a significant amount over the semester. This experience in industry had a profound effect on my skill level in research and in a synthetic lab, as well has helped shape my future career plans. I would also like to thank my thesis committee members, Dr. John Cooper, Dr. Richard Gregory, Dr. Jingdong Mao and Dr. Yuan Zhang at Old Dominion University. I appreciate their valuable recommendations and support. I would like to say very special thank you to all my lab mates in the Wang group for all their help and comradeship over the past 5 years. It was my honor to work and grow alongside all of you: current members: Surya Adhikari, Joedian Morris, Pooja Sharma, and the former members: Dr. Anji Chen, Dr. Kristen Bashaw, Dr. Ifeanyi Okafor, Dr. Lalith Samankumara, Dr. Dan Wang, and Mary Olson. I would also like to say a special thank you to my hard-working REU interns Mary Olson, Cheandri Ackermann, and Samuel Carter, as I learned a significant amount about being a mentor during your internships. I would also like to collectively thank ODU staff members Alicia, Janice, Kristi, Tammy, Dana and Michelle for their help and support at Old Dominion University.

Finally, I would like to thank National Science Foundation grants CHE1313633 and CHE1808609, Boehringer Ingelheim and Old Dominion University for the financial support over the course of my Ph. D.

NOMENCLATURE

Ac	acetyl
AFM	atomic force microscopy
CD	circular dichroism
$CDCl_3$	deuterated chloroform
COSY	correlation spectroscopy
CuAAC	copper-catalyzed azide-alkyne cycloaddition
DCM	dichloromethane
DI	deionized
DIEA	diisopropyl ethyl amine
DMF	*N*, *N*-dimethylformamide
DMSO	dimethyl sulfoxide
DMSO-d_6	deuterated dimethyl sulfoxide
D_2O	deuterium oxide
DSC	differential scanning calorimetry
EG	ethylene glycol
EtOH	ethanol
Gly	glycerol
HCl	hydrochloric acid
Hex	hexane
HSQC	heteronuclear single quantum coherence
IPA	isopropyl alcohol

NaOH	sodium hydroxide
LC-MS	liquid chromatography mass spectrometry
LMWGs	low molecular weight gelator
MeOH	methanol
MGC	minimum gelation concentration
mp	melting point
NMR	nuclear magnetic resonance
OM	optical microscopy
PTSA	*p*-toluenesulfonic acid
Py	pyridine
PXRD	powder X-ray diffraction
SEM	scanning electron microscope
SXRD	single crystal X-ray diffraction
TBO	toluidine blue
TEA	triethylamine
TEG	triethylene glycol
TEM	transmission electron microscopy
THF	tetrahydrofuran
Tol	toluene
UV-Vis	ultraviolet visible

TABLE OF CONTENTS

Page

Page

LIST OF TABLES

Table Page

LIST OF FIGURES

Figure Page

Figure Page

Figure Page

Figure Page

CHAPTER 1

BACKGROUND AND INTRODUCTION

1.1 GENERAL INTRODUCTION TO GELS

Gels are ubiquitous soft viscoelastic solid-like materials that are typically formed by a two component system consisting of a gelator and a solvent.[1-3] Gels have a wide range of applications, such as being used in pharmaceuticals, lubricants, cosmetics, agriculture, environmental remediation, and in the food industry.[4-7] In a gel, the gelators form polymer like fibers that form a three dimensional (3D) network in solution.[3] The solvent then becomes immobilized within the three dimensional matrix due to surface tension and capillary forces, resulting in a viscoelastic material known as a gel.[1-3] Gels can be categorized as either physical gels or chemical gels.[1,3] Chemical gels, also known as polymer gels or macromolecular gels, are formed by a network of polymer fibers which are covalently cross-linked to form the 3D network.[1,3] Macromolecular gels are typically irreversible since the three dimensional network is stabilized by permanent covalent cross-linkages.[1] In physical gels, also known as supramolecular gels, the three dimensional network is formed through non-covalent interactions.[1,3,8] Since the forces holding a supramolecular gel together are non-covalent, these gels are termed reversible, meaning they can undergo a gel to solution transition when exposed to certain stimuli such as a change in temperature.[1,3,8] The reversible nature of supramolecular gels gives them an advantage over macromolecular gels in various applications.[9] Low molecular weight gelators (LMWGs) are a class of small molecules, typically with a mass under 3000 Daltons, which form supramolecular gels.[2,3,10] These small molecules form three dimensional networks of entangled fibers through a process called self-assembly.[3] These three dimensional networks are known as self-assembled

fibrillary networks (SAFiN).[11] LMWGs are turning out to be a very important class of soft materials and attracting attention in a wide range of applications.[1-3]

1.2 SELF-ASSEMBLY AND THE MECHANISM OF GELATION

LMWGs self-assemble through non-covalent interactions such as hydrogen bonding, halogen bonding, hydrophobic interactions, donor-acceptor interactions, aromatic interactions (π-π stacking), metal coordination, Van der Waals interactions and charge transfer interactions.[1,3,8] The self-assembly process that results in gelation, rather than crystallization or precipitation, is dependent on a balance of these non-covalent interactions. Changing the type and spatial arrangement of functional groups capable of these non-covalent interactions allows for the tuning of the gelation properties of a molecule.

There are three tiers of interactions that lead to a supramolecular gel. The primary tier is called molecular recognition and is the beginning of the self-assembly process, where individual gelator molecules are aligning and interacting. The primary tier is found within the Å to nm range. The secondary tier is the one-dimensional growth of the aggregates into individual fibers, which is observed on an nm to μm range. The tertiary tier of interactions occur between various fibers, observed on a μm to mm range, which entangle to create the three-dimensional architecture of the gel. Figure 1 shows a representative schematic depicting each tier of interactions that lead to supramolecular gelation.

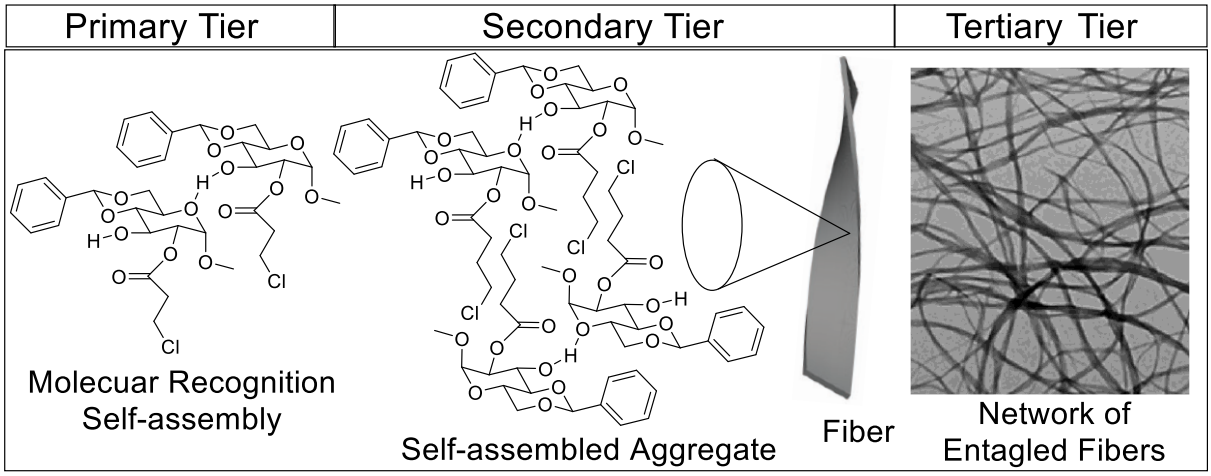

Figure 1. Depiction of tiers of interactions that lead to gelation.[12]

1.3 RATIONAL DESIGN OF LMWGS

Since the serendipitous birth of the LMWG cholesteryl 4-(2-anthrylloxy)butyrate (CAB), depicted in Figure 2, in the late 1980's,[13] the rational design of LMWGs has been a significant challenge. Many additional gelators have since been discovered through serendipitous means; however, significant strides have been made towards rationally designing LMWGs, with moderate success.

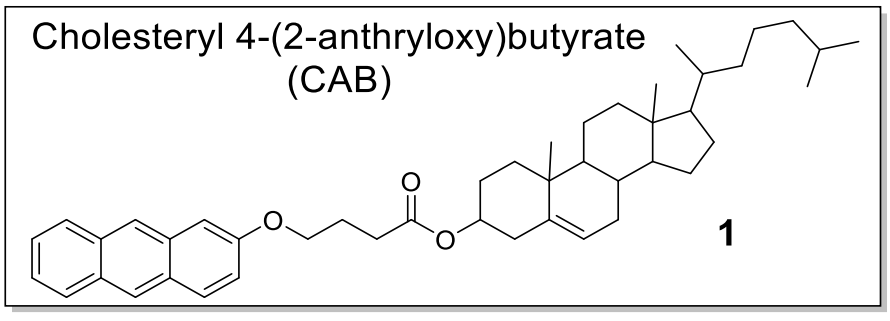

Figure 2. The fist LMWGs, discovered serendipitously in 1980.[13]

A popular strategy utilized by various researchers in this field is termed the "bottom-up" approach, where a central building block is functionalized with various functional groups to give desired gelation properties and/or functionality.[14] This approach allows the small molecules to be tuned, producing optimized desired properties. This method is similar to high throughput screening seen in the medicinal chemistry field, where structure to activity relationships are analyzed by synthesizing and analyzing libraries of analogs built from a core scaffold.

The intermolecular forces controlling the self-assembly of a molecule can be tuned by adding specific functional groups in various spatial arrangements to achieve the required balance of non-covalent forces that lead to gel formation. In order to achieve one dimensional growth through self-assembly, these non-covalent forces must work cooperatively. The proportions of these forces can lead to precipitation, crystallization, insolubility and solubility instead of gelation when not in balance. Hydrogen bonding is one of the strongest forces among the non-covalent interactions and is frequently the driving force in self-assembly. Various hydrogen bond donating groups can be utilized in LMWG design such as amides, ureas, carbamates and hydroxyl groups.[15-18] Hydrophobic forces also play an important role in molecular self-assembly. Functional groups with this property can drive molecules towards each other in polar solvents and increase the solubility of the molecule in more non-polar solvents. The hydrophobic forces of the molecule can be tuned by functionalizing the scaffold with aliphatic chains of various lengths. Another class of non-covalent forces that play an important role in self-assembly are aromatic interactions. Not only do aromatic forces play a role in directing self-assembly, they have also been shown to play a role in stabilizing other intermolecular interactions such as hydrogen bonding.[19] Different aromatic functional groups are capable of various types of aromatic-aromatic interactions, such as the weaker phenyl functional group versus the stronger naphthyl group functional group.[20] Various

activating and deactivating groups can be added to the aromatic moieties to tune the strength of these interactions. The addition of halogen groups on the aromatic functional groups not only deactivates the aromatic ring, but also acts as a halogen bonding source, which is another strong non-covalent force involved in self-assembly. Halogen bonding groups have been utilized sparsely in literature to create LMWGs; however, in several cases, the addition of a halogen bonding moiety has either converted a non-gelator into a gelator or significantly reduced the minimum gelation concentration (MGC) of a gelator, leading to the discovery of "super gelators", which is a term coined to describe gelators with MGC under 1% wt/v. Figure 3 shows a depiction of the functionalization of a carbohydrate based LMWG with various hydrogen bonding groups, aliphatic groups, aromatic groups, and halogen bonding groups to attempt to strike the right balance to achieve strong supramolecular gelators. Through our research, we have shown that it is possible to rationally design gelators from common carbohydrate templates through functional group manipulations.[21-24]

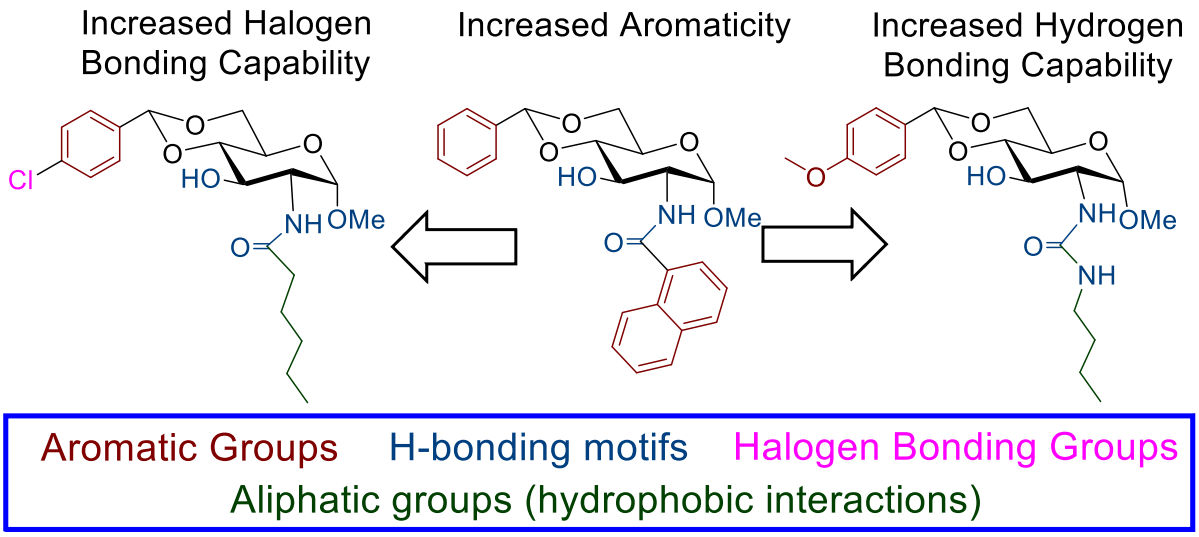

Figure 3. Tuning the gelation properties of glucosamine through structural modification.[16,17,24]

1.4 CHARACTERIZATION OF SUPRAMOLECULAR GELS

Several techniques are utilized to characterize gels and probe the mechanisms of gelation. NMR spectroscopy, FTIR spectroscopy, UV-vis spectroscopy, and differential scanning calorimetry (DSC) are frequently used to probe the mechanisms of gelation. NMR spectroscopy can be utilized to gain information about hydrogen bonding groups and some of the other intermolecular interactions that are occurring. Both changes in chemical shift and peak broadening are frequently observed in ^{1}H NMR studies that probe the self-assembly process. FTIR spectroscopy reveals information about specific functional groups within the gelator molecules. In a self-assembled state, these signals have slight to significant changes in wavenumber and peak size, which can be indicative of hydrogen bonding, aromatic interactions, or hydrophobic interactions. Characterization of the gels themselves is typically carried out by powder X-ray diffraction (PXRD), single crystal x-ray diffraction (SXRD), optical microscopy (OM), atomic force microscopy (AFM), scanning electron microscopy (SEM), transmission electron microscopy (TEM), circular dichroism (CD), rheology, and differential scanning calorimetry (DSC). While x-ray diffraction is typically a technique for characterizing crystalline material, it also gives important packing information on self-assembled systems. The solvent component of the gel generally causes scattering, so most x-ray diffraction analysis is carried out on xerogels,[25] where the solvent component is removed from the gel, leaving just the gels microstructures. Single crystal x-ray diffraction, on the other hand, solely gives information on the arrangement of atoms within a single crystal. While this information does not directly relate to the self-assembled systems, it does allow for conjecture as to how several of the same gelator molecules may interact with each other during the self-assembly process.[26,27] The morphology of the supramolecular architectures can vary significantly from system to system and characterization is carried out through various

microscopy techniques. OM produces low resolution imaging of the gel morphology, which is often not sufficient characterization of the gel networks.[28] Sample preparation typically requires extremely thin aliquots of gel to be dried on a microscope slide. OM imagining can be carried out on wet gels, or gels that are not fully dried; however, the solvent often impedes the network microstructures. Because of this, high resolution imaging such as AFM, SEM, and TEM are typically used to characterize gels. As opposed to OM, SEM and TEM samples need to be completely dried on appropriate platforms for imaging, giving rise to possible artifacts from the drying process. The occurrence of artifacts can be minimized by forming the gels at a low concentration. Staining used in TEM can also lead to structural changes to the gels morphology.[28] These high resolution techniques are capable of imaging the dense areas of a dried sample, which are typically too thick to be imaged by OM, giving them a significant advantage. There are examples in literature of wet gels being imaged by AFM.[29] AFM produces images with resolution on less than a nanometer scale, giving incredibly detailed images of supramolecular structures. AFM imaging is detailed enough to see helical ribbons, as well as various fibers and tubules.[30] While the images are extremely detailed, this instrumentation can have issues with imaging supramolecular structures with high Z height in tapping mode. Several gelators have been found to be capable of chiral self-assembly, leading to a chiral environment within the supramolecular architectures of the gels they form. Circular dichroism is a very useful tool for analyzing these chiral environments. Since the mechanical strength and viscoelastic nature of the gel is important when looking at practical applications, rheology is often utilized to analyze these traits. In addition, rheology is also useful in analyzing the thixotropic properties and self-healing properties of these gels. Since these physical gels are thermally reversible, differential scanning calorimetry can be utilized to analyze the gel to solution and solution to gel transitions.

1.5 POPULAR SCAFOLDS FOR DESIGNING LMWGS

There are several popular classes of compounds frequently used as starting materials for designing LMWGs.[10] Great success in designing supramolecular gelators has been achieved using various classes of naturally occurring starting materials, such as amino acids, nucleotides, cholesterols and carbohydrates.

Peptides are a motif which are known to self assemble into nanostructures, making exploration into peptide based gelators a very popular area of study in the recent decades.[26] Various length peptides have proven to be some of the most successful materials for designing supramolecular gelators. Zhang et al. developed the dipeptide "samogen" abbreviated NapFF, depicted in Figure 4.[26] Samogen is a term for a unit or motif that promotes supramolecular self-assembly.[26] This supramolecular gelator consists of a phenylalanine dipeptide with an N-terminal naphthyl group and was found to be a very versatile hydrogelator. To investigate the efficiency of this samogen, it was functionalized at the *C*-terminal with various bioactive molecules such as β-lactam rings, Taxol, and bisphosphates. Regardless of the size of the bioactive molecules that were attached, the molecule retained its ability to form hydrogels, which is a testament to its extensive gelation properties.

Another class of naturally occurring biological molecules that are notorious for self-assembly are nucleosides. These molecules consist of a five membered sugar ring and a nitrogenous base. There are several positions on the molecules that make up this category of biomolecules which can be functionalized, making them excellent starting materials for the design of supramolecular gelators. Angelerou et al. designed and synthesized the nucleoside-based hydrogelator depicted in Figure 4. These nucleoside derivatives were synthesized by linking fatty acids to 2′-deoxycytidine.[31] Hydrogels created from these supramolecular gelators showed self-

healing capabilities and preliminary *in vitro* studies were carried out to assess potential uses in drug delivery using fluorescently labeled tracers. Cell viability assays were conducted to assess the biocompatibility of the supramolecular gels and no adverse effects on proliferation or cell viability were observed. An interesting property observed during a later study was that the self-assembly of this gelator induces fluorescence.[32] Nucleosides are not typically fluorescent; however, N^4-octanoyl-2′-deoxycytidine displays weak fluorescence when dissolved in methanol. Gels made from N^4-octanoyl-2′-deoxycytidine in a 1:4 solution of ethanol to water showed a significant increase in emission intensity. This indicates that the aromatic-aromatic interactions in the gel state led to aggregation-induced emission (AIE). This study also investigated the self-assembly mechanism through molecular modeling and powder X-ray diffraction. Solvophobic forces initially drive the formation of oligomeric structures, which then rearrange into cylindrical fibers with the aliphatic chains facing the core of the fiber. This creates a hydrophobic core within the fibers and a hydrophilic environment immediately surrounding the fiber. These properties could be ideal for the encapsulation of small hydrophobic drug molecules and the stabilization of hydrophilic biopharmaceuticals such as therapeutic proteins, peptides or mRNA.

Cholesterols are another interesting starting material for the development of low molecular weight gelators. Ghosh et al. designed and synthesized a cholesterol derivative which is coupled to a naphthalene group through a imine containing linker.[33] In this system, gelation occurs though aromatic interactions between the naphthaldimine groups and hydrophobic interactions provided by the large hydrophobic surface of the cholesteryl sections of the molecules. Compound **4**, depicted in Figure 4, is an example of one of the LMWGs discovered over the course of this study. The anion sensitivity of the supramolecular gels formed from this cholesteryl based gelator was analyzed by exposing the gels to concentrated solutions of tetra-butylammonium salts of F^-, Cl^-,

Br^-, AcO^-, $H_2PO_4^-$, $HP_2O_7^-$, HSO_4^-, NO_3^-, and CN^-. The gel was found to be selective to cyanide anions, as it exhibited both a color change from yellow to brown, as well as a gel to solution transition. This selectivity makes this cholesteryl based gelator a good candidate for the detection of cyanide.

Carbohydrates are an excellent starting material for designing supramolecular gelators. Using carbohydrates as a feedstock for the synthesis of LMWGs is an attractive option because of their natural abundance, renewability, biocompatibility, biological activity, biodegradability, structural diversity and capability of chiral self-assembly. The structural diversity of carbohydrates makes them a good scaffold for designing and tuning the gelation properties of LMWGs because multiple positions on the sugar can be functionalized. Additionally, gelators derived from carbohydrates are capable of chiral self-assembly, creating unique chiral environments within the gels. Goyal et al. designed and synthesized a library of 4,6-benzylidene protected α-D-methoxy-glucosamine derivatives containing aliphatic and aromatic amide and urea functional groups at the second position of the sugar ring.[16] Several efficient gelators were discovered over the course of this study. The phenyl amide derivative **5** depicted in Figure 4 was found to be a hydrogelator with a MGC of 2 mg/mL.

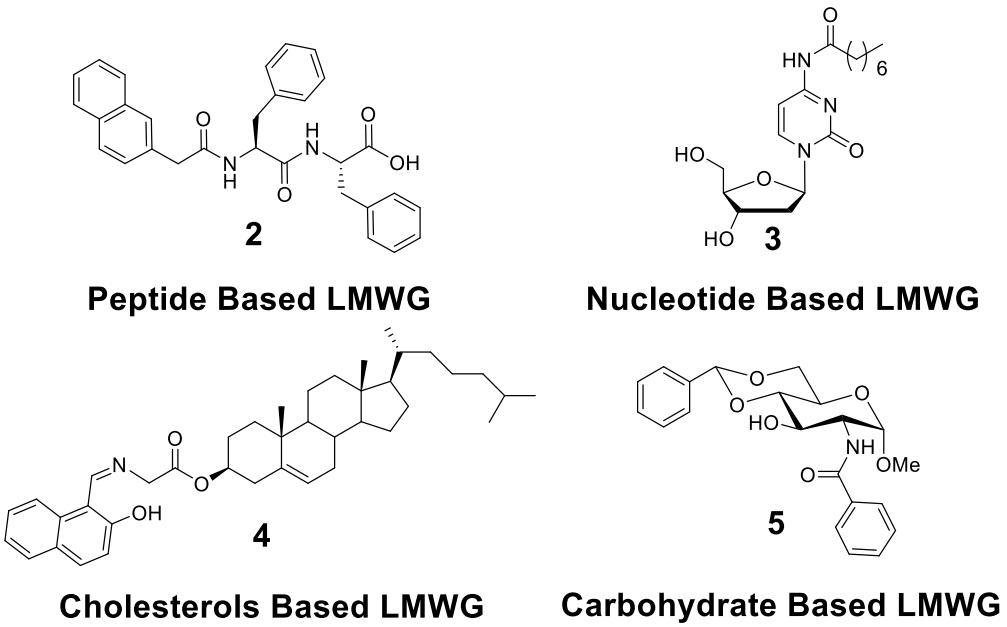

Figure 4. Examples of LMWGs designed from popular scaffods. Peptide based LMWG;[26] Nucleotide based LMWG;[32] Cholesterol based LMWG;[33] Carbohydrate based LMWG.[16]

1.6 DESIGNING CARBOHYDRATE BASED SUPRAMOLECULAR GELATORS

In previous studies, we have had success in designing effective carbohydrate based LMWGs through the selective functionalization of D-glucose or D-glucosamine.[15-17,21,34-42] Figure 5 depicts various successful LMWG's designed from 4,6-benzylidene protected glucose and glucosamine by functionalizing the second and third position of the sugar rings through linking aliphatic and aromatic groups through hydrogen bonding motifs such as amides, ureas, carbamates and esters. Compounds **6** and **7** were synthesized using glucosamine and glucose respectively.[15] These two molecules were very successful supramolecular gelators which were discovered within a study that designed and synthesized *O*-inked and *N*-linked carbamate derivatives to investigate the structural requirements for gelation. Compounds **8** and **9** were both effective gelators that were

discovered during a study that analyzed the effect of adding amide and urea hydrogen bonding groups at the second position of 4,6-benzylidene protected glucosamine.[16] In a later study, a similar series of amide and urea derivatives were synthesized from a 4-methoxybenzylidene protected glucosamine headgroup, leading to the discovery of several effective supramolecular gelators such as compounds **10** and **11**.[17] The addition of the electron donating methoxy group to the 4,6-benzylidene protection causes the acetal protection to become acid labile, and thus the gels formed from these LMWGs will readily degrade when exposed to an acidic environment. Another series of stimuli responsive gelators was synthesized in a later study where 4,6-benzylidene protected glucosamine was used to make amide linked glycolipids.[39] Compound **12** was one of several versatile and effective LMWGs discovered from this study. The ester functional group in this series of LMWGs can be hydrolyzed under basic conditions, making the gels formed by these glucosamine derivatives degrade under basic conditions. Studies exploring the effect of functionalize the third position of the sugar ring of *N*-acetyl glucosamine have also been carried out leading to the discovery of the 3-*O*-ester derivative **13** and the 3-*O*-carbamate derivative **14**.[37,40] Compound **14** was found to have an interesting stimuli response to metal ions and tetrabutylammonium salts, forming spontaneous gels in the presence of specific ions.

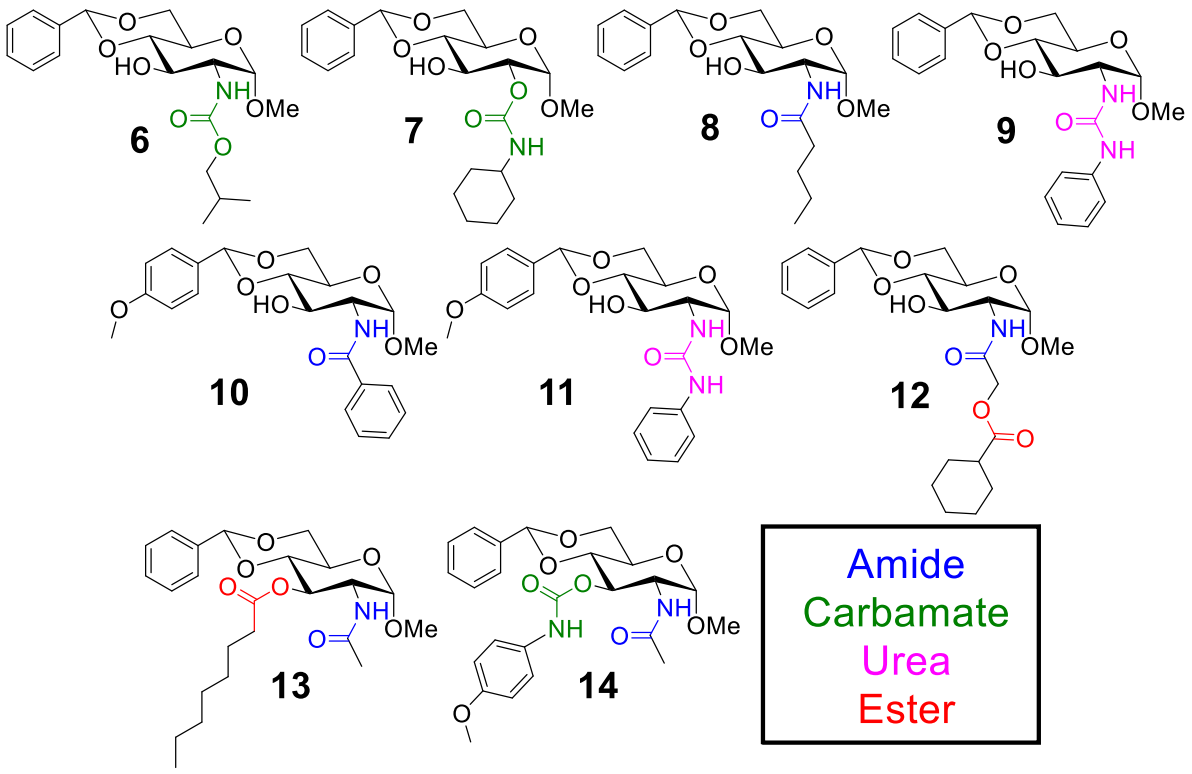

Figure 5. Various carbohydrate derived LMWG's designed from 4,6-protected glucosamine and glucose functionalized at the second and third positions on the sugar ring.[15-17,37,39,40]

We have also had significant success in designing LMWGs through functionalizing carbohydrate derivatives at the anomeric position, or first position of the sugar ring, using copper-catalyzed azide-alkyne cycloaddition (CuAAC) reactions. CuAAC reactions are a useful method for covalently linking building blocks with various functional groups.[43] The resulting 1,2,3 triazole ring linker has a strong dipole moment, heteroaromatic character and is capable of both hydrogen bond donation and accepting. This makes the triazole ring moiety a useful functional group in supramolecular chemistry and it has been successfully utilized as an isosteric substitution for amide groups in self assembling systems.[44] Figure 6 shows several selected LMWGs from various studies where functionalizing carbohydrate derivatives at the anomeric position through β-1,2,3-

triazole linkers was investigated. Compound **15** was one of several peracetylated glucosyl triazole derivatives that were found to be effective supramolecular gelators.[35] Utilizing peracetylated glucosamine instead of peracetylated glucose led to the discovery of very effective gelators, such as compound **16**.[34] Seven out of the sixteen peracetylated glucosamine derivatives synthesized in this study were found to be hydrogelators at concentrations under 1.0 mg/mL.[34] In a later study, 4,6-benzylidene protected glucosamine and glucose head groups were utilized to create a series of 4,6-*O*-benzylidene acetal protected β-1,2,3-triazole derivatives.[41] Several effective gelators were once again obtained from this series, such as compound **17**.[41] Studies utilizing the peracetylated disaccharides, lactose and maltose, also led to the discovery of several LMWGs, such as compound **18**.[42] The effect of adding several methylene spacers in between the sugar head group and the triazole moiety was analyzed in a later study leading to the discovery of several LMWGs, such as compound **19**.

We have also explored linking several sugar units to a central building block to take advantage of the multivalent effect as an approach in the rational design of supramolecular gelaltors.[45] In this study, peracetylated glucose and peracetylated glucosamine were linked to a central pentaerythritol core through triazole groups to create dendritic glycoclusters. The results of this study indicate that increasing the number of branches containing peripheral sugar units can lead to enhance gelation properties. Compared to monovalent and divalent derivatives, trivalent and tetravalent derivatives, such as compound **20**, were much more effective and versatile gelators. This concept was further explored in a later study where trivalent, tetravalent, and hexavalent derivatives were synthesized utilizing trimesic acid, pentaerythritol, and dipentaerythritol cores.[38] Various effective gelators were obtained from this study, such as compound **21**. A majority of the compounds synthesized in this study were also found to act as copper ligands, which accelerated

the rate of CuAAC reactions significantly. Mixtures of compounds that were good gelators and effective at accelerating CuAAC reactions were utilized in supramolecular catalysis.

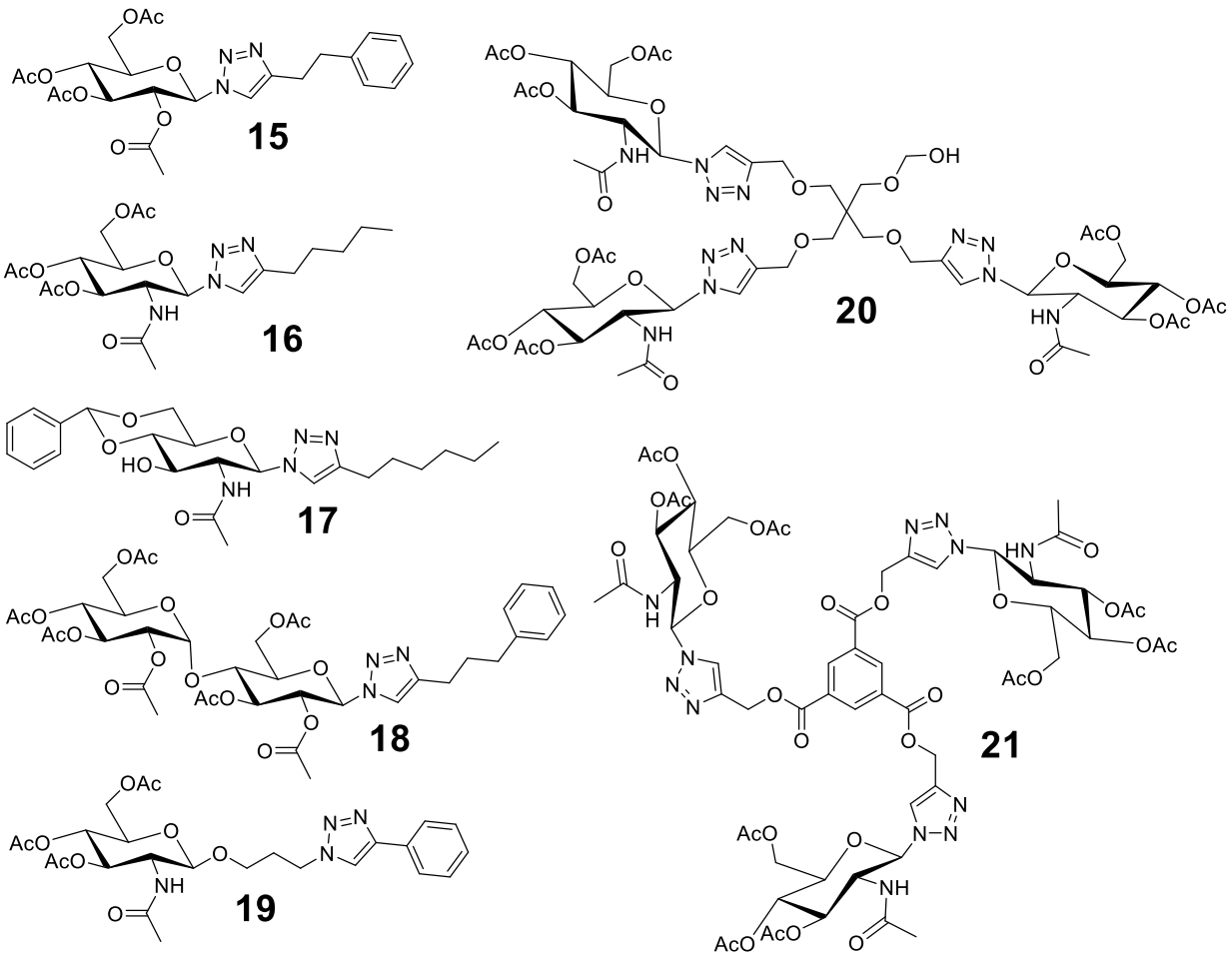

Figure **6**. Various carbohydrate derived LMWG's designed from peracetylated carbohydrates functionalized at the anomeric position through a triazole group.[34-36,38,41,45]

1.7 APPLICATION OF SUPRAMOECUALR GELS

1.7.1 Biomedical Applications

As previously mentioned, the NapFF dipeptide hydrogelator exhibits significant gelation properties and retains these properties after being functionalized with various biofunctional molecules.[26] Due to the ability of this structural motif to act as a building block for designing functional hydrogelators, it is referred to as a samogen, which represents the fundamental unit of a molecule that promotes self-assembly.[26] This molecule has been functionalized though either the "end-on" or "side-on" method, depicted in Figure 7.

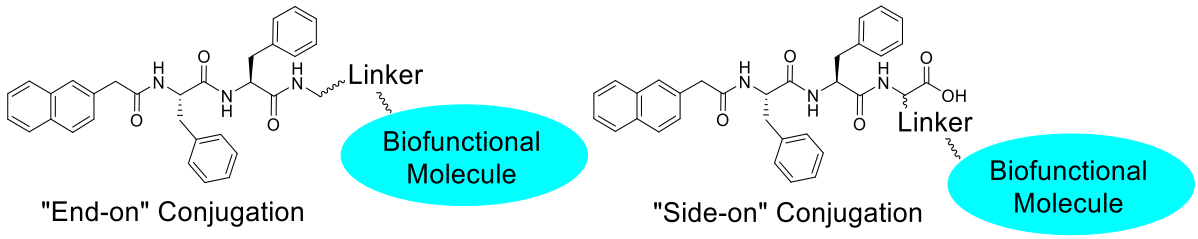

Figure 7. End-on versus Side-on functionalization of Nap-FF.[26]

Using these methods of functionalization, a variety of biofunctional molecules and stimuli responsive groups have been successfully added to Nap-FF, while retaining the ability to form hydrogels.[26] Bisphosphonate, a potent inhibitor of bone resorbing cells, and Taxol, an anticancer agent, were both conjugated with Nap-FF through the end-on functionalization method to create effective biofunctional hydrogelators. The Nap-FF samogen was also functionalized with β-lactam rings to create hydrogels that are sensitive to the presence of β-lactamase, depicted in Figure 8. β-lactamase hydrolyzes the constrained β-lactam ring on the hydrogelator, cleaving the gelator into two non-gelator sections, causing degradation to the supramolecular architecture and a gel to solution transition.[26]

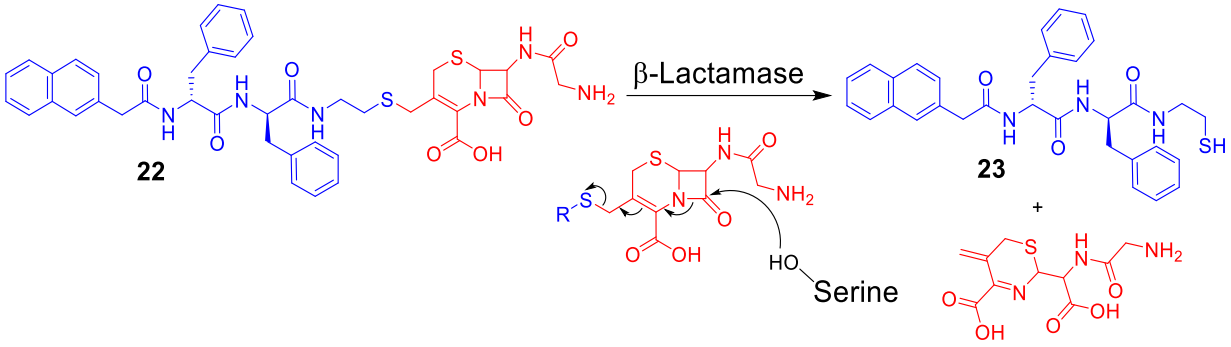

Figure 8. β-lactam functionalized Nap-FF and mechanism of β-lactamase inhibition.[26]

Functionalizing Nap-FF with O-butyric diacid and tyrosine phosphate led to the creation of stimuli responsive hydrogels. In the case of the *O*-butyric diacid functionalized Nap-FF derivative **24**, shown in Figure 9a, either basic conditions or exposure of lipase cleaves the ester group, producing hydrogelator **25**. While this derivative is not functionalized with a biofunctional molecule, previous research by Yang et al. found the amino ethanol derivative **25,** formed after enzymatic cleavage, was capable of self-assembly within cancer cells that led to the inhibition of cell growth.[46] Functionalizing NapFF with tyrosine phosphate led to another hydrogelator that can be triggered enzymatically, shown in Figure 9b. Alkaline phosphatase (ALP) is over expressed by several types of cancer cells and will cleave the phosphate group off of the NapFF-tyrosine phosphate derivative **26**, producing the NapFF-tyrosine derivative **27**, which is a hydrogelator. Both of these Nap-FF derivatives are examples of pregelators that when acted upon by specific stimuli will cleave to produce a gelator *in situ*.

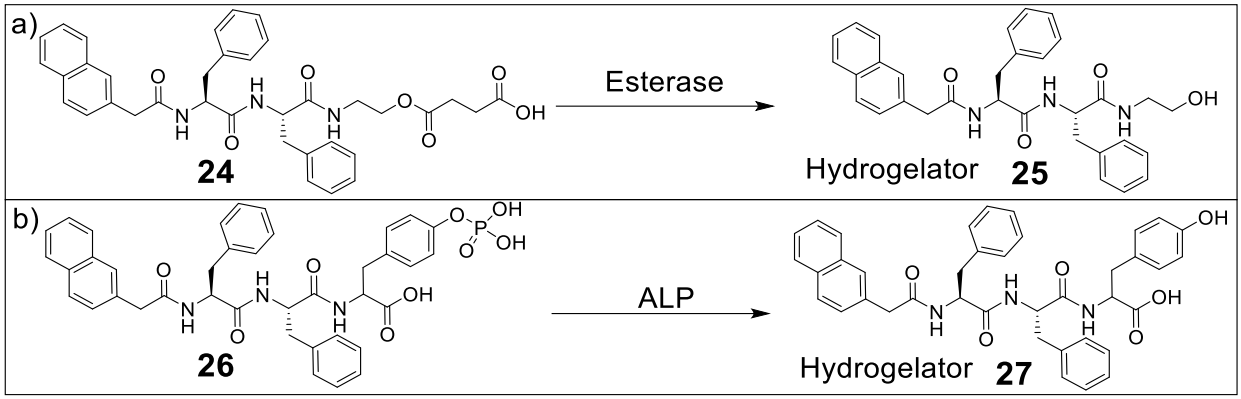

Figure 9. Chemical structures of enzyme responsive Nap-FF pregelators. a) depicts the cleavage of *O*-butyric diacid functionalized Nap-FF derivative to form hydrogelator **25**; b) shows dephosphorylation of NapFF-tyrosine phosphate to produce hydrogelator **27**.[46,47]

In a later study, Gao et al. further functionalized the NapFF samogen to contain both the tyrosine phosphate group and Taxol, through side-on conjugation, creating compound **29**, shown in Figure 10.[48] Even though Taxol is a fairly bulky molecule, the derivative retained the gelation properties in water. This study demonstrated the ability of this system to undergo enzyme instructed self-assembly. In 2013, Li et al. further expanded on this study by functionalizing the scaffold with the fluorescent marker 4-nitro-2,1,3-benzoxadiazole (NBD), creating compound **28**, shown in Figure 10.[49] MTT assays were utilized to examine the efficacy of the Taxol functionalized derivative and found that the antitumor activity was preserved. In vivo studies were then carried out using a mouse model where Bal b/c mice were inoculated with 4T1-luciferase cells. In comparison to the control group and a group treated with Taxol, the hydrogel treated group showed a statistically smaller tumor size, suggesting that it exhibits higher antitumor efficacy. To look at applications in cell imaging, the NBD functionalized derivative was used to treat HeLa cells. NBD containing hydrogelators typically exhibit very little fluorescence unless they are in an

aggregated state, such as in a self-assembled gel. After incubation, strong fluorescence from the area near the nuclei was observed, which indicated that self-assembly around the endoplasmic reticulum (ER) had occurred. The lack of fluorescence outside of the cells suggests that little self-assembly occurred outside of the cells. These studies are excellent examples of functional molecules that can undergo enzyme instructed self-assembly and are an important step in targeted medical treatments.

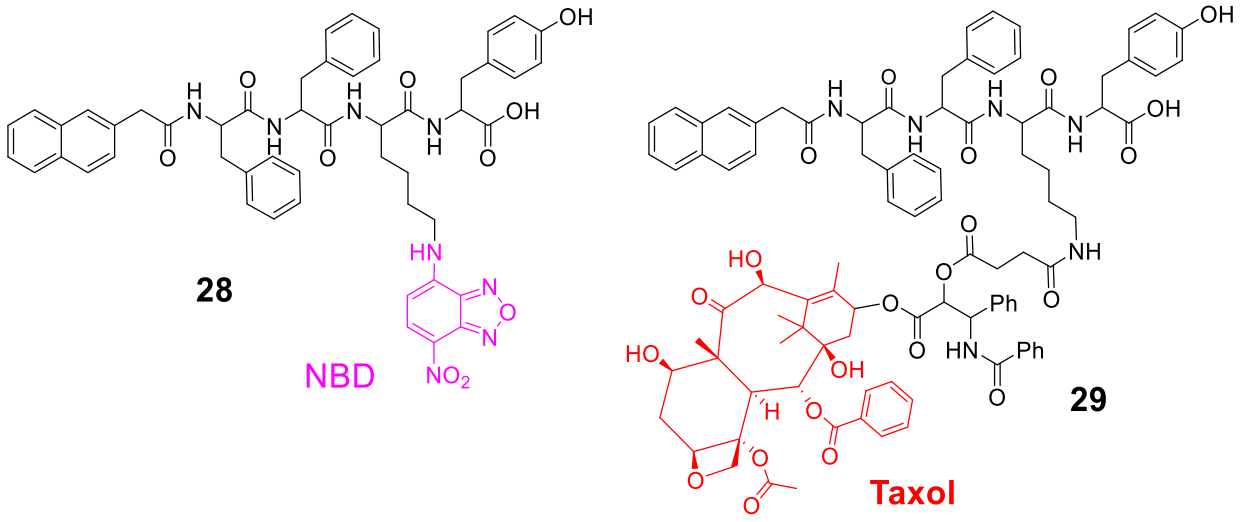

Figure 10. Structure of the short-chained phenylalanine peptide gelators functionalized with a fluorescent marker (NBD) and a chemotherapy drug (Taxol).[48,49]

Another example of a enzyme triggered gelator precursor was developed by Pires et al., which utilized a N-fluorenylmethyloxycarbonylglucosamine derivative which was phosphorylated at the sixth position.[50] Similarly to the previous work on ALP triggered dipeptide gelators, this gelator precursor was treated with alkaline phosphatase (ALP), which then cleaves the phosphate

group to trigger gelation, shown in Figure 11. Since ALP is overexpressed in bone cancer tumors, *in vitro* studies were carried out using osteosarcoma cell lines, which posses membrane bound ALP, and the cartilage cell line ATDC5, which have a lower expression of ALP. The results of this study showed that after treatment with the pregelator, the gelator forms a cytotoxic nanonet or "hydrogel cage" around the osteosarcoma cells, shown in Figure 11. This shielded network was found to disrupt cellullar functions, causing cell death. The cartilage cells on the other hand, were not affected after treatment with the gelator precursor. In a later study, these molecules were found to deprive cancer cells of glucose through competitive binding to the GLUT1 transporter.[51] The supramolecular network formed around the cells acts as a reservoir of GLUT1 inhibitors. These studies showed the synergistic properties of the posphorylated F-moc protected glucosamine that allow it to target and kill specific ALP producing cells, making it a responisve biomaterial that can be utilized for cancer treatments.

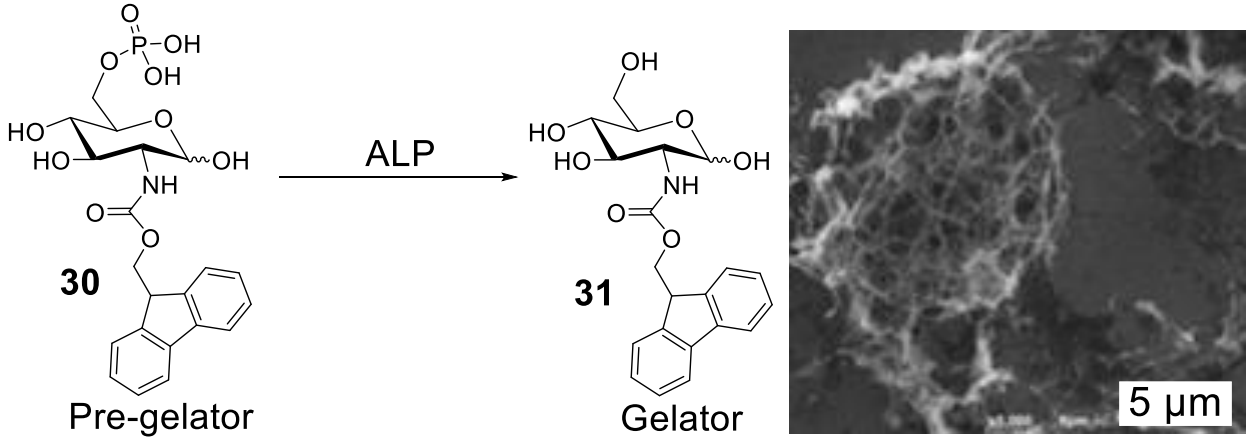

Figure 11. N-Fmoc-glucosamine-6-phosphate (pregelator) treated with ALP to produce N-Fmoc-glucosamine (Gelator) and SEM image of the "hydrogel cage" surrounding a SaOs2 cell.[50] Adapted with permission from ref 50. Copyright (2015) American Chemical Society

Morris et al. designed and synthesized a series of D-glucosamine-derived amide-ester LMWGs.[39] These D-glucosamine derivatives were effective gelators in various organic solvents and aqueous mixtures with polar organic solvents. From this series, gelators such as compound **32**, shown in Figure 12, formed gels that were capable of entraping the model drug naproxen sodium. When exposed to an aqueous medium, diffusion of naproxen sodium was found to occur over several days, showing plausible use in controled drug release applications. UV-vis spectra showing the diffusion of naproxen into the aqueous media over an extended period of time are shown in Figure 12. The ester functional group in this series of molecules make them sensitive to high pH and possibly enzymes such as lipase, making them stimuli-responsive.

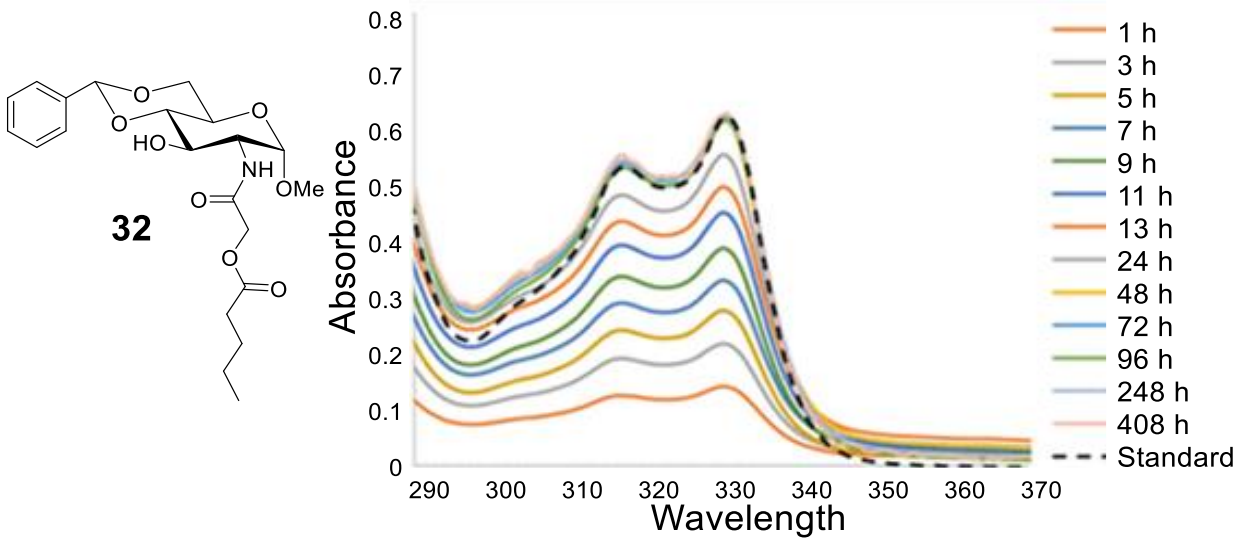

Figure 12. Structure of a D-glucosamine-derived amide-ester LMWG and the UV-vis spectra of naproxin release.[39] Adapted with permission from ref 39. Copyright (2019) American Chemical Society.

In addition to using supramolecular gels to distribute drug molecules, they have also been explored for potential uses in controlled release of certain pheromones, which have biopesticidic properties.[5] Jadhav et al. developed the sugar alcohol based amphiphilic gelator compound **33** shown in Figure 13, and studied the potential applications in sustained release of the model pheromones 2-heptanone and lauryl acetate.[5] The sugar alcohol utilized for this study was mannitol, which was functionallized at the 1 and 6 position with octanoate groups by employing regiospecific enzyme catalysis. The MGC of the pheromone gels were around 3% wt/v, and thus, the gels were composed of over 96% pheromone. The pheromone 2-heptanone is very important in the honey bee industry.[5] While it is naturally produced by honey bees to assist in breaking down various waxes, at elevated levels it acts as a mitocide and inhibits *Varroa destruction* infestations, which are a parasitic mite that quickly destroy honey bee colonies.[5] In order to create an effective controlled release device for anti-mite applications, the device needs to slowly release the 2-heptanone over 42 days, which is the length of two brood cycles. Unfortunately, 2-heptanone has a high vapor pressure, so the controled release device must be capable of controlling the rate of evaporation. Using 2-heptanone gels created from the mannitol dioctanoate gelator **33** concealed within a semi-permeable pouch, a reservoir-type controlled release device was developed. Compared to the current controlled release devices of similar weight, the gel-containing device has a much higher loading capacity and delivered sustained release of almost twice the amount of 2-heptanone.

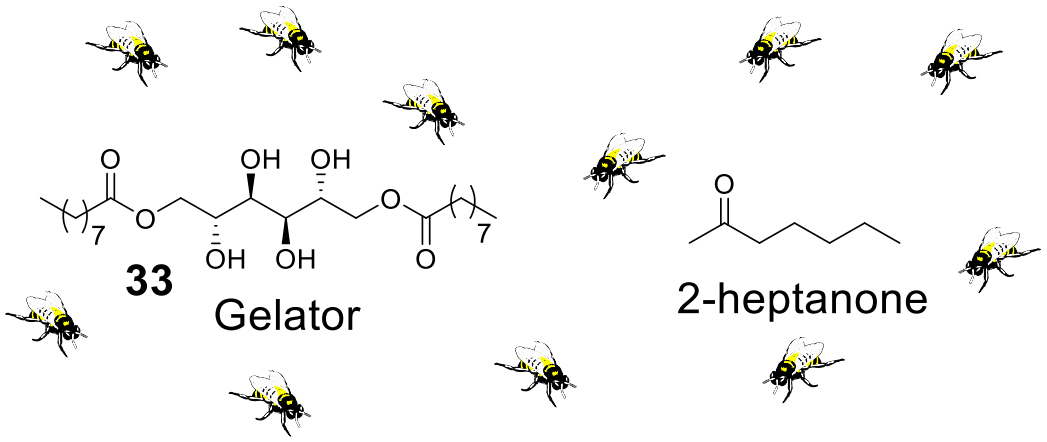

Figure 13. Sugar alcohol based gelator used in the controlled release of pheromones.[5]

Tao et al. designed and synthesized zinc responsive forky peptide **34**, D_3F_3, depicted in Figure 14.[52] This molecule was found to self-assemble in the presence of zinc ions. The concentration of zinc ions required to trigger gelation is within the physiological range found within prostate tissue. For all other cations found to trigger gelation, concentrations much higher than physiological concentrations are required. Because of this, prostate tissue-specific self-assembly *in situ* is possible using this peptide gelator. Doxorubicin (DOX), an anti-cancer drug, was chosen as a model drug to be incorporated in the gel matrix for drug delivery. In rat models, a solution of the gelator and doxorubicin was injected intravenously. Gel formation was observed after the rat prostates were excised and doxorubicin was found to be retained locally at the prostate up to 24 hours after the injection. Additionally, the forky peptide did not exhibit cytotoxicity towards normal fibroblast cells, nor did they damage the prostate tissue in rat models. The results of this study pave the way for tissue-specific drug delivery system triggered by cationic ions within physiological concentration.

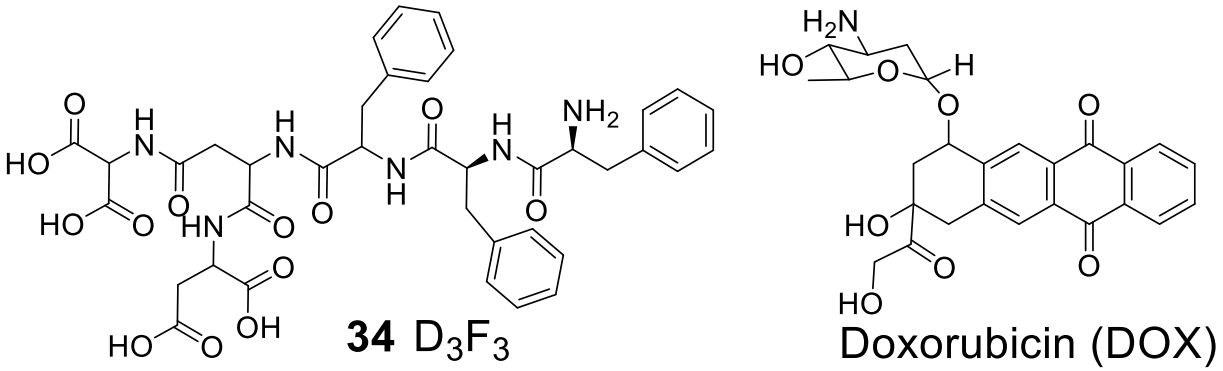

Figure 14. Forky peptide gelator used for prostate tissue targeted drug delivery.[52]

Yang et al. designed and synthesized two hydrogelators composed of D-glucosamine, L- or D-phenylalanine, and a naphthalene group, shown in Figure 15.[53] Glucosamine plays an important role in wound healing and previous work on dendritic glucosamine derivatives has shown the prevention of the formation of scar tissue.[54] Cytotoxicity assays found both hydrogels to be biocompatible; however, the gelator containing the D-phenylalanine group was slightly more biocompatible. To analyze the ability of the hydrogel to enhance wound healing and reduce scar tissue formation, a mouse wound model was utilized. In this experiment, two groups of Balb/C mice had 7 mm incisions made on the middorsal skin. In the experimental trials, 1 mL of the hydrogel was added to the incision, followed by liquid bandage. In the control trials, liquid bandage was added to the incision. Observations of the incisions showed the mice treated with the hydrogel healed much faster and exhibited much smaller scars after 6 days. A higher density of fibroblasts was observed in the day 6 control group on histological examinations, signifying the formation of scar tissue. Additionally, the day 6 control groups showed that a large number of keratinocytes had migrated to the extracellular matrix around the scar tissue, indicating the re-epithelialization phase

of wound healing had started, which is the first of five phases of wound healing. In the experimental group, on day 6, minimal scar tissue formation was observed, along with a larger amount of extracellular matrix forming between the fibroblasts and the keratinocytes, indicating that wound was in the later matrix deposition phase of wound healing. In the 18-day group, no local or systemic infections were observed. The overall results of this study showed that wound treatment with a hydrogel formed from these aminosaccharide derivatives reduces scar tissue formation and increases the rate of wound healing.

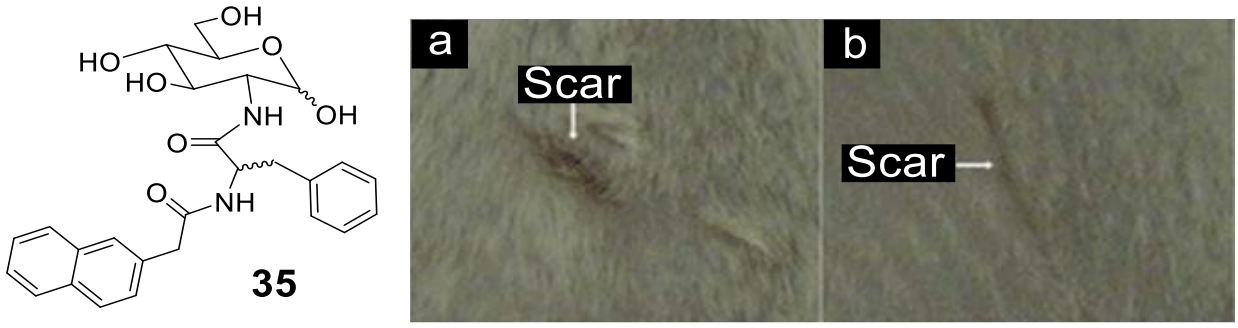

Figure 15. Structure of an aminosaccharide hydrogelator used in wound healing.[53] Adapted with permission from reference 53. Copyright (2007) Royal Society of Chemistry

Gluconamide-based amphiphilic gelators have also been found to have bioactive properties. Siva Prasad et al. synthesized amphiphilic gluconamide derivatives depicted in Figure 16 through linking δ-gluconolactone with phenoxyacetohydrazide and a mixture of 3-alkyphenoxyacetohydrazides which were synthesized utilizing a liquid extract from cashew nut shell as a renewable source of cardanols.[55] The derivative lacking the aliphatic tail was found to

be an effective hydrogelator, while the mixture of derivatives containing hydrophobic aliphatic tails were more effective gelators in organic solvents. These compounds were found to possess antimicrobial properties when tested against various pathogenic bacteria. Additionally, these compounds were found to have significant biofilm inhibitory activity against these bacterial strains. These results indicate that gels formed from gluconamide derived LMWGs could be utilized in the biomedical field to prevent bacterial biofilm related infections.

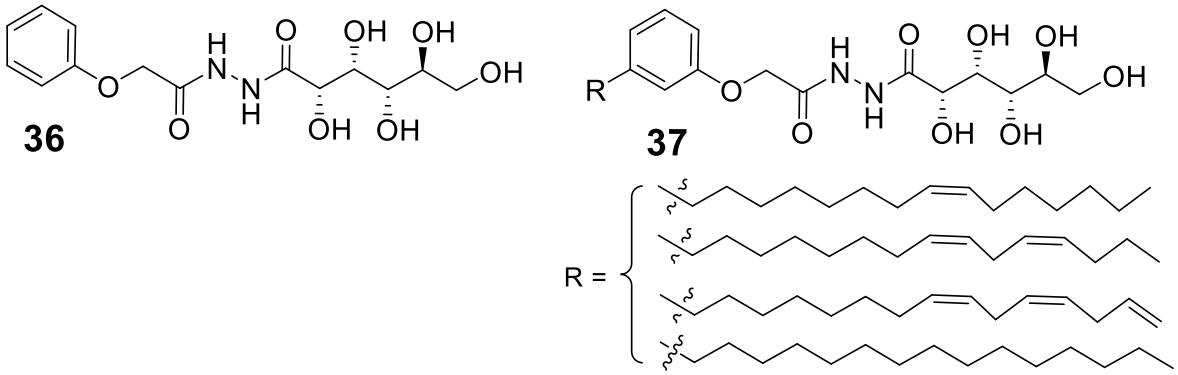

Figure 16. Bioactive gluconamide gelators derived from waste materials obtained from the cashew nut industry.[55]

1.7.2 Tissue Engineering

In 2019, Brito et al. designed a two component gelator system composed of a set of carbohydrate and dipeptide gelators, with the intent of creating a system that mimics proteoglycans in an extracellular matrix.[56] This two component system contained either a sulfonated or phosphorylated N-fluorenylmethyloxycarbonylglucosamine with the fluorenylmethyloxycarbonyl phenylalanine phenylalanine dipeptide gelator depicted in Figure 17. While gelation for the

dipeptide gelator could be controled through pH, the carbohydrate component required high temperatures for triggering gelation. This also means that the carbohydrate component has low solubility at room temperature (rt). Because of this, sulfonation or phosphorylaltion at the sixth position of the sugar was required to increase water solubility at rt so the assembly of the two component system could be carried out under physiological conditions. Several cell lines were used to analyze the ability of these gels to support cell growth and no cytotoxicity was observed. Experiments were carried out using basic fibroblast growth factor (FGF-2), which is crucial for several biological processes such as angiogenesis, cell survival and cell differentiation. FGF-2 is also known for being thermaly unstabel, losing its activity withing 24 hours of incubation at 37 °C. In biological systems, FGF-2 interacts with proteoglycans on cell surfaces, which protect it from degradation. Since the gel networks mimic proteoglycans, the gels' abilty to protect FGF-2 was investigated. Immunostaining using a specific antibody with a fluorescent tag allowed for the visualisation of active FGF-2. These experiments found that the gels could protect the growth factor for 7 days under standard cell culture conditions. Both of the two component systems were more successful at protecting growth factor compared to using a gel formed by the dipeptide component on its own. These results support the hypothesis that the supramollecular scaffold of the two component systems mimics proteoglycans. This, along with the gels' ability to mimic extracellular matrices, make these systems usefull in tissue engineering and regenerative therapies.

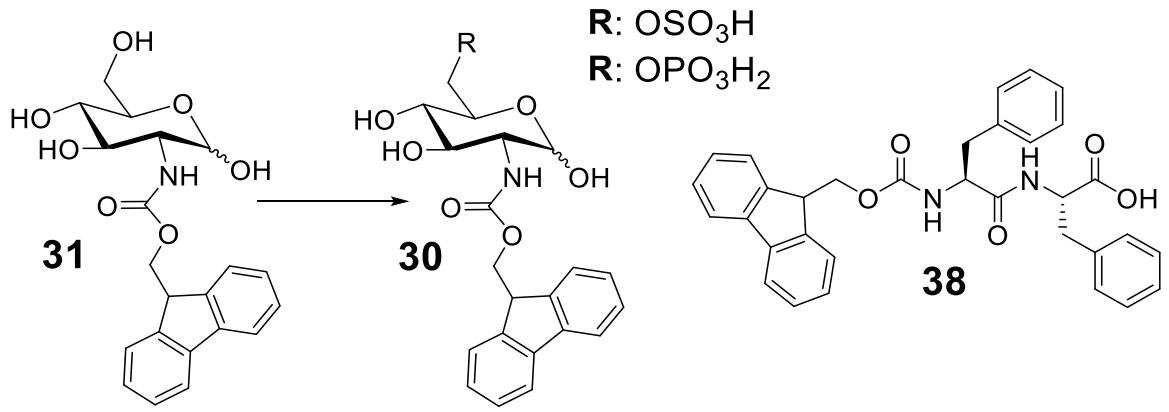

Figure 17. Glucosamine and dipeptide gelators used to create the two component system that mimics proteoglycans in an extracellular matrix.[56]

Chalard et al. carried out a study analyzing the ability of hydrogels formed from N-heptyl-galactonamide, shown in Figure 18, to act as a scaffold for the 3D growth of neuronal cells.[57] N-hexyl-galactonamide and N-octyl-galactonamide were also analyzed in this study; however, live-dead cell assays using the neuronal cell line Neuro2A showed that the N-heptyl-galactonamide hydrogels were the most biocompatible. This study found that controlling the cooling rate during gel formation had a significant effect on the morphology of the supramolecular architecture of the gels, leading to wider, longer and more uniform fibers. The gels formed over a 90-minute controlled cooling period allowed cells to grow into the gel, as opposed to just staying on the surface. Human neural stem cells were seeded on a gel formed through controlled cooling and after 7 days, live stem cells were observed throughout the gel. To visualized cell differentiation, the gels were embedded into polyacrylamide, preserving the cellular network, and dissolving the gel network. Immunostaining for the glial fibrillary acidic protein (GFAP) revealed that some of the human neuronal stem cells had differentiated into glial cells. Additionally, immunostaining for

early neuronal marker tuj-1 showed a significant amount of differentiation into neuronal cells. Fluorescent imaging of the neuronal cells is shown in Figure 18. Combined, these results show that a dense neurofilament network was grown within the 3D network of the gel, showing plausible applications in regenerative medicine and tissue engineering.

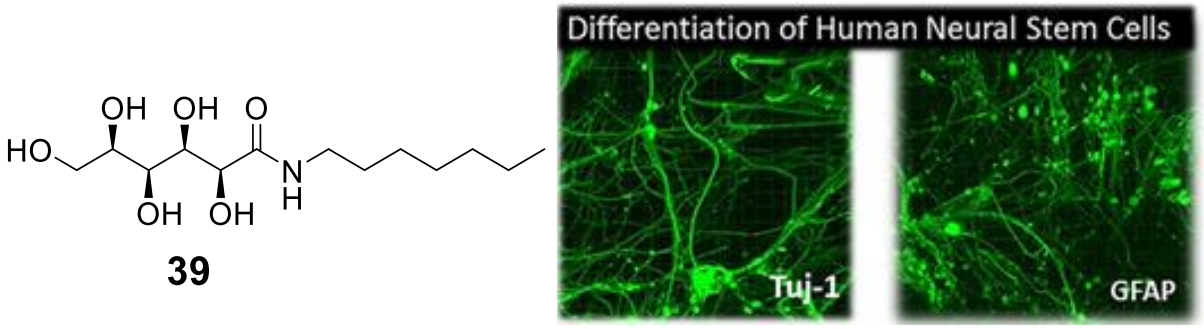

Figure 18. Structure of the N-heptyl-galactonamide gelator and fluorescent imaging of the neuronal cells cultured within the hydrogel matrix.[57] Adapted from ref 57, under the creative commons license. Copyright (2018) American Chemical Society.

Godbe et al. carried out a study where hydrogel stiffness was tuned by varying the length of an oligo-L-lysine peptide gelator.[58] The overall goal of this study was to achieve a gel with mechanical properties that lie within the range of mechanical properties found within the central nervous system. They found that the storage moduli (G′) increased by 10.5 Pa with each lysine monomer added to the peptide chain. When using these gels in 3D neuronal cell cultures, they found that small changes in storage modulus (G′) significantly affected survival and neurite growth in dopaminergic neurons derived from pluripotent stem cells. The results from this study indicate

that with the correct mechanical properties, supramolecular gels have plausible applications as transplantation matrices for neural regeneration.

Hu et al. designed and synthesized amphiphilic phenylboronic acid tripeptide gelators and investigated the ability of the supramolecular gels to culture and differentiate mesenchymal stem cells.[59] Mesenchymal stem cells can differentiate into various cell lines, and it has been found that rigid scaffolds induce osteoblastic differentiation and softer viscoelastic environments induce chondrocytic differentiation. In order to control the mechanical properties of the gels, various concentrations from 40-20 mg/mL were used to change the stiffness. The LMWG synthesized in this study was unable to form a hydrogel, so a biocompatible poly(ethylene glycol) water solution was utilized. The higher concentration gels had a storage modulus (G′) of 20-60 kPa and were found to guide mesenchymal stem cell differentiation towards the osteoblastic lineage, forming osteoid polygonal morphology, similar to osteoblast. The lower concentration gels, on the other hand, had a storage modulus of 0.1-10 kPa and led to oval-shaped cells similar to chondrocytes. Confocal microscope images of meshenchymal stem cell differnitation on the rigid and soft gels are depicted in Figure 19. The results from this study show the matrix elasticity of supramolecular gels can be utilized to direct stem cell differentiation.

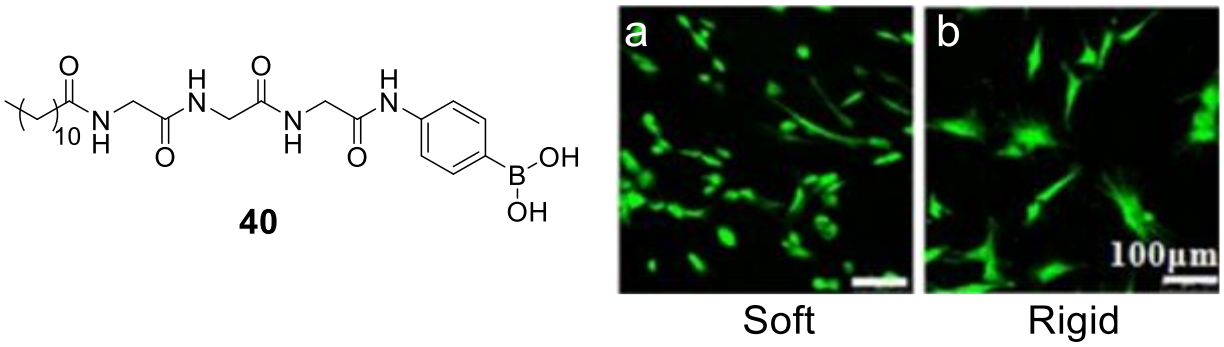

Figure 19. Structure of the amphiphilic LMWG and confocal microscope images of meshenchymal stem cell differnitation. (a) on soft gels (20 mg/mL in PEG:H_2O 4:1); (b) on hard gels (40 mg/mL in PEG:H_2O 4:1).[59] Adapted with permission from reference 59. Copyright (2013) Royal Society of Chemistry.

1.7.3 Environmental Remediation

Rizzo et al. designed gluconate and saccharate derived imidazolium salts capable of supramolecular gelation in ionic liquids, shown in Figure 20.[60] These salts consist of a carbohydrate anion and imidazolium cations containing long alkyl chains. The anionic carbohydrate sections of these salts contribute too self-assembly through multiple hydrogen bond donating groups and the imidazolium sections contribute to self-assembly through aromatic-aromatic interactions as well as the hydrophobic interactions. The gelation properties of these salts were tested in several organic solvents, aqueous solutions, and ionic liquids. Salts formed by an anionic bromide atom were also analyzed in this study and the [C_{18}mim]Br salts were found to be very effective gelators in water, salt solutions and diesel fuel. The carbohydrate salts were found to require a higher ionic strength to form supramolecular gels. 1-Methyl-3-butyl imidazolium [$bmim^+$] with either hexafluorophosphate [$PF6^-$] or N,N-bis(trifluoromethanesulfonyl)imide

[$NTf2^-$] were utilized as ionic liquids in this study. Applications in removing metal ions from waste water using these gels were investigated. These gels were found to selectively adsorb chromium (VI) species, with most removing 60% of chromium within 3 hours. These gels were found to have extremely high adsorption capacities in studies where a small sample was immersed in large chromium solutions. In the case of the $[C_{18}mim]_2$[saccharate] hydrogels, not only was total adsorption observed within 24 hours, but the chromium (VI) species were found to be reduced to the less toxic chromium (III) species. This ability to adsorb and reduce chromium (VI) makes these carbohydrate-based imidazolium salt gels useful in waste water treatment.

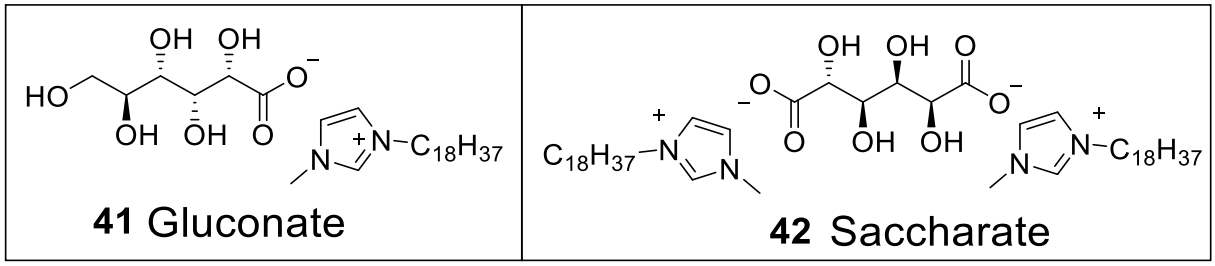

Figure 20. Gluconate and saccharate derived imidazolium salts capable of forming chromium absorbing and reducing gels.[60]

Sekhar et al. designed and synthesized a series of eight glycolipids with varying degrees of unsaturation within the hydrophobic tail, shown in Figure 21.[61] Additionally, they explored the effect of polar head size on the gelation properties by incorporating one or two sugar groups. While the glycolipids with the small polar head groups and the saturated hydrophobic tales did form hydrogels, the overall trend showed that increasing the polar head size increased the glycolipid's

ability to form hydrogels. Encapsulation experiments were carried out to analyze the loading ability of the gels formed. Both hydrophobic and hydrophilic bioactive molecules, curcumin and riboflavin, were successfully encapsulated within the gels. Triggered release of these bioactive molecules was studied by treating the gels with amidase-like trypsin, causing hydrolysis of the glycolipids, leading to the degradation of the gel and release of the bioactive molecules. Additional studies into metal ion removal from vegetable oils found that these gels were capable of chromium and copper removal. The removal capacity of the gels was found to increase with the unsaturation of the hydrophobic tail. These supramolecular gels have potential applications in gel-based delivery systems and in the purification of vegetable oils.

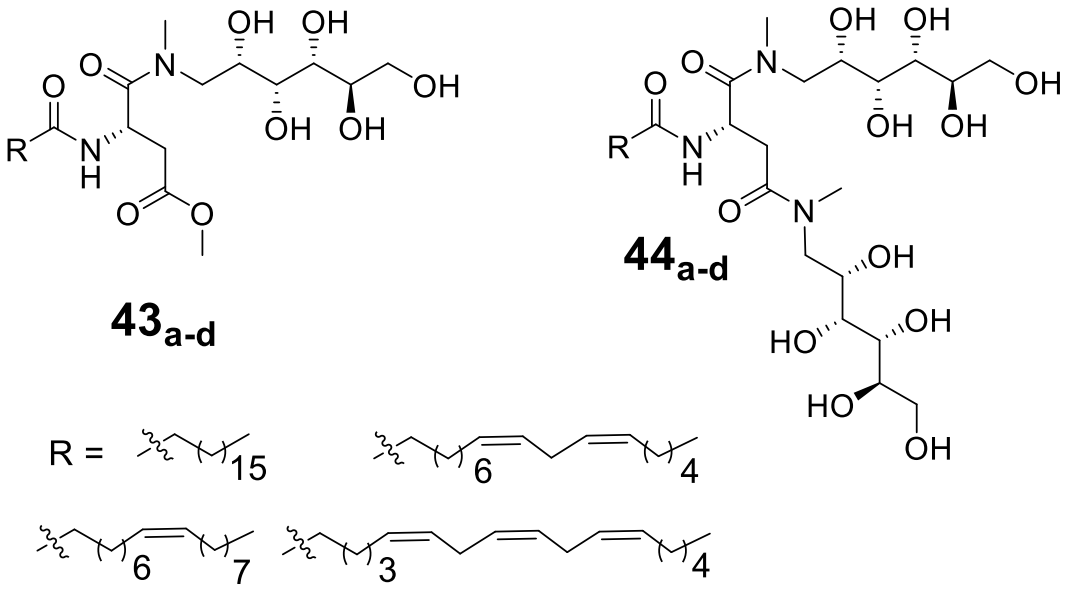

Figure 21. Series of glycolipid gelators used for Cr/Cu removal from vegetable oil.[61]

Basak et al. designed and synthesized a phenylalanine tripeptide super hydrogelator, compound **45** shown in Figure 22, which was found to have a MGC of 0.08% wt/v.[62] Supramolecular hydrogels formed from this tripeptide gelator exhibit interesting self-shrinking or self-compressing properties known as syneresis. Expulsion of water from the gel matrix was observed immediately after the formation. This is thought to be due to the hydrophobic phenylalanine residues. This property was utilized to remove toxic lead ions and organic dyes from water. In both cases, a solution of the respective pollutant was used to form a gel. Upon shrinking, clean water was expelled, and the pollutants remained in the gel matrix. Images of this process are shown in Figure 22. An ethyl acetate extraction was used to recover the gelator and the gelator could be reused for up to four cycles. The high absorption capacity and reusability show potential for uses in waste-water management.

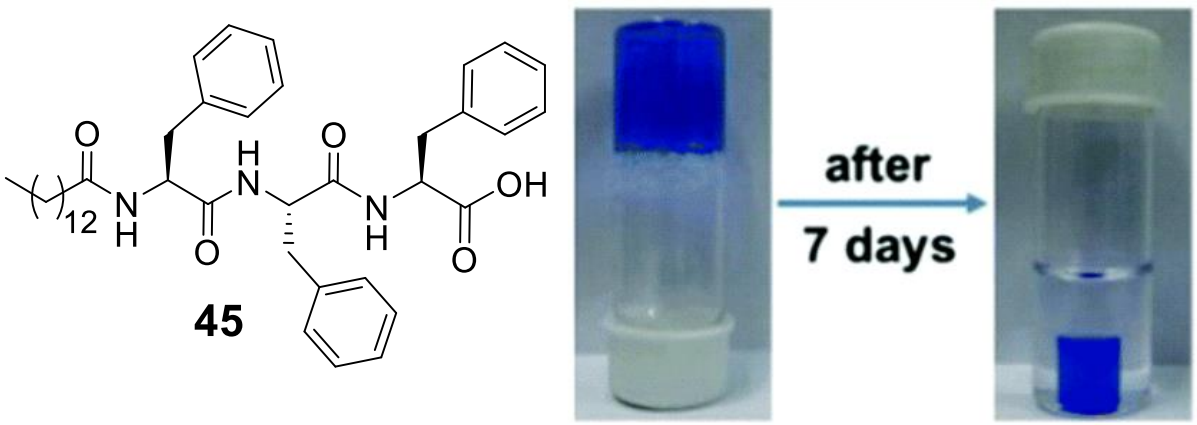

Figure 22. Tripeptide LMWG which was used for removing Pb^{2+} from contaminated water.[62] Adapted with permission from reference 62. Copyright (2017) Royal Society of Chemistry.

Srivastava et al. designed and synthesized a aryl-triazolyl peptide based organogelator and investigated applications in waste water purification and phase selective gelation.[63] The aryl-triazolyl peptide depicted in Figure 23 is capable of gelation in aromatic solvents and several hydrocarbons such as heptane. It formed very transparent gels in petrol and diesel fuel with very low minimum gelation concentrations of 0.1 and 0.3 wt% respectively. Solidification of organic solvents in biphasic solutions was carried out by using THF as a carrier solvent. A solution of the gelator in THF was added to a biphasic solution of petrol and water. The petrol layer was fully solidified within 30 seconds of the addition. The solidified organic layer was then removed, and distillation was used to recover both the petrol and the gelator. The recovered gelator was then reused up to two more times with a 70% efficiency overall. Dye removal was also analyzed in this study by adding small blocks of mesitylene gel to aqueous dye solutions. These gels were found to selectively absorb rhodamine B from aqueous solutions of rhodamine B and methylene blue. UV-vis spectra showed almost full removal of rhodamine B from the aqueous solution and the selectivity is thought to be due to the rhodamine B's equilibrium between the neutral lactone conformation and the cationic conformation. Overall, the aryl-triazolyl peptide LMWG designed in this study has applications in various aspects of wastewater treatment.

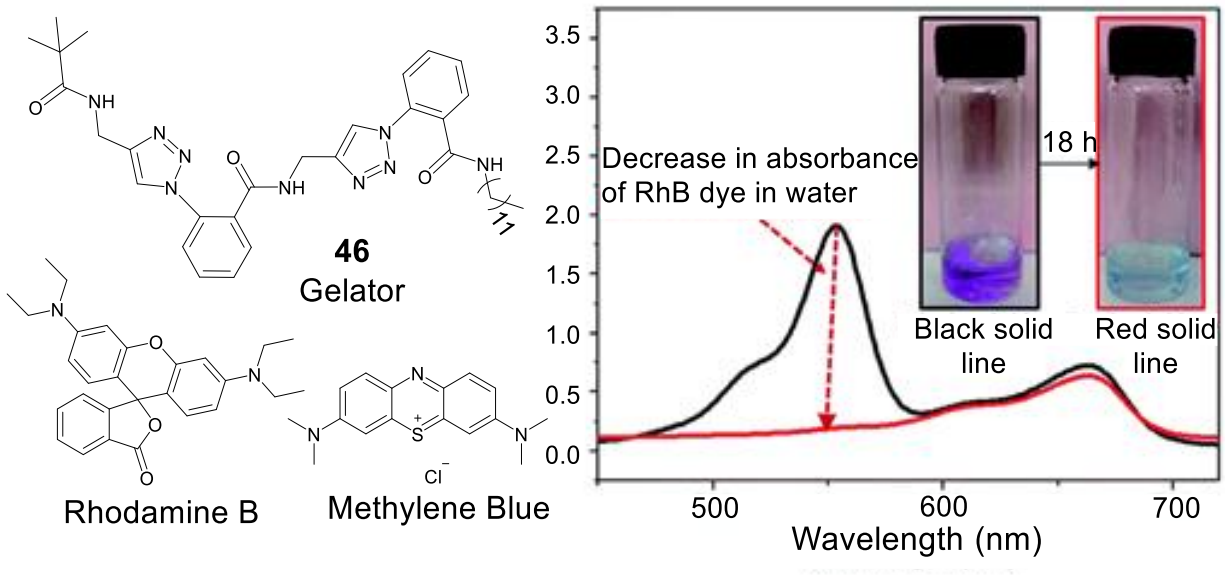

Figure 23. Aryl-triazolyl peptide LMWG which was utilized as a "supramolecular sponge" and the UV-vis overlay of a aqueous mixture of Rhodamine B and methylene blue before and after the addition of the supramolecular gel.[63] Adapted with permission from reference 63. Copyright (2016) Royal Society of Chemistry.

Pathak et al. reported a gelator-natural polymer blend capable of solidifying crude oil in less than 30 seconds at ambient temperatures.[64] The combination of the gelator, compound **47** in Figure 24, and starch causes a uniform dispersion of the gelator throughout the oil layer, leading to fast and uniform gel formation. The starch acts as a solid support for gelator dispersal and minimum gelation concentrations as low as 0.34% w/v were achieved using this method. Figure 24 shows images of the addition of the gelator-starch mixture to a biphasic mixture of crude oil and water, followed by solidification of the oil layer, and separation of the solidified oil from the aqueous layer. The results of this study are a significant step towards using LMWG's in solid form for the solidifications of crude oil from biphasic oil-water mixtures.

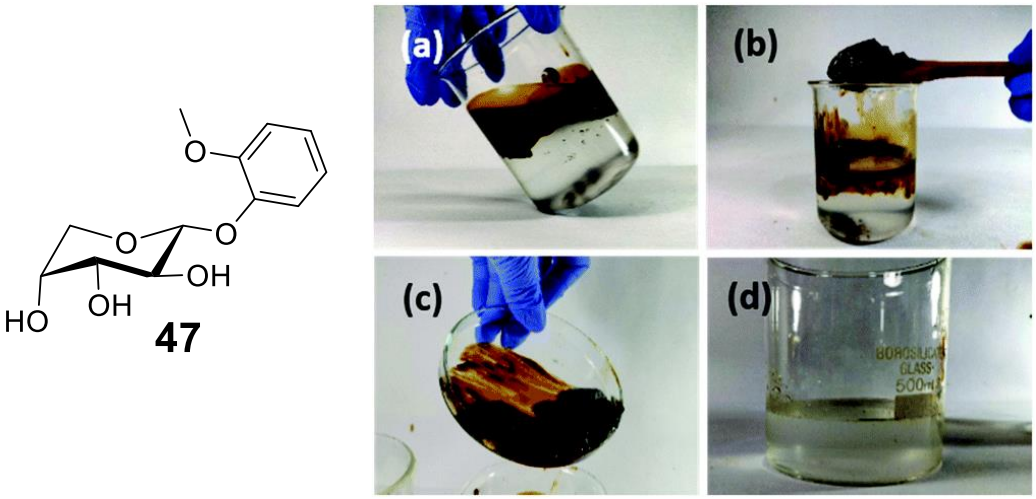

Figure 24. Structure of the arabinopyranoside gelator and phase selective gelation of crude oil. (a) Biphasic mixture of crude oil and seawater (b) Removing the solidified crude oil. (c) Solidified crude oil after removal (d) Residual water.[64] Adapted with permission from reference 64. Copyright (2020) Royal Society of Chemistry.

Zhang et al. designed and synthesized a series of acetal protected gluconic amide derivatives with various aliphatic chains, shown in Figure 25.[65] The addition of the *cis* double bond in the aliphatic chain was found to create a porous amorphous powder capable of phase-selective gelation of aromatic solvents, refined petroleum products and crude oils when added in powder form. Gelation occurred at room temperature, without heating. Gelation occurred very quickly, even in high viscosity oils such as Napo Heavy oil. This phase selective organogelator showed high recovery rates and is applicable in a wide range of oils and aromatic solvents. The introduction of the *cis* double bond, which created an irregular structure in the alkyl chain, is most likely responsible for this compound's ability to gelate solvents at room temperature, when added in solid form. Figure 25 shows the ability of this gelator to solidify toluene in a biphasic mixture of toluene

and water. The solidified toluene layer was then removed, and distillation was utilized to recover both the gelator and organic solvent. This strategy may be used may be very useful in designing future powder form phase selective organogelators.

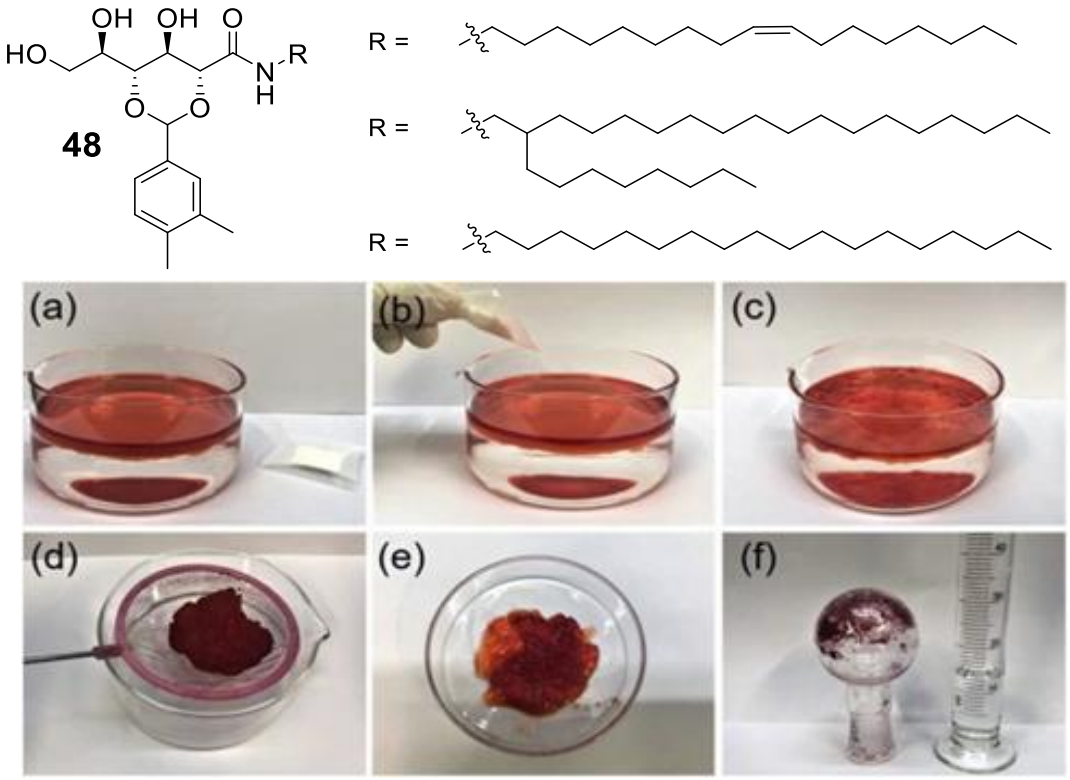

Figure 25. Structures of the acetal protected gluconic amide derivatives synthesized in this study and the removal/recovery of aromatic solvents using the gelator. (a) Aqueous biphasic mixture of toluene that was dyed with Methyl Red; (b) Addition of the gelator powder; (c) Solidification of the toluene layer; (d) Removal of the solidified toluene layer; (e) Separated solidified toluene layer; (f) Recovered gelator and toluene.[65] Adapted with permission from ref 65, Copyright (2020) Elsevier.

Pal et al. reported a mannose-based low molecular weight organogelator (LMOGs) capable of gelling various organic solvents including several fuels, alcohols, aromatic solvents, halogenated solvents, and oils.[66] Phase-selective gelation was found in several mixtures of organic solvents and water. In Figure 26, biphasic solutions of methyl violate solution and toluene was heated with the gelator and the toluene layer formed a gel. After 24 hours, the aqueous layer appears clear and most of the methyl violate had diffused into the organogel. UV-vis spectra, shown in Figure 26, confirm the near complete absorption of the dye into the organogel. Figure 26 also shows that a xerogel formed by compound **49** was capable of removing methyl violet from the aqueous phase effectively. The last image in Figure 26 shows the phase selective gelation of diesel fuel, indicating this molecule may be useful in applications of fuel spill cleanup.

Almost all of the gels formed by the mannose-based gelator **49** were also found to possess significant self-healing properties. Figure 27 shows two blocks of gel, one of which was doped with 4,4’-dihydroxyazobenzene, that were cut into pieces, stacked in alternating order, and pressed together to form one solid bar, demonstrating significant self-healing capability. Diffusion of the azo dye was observed across the fusion interface, indicating the gel segments have merged into one column of gel.

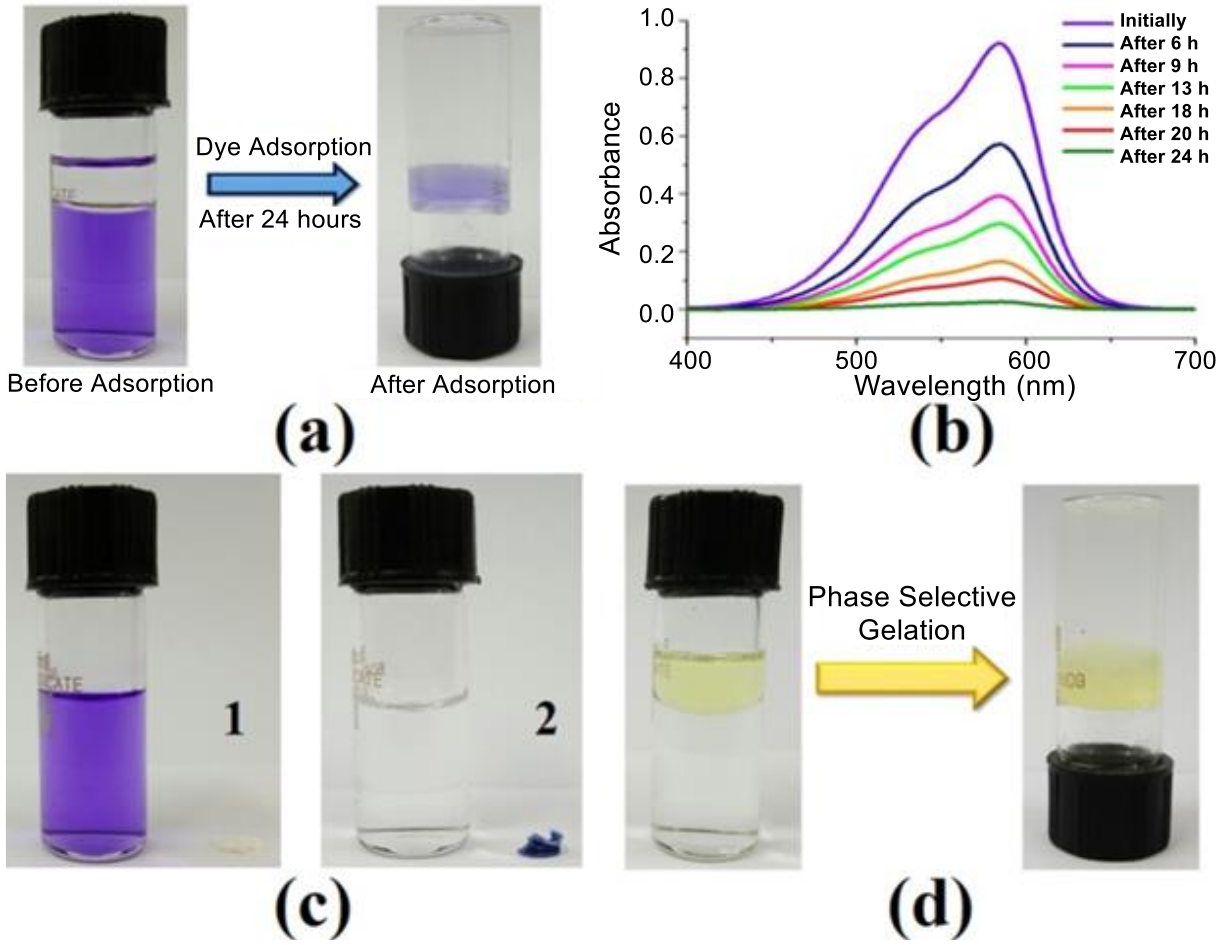

Figure 26. Applications of gels formed from the mannose-based gelator in phase selective gelation and dye absorption. (a) Phase selective gelation (Toluene/water) followed by absorption of dye from the aqueous layer; (b) UV-vis spectra of dye absorption over time; (c) Aqueous methyl violate solution (0.02 mM) (left) and the solution after the addition of a xerogel made in toluene (right); (d) Phase selective gelation of a diesel-water mixture.[66] Adapted with permission from ref 66, Copyright (2017) John Wiley and Sons.

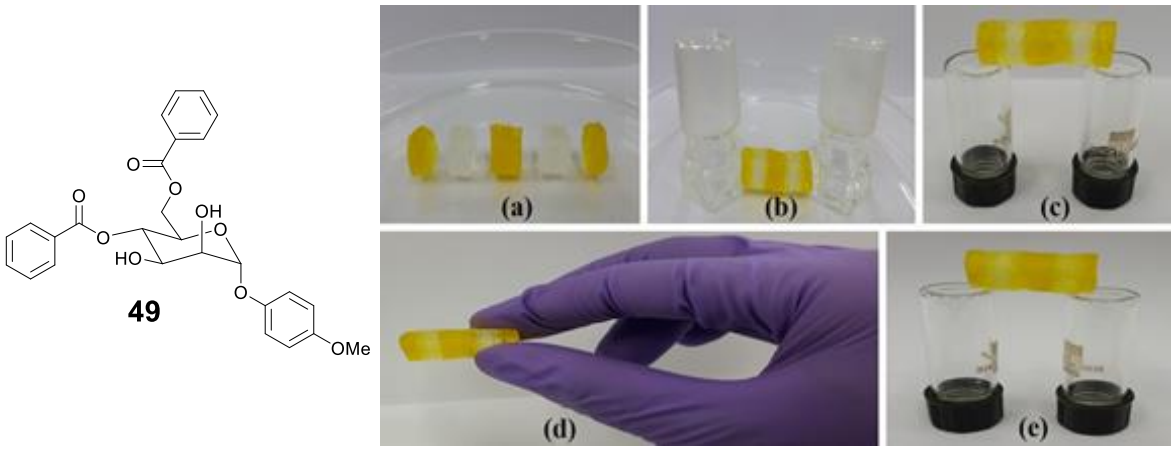

Figure 27. Mannose-based LMWG and 0.3% w/v mesitylene gels. (a) Cut up pieces of doped and undoped gel in alternating order; (b) Compressing the pieces to promote self-healing; (c) Rod of gel after self-healing; (d) A hand holding the gel rod; (e) Image showing the diffusion of the azo dye into the undoped segments of the gel rod.[66] Adapted with permission from ref 66, Copyright (2017) John Wiley and Sons.

1.7.4 Shaping and 3D Printing

Nolan et al. carried out a study optimizing the conditions for the successful extrusion based 3D printing of supramolecular gels.[6] They set out to better understand the morphological and rheological requirements for printable gels. The morphology of the gel architecture was found to be impacted by the method of triggering gelation. The solvent-triggered gels exhibited spherical domains composed of tightly packed primary fibers, while pH triggering led to the formation of continuous smooth fibrous networks. The gels exhibiting the spherulitic microstructures were found to be favorable in extrusion-based 3D printing applications. Solvent triggered gels formed from the Fmoc- diphenylalanine derivative **50**, shown in Figure 28, were successfully printed via extrusion-based 3D printing. Figure 28 also shows three- and six-layer structures that were printed

using the supramolecular gel. In this study, several printing parameters were optimized such as the speed of extrusion, the speed the printing accessory moved along the axis, the height of the printing accessory from the printing bed and the volume of gel extruded. This study is a big step in opening the door to shaping supramolecular gels through 3D printing.

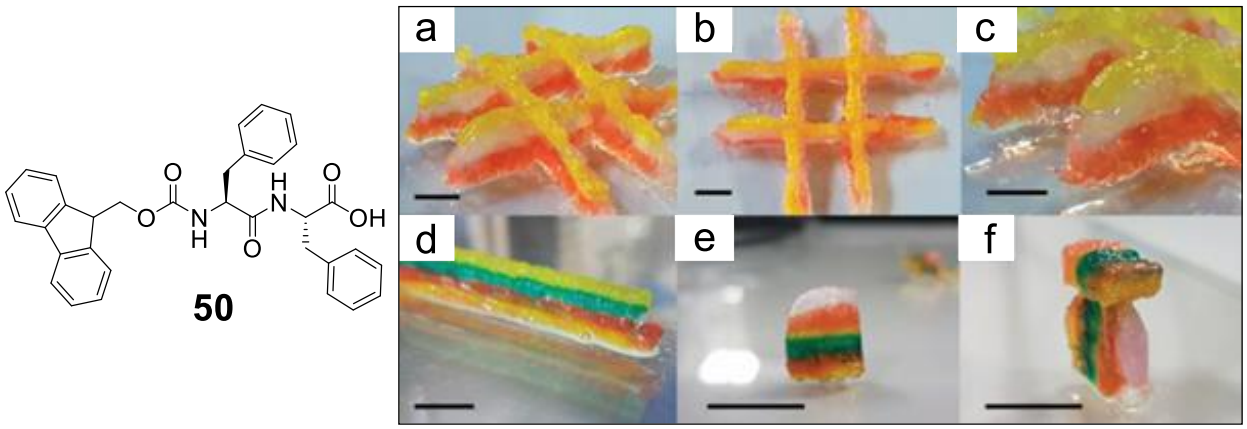

Figure 28. Structure of the Fmoc-diphenylalanine gelator and images of 3D printed structures. (a-c) a three layer printed structure and (d-f) six layer printed structures, scale bar represents 1 cm.[6] Adapted from ref 6, under the creative commons license. Copyright (2017) Royal Society of Chemistry.

Chalard et al. showed that well organized hydrogel filaments could be formed through DMSO-H_2O solvent exchange.[67] The hydrogels formed by N-heptyl-*D*-galactonamide, compound **39** in Figure 18, cannot be successfully extruded because they are fragile and undergo syneresis when they undergo a shear force, similar to many other supramolecular gels formed from LMWGs. In this study, a DMSO solution of N-heptyl-*D*-galactonamide was injected into a water bath at an

optimized rate controlled by a syringe pump, resulting in the formation of a continuous uniform hydrogel filament shown in Figure 29. This result opens up the possibility of 3D printing non-thixotropic gels, as gel can be formed on a surface through this solvent exchange.

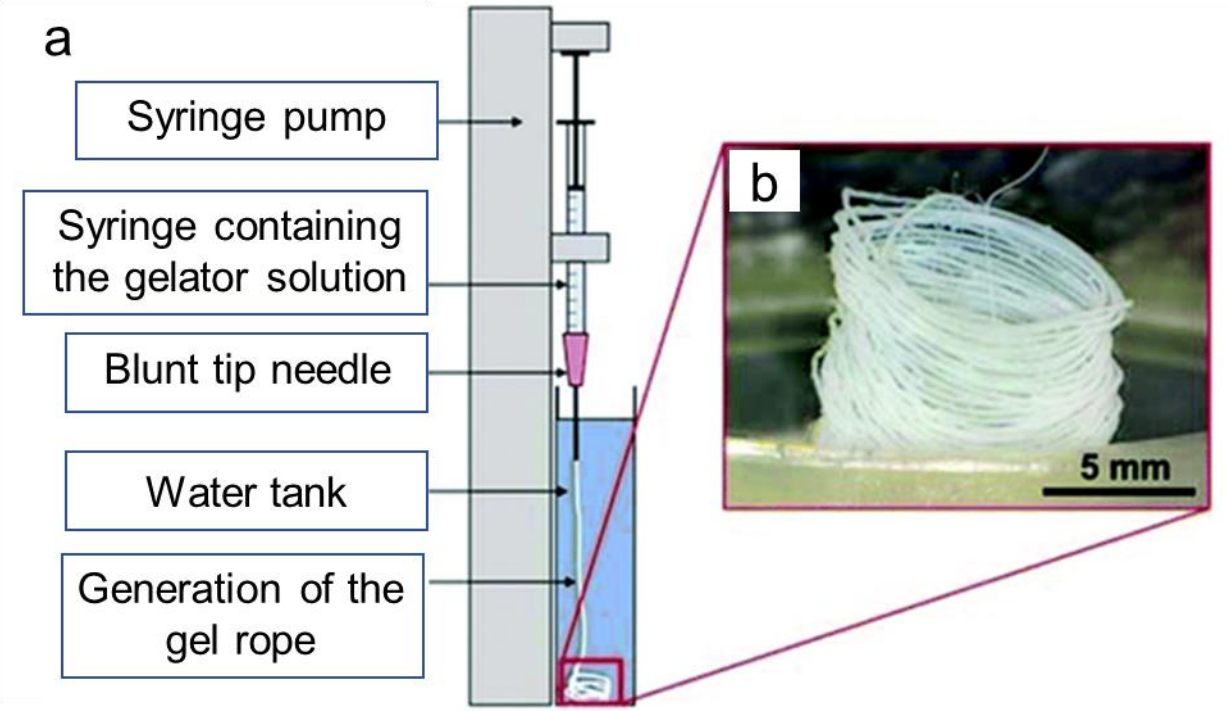

Figure 29. Wet spinning set-up, extrusion schematic and filament image. (a) Wet spinning apparatus set-up; (b) Gel filament after extrusion.[67] Adapted from ref 67, under the creative commons license. Copyright (2019) Royal Society of Chemistry.

In a later study, Chalard et al. showed that solvent exchange can be used to 3D print these non-thixotropic carbohydrate based supramolecular gels.[68] Using a syringe pump, a XY-translation stage and a handheld Z-adjustable platform, a DMSO solution of N-heptyl-*D*-

galactonamide, was extruded into a water bath and onto a glass slide covered in a hydrophobic polycarbonate membrane. The flow rate was adjusted until good adhesion to the polycarbonate membrane was achieved. Using this technique, 3D printed biocompatible supramolecular gel scaffolds can be custom printed using carbohydrate based LMWGs. This work opens the door for 3D printing other non-thixotropic supramolecular gelators.

1.7.5 Supramolecular Catalysis

In 2016, Okesola et al. reported the ability of hydrogels formed from a 1,3:2,4-dibenzylidene sorbitol functionalized with acyl hydrazides groups (DBS-$CONHNH_2$), compound **51** in Figure 30, to extract precious metals from waste water and reduce them into nanoparticles *in situ*.[69] Two years later, Slavik et al. investigated the ability of a DBS-$CONHNH_2$ and agarose co-gel to scavenge palladium and reduce it in situ, producing a gel embedded with palladium nanoparticles.[70] The resulting gel was then utilized in the catalysis of Suzuki-Miyaura cross-coupling reactions. These reactions were carried out by simply adding the gel to solutions of reagents and removing the gel once the reaction is complete. Excellent recyclability and reusability were observed with the gels successfully catalyzing over ten reactions. The gel matrix was effective at stabilizing the nanoparticles, preventing aggregation, and preventing leaching. A flow-through model was created by forming the gel in a syringe and allowing reaction mixture to flow through the gel. This protocol allowed efficient, rapid reactions along with an easy workup. These nanoparticle embedded hydrogels combine the advantages of homogeneous and heterogeneous catalysts.

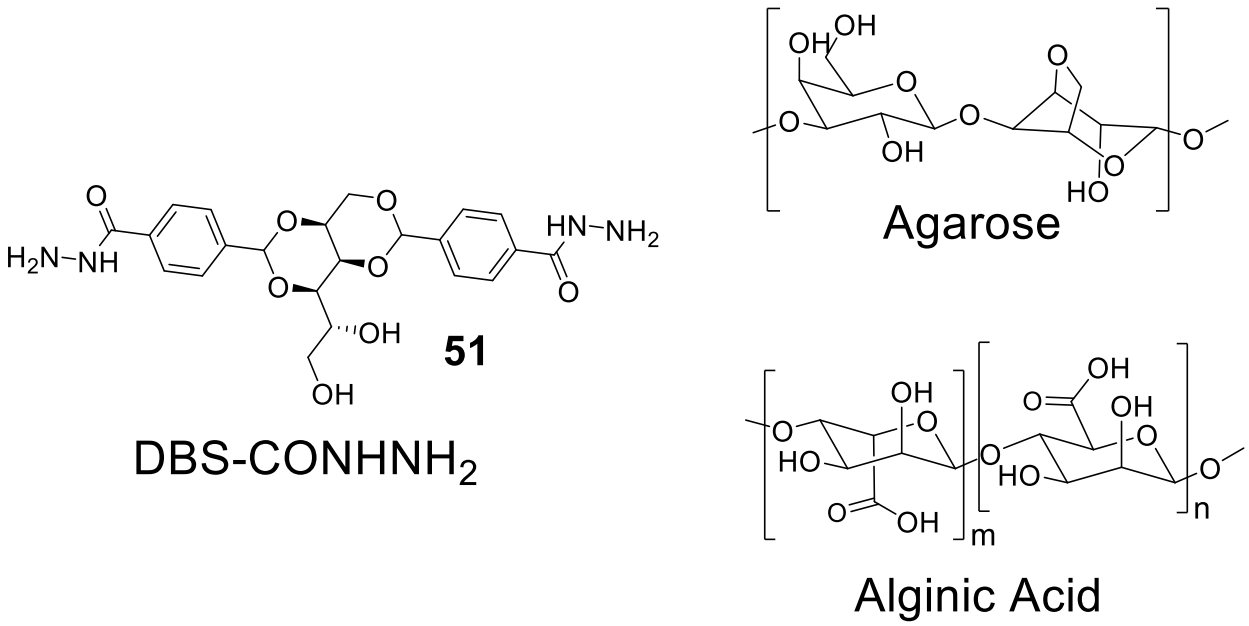

Figure 30. Structures of the polymer gelators and sorbitol based LMWG.[70]

In 2020, Piras et al. continued work on the DBS-$CONHNH_2$ hydrogelator system, setting out to gain control over the shape of the gels formed.[71] To accomplish this control over the shape and create spatially resolved structures, they formed a co-gel with alginic acid, which is a natural polysaccharide composed of β-D-mannuronic acid and α-D-mannuronic acid units linked through β-1,4 bonds. Alginate salts are water soluble and form hydrogels when mixed with multivalent cations such as Ca^{2+}. Combining LMWG DBS-$CONHNH_2$ and polymer gelator sodium alginate, created a multicomponent gel system where the polymer gel network acts as a spherical mold to constrain LMWG self-assembly. This study carried out shaping gelation in two different ways, forming either "core-shell" gels or an interpenetrating network, depicted in Figure 31. For each method, a mixture of DBS-$CONHNH_2$ and sodium alginate was heated until all of the LMWG was dissolved. For the creation of the interpenetrating network, a calcium chloride solution was added

on top of the hot solution of DBS-$CONHNH_2$ and sodium alginate. To create “core-shell” gels, this hot solution was added to a calcium chloride solution with a micropipette. Adding the solution dropwise led to the formation of gel beads and adding larger quantities all at once led to the formation of gel worms. Optical and SEM imaging of cross sections of the gel beads showed very different gel morphologies for the surface of the bead, composed of alginate, and the interior cross-section, formed from DBS-$CONHNH_2$. Staining with toluidine blue showed a clear difference between the interior of the gel bead and the outer shell. To explore the application in supramolecular catalysis, the gel beads were added to aqueous solutions of $PdCl_2$. A color change from bright yellow to dark brown indicated that the Pd^{2+} was reduced to Pd^0 nanoparticles. SEM and TEM were also utilized to confirm nanoparticle formation. Reduction in the Pd^{2+} signal on UV-vis was used to quantify the uptake of palladium into the gel bead. High catalytic activity was observed, with a single bead being capable of catalyzing up to five coupling reactions with acceptable yields. In these reactions, the reaction mixture was simply decanted, and the gel bead was rinsed with an organic solvent, preparing the gel bead to be reused for additional reactions. This study is an excellent example of fusing the function of a low molecular weight gelator with the shaping potential of a polymer gelator.

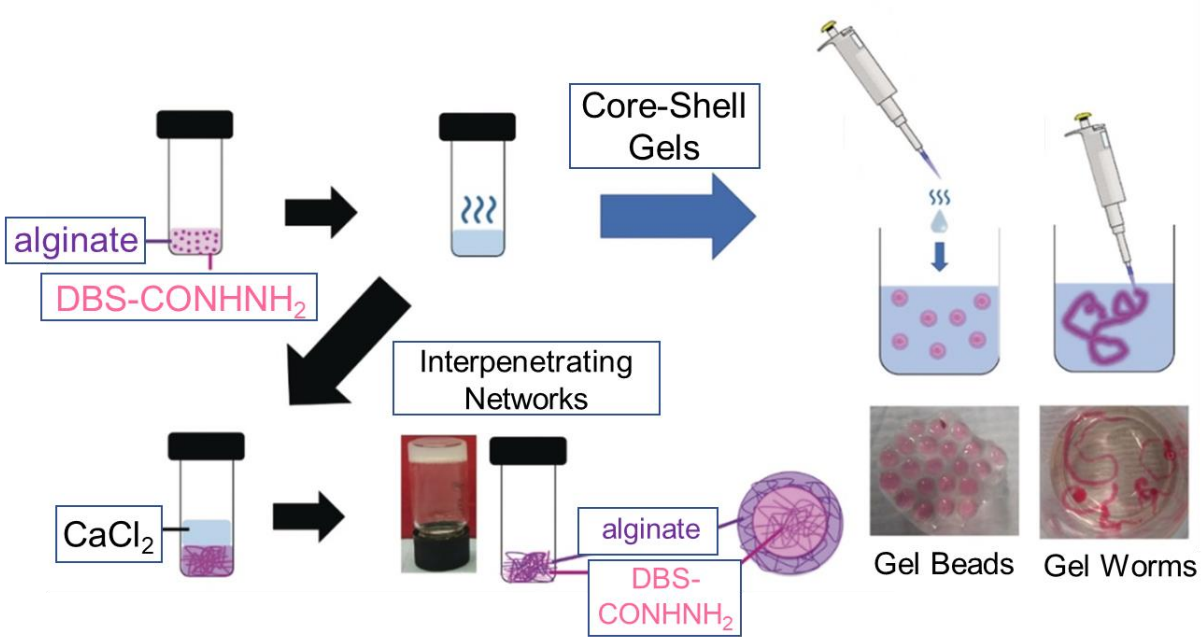

Figure 31. Schematic depicting the formation of hybrid hydrogel beads and worms which can be utilized for Pd cross coupling reactions.[71] Adapted from ref 71, under the creative commons license. Copyright (2019) John Wiley and Sons.

Wang et al. designed and synthesized a series of glycoclusters with three, four and six arms containing peripheral sugar units linked to a central core through triazole groups.[38] Several of the compounds were found to be supramolecular gelators in various solvents. Additionally, these compounds were found to accelerate CuAAC reactions, especially the glycoclusters with six arms. Copper metallogels were more effective at accelerating the reaction rates compared to adding the compound to the reaction mixtures in solid form. Several of these gelators were utilized to create copper metallogel columns which were used for flow type CuAAC reactions, depicted in Figure 32. The gel columns produced acceptable yields and were capable of being reused at least six

times. These supramolecular metallogels should be capable of catalyzing various copper catalyzed reactions with similar results.

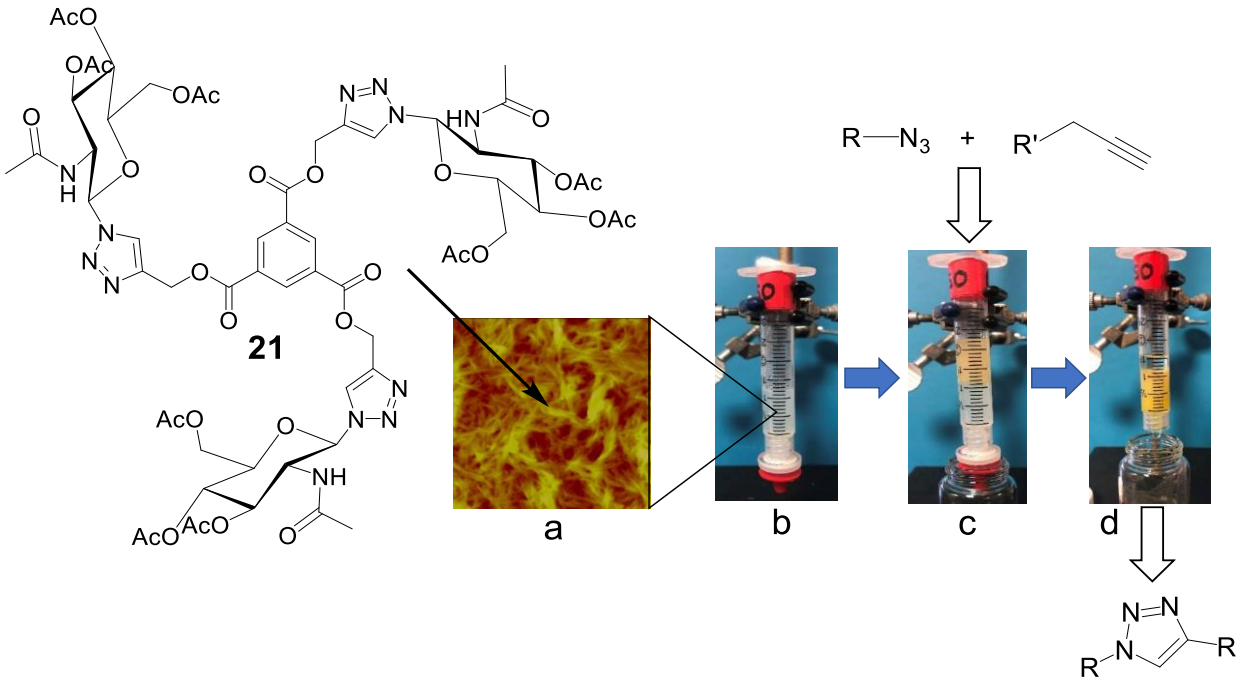

Figure 32. Trimeric glycocluster utilized for supramolecular catalysis of CuAAC reactions. (a) AFM image of the supramolecular gel; (b) Gel column; (c) Gel column loaded with a reaction mixture; (d) Gel column after elution of reaction mixture.[38] Adapted with permission from ref 38. Copyright (2020) American Chemical Society.

Hawkins et al. designed and synthesized a glutamine amide derivative capable of forming organocatalytic hydrogels, shown in Figure 33. These gels were utilized in catalyzing the prebiotically relevant aldol dimerization of glycolaldehyde, producing threose and erythrose.[72] The self-assembled hydrogels were found to be much better at catalyzing these reactions compared to

non-assembled. Reactions run on the gels showed very good diastereoselectivity, a little enantioselectivity, and excellent conversions. This study in an important example of the advantages of using gels as supramolecular catalysts.

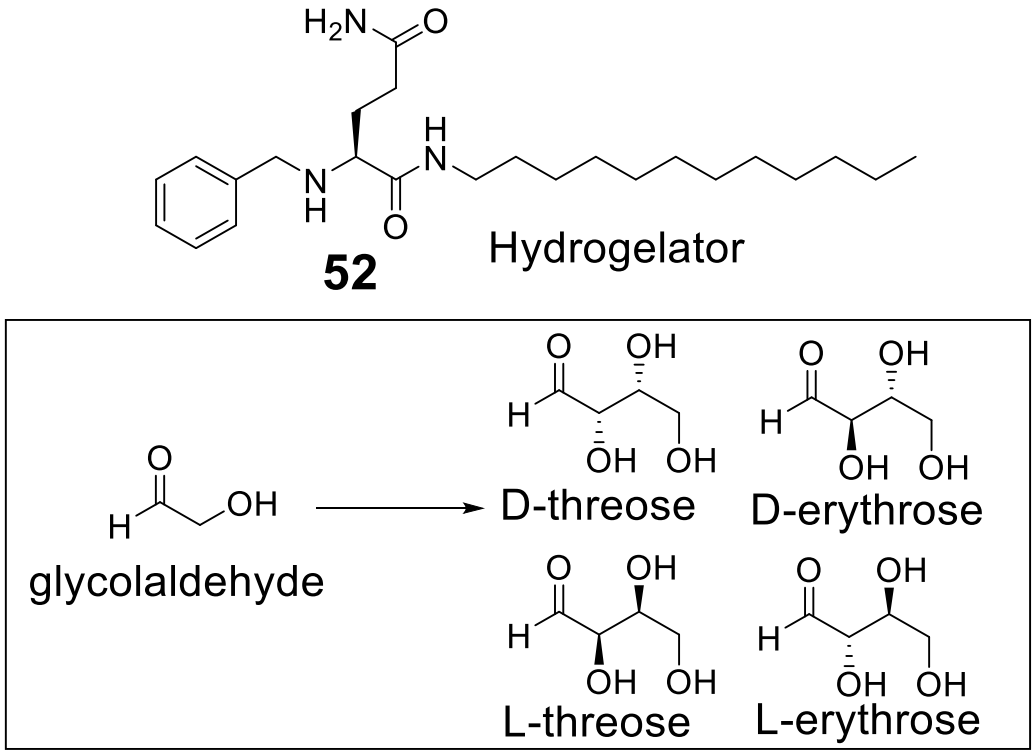

Figure 33. Organocatalytic glutamine gelator and the aldol reaction of glycolaldehyde.[72]

CHAPTER 2

SYNTHESIS AND CHARACTERIZATION OF 4,6-(1-NAPHTHYLIDENE) ACETAL PROTECTED GLUCOSAMINE DERIVATIVES AS LMWGS

2.1. INTRODUCTION

It is well known in supramolecular chemistry that aromatic interactions are important non-covalent interactions that provide a significant stabilizing force during self-assembly.[1,73,74] Peptides containing fmoc groups and naphthyl groups have been shown to have increased gelation capabilities in water and various other organic solvents/solutions.[26,48,73] The 2-naphthyl phenylalanine phenylalanine dipeptide gelator in Figure 34 was found to be an incredibly strong hydrogelator, which was found to retain its gelation capabilities after being derivatized.[26] Single crystal X-ray diffraction shown in Figure 34 shows how the aromatic groups interact to create a hydrophobic pocket that reinforces hydrogen bonding between molecules.[26]

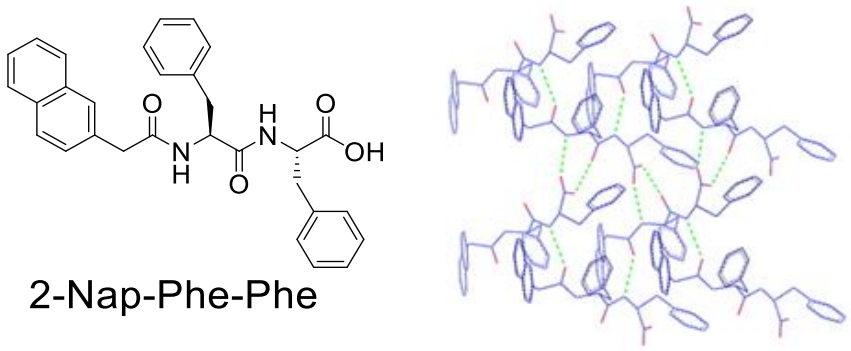

Figure 34. Structure of a 2-naphthyl dipeptide LMWG and its X-ray crystal structure.[26] Adapted with permission from ref 26. Copyright (2011) American Chemical Society

Many similar short chained peptide based LMWGs containing *N*-terminal naphthyl functional groups have been found to be very versatile gelators.[9, 19,27, 75] A diphenylalanine tyrosine tripeptide with a terminal naphthyl group was found to be such a strong hydrogelator that the gelation properties were retained after being functionalized with large molecules such as a fluorescent marker (4-chloro-7-nitrobenzo-2-oxa-1,3-diazole, NBD) and the anti-cancer drug taxol.[48] Zhou et al. utilized aromatic-aromatic interactions in the rational design of a phenyl aniline-lysine-tyrosine tripeptide containing a naphthyl group at the *N*-terminus, which was capable of enzyme instructed molecular self-assembly.[75] Introducing functional groups capable of aromatic interactions has also been a successful technique employed in the rational design of carbohydrate based LMWGs. A glucosamine derivative, which was functionalized with a naphthyl group attached at the second position through a phenylalanine linkage, was found to be very effective hydrogelator and improved wound healing in studies utilizing mouse models.[53] Several very effective LMWGs have been discovered through adding either one or two benzylidene acetal protecting groups to gluconic acid derivatives, xylitol derivatives and sorbitol derivatives.[65,76-79] Various 4,6-benzylidine acetal protected glucosamine and glucose derivatives have also been reported to be efficient LMWGs.[12,15,16,37,39-41,80,81] In an effort to understand the importance of the aromatic 4,6-benzylidene protection on glucosamide derivatives, Williams et al. replaced the 4,6-benzylidene protection with a isopropylidene protection.[82] Several benzylidene protected glucosamide derivatives were previously reported to be effective LMWGs.[16] Exchanging the aromatic group for the short aliphatic isopropylidene group resulted in a significant reduction in gelation properties compared to analogous benzylidene protected derivatives. In an effort to further understand the structure to gelation properties relationship, three series of 1-naphthylidene acetal protected glucosamine derivatives were synthesized, characterized and analyzed. As shown in

Figure 35, the 4,6-benzylidene acetal protection was replaced with a 1-naphthylidene acetal protection. We hypothesized that the increased aromatic interactions would lead to stronger intramolecular interactions and improved gelation properties. To further investigate the structural requirements that promote self-assembly and gelation for this new 1-naphthylidene acetal protected glucosamine scaffold, the second position was functionalized with various aliphatic and aromatic groups through amide, carbamate, or urea linkages.

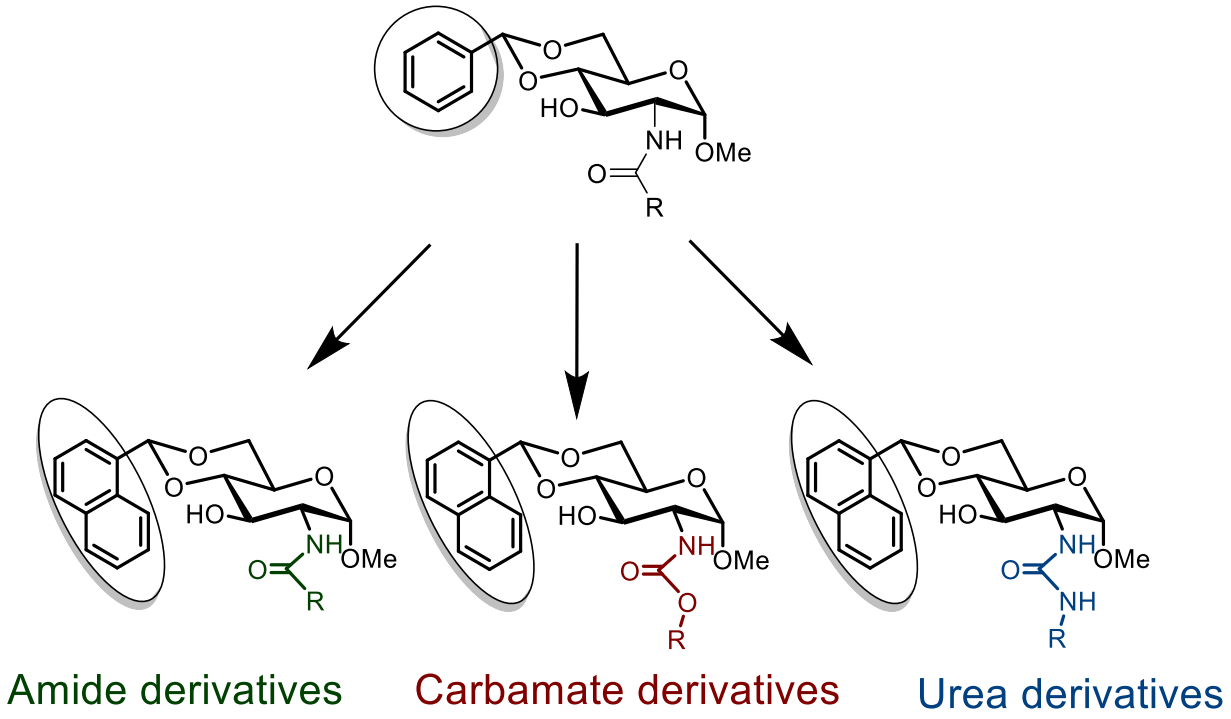

Figure 35. Rational design for the synthesis of 1-naphthylidene acetal protected glucosamine derivatives.

2.2. RESULTS AND DISCUSSIONS

Scheme 1 depicts the synthesis of the 4,6-(1-naphthylidene) acetal protected glucosamine headgroup **IV**. Starting with N-acetyl glucosamine, an *O*-methoxy group was installed in the anomeric position via a glycosylation reaction utilizing amberlite IR120 acidic resin in methanol, producing compound **II**. Compound **II** then underwent a 4,6-acetal protection using 1-naphthaldihyde dimethyl acetal, producing compound **III**. Compound **III** then underwent a deacetylation reaction under microwave conditions, producing the final 4,6-(1-naphthylidene) acetal protected glucosamine headgroup, compound **IV**.

Scheme 1. Synthesis of the 4,6-(1-naphthylidene) acetal protected glucosamine headgroup

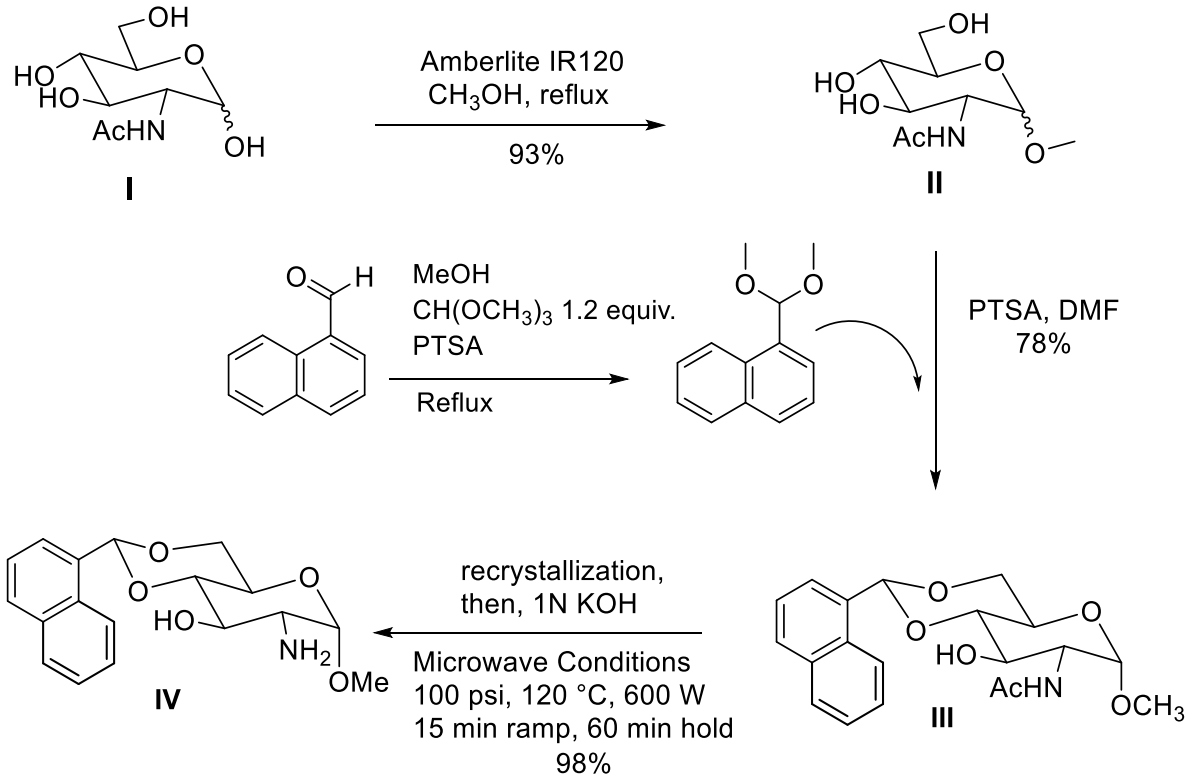

Gelation testing was carried out on compound **III**, with the acetamide group at the second position, to help predict whether the new 1-naphthylidene acetal protected glucosamine scaffold would in fact have good gelation properties when functionalized at the second position. Compound **III** formed gels in various alcohols, aqueous mixtures of ethanol, and aqueous mixtures of DMSO, shown in Table 1. Compound **III** was found to be insoluble in H_2O and toluene, and soluble in triethylene glycol. All gels formed were opaque in appearance.

Table 1. Gelation test results of the 4,6-(1-naphthylidene) acetal protected head group **III**

No.	**Gly**	**EG**	**IPA**	**EtOH**	**H_2O:EtOH (1:1)**	**H_2O:EtOH (2:1)**	**H_2O:DMSO (1:1)**	**H_2O:DMSO (2:1)**
III	20.0	20.0	10.0	10.0	5.0	10.0	20.0	20.0

Numbers are the minimum gelation concentrations (MGCs) in mg/mL.

With promising results from the initial gel test of compound **III**, compound **IV** was used to make a series of amide derivatives. Scheme 2 shows the synthesis of amide derivatives with the general structure **V**. Two methods were utilized in the synthesis of the amide derivatives with the general structure **V**. Derivative **1-6** and **9-10** were synthesized by reacting compound **IV** with respective acid chlorides in a solution of anhydrous DCM with pyridine. Derivatives **7-8** were synthesized using the respective anhydrides in a solution of DCM with triethylamine.

Scheme 2. Synthesis of the 4,6-(1-naphthylidene) acetal protected amide derivatives

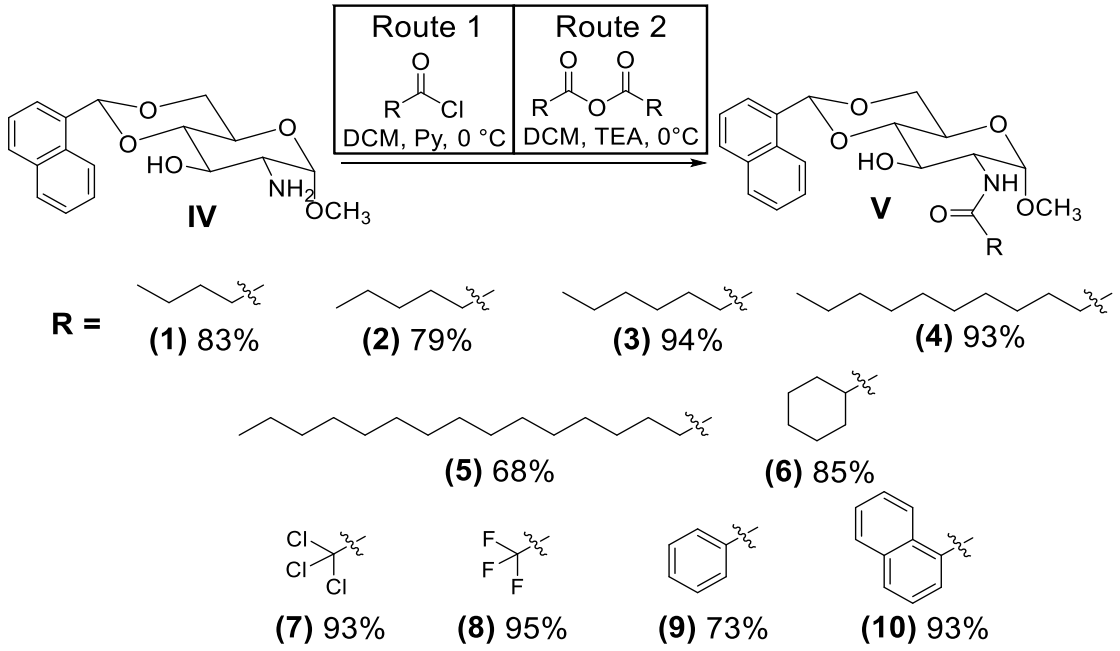

After completing the synthesis of amide derivatives **1**-**10**, gelation testing was carried out in various organic solvents, aqueous mixtures of DMSO and ethanol, and in water. The results of the gel tests can be found in Table 2. Unfortunately, all derivatives were found to be insoluble in water and hexanes from 20 mg/mL to 4 mg/mL. In general, the amide derivatives preformed best in organic solvents and alcohols. The valeryl amide derivative **1** was the most versatile gelator, forming gels in all tested solvents except triethylene glycol and water. Increasing the aliphatic chain further in derivatives **2**-**5**, seemed to reduce the gelation tendency in aqueous solutions of DMSO or ethanol. The gelation properties of these aliphatic derivatives in alcohols, glycols, and toluene remained mostly constant as the chain length increased. The hexadecyl amide derivative **5** saw a reduction in gelation properties compared to the other aliphatic derivatives and was the only one to not form a gel in toluene. The cyclohexyl amide derivative **6** performed fairly similar to the

hexyl amide derivative **2** and heptyl derivative **3**. The trichloro acetamide derivative **7** formed gels in glycerol, ethylene glycol, ethanol and both mixtures of DMSO/H_2O at high concentrations; however, the trifluoro acetamide derivative **8** was either soluble at 20 mg/mL or precipitated in all solvents tested. The benzamide derivative **9** only formed gels in toluene, glycerol and both DMSO/H_2O mixtures; however, the minimum gelation concentration was found to be fairly low in each of these solvents. The 1-naphthyl amide derivative **10** was found to only form gels in toluene. The results from these gel tests show that balancing non-covalent forces to tune gelation properties can lead to versatile LMWGs such as amide derivative **1**.

Table 2. Gelation test results of the 4,6-(1-naphthylidene) acetal protected amide derivatives

No.	**Tol**	**Gly**	**EG**	**TEG**	**IPA**	**EtOH**	**H_2O: EtOH (1:1)**	**H_2O: EtOH (2:1)**	**H_2O: DMSO (1:1)**	**H_2O: DMSO (2:1)**
1	**3.3**	**5.0**	**2.2**	S	6.7	10.0	**1.7**	**0.8**	**1.8**	**1.1**
2	**5.0**	**5.0**	S	S	5.0	5.0	I	I	**5.0**	**5.0**
3	**2.5**	10.0	3.3	S	5.0	5.0	**5.0**	I	**5.0**	I
4	**2.2**	6.7	6.7	**4.0**	20.0	2.2	I	I	I	I
5	P	6.7	6.7	10.0	20.0	4.0	I	I	I	I
6	6.7	10.0	5.0	P	**3.3**	6.7	I	I	6.7	10.0
7	P	6.7	6.7	S	P	20.0	I	I	20.0	20.0
8	S	S	S	S	S	S	P	P	P	P
9	**2.5**	**5.0**	S	S	P	P	I	I	**3.3**	**3.3**
10	10.0	S	P	S	P	P	I	I	I	I

Numbers are the MGCs in mg/mL for those compounds that formed stable gels. P = precipitation; S = soluble; I = insoluble (all at 20 mg/mL). All compounds were found to be insoluble in H_2O.

With the synthesis of the amide derivatives complete, we decided to make a second set of derivatives containing urea linkage, which is well-known hydrogen bonding functional group frequently used in supramolecular self-assembly. With a second NH available for both hydrogen bonding donating and accepting, we hypothesized these derivatives would have enhanced self-assembling properties. Scheme 3 shows the synthesis of urea derivatives with the general structure **VI,** where compound **IV** was reacted with respective isocyanates in THF. Similar to the amide series, several aliphatic and aromatic functional groups were chosen for analyzing structure to gelation properties relationships.

Scheme 3. Synthesis of the 4,6-(1-naphthylidene) acetal protected urea derivatives

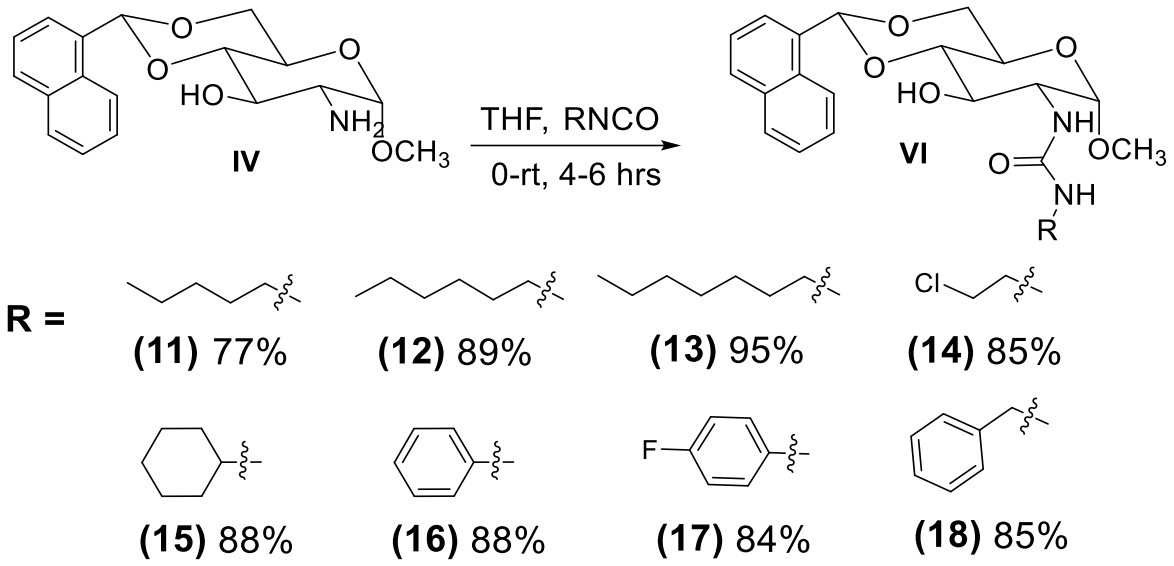

Once the urea derivatives **11-18** were obtained, gelation testing was carried out in various organic solvents, aqueous mixtures of DMSO and ethanol, and in water, as shown in Table 3. In

general, these derivatives were found to be less versatile gelators than the amide derivatives. Like the amide derivatives, all of the urea derivatives were insoluble in water and hexanes. Additionally, the urea derivatives were found to be insoluble in DMSO-water 1:2. With that said, several of the urea derivatives were found to be very effective gelators in specific solvents with fairly low MGCs. All of the urea derivatives, except for the 2-chloroethyl derivative **14**, were found to form a gel at less than 5 mg/mL in at least one of the solvent systems tested. The pentyl urea derivative **11**, for instance, formed gels in glycerol and both ethanol-water mixtures at under 5 mg/mL. The straight aliphatic derivatives performed well in protic organic solvents, but were mainly insoluble in the aqueous mixtures of DMSO and EtOH. The hexyl urea derivative **12** has a MGC of 5 mg/mL in both toluene and ethanol, as well as a very low MGC of 2.9 mg/mL in ethanol-water 1:1. The heptyl urea derivative **13** also performed well in toluene, with a MGC of 2.2 mg/mL. Adding a terminal chloro group the aliphatic chain reduced gelation properties, with the 2-chloroethyl urea derivative **14** only forming gels in isopropyl alcohol and ethanol at MGCs of 10 mg/mL and 6.7 mg/mL respectively. The cyclohexyl urea derivative **15** performed very well in both ethanol-water 1:1 and DMSO-water 1:1, with MGCs of 3.3 mg/mL and 2.5 mg/mL respectively. The phenyl urea derivative **16** only formed gels in ethylene glycol and DMSO-water 1:1 at MGS of 4.0 mg/mL and 3.3 mg/mL respectively. Adding a fluoro group to the para position of the phenyl group, resulting in urea derivative **17**, did not have a dramatic effect on the gelation properties of the molecule. Derivative **17** formed gels in both glycerol and ethanol at 5 mg/mL, as well as isopropanol at 10 mg/mL. The benzyl urea derivative **18** formed gels in both ethylene glycol and ethanol at MGCs of 5.0 mg/mL and ethylene glycol at 3.3 mg/mL. The results of the gelation testing suggest that hydrogen bonding caused by the urea functional group, whether intramolecular or intermolecular,

may be interfering with the ability of these derivatives to be solubilized in several desired solvent systems.

Table 3. Gelation test results of the 4,6-(1-naphthylidene) acetal protected urea derivatives

No.	Tol	Gly	EG	TEG	IPA	EtOH	H_2O:EtOH (1:1)	H_2O:EtOH (1:2)	H_2O:DMSO (1:1)
11	I	**5.0**	10.0	10.0	S	I	**5.0**	**4.0**	I
12	**5.0**	10.0	**3.3**	S	10.0	**5.0**	**2.9**	I	I
13	**2.2**	10.0	**5.0**	S	10.0	10.0	P	I	I
14	P	I	S	S	10.0	6.7	P	I	S
15	P	I	10.0	S	P	10.0	**3.3**	I	**2.5**
16	P	S	**4.0**	S	P	P	P	I	**3.3**
17	I	**5.0**	P	S	10.0	**5.0**	I	I	I
18	I	S	**5.0**	S	**3.3**	**5.0**	I	I	I

Numbers are the minimum gelation concentration in mg/mL. P = precipitation; S = soluble; I = insoluble (all at 20 mg/mL). All compounds were found to be insoluble in H_2O, hexanes, and DMSO:H_2O 1:2.

To further study the structure to gelation properties relationship in the 1-naphthylidine protected glucosamine series; a series of derivatives utilizing a carbamate linkage was designed and synthesized. Carbamate groups are another popular hydrogen bonding group frequently utilized in supramolecular self-assembly. The synthesis of the carbamate linked derivatives with the general structure **VII**, is depicted in Scheme 4. Compound **IV** was reacted with the respective chloroformates in anhydrous DCM with triethylamine. Similar to the amide and urea series, several

aliphatic and aromatic functional groups were chosen for analyzing the structure to gelation properties relationships.

Scheme 4. Synthesis of the 4,6-(1-naphthylidene) acetal protected carbamate derivatives

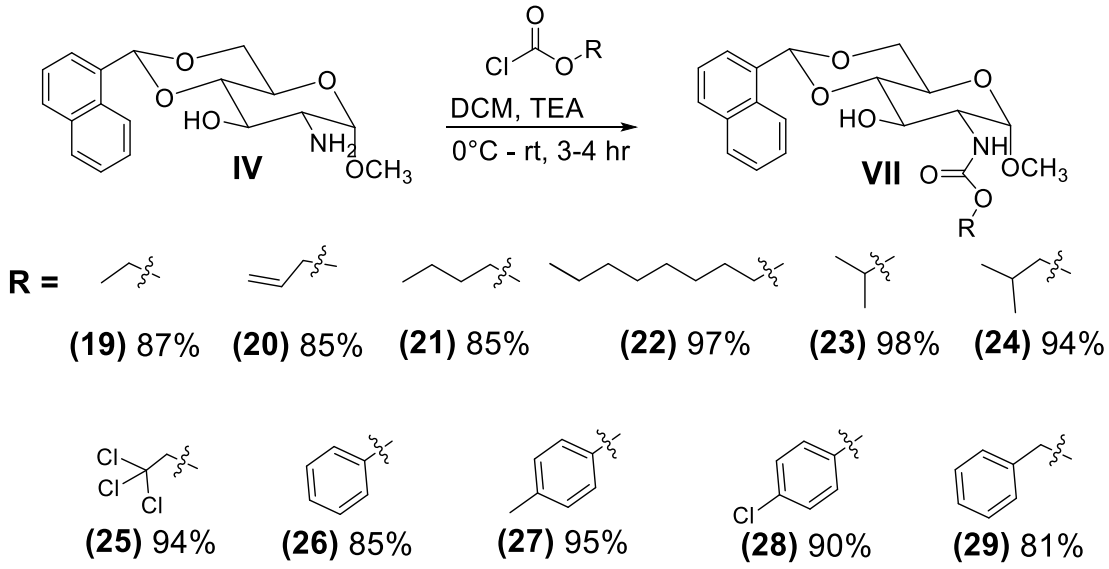

Like the other series, once pure compounds were obtained, gelation testing was carried out in various organic solvents, aqueous mixtures of DMSO and ethanol, and in water. Unfortunately, like the amide and urea series, all of the compounds were found to be insoluble in water. All compounds were also found to be insoluble in hexanes and soluble in triethylene glycol. The carbamate series performed similarly to the amide series in the tested solvents, with several of the derivatives being found to be fairly versatile gelators. As shown in Table 4, the ethyl carbamate derivative **19** was found to be very versatile, forming gels in a total of 7 solvents at higher concentrations. The allyl carbamate derivative **20** was also very versatile forming gels in 8 of the

solvents tested. Compound **20** was also found to have fairly low MGCs of 3.3 mg/mL in ethanol and 4.0 mg/mL in both ethanol-water solutions. The butyl carbamate derivative **21** formed gels in six of the tested solvents at higher concentrations, except for glycerol, which had a MGC of 5.0 mg/mL. The octyl carbamate derivative **22** was also a very versatile gelator, forming gels in 7 of the solvents tested. Compound **22** was found to have fairly low MGCs of 5.0 mg/mL and 2.9 mg/mL in ethanol-water 1:1 and DMSO-water 1:1 respectively. Additionally, compound **22** was found to be a supergelator for ethylene glycol, with a MGC of 1 mg/mL or 0.1 wt%. The isopropyl carbamate derivative **23** formed gels in seven of the tested solvents, with very similar results to compound **19**. The additional steric hindrance of the isopropyl group seemed to enhance the gelation properties of compound **23** compared to compound **19**. While the formed gels in the exact same solvents, compound **23** had lower MGCs in ethylene glycol, ethanol, ethanol-water 1:1, and DMSO-water 1:1. Increasing the steric hindrance further with an isobutyl group significantly reduced gelation versatility. The isobutyl carbamate derivative **24** only formed gels in four of the tested solvents; however, it was found to have fairly low MGCs of 5.0 mg/mL in both DMSO-water solutions. Adding chloro substituents to the end of the aliphatic chain was found to have a similar effect in the carbamate series. Like the chloroethyl urea derivative **14**, the trichloroethyl carbamate derivative **25** was also found to have reduced gelation properties, only forming gels in two of the tested solvents. The aromatic carbamate derivatives **26-29** saw a reduction in gelation properties compared with the aliphatic carbamate derivatives. Out of the aromatic derivatives, the 4-methylphenyl carbamate derivative **27** was the most versatile, forming gels in 5 solvents at fairly high concentrations. The phenyl carbamate derivative **26** and 4-chlorophenyl carbamate derivative **28** formed gels in four and three solvents respectively. The benzyl carbamate derivative **29** also only formed gels in four of the tested solvent; however, it did form a fairly strong gel in DMSO-

water 1:1 at 4.0 mg/mL. Fewer of the gels, on the other hand, were found to have MGCs under 5 mg/mL compared to the amide and urea series.

Table 4. Gelation test results of the 4,6-(1-naphthylidene) acetal protected carbamate derivatives

No.	Tol	Gly	EG	IPA	EtOH	H_2O:EtOH (1:1)	H_2O:EtOH (2:1)	H_2O:DMSO (1:1)	H_2O:DMSO (2:1)
19	10.0	10.0	10.0	6.7	6.7	6.7	P	20.0	P
20	6.7	S	10.0	6.7	**3.3**	**4.0**	**4.0**	10.0	10.0
21	P	**5.0**	6.7	P	10	10.0	I	10.0	10.0
22	10.0	6.7	**1.0**	20.0	6.7	**5.0**	P	**2.9**	P
23	10.0	20.0	**5.0**	10.0	**5.0**	10.0	P	6.7	P
24	20.0	S	6.7	P	P	P	P	**5.0**	**5.0**
25	S	10.0	10.0	P	P	P	P	P	P
26	P	P	20.0	6.7	P	P	10.0	P	10.0
27	10.0	20.0	P	10.0	10.0	10.0	P	I	I
28	P	P	S	10.0	P	6.7	P	P	10.0
29	P	S	6.7	10.0	10.0	I	I	**4.0**	I

Numbers are the minimum gelation concentration in mg/mL. P = precipitation; S = soluble; I = insoluble (all at 20 mg/mL). All compounds were found to be insoluble in H_2O and hexanes. All compounds were found to be soluble in triethylene glycol.

Several images of gels in vials at the MGCs are shown in Figure 36. Various gels from each of these series were characterized via optical microscopy to analyze the morphology of the gel supramolecular architecture. Figure 37a-f shows several optical micrographic images of the

self-assembled networks that form the supramolecular gels. Various morphologies have been observed from these gelators. The image in Figure 37a was taken from a gel formed by compound **1** in ethanol-water 1:2 at 0.8 mg/mL. The gel is comprised of short straight hair like fibers that bunch together in a bowtie type morphology. Figure 37b also shows a gel formed by compound **1**, except in DMSO-water 1:1 at 1.1 mg/mL. This gel is comprised of long winding fibers which entangle to create the supramolecular architecture. Figure 37c shows the feather like morphology of a gel formed by compound **15** in DMSO-water 1:1. This image shows small uniform straight fibers that assemble into a feather like structures, which overlap to form the gel matrix. Figure 37d shows a network of very uniform long winding fibers that make up the network of a gel formed by compound **18** in isopropanol at 3.3 mg/mL. The image in Figure 37e is of a gel formed by compound **24** in DMSO/H_2O 1:2 at 5.0 mg/mL, which was captured before the gel was completely dry and shows solvent still entrapped in between long straight fibers. These fibers lay over each other to form high density intersections where multiple fibers cross. Figure 37f shows an image of a gel formed from compound **29** in DMSO/H_2O 1:1 at 4.0 mg/mL. This image shows incredibly small hair like fibers that pile together to make form the gel's microstructure. Imaging of these gels shows a diverse range of morphologies that form supramolecular gels.

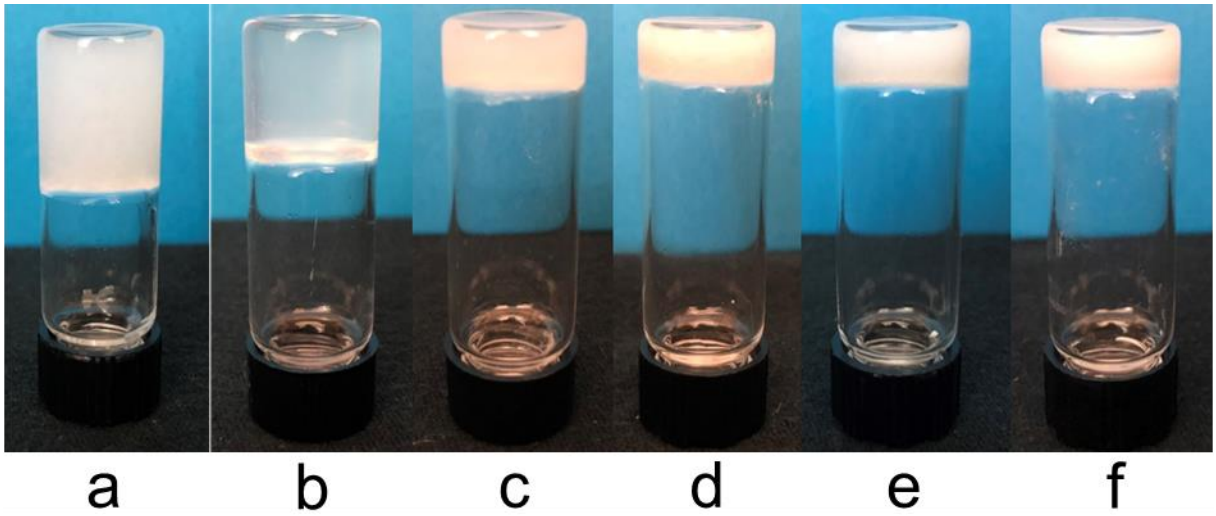

Figure 36. Gel photos for compounds **1**, **15**, **18**, **24**, and **29**. (a) Compound **1** in EtOH/H_2O (v/v 1:2) at 0.8 mg/mL; (b) Compound **1** in DMSO/H_2O (v/v 1:1) at 1.1 mg/mL; (c) Compound **15** in DMSO/H_2O (v/v 1:1) at 2.5 mg/mL; (d) Compound 18 in isopropyl alcohol at 3.3 mg/mL; (e) Compound 24 in DMSO/H_2O (v/v 1:2) at 5.0 mg/mL; (f) Compound **29** in DMSO/H_2O (v/v 1:1) at 4.0 mg/mL.

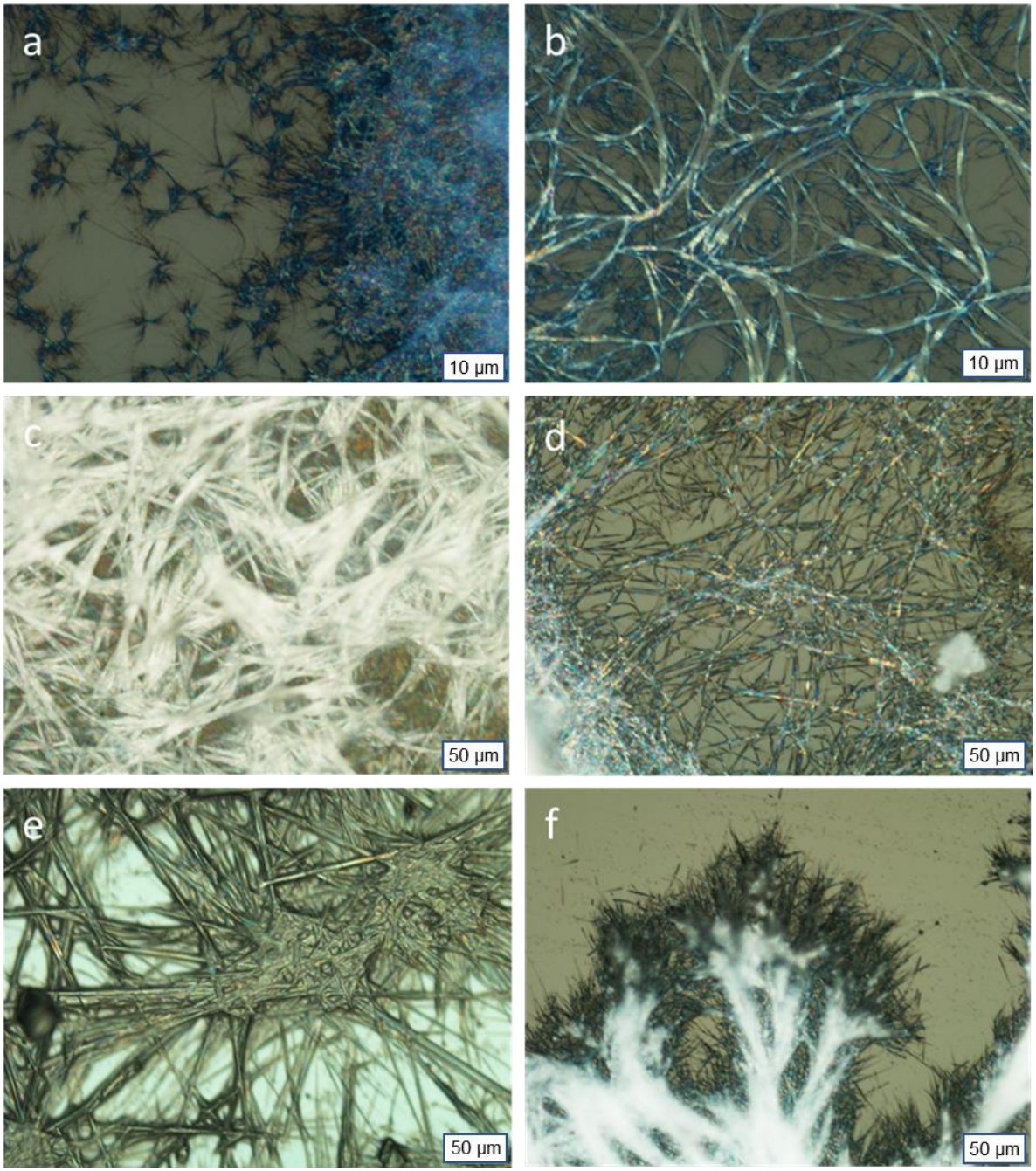

Figure 37. OM imaging of gels formed from compound **1**, **15**, **18**, **24**, and **29**. (a) compound **1** in EtOH/H_2O (v/v 1:2) at 0.8 mg/mL; (b) compound **1** in DMSO/H_2O (v/v 1:1) at 1.1 mg/mL; (c) compound **15** in DMSO/H_2O (v/v 1:1) at 2.5 mg/mL; (d) compound **18** in isopropyl alcohol at 3.3 mg/mL; (e) compound **24** in DMSO/H_2O (v/v 1:2) at 5.0 mg/mL; (f) compound **29** in DMSO/H_2O (v/v 1:1) at 4.0 mg/mL.

SEM was utilized to obtain high resolution images of the fibrous networks created by several gelators. Images of various types of entangled fibrous networks are shown in Figure 38a-f. Figure 38a shows an image of long flat fibers of various widths that intertwine to form the gel matrix of a gel formed by compound **1** in EtOH/H_2O 1:2. The DMSO/H_2O 1:2 gel formed by compound **1** was also observed to be composed of long flat intertwined fibers; however, the fibers are smaller and much more uniform in size, seen in Figure 38b. Both DMSO/H_2O 1:1 gels formed by compounds **9** and **15** were also observed to be composed of long flat entangled ribbon like fibers of various sizes, shown in Figure 38c and Figure 38d respectively. Figure 38e shows that the DMSO/H_2O 1:1 gel formed by compound **16** is composed of short flat uniform feather like fibers. The DMSO/H_2O 1:1 gel formed by compound **29** is composed of very small round fibers that wrap around each other to form larger rope like fibers that entangle to form the gel matrix, seen in Figure 38f.

The viscoelastic properties of several gels were analyzed via rheometric analysis. Figure 39 show frequency sweep overlays of several gels formed at their minimum gelation concentrations. For each gel, the storage modulus (G′) remained higher than the loss modulus (G″) over the entire range of angular frequencies ω analyzed, indicating the gels are both stable and possess viscoelastic properties.

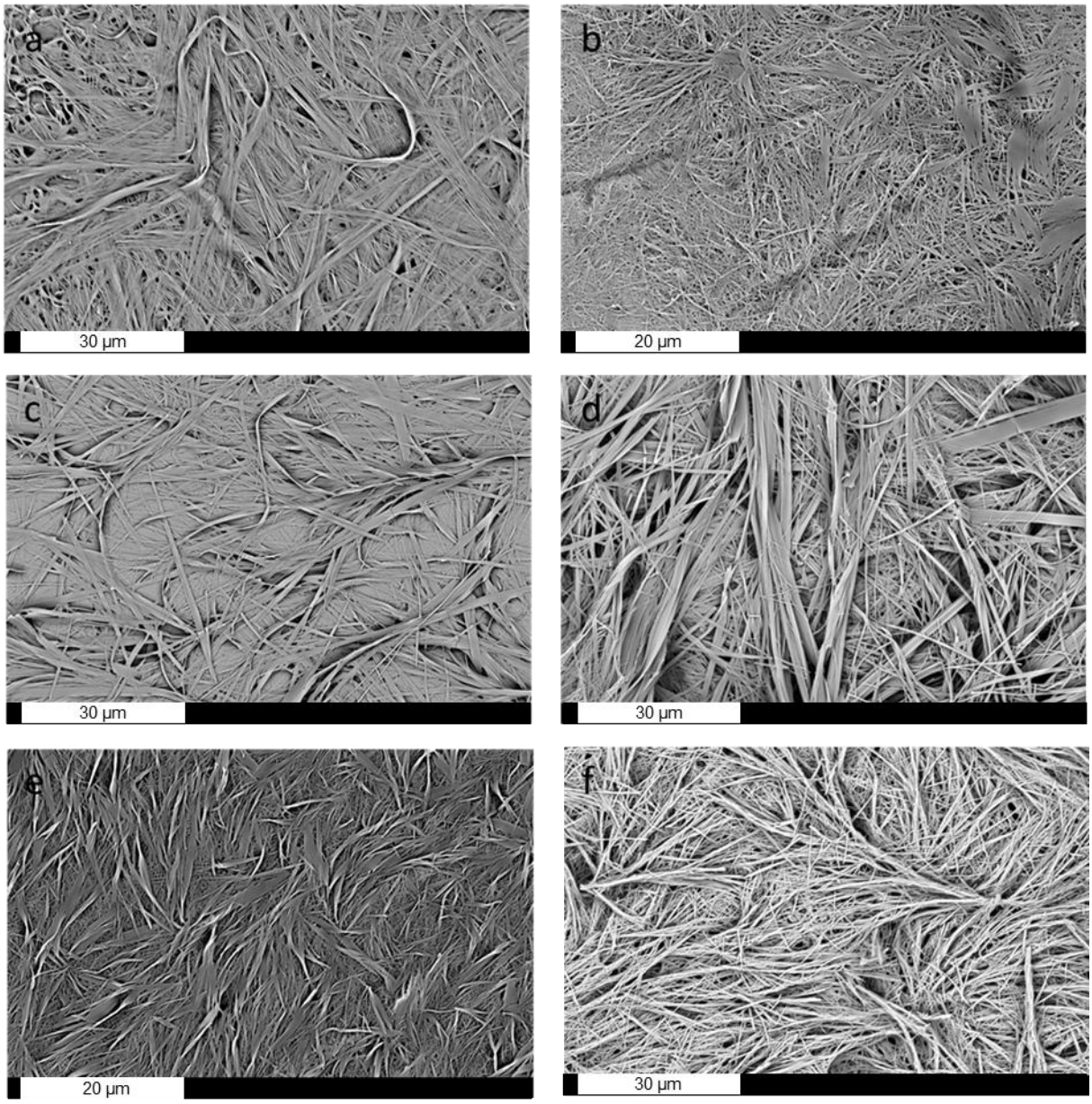

Figure 38. SEM imaging of a gels formed from compound **1**, **9, 15**, **16**, and **29**. (a) compound **1** in EtOH/H_2O (v/v 1:2) at 0.8 mg/mL; (b) compound **1** in DMSO/H_2O (v/v 1:1) at 1.1 mg/mL; (c) compound **9** in DMSO/H_2O (v/v 1:1) at 3.3 mg/mL; (d) compound **15** in DMSO/H_2O (v/v 1:1) at 2.5 mg/mL; (e) compound **16** in DMSO/H_2O (v/v 1:1) at 2.3 mg/mL; (f) compound **29** in DMSO/H_2O (v/v 1:1) at 4.0 mg/mL.

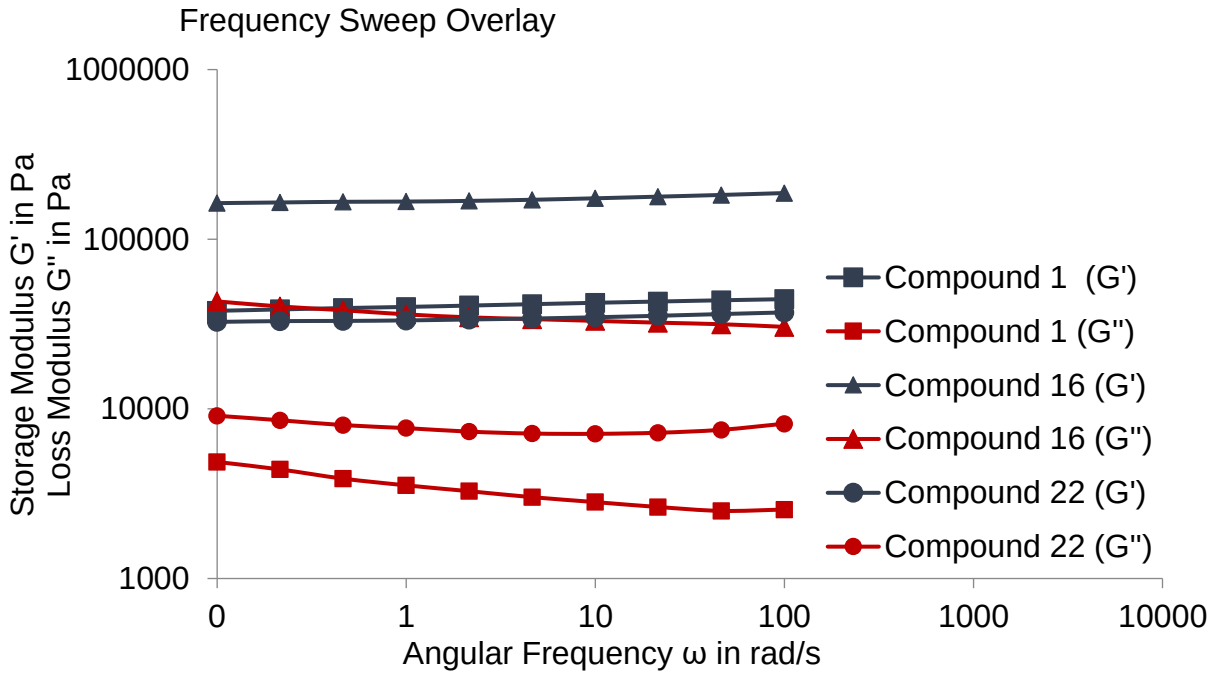

Figure 39. Overlaid rheology spectra of gels formed by compounds **1**, **16**, **22**. Compound **1** in DMSO-water 1:2 at 1.1 mg/mL, compound **16** in DMSO-water 1:1 at 3.3 mg/mL, and compound **22** ethylene glycol at 1.0 mg/mL. The applied strain for all samples was 0.5%.

To investigate why the gelation properties varied between the three series of 1-naphthylidene derivatives, three analogous compounds were chosen for further analysis via ^{1}H NMR. The compound selected for these studies were the valeryl amide derivative **1**, the pentyl urea derivative **11**, and the butyl carbamate derivative **21**. The first study carried out was variable temperature ^{1}H NMR. Elevated temperatures reduce the concentration of intermolecular hydrogen bonding, and therefore, changes in chemical shift caused by increasing temperature indicate that an exchangeable proton is partaking in intermolecular hydrogen bonding. A larger change in chemical shift would indicate frequent hydrogen bonding events, while a very small change in

chemical shift would indicate very few hydrogen bonding events. The samples for this study were prepared in d_6-DMSO at 10 mg/mL and ^{1}H NMR spectra were obtained from 30-60 °C in 5 °C intervals. Figure 40 shows the overlaid ^{1}H NMR spectra obtained from the study using compound **1**, which was both a very versatile gelator and produced gels with fairly low MGCs, especially in DMSO-water solutions. The amide proton showed a significant change in chemical shift over the range of temperatures. The NH signal initially showed up at 7.78 ppm at 30 °C and shifted upfield to 7.58 ppm at 60 °C, which is an overall change of 0.20 ppm, indicating that in solution this molecule is taking part in intermolecular hydrogen bonding. This is not a shock since amides, ureas, and carbamates are known as hydrogen bonding functional groups, which is the overall reason for employing them in the synthesis of these series. The variable temperature study of the pentyl urea derivative **11**; however, presented some unexpected results. Since the urea functional group contains two NH groups, it was predicted to readily hydrogen bond with other molecules. The overlaid ^{1}H NMR spectra shown in Figure 41 show that neither the inner or outer NH peak shifted significantly at elevated temperatures. The inner NH peak started at 5.75 ppm at 30 °C and shifted upfield to 5.68 ppm at 60 °C, which is only a change of 0.07 ppm. The outer NH had an even smaller change in chemical shift, starting at 6.05 ppm at 30 °C and shifting to 6.02 ppm at 60 °C. This evidence suggests that this urea derivative may be in a conformation that is preventing hydrogen bonding. Similar to the amide derivatives results, the variable temperature studies carried out on carbamate derivative **21**, shown in Figure 42**,** showed a significant up field shift of the NH proton signal from 7.03 ppm at 30 °C to 6.75 ppm at 60 °C.

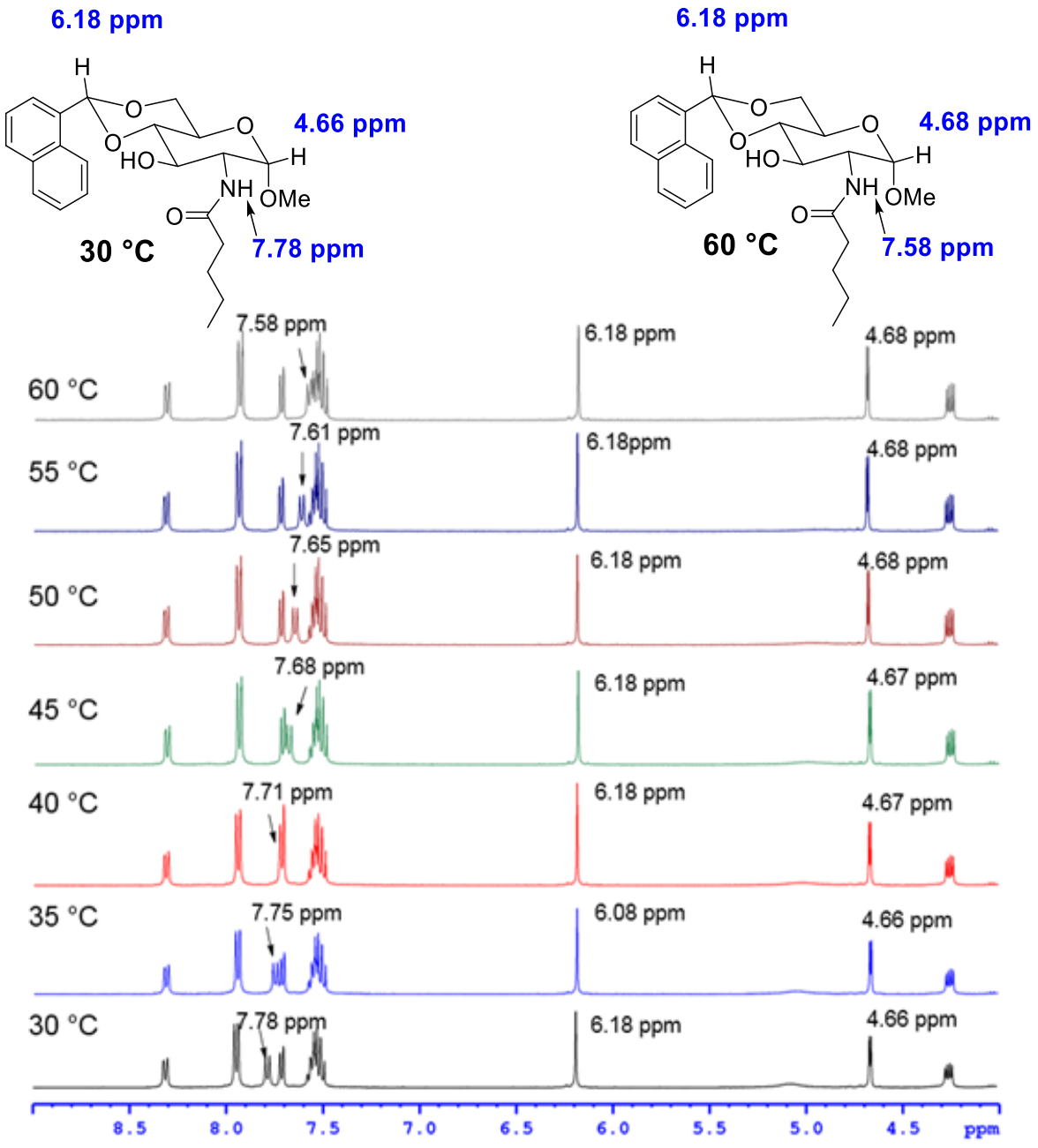

Figure 40. ^{1}H NMR spectra of compound **1** from 30 °C to 60 °C in d_6-DMSO (10 mg/mL).

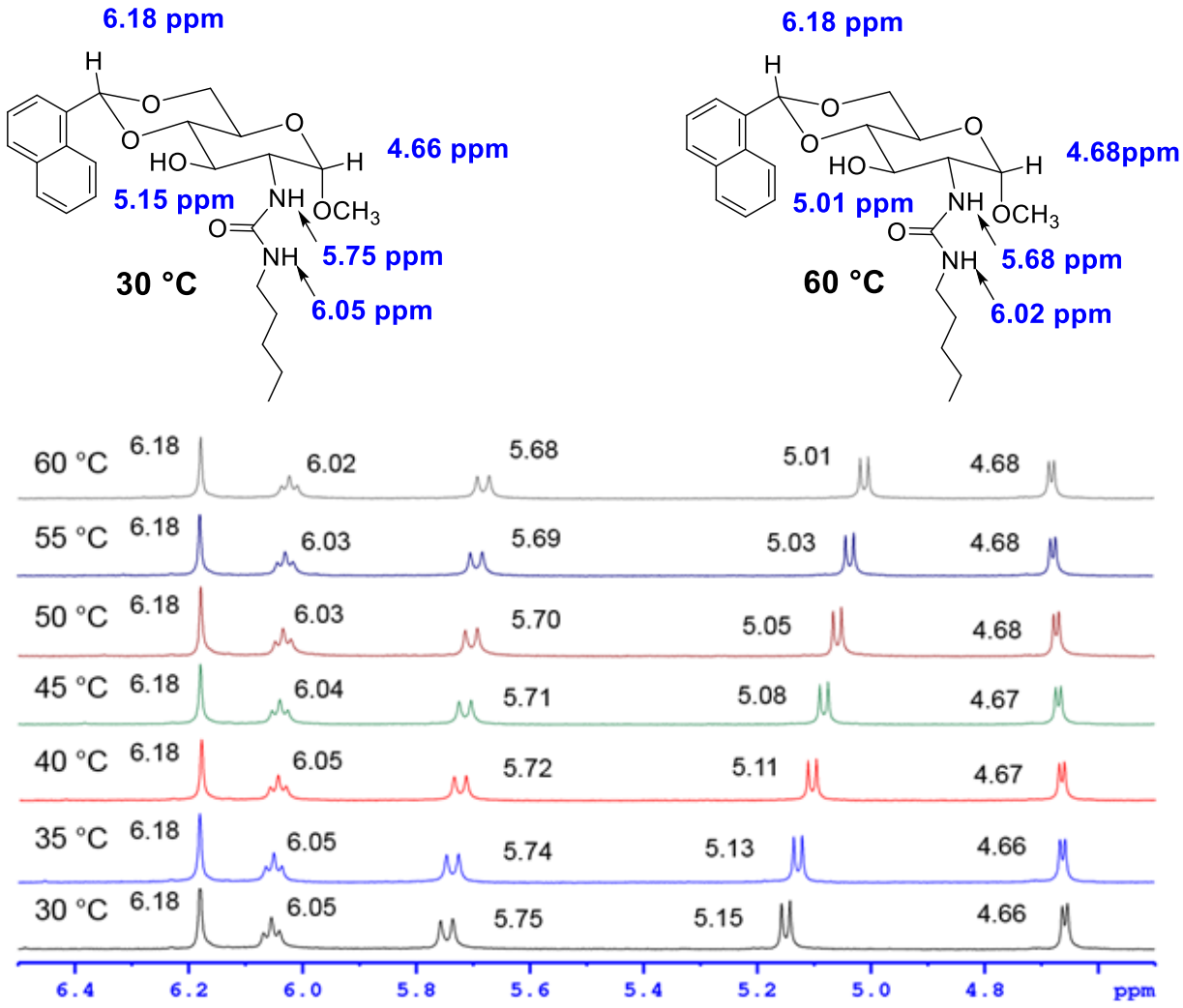

Figure 41. ^{1}H NMR spectra of compound **11** from 30 °C to 60 °C in d_6-DMSO (10 mg/mL).

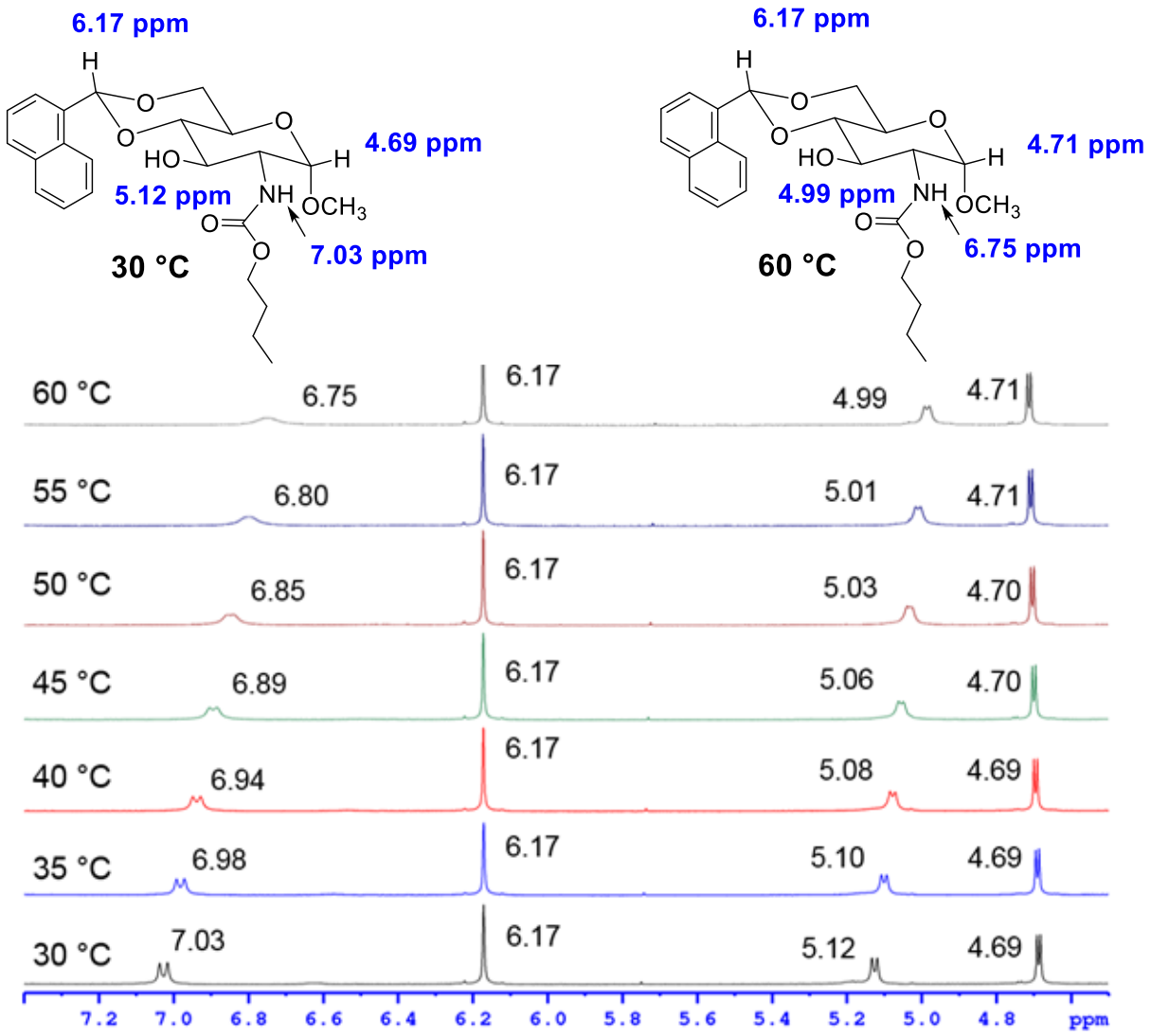

Figure 42. ^{1}H NMR spectra of compound **21** from 30 °C to 60 °C in d_6-DMSO (10 mg/mL).

To further investigate the hydrogen bonding abilities of the amide, urea, and carbamate functional groups in this series of 1-naphthylidene protected glucosamine derivatives, deuterium exchange studies were carried out. NMR samples were prepared by weighing out 1.6 mg of each compound and dissolving it in 0.4 mL of d_6-DMSO, giving an overall concentration of 4.0 mg/mL. An initial ^{1}H NMR was acquired as the starting point, or t = 0 min, for the experiment. 100 µL of

D_2O was then added to the NMR tube and ^1H NMR was acquired at various time points. During these experiments, deuterium is exchanging with any exchangeable protons on the molecule, reducing the ^1H NMR signal over time. Similar to large changes in chemical shift observed in the variable temperature studies, a fast exchange rate indicates frequent hydrogen bonding. In order to appropriately analyze the results of the deuterium exchange study, the integrated rate law for first order reactions, derived in Figure 43, must be applied. The integrated rate law allows us to confirm the deuterium exchange is first order and allows us to determine the rate constant and the half-life of the exchange from plotted data. The integrated rate law is arranged in the form of an equation of a line and in exponential form in Figure 43. The half-life of the exchange is also shown in Figure 43.

For a first order exchange, $[A]^n$, n = 1, so

$$Rate = k[A] \rightarrow k[A] = -\frac{d[A]}{dt} \rightarrow \frac{d[A]}{[A]} = -kdt \rightarrow \int_{[A]_0}^{[A]} \frac{d[A]}{[A]} = -k\int_{t_0}^{t} dt$$

$$ln[A] - ln[A]_0 = -k(t - t_0)$$

The two final equations used to analyze this study

$$Equation\ in\ the\ form\ of\ a\ line\ (y = mx + b): ln[A] = -kt + ln[A]_0$$

$$Equation\ exponential\ form: [A] = [A]_0 e^{-kt}$$

$$Equation\ for\ the\ half\ life: t_{\frac{1}{2}} = \frac{ln2}{k} = \frac{0.693}{k}$$

Figure 43. Differential rate law for first order exchange and integrated rate law for a first order exchange.

Figure 44 shows overlaid ^{1}H NMR spectra obtained from the deuterium exchange study carried out using compound **1**. The amide peak, located at 7.78 ppm, starts off integrated to 1.00 and after the 100 µL of D_2O was added, the peak begins to dissipate. The plot of the integration versus time and the natural logarithm of the NH peak integration versus time can be found in Figure 45a-b. Using a trend line, the rate constant was found to be 0.0238 min^{-1}. The half-life of the exchange was calculated to be 29.1 minutes, indicating the amide group is capable of strong hydrogen bonding.

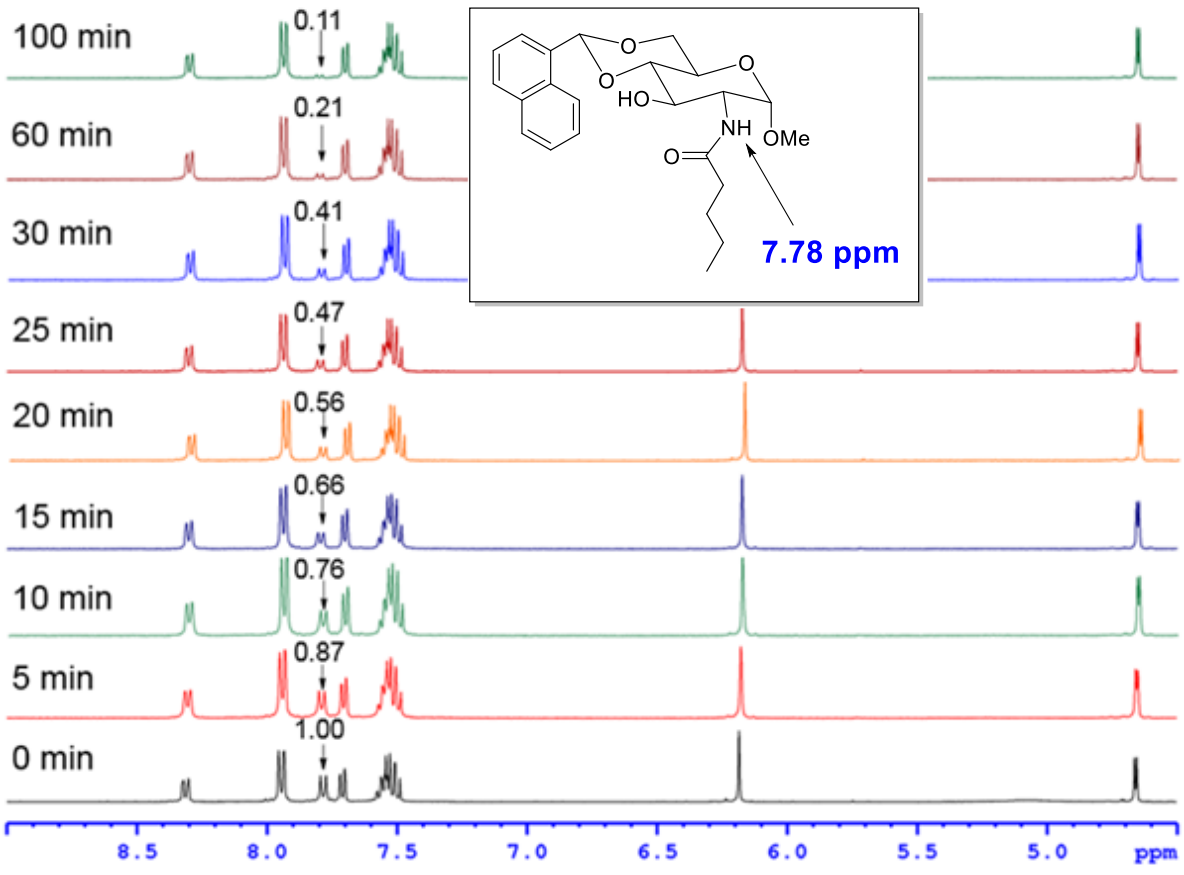

Figure 44. ^{1}H NMR spectra of compound **1** during the deuterium exchange study. The NMR spectra were all acquired at 30 °C.

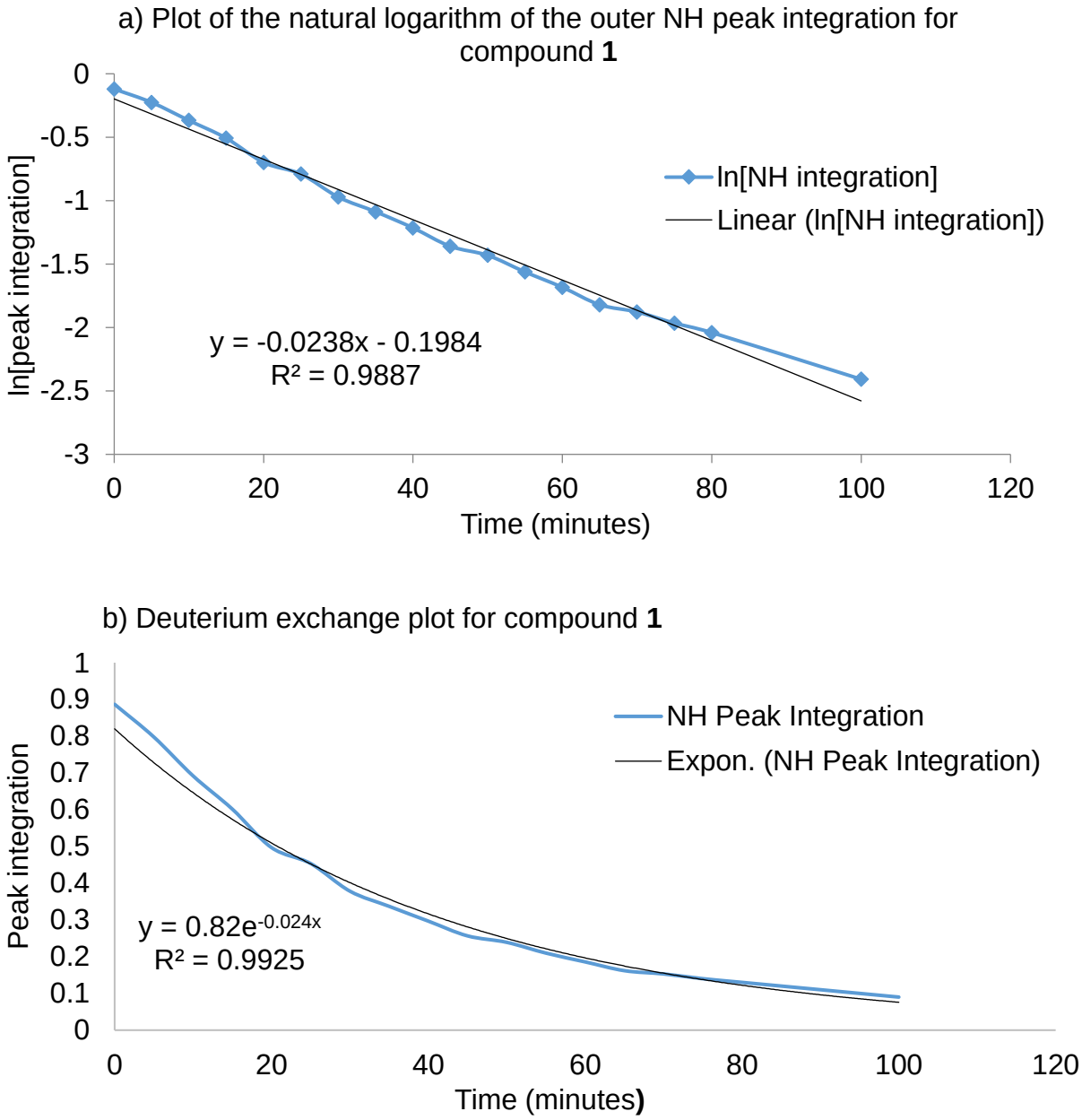

Figure 45. Plots of the deuterium exchange of the N-H peak of compound **1**. (a) Plot of the natural logarithm of the exchange versus time; (b) Plot of deuterium exchange versus time.

Figures 46 and 48 show overlaid ^{1}H NMR spectra obtained from the deuterium exchange study carried out using compound **11**. The urea functional group contains two exchangeable NH

peaks which were found to exchange at very different rates. Figure 46 shows the disappearance of the outer NH peak, which shows up as a triplet at 6.05 ppm. The plot of the integration versus time and the natural logarithm of the outer NH peak versus time integration can be found in Figure 47. Using a trend line, the rate constant was found to be 0.0119 min^{-1}. The half-life of the exchange was calculated to be 58.2 minutes, which is almost twice as long as the amides NH exchange half-life.

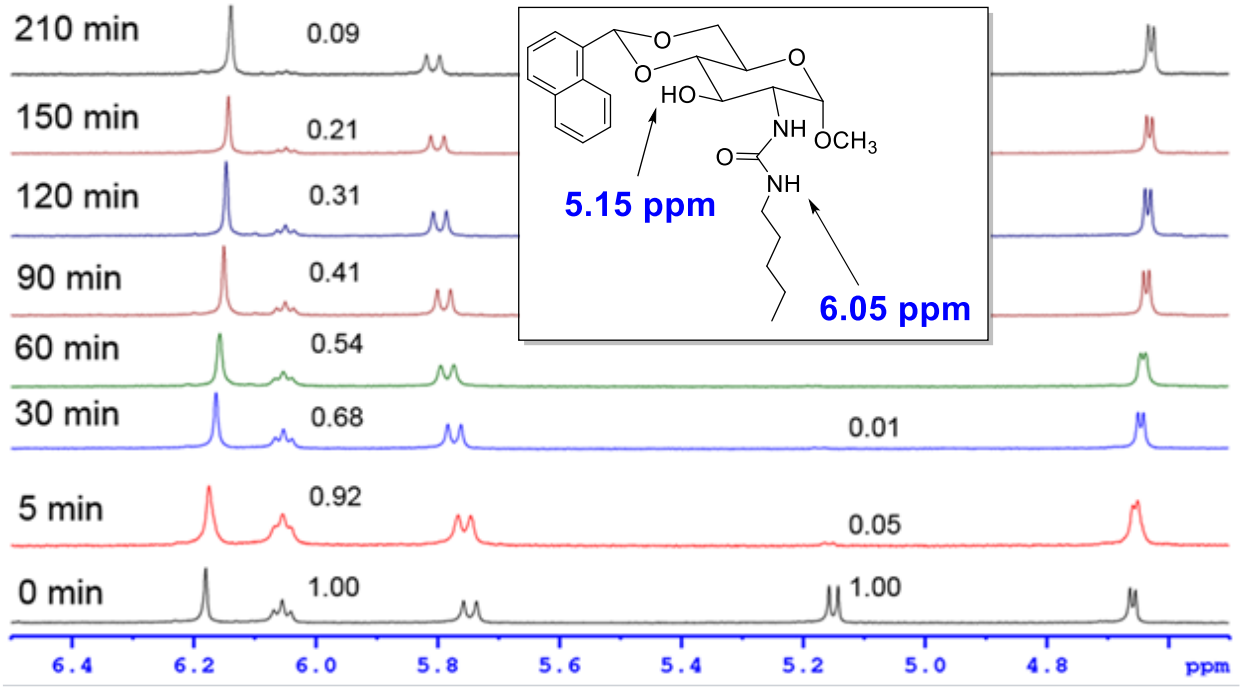

Figure 46. ^{1}H NMR spectra of compound **11** (outer NH) during the deuterium exchange study. The NMR spectra were all acquired at 30 °C.

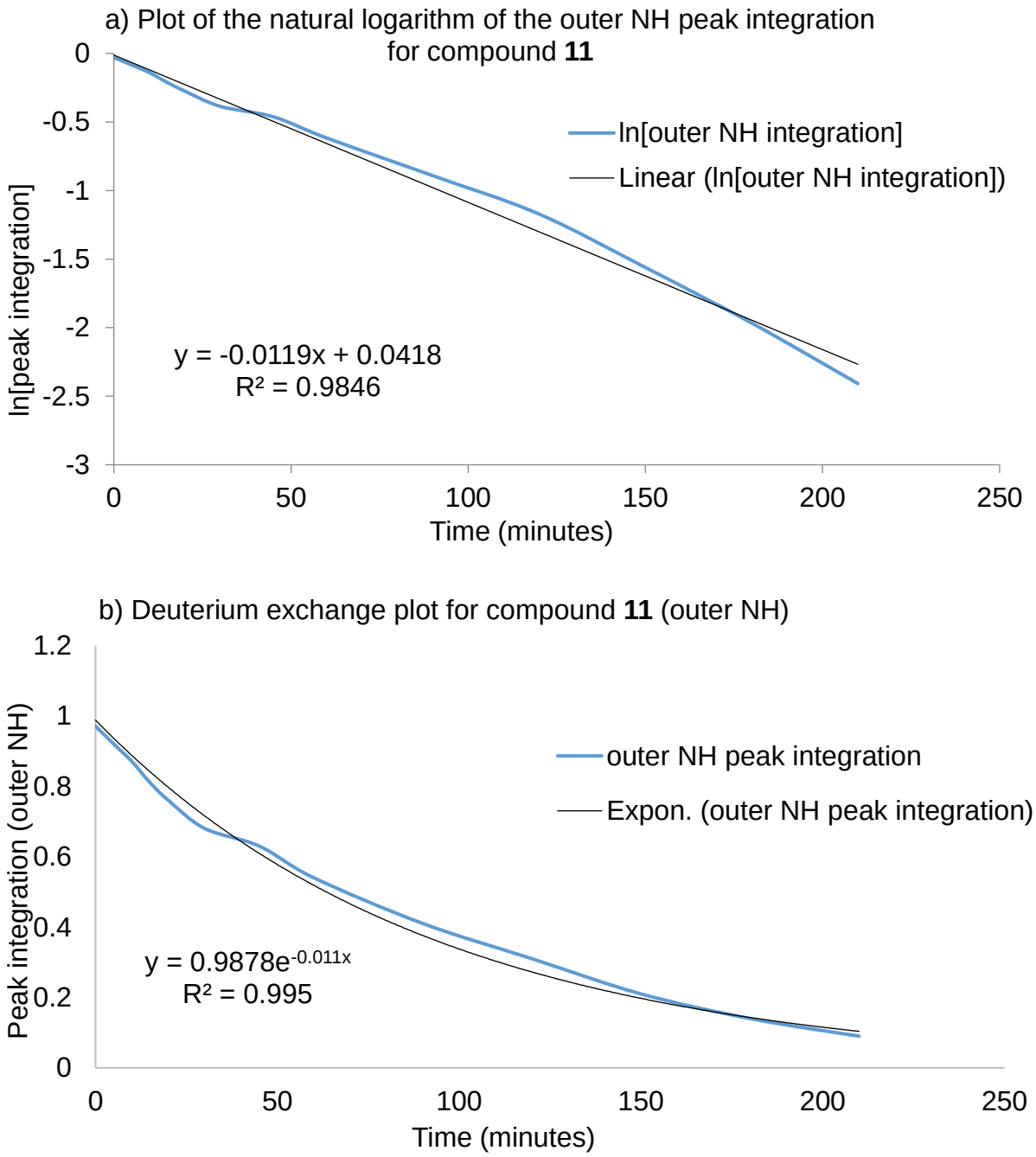

Figure 47. Plots of the deuterium exchange of the outer N-H peak of compound **11**. (a) Plot of the natural logarithm of the exchange versus time; (b) Plot of deuterium exchange versus time**.**

Figure 48 shows the disappearance of the inner NH peak of compound **11** during the deuterium exchange study, which shows up as a doublet at 5.75 ppm. The plot of the integration versus time and the natural logarithm of the inner NH peak integration versus time can be found in Figure 49. Using a trend line, the rate constant was found to be 0.0042 min^{-1}. The half-life of the exchange was calculated to be 165.0 minutes, which is several times longer as the amides NH exchange half-life and over twice as long as the half-life for the urea's outer NH. These were unexpected results as urea functional groups are known for strong hydrogen bonding activity.

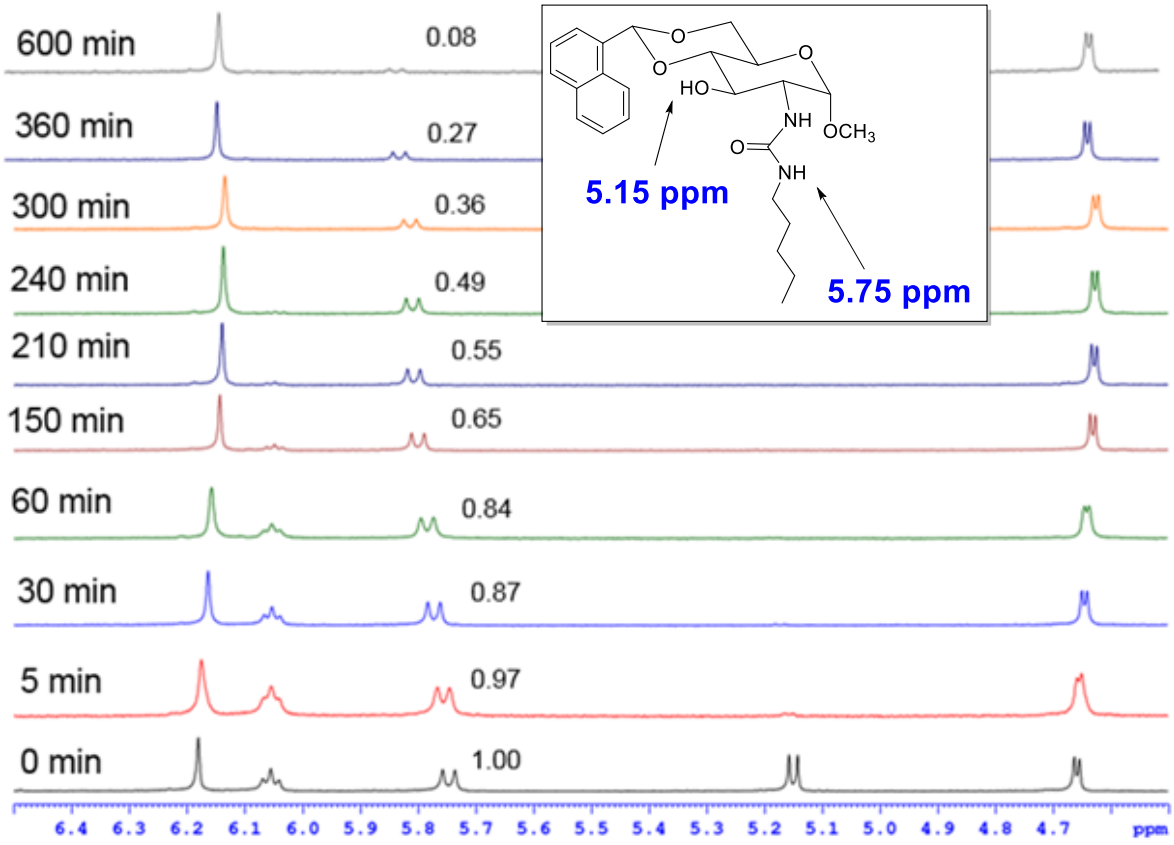

Figure 48. ^{1}H NMR spectra of compound **11** (inner NH) during the deuterium exchange study. The NMR spectra were all acquired at 30 °C.

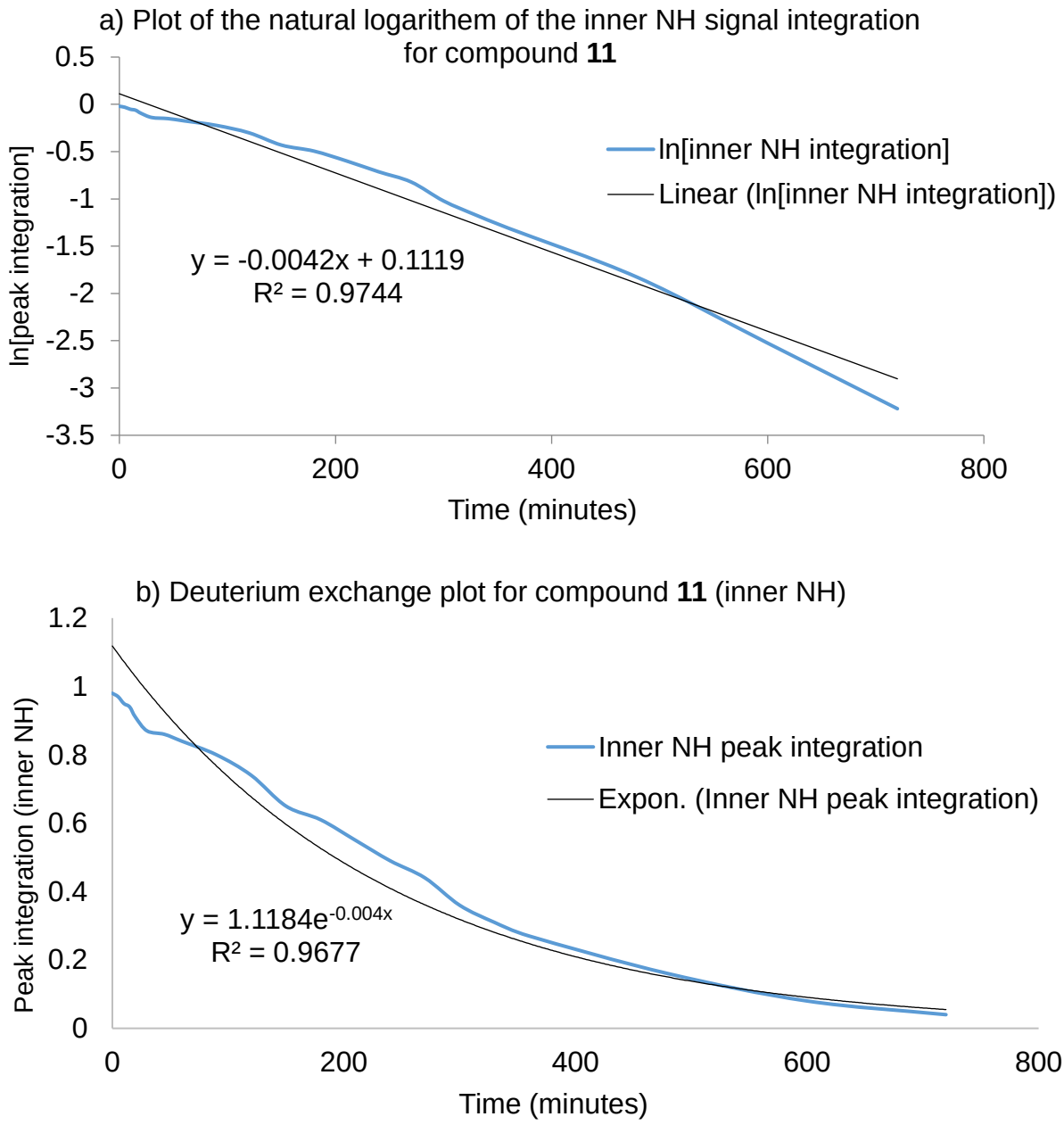

Figure 49. Plots of the deuterium exchange of the inner N-H peak of compound **11**. (a) Plot of the natural logarithm of the exchange versus time; (b) Plot of deuterium exchange versus time**.**

Figure 50 shows overlaid ^{1}H NMR spectra obtained from the deuterium exchange study carried out using compound **21**. The carbamate NH peak appears as a doublet located at 7.03 ppm.

The plot of the integration versus time and the natural logarithm of the peak integration versus time can be found in Figure 51. Using a trend line, the rate constant was found to be 0.0225 min^{-1}. The half-life of the exchange was calculated to be 38.5 minutes, indicating the carbamate group is capable of strong hydrogen bonding.

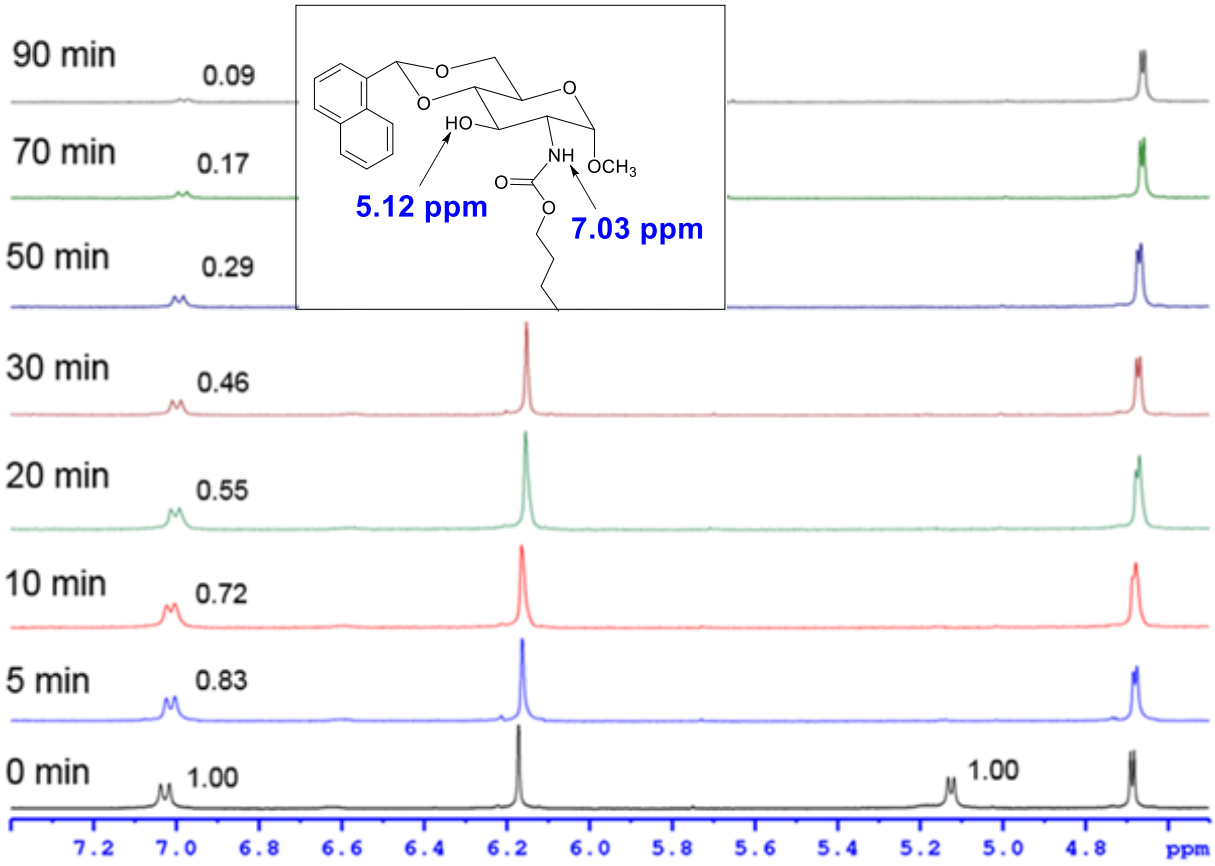

Figure 50. ^{1}H NMR spectra of compound **21** during the deuterium exchange study. The NMR spectra were all acquired at 30 °C.

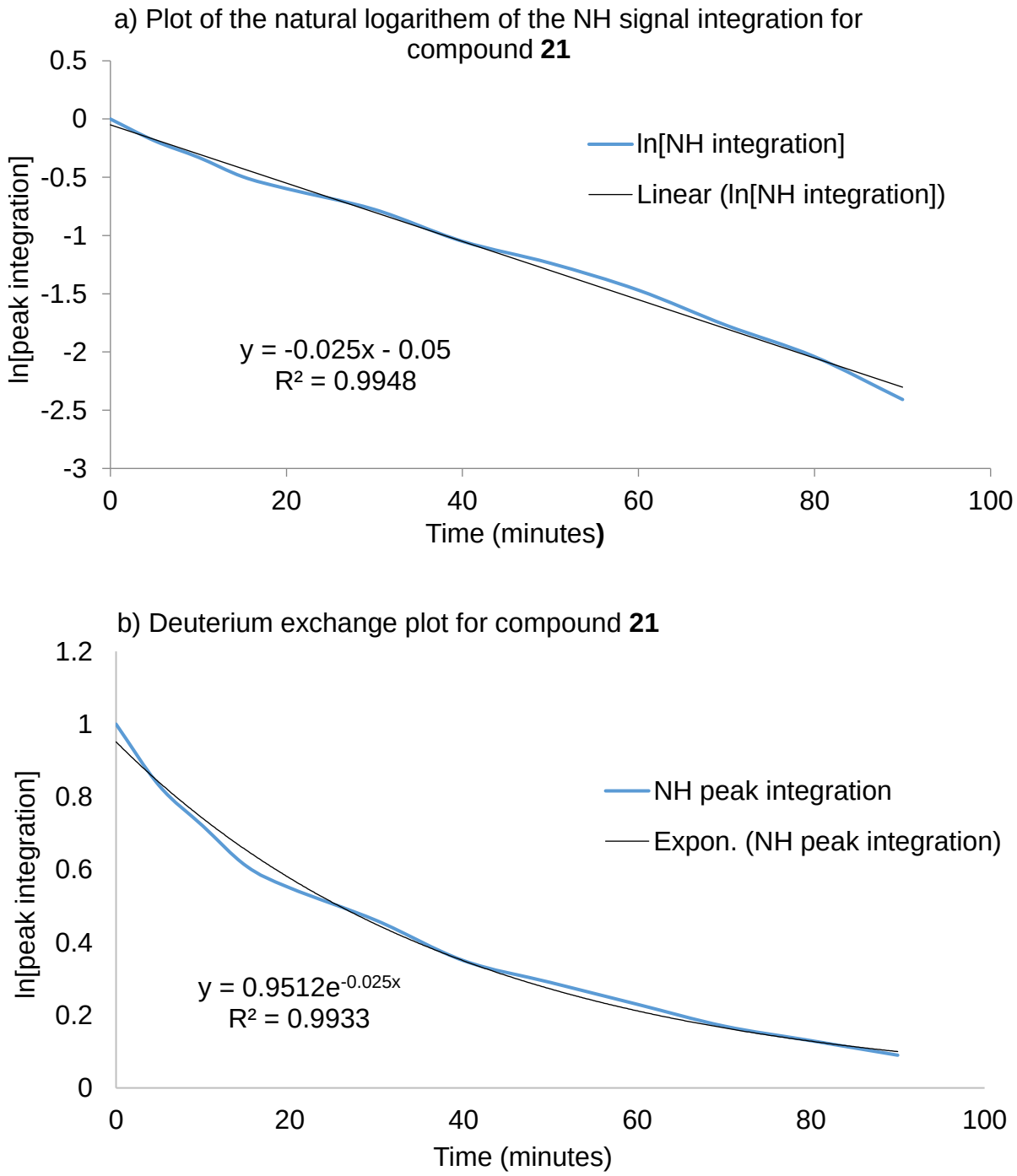

Figure 51 Plots of the deuterium exchange of the N-H peak of compound **21**. (a) Plot of the natural logarithm of the exchange versus time; (b) Plot of deuterium exchange versus time.

With the surprising results from the variable temperature ^{1}H NMR studies and the deuterium exchange studies, we decided to see if computational modeling could shed some light on why urea derivative behaved so much differently than both the amide and carbamate derivatives. Using Chem-3D, two molecular structures were inserted and MM2 calculations were run to minimize the energy between the two molecules. This produced 3D modes of energy minimized two molecule stacking conformations. The model produced for the amide derivative is shown in Figure 52a. The model shows the two molecules aligning to allow multiple hydrogen bonding interactions, as well as aromatic interactions and hydrophobic interactions. The oxygen in the carbonyl of the amide is 1.871 Å and 2.052 Å away from the amides' NH and the 3-hydroxyls OH in the adjacent molecule, which would support strong hydrogen bonding interactions. Additionally, the molecules are aligned for both aromatic interactions as well as hydrophobic interactions. The computational models produced for the urea derivative, shown in Figure 52b, also showed an alignment that would support aromatic and hydrophobic interactions; however, these sections of the molecules were much further away from each other compared to the amide derivative. The urea models were also in a confirmation that would suggest strong intramolecular hydrogen bonding, which may explain the results of the variable temperature study and the deuterium exchange study. The outer NH proton has a close proximity to the oxygen in the 3-hydroxyl group of 2.168 Å. Typically; hydrogen bond donor-acceptor distances in between 2.2-2.5 Å are very strong and considered mostly covalent. If this intramolecular hydrogen bonding is occurring in the way the model is predicting, then the inner NH would be entombed within a pocket created by interactions between the outer NH and the 3-OH. This would prevent the inner NH from interacting as a hydrogen bond donor and reduce its ability to quickly exchange with deuterium. The computational models produced for the carbamate derivative **21**, shown in Figure 52c, showed

some alignment of the aromatic and aliphatic groups; however, similar to the urea derivative, these sections of the molecules were much further away from each other compared to the amide derivative. No hydrogen bonding groups are within a proximity of each other that would suggest strong or moderate hydrogen bonding was occurring. The NH of the carbamate functional group was closest to the oxygen in the adjacent sugar ring and *O*-methoxy group at the anomeric position. Both distances were well over 5.0 Å, which would put it in the range of no hydrogen bonding interactions at all to very weak electrostatic interactions. Unfortunately, the modeling of the carbamate derivative gave very little insight into the self-assembling properties of this molecule.

Characterization of the head group and the final amide, urea and carbamate derivatives were carried out through one dimensional ^{1}H NMR and ^{13}C NMR spectroscopy, 2-dimensional HSQC and COSY NMR spectroscopy, and LC-MS. Figures 53-58 show the 1D and 2D NMR spectra obtained from compounds **1**, **12**, and **29**. These spectra are included as representative spectra that are obtained during the characterization of each of the final derivatives after purification.

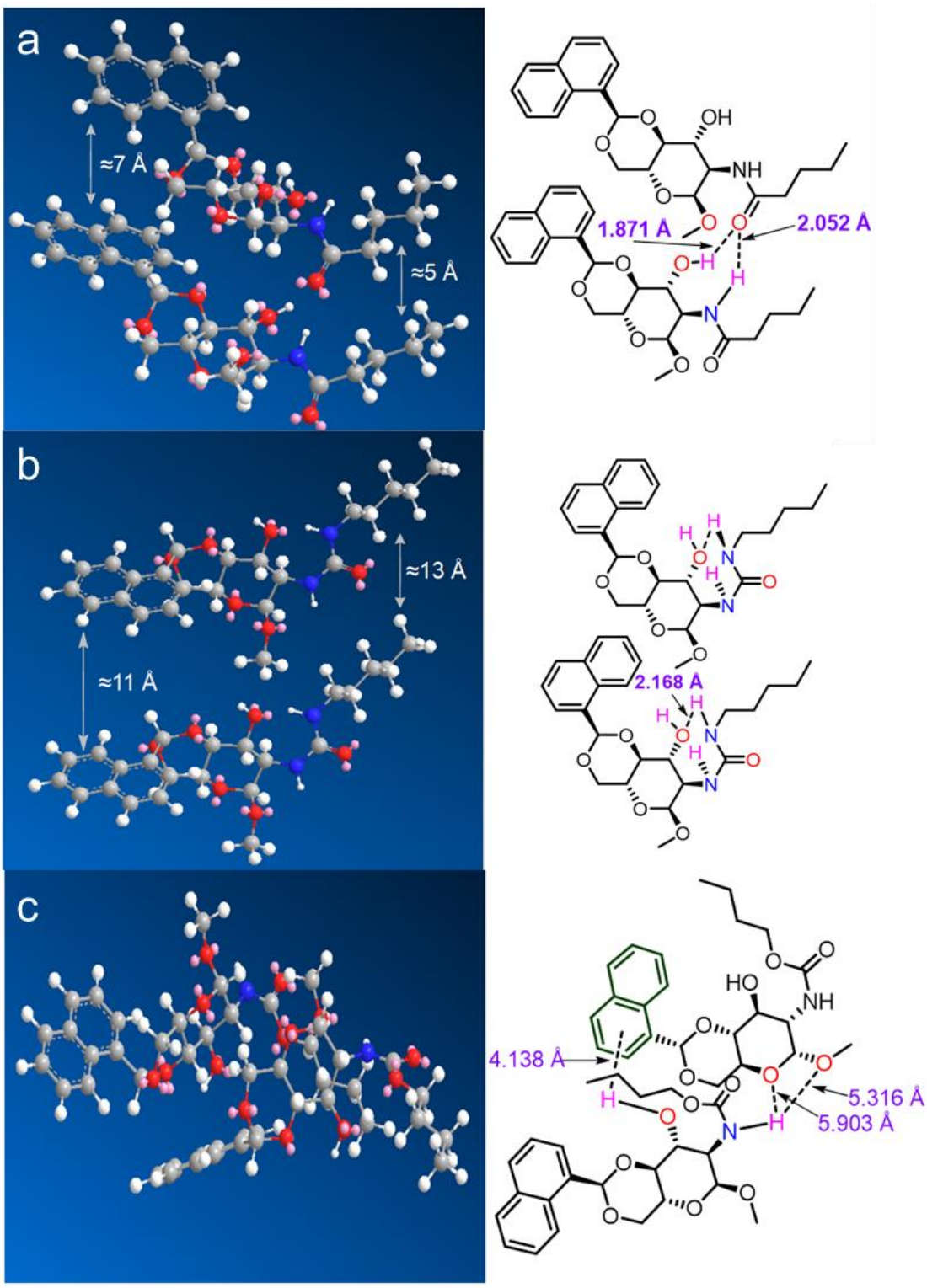

Figure 52. CHEM 3D molecular modeling of analogous derivatives with MM2 calculations. (a) compound **1**; (b) compound **11**; (c) compound **21** with MM2 calculations to minimize energy.

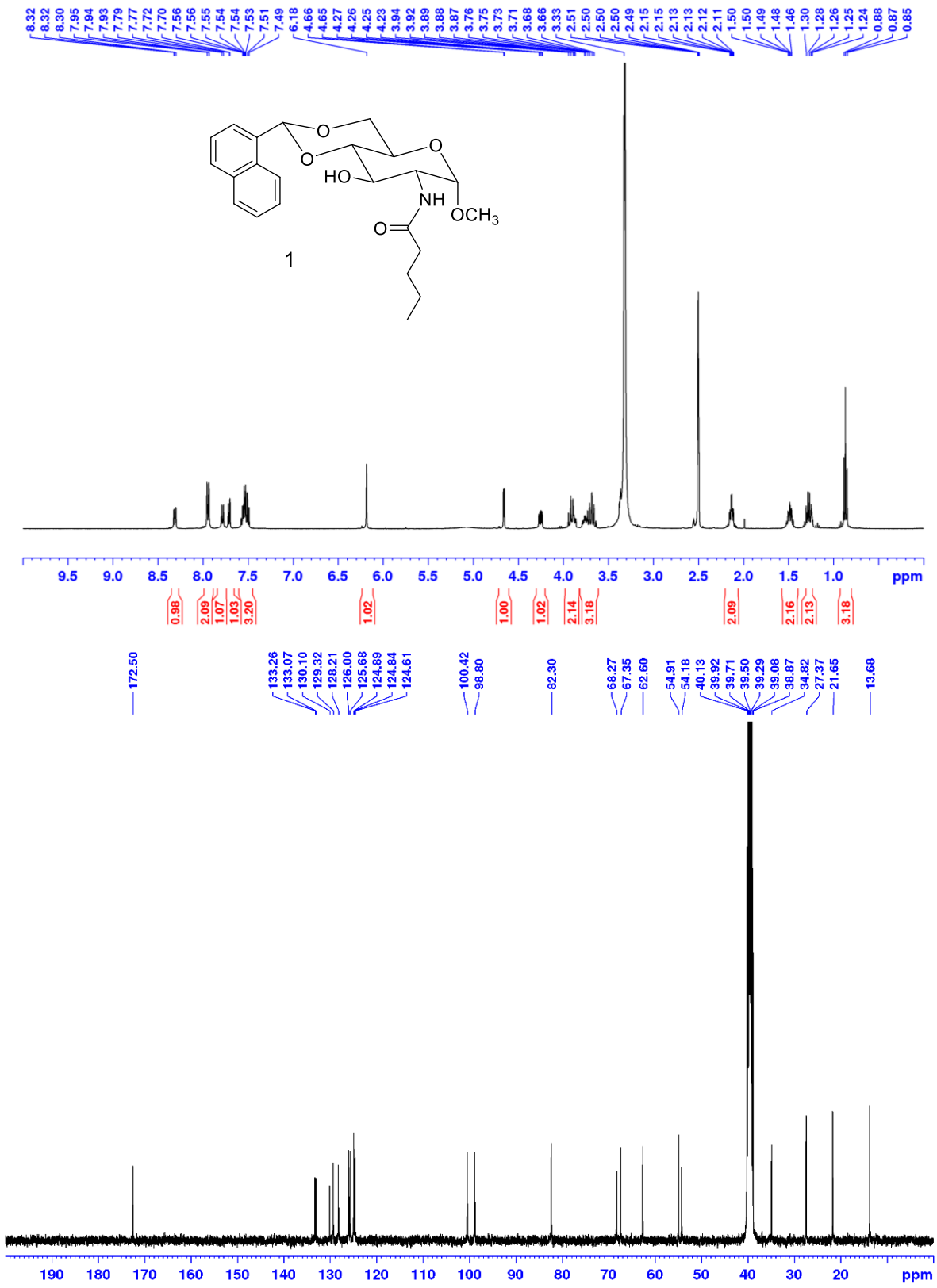

Figure 53. ^{1}H NMR and ^{13}C NMR spectra of amide derivative **1** in d_6-DMSO.

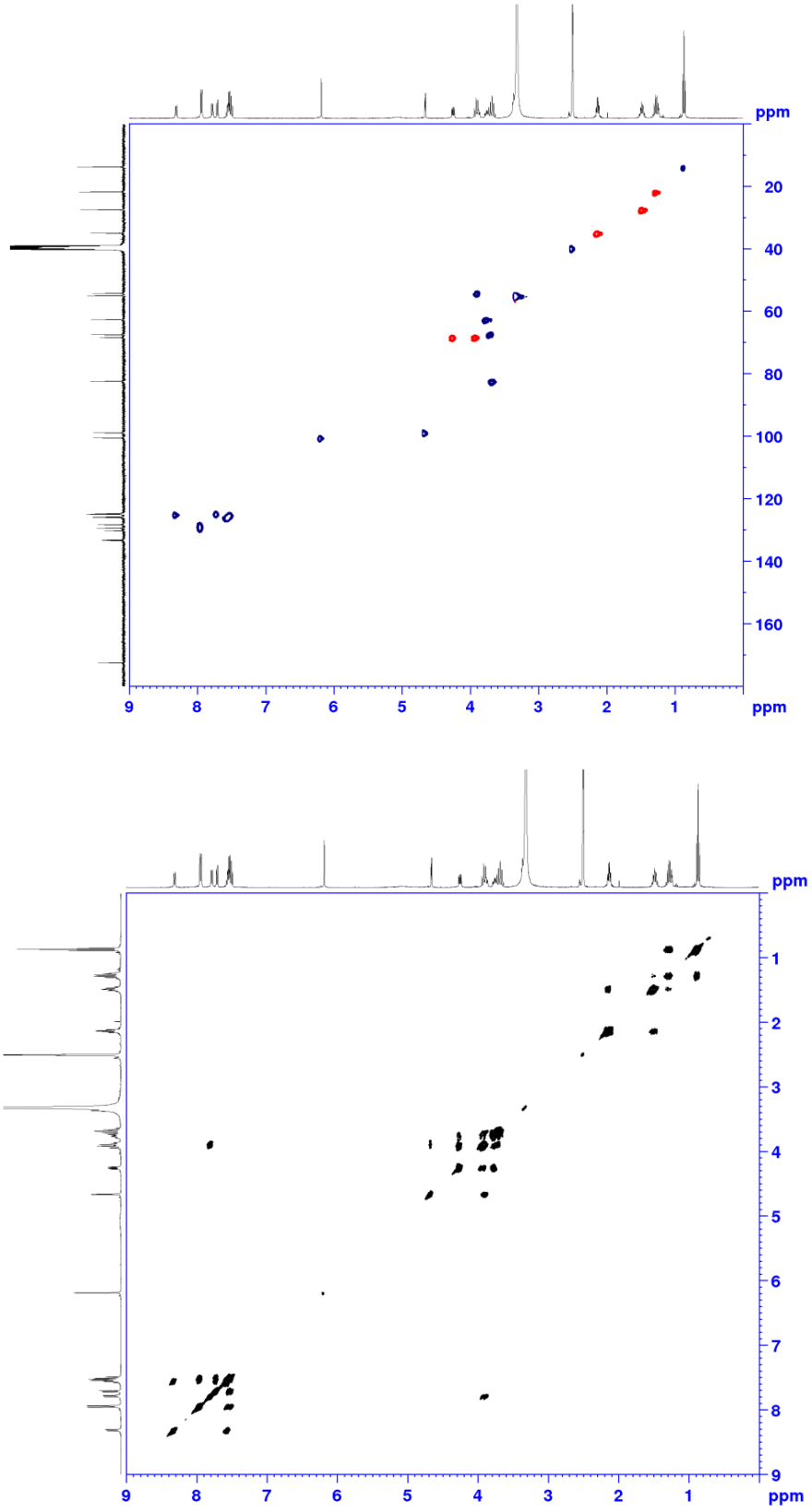

Figure 54. HSQC and COSY spectra of amide derivative **1** in d_6-DMSO.

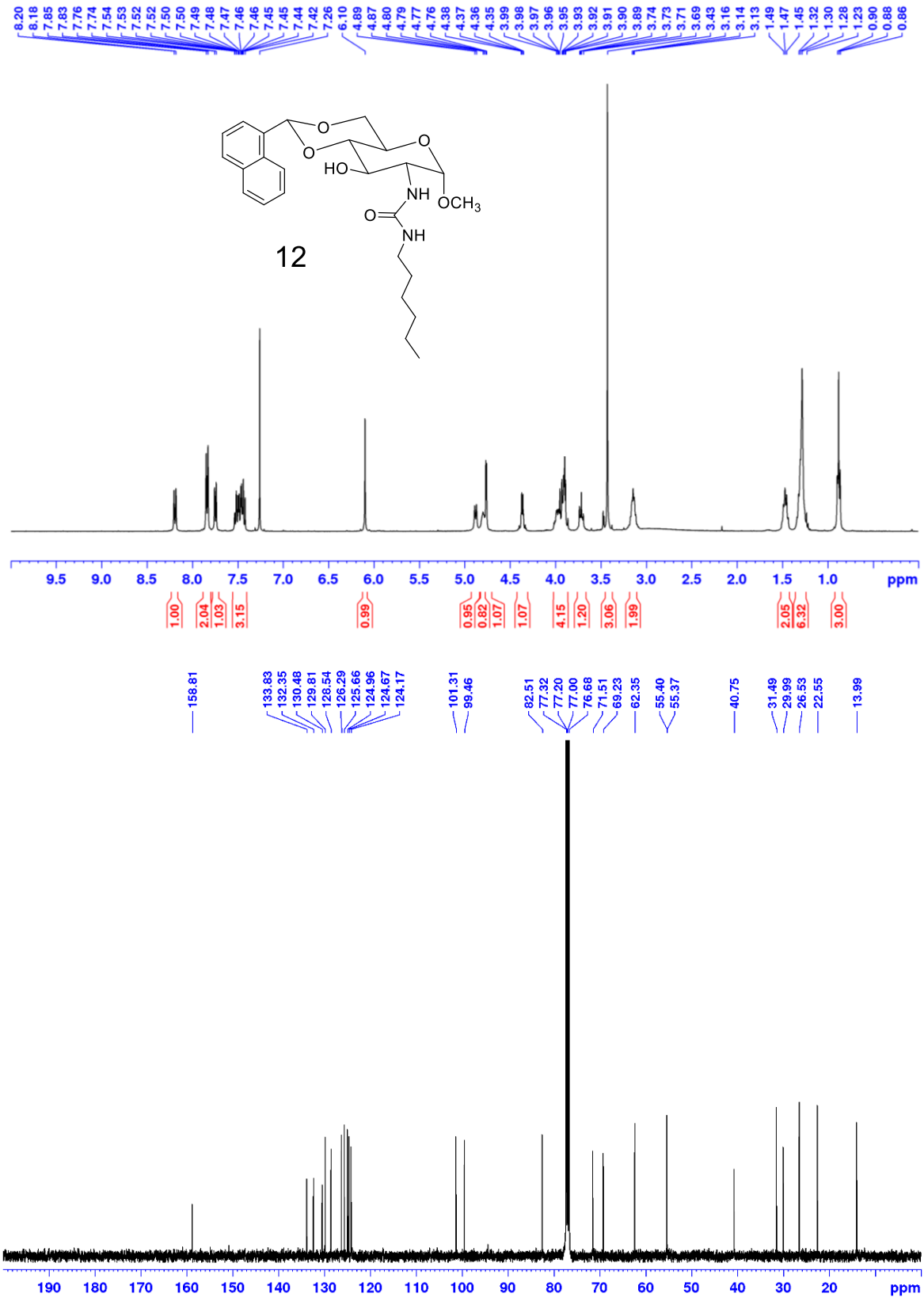

Figure 55. ^{1}H NMR and ^{13}C NMR spectra of urea derivative **12** in $CDCl_3$.

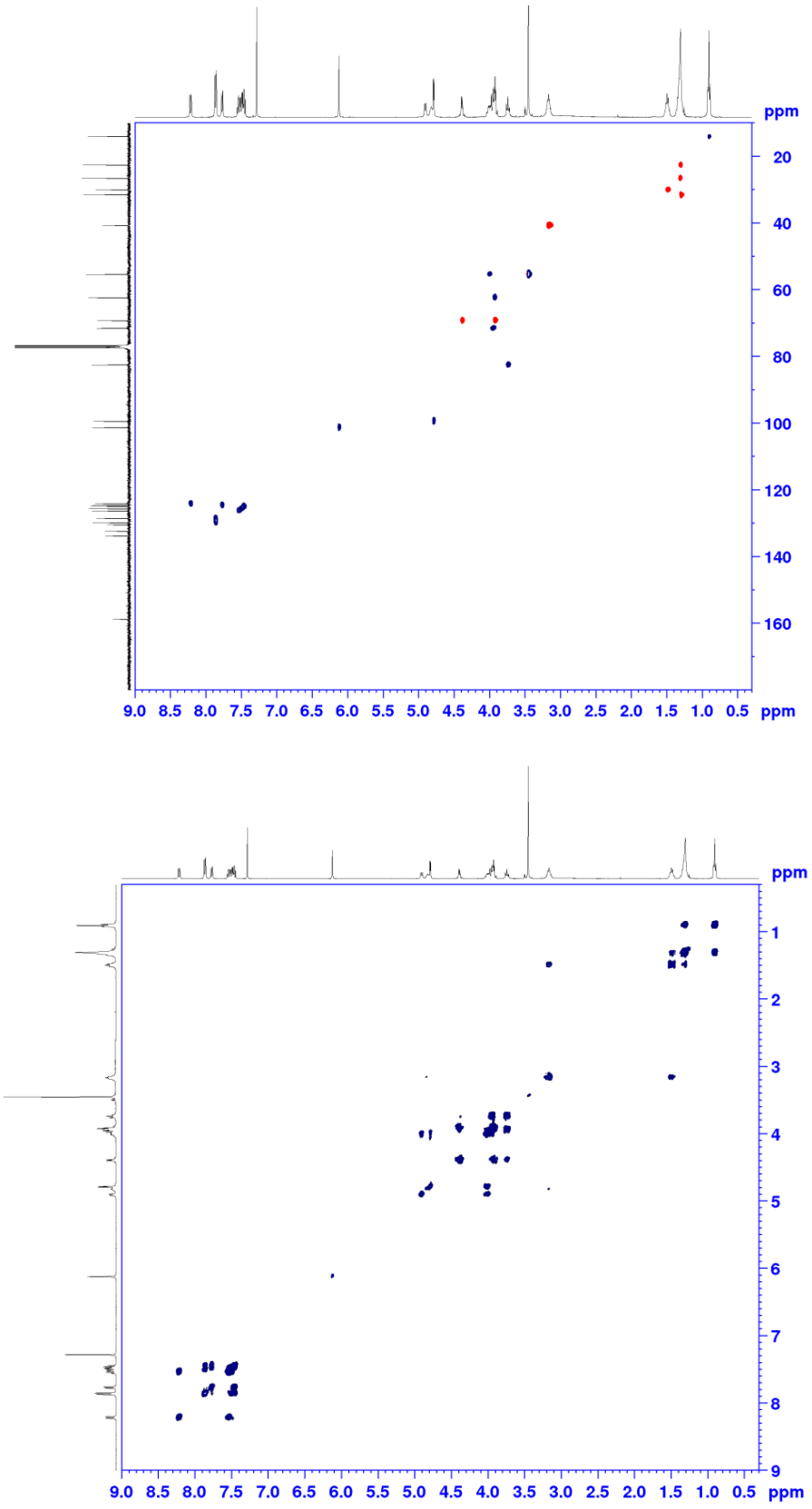

Figure 56. HSQC and COSY spectra of urea derivative **12** in $CDCl_3$.

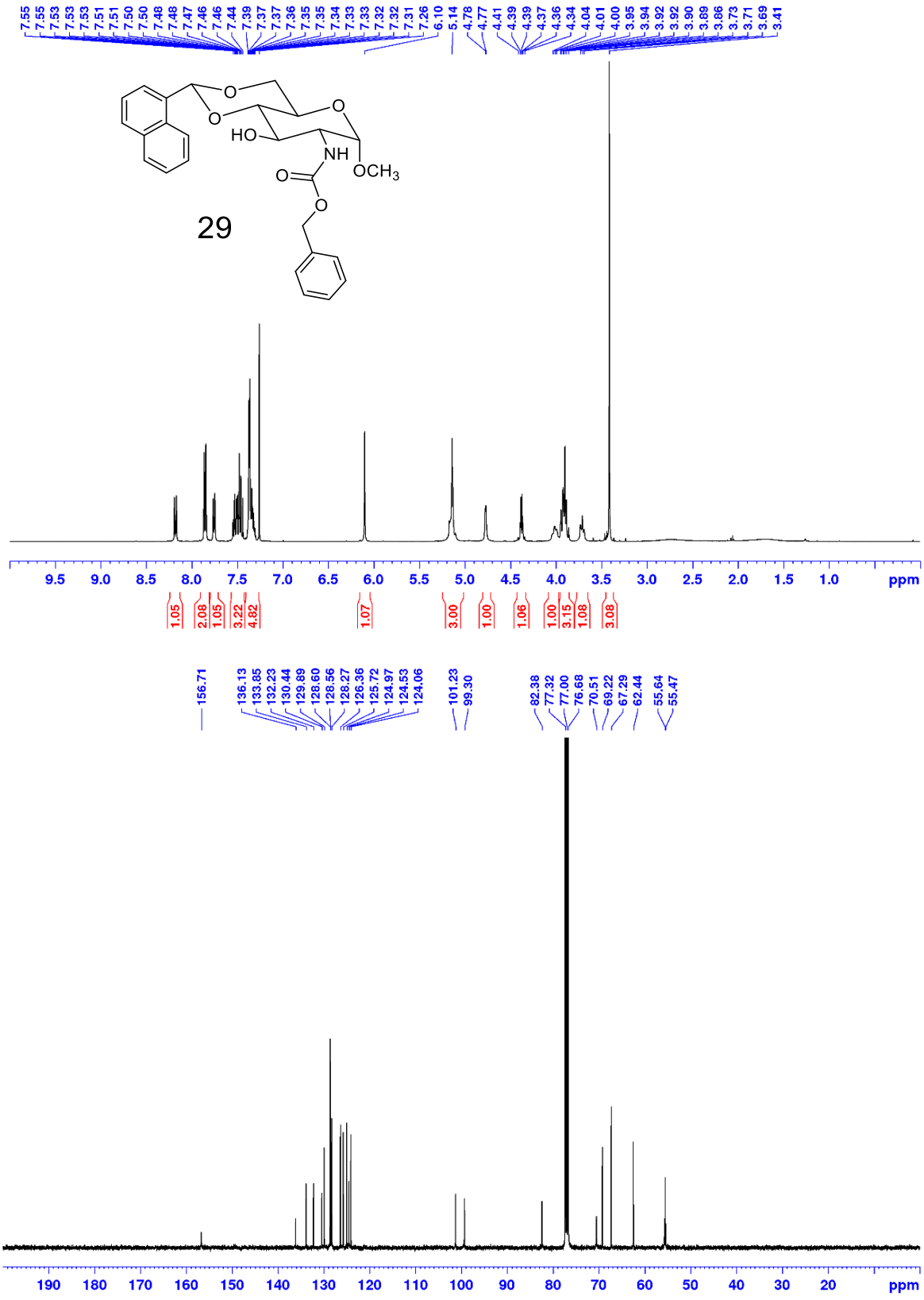

Figure 57. ^{1}H NMR and ^{13}C NMR spectra of carbamate derivative **29** in $CDCl_3$.

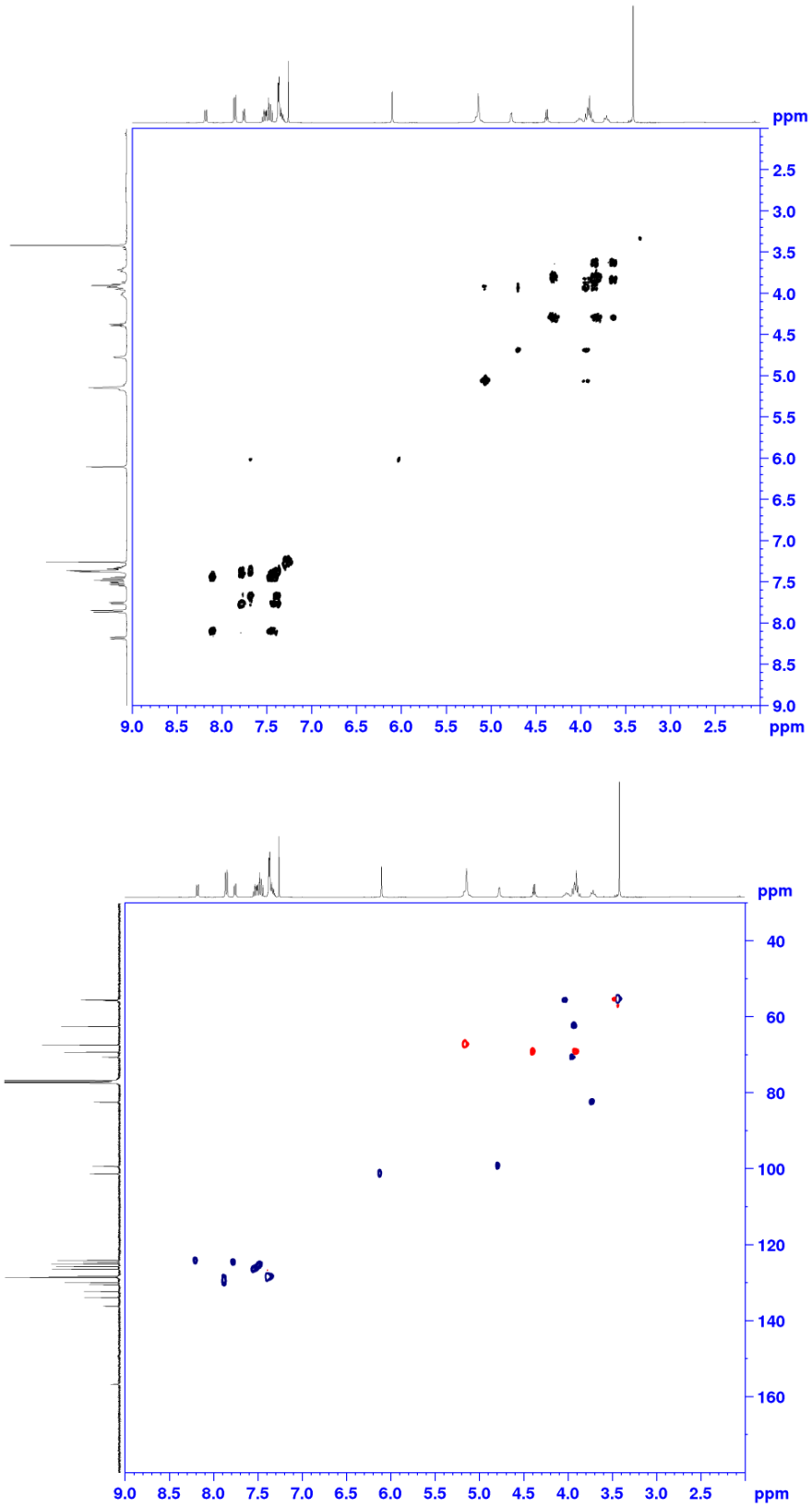

Figure 58. HSQC and COSY spectra of carbamate derivative **29** in $CDCl_3$.

2.3. CONCLUSION

To explore the effect that increased aromatic interactions on the self-assembly and gelation properties of 4,6 acetal protected glucosamine derivatives, a 1-naphthylidene protected glucosamine head group was synthesized. Preliminary gelation testing on compound **III** showed promising results that the head group could be used as a scaffold for increasing the gelation properties through further functionalization. Headgroup **IV** was then used to synthesize three series of derivatives utilizing amide, urea, and carbamate hydrogen bonding groups to link various aliphatic and aromatic groups to the sugar scaffold. The amide derivatives were found to be very versatile gelators in protic organic solvents and toluene. Several of these derivatives were also very effective gelators in aqueous mixtures of ethanol and DMSO. The urea derivatives were less versatile than the amide or carbamate derivatives; however, most of these derivatives were very effective gelators, forming gels at low concentrations in two to three solvents. Like the amide derivatives, the carbamate derivatives were very versatile gelator, which typically formed gels in multiple solvents; however, at higher concentration. The valeryl amide derivative **1** was found to be not only the most versatile gelator out of all of the series, but also formed gels at very low MGCs in various solvents. This indicates that design of compound **1** led to a good balance between various intermolecular forces which promoted self-assembly and increased gelation properties. The morphology of several gels was analyzed under optical microscope. The supramolecular architecture of several gels was investigated under optical microscopy and various types of fibrous morphologies were observed. The viscoelastic properties of several gels were also analyzed via rheometric analysis. To investigate the self-assembly mechanism, variable temperature studies were carried out on analogous amide, urea, and carbamate derivatives. Both the amide and carbamate derivatives saw significant upfield changes in chemical shifts for exchangeable protons

as temperature was increased, while very small upfield changes in chemical shifts were observed for the urea derivatives. Deuterium exchange studies were then carried out to further probe the ability of the amide, urea, and carbamate groups to partake in intermolecular hydrogen bonding. The amide and carbamate derivatives showed a fairly fast exchange rate, with the half-life of the exchange being found to be 29 minutes and 38 minutes respectively. The urea derivative, on the other hand, exhibited a very slow exchange rate. The half-life of the exchange for the outer and inner NH protons of the urea derivative were found to be 58 minutes and 165 minutes respectively. The urea derivatives' results from the variable temperature studies and the deuterium exchange studies were surprising since urea functional groups are notorious for hydrogen bonding. To gain insight into why these results were obtained, computational modeling was carried out on each of the analogous derivatives. The modeling not only suggested why amide derivative **1** was so effective at self-assembling into gels, but also suggested that strong intramolecular hydrogen bonding between may be the reason the urea derivative isn't. The modeling suggests that the outer NH of the urea group and the 3-hydroxyl are hydrogen bonding, which not only prevents the outer NH of the urea from partaking in intermolecular hydrogen bonding, but also creates a pocket that entraps the inner NH of the urea, preventing it from intermolecular hydrogen bonding also. The results of this study show the rational based design of LMWGs through the study of structure to gelation properties relationships, as well as useful methods to probing self-assembly mechanism.

2.4. EXPERIMENTAL SECTION

General method and materials: All reagents and solvents were purchased from chemical suppliers and uses as they were received. Purifications were carried out through recrystallization, trituration, or column chromatography using 230-400 mesh silica gel using gradient solvent

systems. A Bruker 400 MHz spectrometer was utilized to obtain ^{1}H NMR, proton-decoupled ^{13}C NMR, HSQC, and COSY in either $CDCl_3$ or DMSO-d_6. The chemical shifts reported are based off of using $CDCl_3$/DMSO-d_6 as internal standards at 7.26/2.50 ppm (^{1}H NMR) and at 77.00/39.50 ppm (^{13}C NMR), respectively. Carbon and proton assignment was determined with the assistance of 2D NMR experiments (HSQC, COSY). Melting point analysis was carried out using a Fisher Jones melting point apparatus. Rheological experiments were carried out using a HR-2 Discovery Hybrid Rheometer from TA instrument, equipped with a 25 mm Peltier Plate. Mass spectroscopy was carried out using a LC-MS on an Agilent 6120B Single Quad Mass Spectrometer.

Optical Microscopy: Olympus BX60M optical microscope, equipped with an Olympus DP73-1-51 high performance Peltier cooled 17MP digital camera with pixel shifting, was used to analyze the morphology of gel samples. Gel samples were placed on clean glass slides and allowed to air dry before analysis. Images were captured using CellSens 1.11 computer software.

Gel Testing: All experiments were started at 20 mg/mL by measuring out about 2 mg of compound in a 1-dram vial and 0.1 mL of the appropriate solvent. The sample was then heated gentility until the compound dissolved, forming a homogeneous solution. The solution was then allowed to cool to room temperature and sit undisturbed for 30 minutes. The vial inversion method was used to determine gel formation, where an inverted vial containing a gel has no flow under gravity. Serial dilutions were carried out on all gels that were found to be stable at 20 mg/mL until the minimum gelation concentration was discovered.

Rheological Analyses: HR-2 Discovery hybrid rheometer (TA instruments) using TRIOS software was utilized to analyze the rheological behavior of several gels. Typically, >500 µL of gel was centered on the fixed plate of the rheometer. For all experiments, a 25 mm Peltier plate was used, the instrument was set to a 100 µm gap and the temperature was held constant at 25 °C.

Amplitude sweeps were carried out first, from 0.125% to 10% to determine the linear range of the gel. Frequency sweeps were then carried out over a range of oscillation frequencies, 0.1 to 500 rad/s, at an amplitude within the linear range determine in the amplitude sweeps, typically 0.1-0.5%.

Time dependent Deuterium-Hydrogen exchange study: NMR samples were prepared from compounds **1**, **11**, and **22** by dissolving 1.6 mg of each respective compound in 0.4 mL of d_6-DMSO in an NMR tube. An initial ^{1}H NMR spectrum was acquired at this concentration of 3.2 mg/mL and represents the initial time of 0 minutes. 0.1 mL of D_2O was then added to the NMR tube and ^{1}H NMR spectra were acquired at various time points up to 600 minutes. Integration of the signals that belong to exchangeable protons was monitored as deuterium exchanged with these protons over time. Distinct non-exchangeable proton signals, such as the anomeric or acetal signals, are used as internal integration references. The integrations of the exchangeable proton signals were plotted versus time in Microsoft Excel. The best fit curves generated by the software followed the simplified rate law $[A] = [A_o]e^{-kt}$, which confirmed first order kinetics. Another way to test if the deuterium exchange is first order is to plot the natural logarithm of the integration versus time. If the graph is linear and the slope is negative, the reaction is first order. The integrated rate law, arranged into the form of $y = mx + b$, is $\ln[A] = -kt + \ln[A_o]$, where k is the first order rate constant. Further simplifying the rate law gives $[A] = [A_o]e^{-kt}$, which is the equation confirmed by Kinetic Studio software. The rate constant was calculated via Kinetic Studio software and confirmed via the natural logarithm plot in Microsoft Excel. Using the rate constant, the half-life of the deuterium exchange was calculated using the following equation, $t_{1/2} = \ln(2)/k$.

Computational modeling: Chem3D software was utilized to carry out MM2 energy minimization to investigate possible intermolecular interaction occurring between two gelator molecules.

Liquid chromatography-mass spectrometer (LC-MS) conditions: An Agilent 1260 Infinity LC system coupled to a G6120B single quadrupole mass spectrometer, utilizing an atmospheric pressure ionization electrospray (API-ES) ionization source was used for molecular mass acquisition. Agilent poroshell 120 EC-C18 4.6 mm x 50 mm columns with 2.7 μm particle size were used for chromatographic separation. The system was linked to a diode array detector (DAD), which analyzes at 254 nm. The injection volume for each run was 5 μL. The flow rate for each experiment was 0.40 mL/min and each experiment's run time was 8 minutes. Agilent OpenLAB CDS ChemStation (Version C.01.05) was used to process data. The mass spectrometer's range was set from 0-2000.

Synthesis of Compound II: Amberlite IR 120 resin (10.000 g, 1 weight equivalent) was activated by stirring with anhydrous methanol (30 mL) for 30 minutes in a 500 mL round bottomed flask. The flask was then charged with N-acetyl glucosamine (10.000 g, 0.045 mol, 1 equiv) and heated to reflux. The reaction stirred at reflux for 24 hours. Solution was then decanted, and resin was washed with methanol (30 mL x 1). The solvent was then removed under reduced pressure and the crude product was co-distilled with toluene (30 mL). Yield: 8.9714 g (85%).

Synthesis of compound III: 1-napthaldehyde (2.2 mL, 15.6 mmol, 1.2 equiv), trimethyl orthoformate (1.7 mL, 15.6 mmol, 1.2 equiv), and pTSA (247 mg, 1.3 mmol, 0.1 equiv) were dissolved in anhydrous methanol (10 mL) in a nitrogen flushed 100 mL round bottomed flask. The reaction was brought to reflux for 1.5 hours. Methanol and excess trimethyl orthoformate were removed under reduced pressure at 60 °C. The resulting crude dimethyl acetal was dissolved in

anhydrous DMF (5 mL). Compound II (3.000 g, 13.0 mmol, 1 equiv) was co-distilled with toluene (15 mL x 3) and dissolved in anhydrous DMF (5 mL) in a dry, nitrogen flushed 100 mL round bottomed flask, which was then placed in a pre-heated oil bath (80 °C). The crude dimethyl acetal mixture was then added to the flask all at once. The reaction stirred at 80 °C for 5 hours, at which point, the reaction mixture was placed on the rotary vaporizer at 60 °C for 30 minutes to drive the reaction forward by removing methanol side products. The reaction mixture was then cooled to rt, while still under vacuum. Once at rt, $NaHCO_3$ (550 mg, 0.065 mmol, 0.5 equiv) was added to quench the reaction and the mixture was allowed to stirr for 30 minutes. The reaction mixture was then poured into to a cold half sataturated NaCl solution resulting in a white solid percipitating. The white precipitate was filtered and the filtrate was extracted with EtOAc (30 mL x 3). The organic layers were combined and washed with DI water (30 mL x 3). The organic layer was then dried over Na_2SO_4, filtered and the solvent was removed under reduced pressure. The precipitate and the crude product obtained from extracting the filtrate were combined and recrystallized in reagent alcohol, producing a white solid. The mother liquor was further purified via column chromatography using pure DCM to 3% MeOH/DCM to yield a white solid. Yield: 3.7970g (78%) R_f = 0.39 in 5% MeOH/DCM. mp = 292.1–294.6 °C. ^{1}H NMR (400 MHz, $CDCl_3$) δ 8.18 (d, J = 8.4 Hz, 1H), 7.85 (d, J = 8.4 Hz, 2H), 7.76 (d, J = 7.0 Hz, 1H), 7.43–7.56 (m, 3H), 6.11 (s, 1H), 5.85 (d, J = 8.7, 1H), 4.76 (d, J = 3.8 Hz, 1H), 4.33–4.43 (m, 1H), 4.25–4.32 (m, 1H), 3.87–3.99 (m, 3H), 3.69-3.76 (m, 1H), 3.44 (s, 3H), 2.97 (d, J = 3.2, 1H), 2.06 (s, 3H). ^{13}C NMR (100 MHz, $CDCl_3$) δ 171.3, 133.8, 132.3, 130.5, 129.9, 128.6, 126.3, 125.7, 125.0, 124.6, 124.1, 101.2, 99.0, 82.5, 70.7, 69.2, 62.4, 55.4, 54.0, 23.3. LC-MS m/z calculated for $C_{20}H_{24}NO_6$ $[M+H]^+$ 374.2 found 374.1.

Synthesis of compound IV: Compound III (2.000 g, 5.4 mmol, 1 equiv) was divided into two ≈ 1 g portions and added to two microwave vials containing 1 N NaOH in EtOH (40 mL). The reaction was carried out under microwave conditions: 100 psi, 600 watts, 150 °C for a 15-minute ramp and 30-minute hold. Solvent was then removed under reduced pressure. The crude product was dissolved in DCM (30 mL) washed with DI water (30 mL x 3). The organic layer was dried over Na_2SO_4, filtered and the solvent was removed under reduced pressure. The crude product was purified via column chromatography using pure DCM to 5% MeOH/DCM to yield a white solid. Yield: 1.7290 g (97%). R_f = 0.12 in 5% MeOH/DCM. mp = 211.1–212.2 °C ^{1}H NMR (400 MHz, $CDCl_3$) δ 8.21 (d, J = 8.5 Hz, 1H), 7.86 (d, J = 8.2 Hz, 2H), 7.75 (d, J = 7.3 Hz, 1H), 7.43–7.58 (m, 3H), 6.08 (s, 1H), 4.70 (d, J = 3.7 Hz, 1H), 4.32–4.40 (m, 1H), 3.82–3.97 (m, 2H), 3.74 (t, J = 9.4 Hz, 1H), 3.58 (t, J = 9.1 Hz, 1H), 3.44 (s, 3H), 2.83 (dd, J = 9.6, 3.7 Hz, 1H); ^{13}C NMR (100 MHz, $CDCl_3$) δ 133.9, 132.4, 130.5, 129.5, 128.6, 126.3, 125.7, 125.0, 124.7, 124.2, 101.3, 82.5, 71.9, 69.4, 62.6, 56.7, 55.5. LC-MS m/z calculated for $C_{18}H_{22}NO_5$ $[M+H]^+$ 332.14 found332.1.

General procedure for the synthesis of amide derivatives 1-10: The amide derivatives were synthesized using the corresponding acid chlorides (for compounds **1-8)** or anhydrides (for compounds **9-10**). In general, compound **IV** (1 equiv) was dissolved in either anhydrous THF or anhydrous DCM in a dried 50 mL round bottomed flask under nitrogen atmosphere. Then, either pyridine (3-5 equiv) or triethylamine (3 equiv) was added to the reaction mixture and the temperature was reduced to 0 °C via an ice bath. The acid chlorides or anhydrides (1.1 equiv) were diluted in anhydrous THF (1 mL) or anhydrous DCM (1 mL) and added dropwise to the reaction mixture. The reactions were typically stirred at 0 °C for 4-6 hours. Reaction progress was monitored via ^{1}H NMR and TLC. After completion, the reaction mixtures were quenched with 5%

$NaHCO_3$ solution. If the reaction was carried out in THF, solvent was removed under reduced pressure and the resulting solid was dissolved in DCM (5 mL) before an aqueous workup was carried out. If the reaction was carried out in DCM, the reaction mixture was diluted with DCM (5 mL) before undergoing an aqueous workup. The aqueous workups were carried out using saturated $NaHCO_3$ solutions, saturated NH_4Cl solutions, DI water and DCM (x 2). The combined organic layers were dried over Na_2SO_4 and solvent was removed under reduced pressure. The crude products were purified either through column chromatography (SiO_2) using a gradient solvent system or through recrystallization in reagent alcohol. The detailed preparation for compound **1** is provided below and only amounts used and characterization data are provided for all other compounds. All compounds were synthesized using 75 mg (0.23 mmol) of compound **IV.**

General procedure for the synthesis of acid chlorides: Corresponding acids (1.1 equiv) were dissolved in anhydrous DCM with 1 drop of a DMF/DCM solution in nitrogen flushed 50 mL round bottomed flasks. The temperature was reduced to 0 °C via an ice bath and oxalyl chloride (1.2-1.5 equiv) was added to the reaction mixture. The reaction stirred at 0 °C for 10 minutes, at which point the ice bath was removed. The reaction mixtures then stirred at room temperature for 4-16 hours. Conversion to the acid chloride was monitored via ^1H NMR. Excess oxalyl chloride was removed in vacuo and the crude acid chloride was dissolved in either anhydrous THF or anhydrous DCM to be used in the amide synthesis.

Synthesis of compound 1: Valeric acid (27 µL, 0.25 mmol, 1.1 equiv), DCM (1 mL) and DMF/DCM solution (2 drops) were added to a dried nitrogen flushed 50 mL round bottomed flask. The temperature was reduced to 0 °C via an ice bath. Oxalyl chloride (30 µL, 0.33 mmol, 1.5 equiv) was added and the reaction was allowed to warm to room temperature. The reaction stirred for 16 hours. Excess oxalyl chloride was removed under reduced pressure and the crude product

was used without further purification. Compound IV (75.0 mg, 0.23 mmol, 1.0 equiv) was dissolved in anhydrous DCM (3 mL) in a dried nitrogen flushed 50 mL round bottomed flask. Pyridine (100 µL, 1.15 mmol, 5 equiv) was added to the reaction mixture and the temperature was reduced to 0 °C via an ice bath. The crude valeroyl chloride was dissolved in anhydrous DCM (1 mL) and added dropwise to the reaction mixture. The reaction stirred for 4 hours at 0 °C, at which point the reaction was quenched with 0.5 mL of 5% $NaHCO_3$ solution. The reaction mixture was diluted with DCM (5 mL), washed with saturated $NaHCO_3$ solution (5 mL), saturated NH_4Cl solution and then DI water (5 mL x 2). The aqueous layers were then back extracted with DCM (5 mL x 2). The organic layers were dried over Na_2SO_4, filtered and solvent was removed under reduced pressure. The crude product was purified via column chromatography using 30-60% EtOAc/hexanes to afford a white solid. Yield: 78.9 mg (83%). R_f = 0.35 in 40% EtOAc/hexanes. mp = 227.0–229.0 °C. ^{1}H NMR (400 MHz, d_6-DMSO) δ 8.29–8.34 (m, 1H), 8.92–8.97 (m, 2H), 7.78 (d, J = 8.3 Hz, 1H), 7.71 (d, J = 6.6 Hz, 1H), 7.48–7.59 (m, 3H), 6.18 (s, 1H), 4.66 (d, J = 3.6 Hz, 1H), 4.22–4.28 (m, 1H), 3.84–3.96 (m, 2H), 3.62–3.80 (m, 3H), 3.33 (s, 3H), 2.13 (t, J = 7.4, 2.8 Hz, 2H), 1.42–1.56 (m, 2H), 1.21–1.35 (m, 2H), 0.87 (t, J = 7.3 Hz, 3H); ^{13}C NMR (100 MHz, d_6-DMSO) δ 172.5, 133.3, 133.1, 130.1, 129.3, 128.2, 126.0, 125.7, 124.9, 124.8, 124.6, 100.4, 98.8, 82.3, 68.3, 67.4, 62.6, 54.9, 54.2, 34.8, 27.4, 27.4, 21.6, 13.7. LC-MS m/z calculated for $C_{23}H_{30}NO_6$ $[M+H]^+$ 416.2 found 416.2.

Synthesis of compound 2: Hexanoyl chloride (30 µL, 0.23 mmol, 1.0 equiv) was dissolved in anhydrous THF and added dropwise to a flask containing compound **IV** and pyridine (60 µL, 0.69 mmol, 3 equiv) dissolved in anhydrous THF at 0 °C. The reaction stirred for 6 hours. The crude product was purified via column chromatography using pure DCM to 3% MeOH/DCM to afford a white solid. Yield: 78.4 mg (79%). R_f = 0.61 in 5% MeOH/DCM. mp = 214.0–215.0 °C.

^{1}H NMR (400 MHz, $CDCl_3$) δ 8.18 (d, J = 8.3 Hz, 1H), 7.85 (d, J = 8.0 Hz, 2H), 7.76 (d, J = 7.0 Hz, 1H), 7.42–7.58 (m, 3H), 6.12 (s, 1H), 5.87 (d, J = 8.5 Hz, 1H), 4.77 (d, J = 3.8 Hz, 1H), 4.33–4.44 (m, 1H), 4.24–4.33 (m, 1H), 3.86–4.02 (m, 1H), 3.74 (t, J = 8.9 Hz, 1H), 3.44 (s, 3H), 2.28 (t, J = 7.5 Hz, 2H), 1.57–1.73 (m, 2H), 1.28–1.39 (m, 4H), 0.89 (t, J = 6.7 Hz, 3H); ^{13}C NMR (100 MHz, $CDCl_3$) δ 174.5, 133.8, 132.3, 130.5, 129.8, 128.6, 126.3, 125.7, 125.0, 124.6, 124.1, 101.3, 99.0, 82.5, 70.7, 69.2, 62.4, 55.4, 54.0, 36.7, 31.3, 25.3, 22.4, 13.9. LC-MS m/z calculated for $C_{24}H_{32}NO_6$ $[M+H]^+$ 430.2 found 430.2.

Synthesis of compound 3: Heptanoyl chloride (40 µL, 0.25 mmol, 1.1 equiv) was dissolved in anhydrous THF and added dropwise to a flask containing compound **IV** and pyridine (60 µL, 0.69 mmol, 3 equiv) dissolved in anhydrous THF at 0 °C. Reaction stirred for 6 hours. The crude product was purified via column chromatography using pure DCM to 3% MeOH/DCM to afford a white solid. Yield: 97.9 mg (94%) R_f = 0.49 in 5% MeOH/DCM. mp = 216.0–218.0 °C. ^{1}H NMR (400 MHz, $CDCl_3$) δ 8.18 (d, J = 8.3 Hz, 1H), 7.85 (d, J = 8.1 Hz, 2H), 7.76 (d, J = 6.9 Hz, 1H), 7.41–7.57 (m, 3H), 6.12 (s, 1H), 5.84 (d, J = 8.4 Hz, 1H), 4.77 (d, J = 3.7 Hz, 1H), 4.33–4.44 (m, 1H), 4.24–4.33 (m, 1H), 3.86–4.02 (m, 3H), 3.74 (t, J = 8.6 Hz, 1H), 3.44 (s, 3H), 2.26 (t, J = 7.5 Hz, 2H), 1.59–1.72 (m, 2H), 1.21–1.44 (m, 6H), 0.88 (t, J = 6.8 Hz, 3H); ^{13}C NMR (100 MHz, $CDCl_3$) δ 174.5, 133.8, 132.3, 130.5, 129.9, 128.6, 126.3, 125.7, 125.0, 124.6, 124.1, 101.2, 99.0, 82.5, 70.7, 69.2, 62.4, 55.4, 54.0, 36.7, 31.4, 28.8, 25.6, 22.5, 14.0. LC-MS m/z calculated for $C_{25}H_{34}NO_6$ $[M+H]^+$ 444.2 found 444.3.

Synthesis of compound 4: Lauroyl chloride (0.25 mmol, 1.1 equiv) was synthesized from lauric acid (50.1 mg, 0.25 mmol, 1.1 equiv) and oxalyl chloride (26 µL, 0.30 mmol, 1.2 equiv). The crude acid chloride was dissolve in anhydrous DCM and added dropwise to a flask containing compound **IV** and pyridine (100 µL, 1.1 mmol, 5.0 equiv) dissolved in anhydrous DCM at 0 °C.

The reaction stirred for 4 hours. The crude product was purified via recrystallization in reagent alcohol and the mother liquor was purified via column chromatography using DCM/hexanes 1:1 to 1.5% MeOH in DCM/Hexanes 1:1 to afford a white solid. Yield: 99.5 mg (93%) R_f = 0.19 in 1.5% MeOH in DCM/hexanes 1:1. mp = 188.0–190.0 °C. ^{1}H NMR (400 MHz, $CDCl_3$) δ 8.18 (d, J = 8.4 Hz, 1H), 7.85 (d, J = 8.2 Hz, 2H), 7.76 (d, J = 7.1 Hz, 1H), 7.41–7.56 (m, 3H), 6.11 (s, 1H), 5.84 (d, J = 8.6 Hz, 1H), 4.76 (d, J = 3.8 Hz, 1H), 4.33–4.42 (m, 1H), 4.24–4.33 (m, 1H), 3.86–3.99 (m, 3H), 3.67-3.77 (m, 1H), 3.44 (s, 3H), 2.25 (t, J = 7.6 Hz, 2H), 1.59–1.72 (m, 2H), 1.16–1.41 (m, 16H), 0.88 (t, J = 6.8 Hz, 3H); ^{13}C NMR (100 MHz, $CDCl_3$) δ 174.5, 133.8, 132.3, 130.5, 129.9, 128.6, 126.3, 125.7, 125.0, 124.6, 124.1, 101.2, 99.0, 82.5, 70.7, 69.2, 62.4, 55.4, 54.0, 36.7, 31.9, 29.6, 29.58, 29.5, 29.33, 29.30, 29.2, 25.6, 22.7, 14.1. LC-MS m/z calculated for $C_{30}H_{44}NO_6$ $[M+H]^+$ 514.3 found 514.3.

Synthesis of compound 5: Palmitoyl chloride (0.25 mmol, 1.1 equiv) was synthesized from palmitic acid (64.7 mg, 0.25 mmol, 1.1 equiv) and oxalyl chloride (26 µL, 0.30 mmol, 1.2 equiv). The crude acid chloride was dissolve in anhydrous DCM and added dropwise to a flask containing compound **IV** and pyridine (60 µL, 0.69 mmol, 3 equiv) dissolved in anhydrous DCM at 0 °C. The reaction stirred for 5 hours. The crude product was purified via recrystallization in reagent alcohol and the mother liquor was purified via column chromatography using DCM/hexanes 1:1 to 1.5% MeOH in DCM/Hexanes 1:1 to afford a white solid. Yield: 81.6 mg (68%) R_f = 0.53 in 5% MeOH/DCM. mp = 185.0–187.0 °C. ^{1}H NMR (400 MHz, $CDCl_3$) δ 8.18 (d, J = 8.3 Hz, 1H), 7.85 (d, J = 8.4 Hz, 2H), 7.77 (d, J = 7.0 Hz, 1H), 7.42–7.56 (m, 3H), 6.11 (s, 1H), 5.83 (d, J = 8.7 Hz, 1H), 4.76 (d, J = 3.8 Hz, 1H), 4.33–4.43 (m, 1H), 4.24–4.33 (m, 1H), 3.85–4.00 (m, 3H), 3.74 (t, J = 8.9 Hz, 1H), 3.44 (s, 3H), 2.25 (t, J = 7.6 Hz, 2H), 1.59–1.72 (m, 2H), 1.17–1.38 (m, 24H), 0.88 (t, J = 6.8 Hz, 3H); ^{13}C NMR (100 MHz, $CDCl_3$) δ 174.5, 133.8,

132.3, 130.5, 129.9, 128.6, 126.3, 125.7, 125.0, 124.5, 124.1, 101.2, 99.0, 82.5, 70.8, 69.2, 62.4, 55.4, 54.0, 36.7, 31.9, 29.67, 29.63, 29.61, 29.5, 29.3, 29.2, 25.6, 22.7, 14.1. LC-MS m/z calculated for $C_{34}H_{52}NO_6$ $[M+H]^+$ 570.4 found 570.3.

Synthesis of compound 6: Cyclohexanecarbonoyl chloride (0.25 mmol, 1.1 equiv) was synthesized from cyclohexanecarboxylic acid (31 µL, 0.25 mmol, 1.1 equiv) and oxalyl chloride (26 µL, 0.30 mmol, 1.2 equiv). The crude acid chloride was dissolve in anhydrous DCM and added dropwise to a flask containing compound **IV** and pyridine (100 µL, 1.1 mmol, 5 equiv) dissolved in anhydrous DCM at 0 °C. The reaction stirred for 4 hours. The crude product was purified via column chromatography using DCM/hexanes 1:1 to 1.5% MeOH in DCM/Hexanes 1:1 to afford a white solid. Yield: 85.7 mg (85%) R_f = 0.33 in 1.5% MeOH in DCM/hexanes 1:1. mp = 219.6–221.3 °C. ^{1}H NMR (400 MHz, $CDCl_3$) δ 8.17 (d, J = 8.4 Hz, 1H), 7.85 (d, J = 7.4 Hz, 2H), 7.77 (d, J = 6.6 Hz, 1H), 7.42–7.56 (m, 3H), 6.12 (s, 1H), 5.85 (d, J = 8.6 Hz, 1H), 4.75 (d, J = 3.8 Hz, 1H), 4.33–4.38 (m, 1H), 4.22–4.32 (m, 1H), 3.86–4.00 (m, 1H), 3.73 (t, J = 9.1 Hz, 1H), 3.44 (s, 3H), 2.16 (tt, J = 11.6, 3.5 Hz, 1H), 1.61–1.95 (m, 5H), 1.39–1.54 (m, 2H), 1.15-1.36 (m, 3H); ^{13}C NMR (100 MHz, $CDCl_3$) δ 177.6, 133.8, 132.3, 130.5, 129.8, 128.6, 126.3, 125.7, 125.0, 124.5, 124.1, 101.2, 99.0, 82.5, 71.0, 69.2, 62.4, 55.4, 53.8, 45.4, 29.6, 25.7, 25.64, 25.61. LC-MS m/z calculated for $C_{25}H_{32}NO_6$ $[M+H]^+$ 442.2 found 442.2.

Synthesis of compound 7: Trichloroacetic anhydride (46 µL, 0.25 mmol, 1.1 equiv) was dissolved in anhydrous DCM and added dropwise to a flask containing compound **IV** and triethylamine (100 µL, 0.69 mmol, 3 equiv) dissolved in anhydrous DCM at 0 °C. The reaction was warmed to room temperature and stirred for 1 hour. Crude product was purified via column chromatography (SiO_2) using 10-40% EtOAc/hexanes to afford a white solid. Yield: 97.1 mg (93%). R_f = 0.44 in 25% EtOAc/hexanes. mp = 200.5–201.9 °C. ^{1}H NMR (400 MHz, $CDCl_3$) δ

8.17 (d, *J* = 8.1 Hz, 1H), 7.87 (d, *J* = 7.9 Hz, 2H), 7.75 (d, *J* = 6.9 Hz, 1H), 7.43–7.56 (m, 3H), 6.92 (d, *J* = 8.7, 1H), 6.10 (s, 1H), 4.87 (d, *J* = 3.7 Hz, 1H), 4.36–4.42 (m, 1H), 4.18–4.26 (m, 1H), 4.05 (t, *J* = 9.6 Hz, 1H), 3.84–3.99 (m, 2H), 3.72 (t, *J* = 9.1 Hz, 1H), 3.47 (s, 3H); ^{13}C NMR (100 MHz, $CDCl_3$) δ 162.4, 133.8, 132.1, 130.4, 130.0, 128.6, 126.4, 125.8, 125.0, 124.5, 124.0, 101.3, 98.4, 92.4, 82.1, 69.8, 69.1, 55.7, 55.5. MS m/z calculated for $C_{20}H_{21}Cl_3NO_6$ $[M+H]^+$ 476.0 found 476.0.

Synthesis of compound 8: Trifluoroacetic anhydride (34 µL, 0.25 mmol, 1.1 equiv) was dissolved in anhydrous DCM and added dropwise to a flask containing compound **IV** and triethylamine (100 µL, 0.69 mmol, 3 equiv) dissolved in anhydrous DCM at 0 °C. The reaction was warmed to room temperature and stirred for 4 hours. The crude product was purified via column chromatography (SiO_2) using 10-40% EtOAc/hexanes afford a white solid. Yield: 89.0 mg (95%). R_f = 0.34 in 25% EtOAc/hexanes. mp = 189.8–192.1 °C. ^{1}H NMR (400 MHz, $CDCl_3$) δ 8.15 (d, *J* = 8.2 Hz, 1H), 7.87 (d, *J* = 7.9 Hz, 2H), 7.74 (d, *J* = 7.0 Hz, 1H), 7.43–7.58 (m, 3H), 6.54 (d, *J* = 8.8, 1H), 6.10 (s, 1H), 4.83 (d, *J* = 3.7 Hz, 1H), 4.36–4.43 (m, 1H), 4.29 (dt, *J* = 9.6, 3.7 Hz, 1H), 4.00 (t, *J* = 9.7 Hz, 1H), 3.84–3.97 (m, 2H), 3.71 (t, *J* = 9.0 Hz, 1H), 3.46 (s, 3H); ^{13}C NMR (100 MHz, $CDCl_3$) δ 158.0, 157.7, 157.3, 156.9, 133.9, 132.0, 130.4, 130.0, 128.7, 126.4, 125.8, 125.0, 124.5, 124.0, 120.1, 117.2, 114.4, 111.5, 101.3, 98.2, 82.0, 69.6, 69.1, 62.6, 55.6, 54.0. MS m/z calculated for $C_{20}H_{21}F_3NO_6$ $[M+H]^+$ 428.1 found 428.1.

Synthesis of compound 9: Benzoyl chloride (40 µL, 0.253 mmol, 1.1 equiv) was dissolved in anhydrous THF and added dropwise to a flask containing compound **IV** and pyridine (60 µL, 0.69 mmol, 3 equiv) dissolved in anhydrous THF at 0 °C. The reaction stirred for 6 hours. The crude product was purified via column chromatography using pure DCM to 3% MeOH/DCM to afford a white solid. Yield: 72.9 mg (74%). R_f = 0.67 in 5% MeOH/DCM. mp = 251.5–253.8 °C.

^{1}H NMR (400 MHz, $CDCl_3$) δ 8.20 (d, J = 8.3 Hz, 1H), 7.57–7.90 (mm, 5H), 7.42–7.60 (m, 6H), 6.51 (d, J = 8.9, 1H), 6.15 (s, 1H), 4.89 (d, J = 3.8 Hz, 1H), 4.47–4.58 (m, 1H), 4.35–4.45 (m, 1H), 4.08 (t, J = 9.7 Hz, 1H), 3.89–4.03 (m, 2H), 3.81 (t, J = 9.1 Hz, 1H), 3.48 (s, 3H); ^{13}C NMR (100 MHz, $CDCl_3$) δ 168.4, 133.9, 133.8, 132.3, 131.9, 130.5, 129.9, 128.7, 128.6, 127.2, 126.4, 125.7, 125.0, 124.6, 124.1, 101.3, 98.1, 82.6, 70.8, 69.2, 62.5, 55.5, 54.4. LC-MS m/z calculated for $C_{25}H_{26}NO_6$ $[M+H]^+$ 436.2 found 436.2.

Synthesis of compound 10: 1-napthoyl chloride (50 µL, 0.25 mmol, 1.1 equiv) was dissolved in anhydrous THF and added dropwise to a flask containing compound **IV** and pyridine (60 µL, 0.69 mmol, 3 equiv) dissolved in anhydrous THF at 0 °C. The reaction stirred for 8 hours. The crude product was purified via column chromatography using pure DCM to 3% MeOH/DCM, to afford a light-yellow solid. Yield: 102.9 g (93%) R_f = 0.53 in 5% MeOH/DCM. mp = 227.0–229.0 °C. ^{1}H NMR (400 MHz, $CDCl_3$) δ 8.35 (d, J = 7.1, 1H), 8.20 (d, J = 8.5 Hz, 1H), 7.94 (d, J = 8.3, 1H), 7.84–7.90 (m, 3H), 7.79 (d, J = 7.1 Hz, 1 H), 7.65–7.69 (m, 1H), 7.44–7.58 (m, 6H), 6.35 (d, J = 8.9, 1H), 6.17 (s, 1H), 4.98 (d, J = 3.8 Hz, 1H), 4.64 (td, J = 9.6, 3.8 Hz, 1H), 4.39–4.47 (m, 1H), 4.10 (t, J = 9.7 Hz, 1H), 3.93–4.02 (m, 2H), 3.81–3.87 (m, 1H), 3.47 (s, 3H); ^{13}C NMR (100 MHz, $CDCl_3$) δ 170.5, 133.9, 133.8, 133.7, 132.2, 130.9, 130.5, 129.9, 128.6, 128.3, 127.3, 126.5, 126.4, 125.7, 125.3, 125.2, 125.0, 124.7, 124.5, 124.0, 101.1, 98.1, 82.6, 70.8, 69.2, 62.6, 55.5, 54.4. MS m/z calculated for $C_{29}H_{28}NO_6$ $[M+H]^+$ 486.2 found 486.2.

General procedure for the synthesis of urea derivatives 11-17: The urea derivatives were synthesized using the corresponding isocyanates. In general, compound **IV** (1 equiv) was dissolved in anhydrous THF in a dried 50 mL round bottomed flask under nitrogen atmosphere. The temperature was reduced to 0 °C via an ice bath. The isocyanates were dissolved in anhydrous THF (1 mL) and added dropwise to the reaction mixture. The ice bath was then removed and the

reaction mixture warmed to room temperature. Reactions typically stirred at room temperature for 4-6 hours. Reaction progress was monitored via ^{1}H NMR and TLC. After completion, THF was removed under reduced pressure. The crude products were the purified via column chromatography using gradient solvent systems, recrystallization in ethanol, or trituration with ethanol or acetone. The detailed preparation for compound **11** is provided below and only amounts used and characterization data are provided for all other compounds. All compounds were synthesized using 75 mg (0.23 mmol) of compound **IV**.

Synthesis of compound 11: Compound **IV** (74.5 mg, 0.23 mmol, 1.0 equiv) was dissolved in anhydrous THF (3 mL) in a dried nitrogen flushed 50 mL round bottomed flask. The temperature was reduced to 0 °C via an ice bath. Pentyl isocyanate (29 µL, 0.23 mmol, 1.0 equiv) was dissolved in anhydrous THF (1 mL) and added dropwise to the reaction mixture. The ice bath was then removed and the reaction mixture was warmed to room temperature. The reaction stirred for 6 hours. THF was removed under reduced pressure. The crude product was purified via column chromatography using pure DCM to 5% MeOH/DCM to afford a white solid. Yield: 77.3 mg (77%). R_f = 0.19 in 1% MeOH/DCM. mp = 293.8–295.5 °C. ^{1}H NMR (400 MHz, d_6-DMSO) δ 8.31 (d, J = 7.6 Hz, 1H), 7.94 (d, J = 7.8 Hz, 2H), 7.70 (d, J = 6.9 Hz, 1H), 7.45–7.62 (m, 3H), 6.18 (s, 1H), 6.00-6.10 (m, 1H), 5.75 (d, J = 8.3 Hz, 1H), 5.15 (d, J = 5.8 Hz, 1H), 4.66 (d, J = 3.08 Hz, 1H), 4.20–4.30 (m, 1H), 3.91 (t, J = 10.0 Hz, 1H), 3.67–3.79 (m, 2H), 3.65 (t, J = 9.1, 1H), 3.50–3.59 (m, 1H), 3.34 (s, 3H), 2.94–3.03 (m, 2H), 1.16–1.44 (m, 6H), 0.86 (t, J = 6.7, 3H). ^{13}C NMR (100 MHz, d_6-DMSO) δ 157.9, 133.3, 133.1, 130.1, 129.3, 128.2, 126.0, 125.7, 124.9, 124.8, 124.6, 100.4, 99.6, 82.3, 68.6, 68.3, 62.6, 54.8, 54.7, 29.6, 28.5, 21.8, 13.9. LC-MS m/z calculated for $C_{24}H_{33}N_2O_6$ $[M+H]^+$ 445.2 found 445.2.

Synthesis of compound 12: Hexyl isocyanate (32 µL, 0.23 mmol, 1 equiv) was dissolved in anhydrous THF and added dropwise to a flask containing compound IV dissolved in anhydrous THF at 0 °C. The reaction warmed to room temperature and stirred for 6 hours. The crude product was purified via recrystallization in reagent alcohol and the mother liquor was further purified via column chromatography using pure DCM to 3% MeOH/DCM. Yield: 89.3 mg (89%). R_f = 0.16 in 1% MeOH/DCM. mp = 289.3–292.1 °C. ^{1}H NMR (400 MHz, $CDCl_3$) δ 8.19 (d, J = 8.4 Hz, 1H), 7.84 (d, J = 8.1 Hz, 2H), 7.75 (d, J = 6.9 Hz, 1H), 7.40–7.56 (m, 3H), 6.10 (s, 1H), 4.88 (d, J = 8.0 Hz, 1H), 4.78–4.83 (m, 1H), 4.76 (d, J = 3.6 Hz, 1H), 4.31–4.43 (m, 1H), 3.84–4.04 (m, 4H), 3.67–3.77 (m, 1H) 3.43 (s, 3H), 3.06–3.24 (m, 2H), 1.40–1.54 (m, 2H), 1.20–1.38 (m, 6H), 0.88 (t, J = 6.8 Hz, 3H); ^{13}C NMR (100 MHz, $CDCl_3$) δ 158.8, 133.8, 132.4, 130.5, 129.8, 128.5, 126.3, 125.7, 125.0, 124.7, 124.2, 101.3, 99.5, 82.5, 71.5, 69.2, 62.4, 55.4, 55.3, 40.8, 31.5, 30.0, 26.5, 22.5, 14.0. LC-MS m/z calculated for $C_{25}H_{35}N_2O_6$ $[M+H]^+$ 459.2 found 459.2.

Synthesis of compound 13: Heptyl isocyanate (38 µL, 0.23 mmol, 1 equiv) was dissolved in anhydrous THF and added dropwise to a flask containing compound IV dissolved in anhydrous THF at 0 °C. The reaction warmed to room temperature and stirred for 5 hours. The crude product was purified via trituration in reagent alcohol to afford a white solid. Yield: 95.6 mg (96%). R_f = 0.21 in 1% MeOH/DCM. mp = 281.7–283.3 °C. ^{1}H NMR (400 MHz, $CDCl_3$) δ 8.19 (d, J = 8.4 Hz, 1H), 7.85 (d, J = 8.4 Hz, 2H), 7.76 (d, J = 7.2 Hz, 1H), 7.42–7.55 (m, 3H), 6.12 (s, 1H), 4.79 (d, J = 3.0 Hz, 1H), 4.34–4.43 (m, 1H), 3.85–4.00 (m, 4H), 3.66–3.77 (m, 1H) 3.46 (s, 3H), 3.18 (td, J = 7.1, 2.5 Hz, 2H), 1.42-1.58 (m, 2H), 1.16–1.38 (m, 4H), 0.88 (t, J = 6.9 Hz, 3H); ^{13}C NMR (100 MHz, $CDCl_3$) δ 158.8, 133.8, 132.3, 130.5, 129.8, 128.5, 126.3, 125.7, 125.0, 124.7, 124.2, 101.3, 99.5, 82.5, 71.5, 69.2, 62.4, 55.4, 55.3, 40.7, 31.7, 30.0, 28.8, 26.5, 22.6, 14.0. LC-MS m/z calculated for $C_{26}H_{37}N_2O_6$ $[M+H]^+$ 473.3 found 473.2.

Synthesis of compound 14: 2-chloroethyl isocyanate (20 µL, 0.23 mmol, 1 equiv) was dissolved in anhydrous THF and added dropwise to a flask containing compound **IV** dissolved in anhydrous THF at 0 °C. The reaction warmed to room temperature and stirred for 5 hours. The crude product was purified via trituration with acetone to afford a white solid. Yield: 85.8 mg (85%). R_f = 0.12 in 1% MeOH/DCM. mp = 214.3–216.4 °C. ^{1}H NMR (400 MHz, d_6-DMSO) δ 8.31 (d, J = 7.4 Hz, 1H), 7.94 (d, J = 8.3 Hz, 2H), 7.70 (d, J = 7.1 Hz, 1H), 7.48–7.59 (m, 3H), 6.37 (t, J = 5.8 Hz, 1H), 6.18 (s, 1H), 6.06 (d, J = 8.6 Hz, 1H), 5.16 (d, J = 6.0 Hz, 1H), 4.67 (d, J = 3.6 Hz, 1H), 4.22–4.29 (m, 1H), 3.91 (t, J = 10.1 Hz, 1H), 3.70–3.79 (m, 2H), 3.65 (t, J = 9.2, 1H), 3.52–3.61 (m, 3H), 3.32–3.37 (m, 5H). ^{13}C NMR (100 MHz, d_6-DMSO) δ 157.7, 133.3, 133.1, 130.1, 129.3, 128.2, 126.0, 125.7, 124.9, 124.8, 124.6, 100.4, 99.5, 82.3, 68.4, 68.3, 62.6, 54.8, 54.7, 42.7, 41.4. LC-MS m/z calculated for $C_{21}H_{26}ClN_2O_6$ $[M+H]^+$ 437.1 found 437.1.

Synthesis of compound 15: Cyclohexyl isocyanate (28 µL, 0.23 mmol, 1 equiv) was dissolved in anhydrous THF and added dropwise to a flask containing compound IV dissolved in anhydrous THF at 0 °C. The reaction warmed to room temperature and stirred for 3 hours. The crude product was purified via trituration with acetone to afford a white solid. Yield: 88.9 mg (89%). R_f = 0.18 in 1% MeOH/DCM. mp = 309.1–311.5 °C. ^{1}H NMR (400 MHz, d_6-DMSO) δ 8.31 (d, J = 7.8 Hz, 1H), 7.94 (d, J = 8.5 Hz, 2H), 7.70 (d, J = 7.0 Hz, 1H), 7.45–7.60 (m, 3H), 6.18 (s, 1H), 6.03 (d, J = 7.8 Hz, 1H), 5.71 (d, J = 8.5 Hz, 1H), 5.17 (d, J = 5.9 Hz, 1H), 4.66 (d, J = 3.6 Hz, 1H), 4.19–4.32 (m, 1H), 3.91 (t, J = 10.1 Hz, 1H), 3.68–3.78 (m, 2H), 3.65 (t, J = 9.2, 1H), 3.49–3.58 (m, 1H), 3.34–3.38 (m, 4H), 1.44–1.86 (m, 5H), 0.97–1.37 (m, 5H). ^{13}C NMR (100 MHz, d_6-DMSO) δ 157.3, 133.3, 133.1, 130.1, 129.3, 128.2, 126.0, 125.7, 124.9, 124.8, 124.6, 100.4, 99.6, 82.3, 68.7, 68.3, 62.6, 54.8, 54.6, 47.7, 33.22, 33.19, 25.3, 24.3. LC-MS m/z calculated for $C_{25}H_{33}N_2O_6$ $[M+H]^+$ 457.2 found 457.2.

Synthesis of compound 16: Phenyl isocyanate (25 µL, 0.23 mmol, 1 equiv) was dissolved in anhydrous THF and added dropwise to a flask containing compound IV dissolved in anhydrous THF at 0 °C. The reaction warmed to room temperature and stirred for 4 hours. The crude product was purified via trituration with acetone to afford a white solid. Yield: 96.9 mg (94%). R_f = 0.23 in 5% MeOH/DCM. mp = 285.8–288.3 °C. ^{1}H NMR (400 MHz, d_6-DMSO) δ 8.63 (s, 1H), 8.32 (d, *J* = 8.0 Hz, 1H), 7.95 (d, *J* = 7.7 Hz, 2H), 7.73 (d, *J* = 6.9 Hz, 1H), 7.48–7.61 (m, 3H), 7.38 (d, *J* = 8.5 Hz, 2H), 7.22 (t, *J* = 7.9 Hz, 2 H), 6.89 (t, *J* = 7.3 Hz, 1H), 6.21 (s, 1H), 6.12 (d, *J* = 8.8 Hz, 1H), 5.28 (d, *J* = 6.0 Hz, 1H), 4.75 (d, *J* = 3.6 Hz, 1H), 4.22–4.32 (m, 1H), 3.94 (t, *J* = 10.0 Hz, 1H), 3.74–3.88 (m, 2H), 3.71 (t, *J* = 9.1, 1H), 3.55–3.66 (m, 1H), 3.83 (s, 3H), ^{13}C NMR (100 MHz, d_6-DMSO) δ 154.9, 140.3, 133.3, 133.1, 130.1, 129.3, 128.7, 128.2, 126.0, 125.7, 124.9, 124.8, 124.6, 121.0, 117.4, 100.4, 99.4, 82.1, 68.5, 68.3, 62.8, 54.8, 54.4. LC-MS m/z calculated for $C_{25}H_{27}N_2O_6$ $[M+H]^+$ 451.2 found 451.1.

Synthesis of compound 17: 4-fluorophenyl isocyanate (24 µL, 0.23 mmol, 1.0 equiv) was dissolved in anhydrous THF and added dropwise to a flask containing compound IV dissolved in anhydrous THF at 0 °C. The reaction warmed to room temperature and stirred for 5 hours. The crude product was purified via recrystallization in reagent alcohol and the mother liquor was purified via column chromatography using 3:6:1 DCM/hexanes/acetone to 3:6:2: DCM/hexanes/acetone to afford a white solid. Yield: 84.8 mg (84%). R_f = 0.36 in 3:6:2: DCM/hexanes/acetone (also, R_f = 0.12 in 1% MeOH/DCM). mp = 288.5–290.1 °C. ^{1}H NMR (400 MHz, d_6-DMSO) δ 8.67 (s, 1H), 8.32 (d, *J* = 8.0 Hz, 1H), 7.95 (d, *J* = 7.7 Hz, 2H), 7.72 (d, *J* = 6.4 Hz, 1H), 7.47–7.61 (m, 3H), 7.35–7.43 (m, 2H), 7.06 (t, *J* = 8.9 Hz, 2 H), 6.21 (s, 1H), 6.09 (d, *J* = 8.8 Hz, 1H), 5.19–5.40 (m, 1H), 4.74 (d, *J* = 3.6 Hz, 1H), 4.22–4.33 (m, 1H), 3.94 (t, *J* = 10.0 Hz, 1H), 3.74–3.87 (m, 2H), 3.70 (t, *J* = 9.1, 1H), 3.57–3.66 (m, 1H), 3.38 (s, 3H), ^{13}C NMR

(100 MHz, d_6-DMSO) δ 158.0, 155.7, 154.9, 136.7, 136.6, 133.3, 133.1, 130.1, 129.3, 128.2, 126.0, 125.7, 124.9, 124.8, 124.6, 119.0, 118.9, 115.2, 115.0, 100.4, 99.4, 82.1, 68.5, 68.3, 62.8, 54.8, 54.4. LC-MS m/z calculated for $C_{25}H_{26}FN_2O_6$ $[M+H]^+$ 469.2 found 469.2.

Synthesis of compound 18: Benzyl isocyanate (26 µL, 0.215 mmol, 1 equiv) was dissolved in anhydrous THF and added dropwise to a flask containing compound IV dissolved in anhydrous THF at 0 °C. The reaction warmed to room temperature and stirred for 5 hours. The crude product was purified via trituration in reagent alcohol to afford a white solid. Yield: 84.8 mg (85%). R_f = 0.19 in 1% MeOH/DCM. mp = 298.3–299.8 °C. ^{1}H NMR (400 MHz, d_6-DMSO) δ 8.31 (d, J = 7.8 Hz, 1H), 7.94 (d, J = 8.1 Hz, 2H), 7.71 (d, J = 6.7 Hz, 1H), 7.47–7.60 (m, 3H), 7.18–7.37 (m, 5H), 6.53 (t, J = 5.9 Hz, 1 H), 6.19 (s, 1H), 5.92 (d, J = 8.6 Hz, 1H), 5.18 (d, J = 6.0 Hz, 1H), 4.69 (d, J = 3.6 Hz, 1H), 4.33 (t, J = 5.1 Hz, 1H), 4.18–4.29 (m, 3H), 3.92 (t, J = 10.0 Hz, 1H), 3.71–3.83 (m, 2H), 3.67 (t, J = 9.1, 1H), 3.53–3.62 (m, 1H), 3.44 (qd, J = 7.0, 5.1 Hz, 1H), 3.35 (s, 3H). ^{13}C NMR (100 MHz, d_6-DMSO) δ 158.0, 140.6, 133.3, 133.1, 130.1, 129.3, 128.2, 128.1, 127.0, 126.5, 126.0, 125.7, 124.9, 124.8, 124.6, 100.4, 99.6, 82.3, 68.6, 68.3, 56.0, 54.9, 54.8, 42.9. LC-MS m/z calculated for $C_{26}H_{29}N_2O_6$ $[M+H]^+$ 465.2 found 465.2.

General procedure for the synthesis of carbamate derivatives 19-29: The carbamate derivatives were synthesized using the corresponding chloroformates. In general, compound IV (1 equiv) was dissolved in anhydrous DCM in a dried 50 mL round bottomed flask under nitrogen atmosphere. Either triethylamine (TEA, 2 equiv), potassium carbonate (K_2CO_3, 2 equiv) or diisopropylethylamine (DIEA, 3 equiv) was added to the reaction mixture and the temperature was reduced to 0 °C via an ice bath. The chloroformates were then dissolved in anhydrous DCM (1 mL) and added dropwise to the reaction mixture. The ice bath was then removed, and the reaction mixture warmed to room temperature. Reactions typically stirred at room temperature for 1-4

hours. Reaction progress was monitored via ^{1}H NMR and TLC. After completion, the reaction mixture was diluted with DCM and underwent aqueous workups using saturated $NaHCO_3$ solution, DI water (x 2) and DCM (x 2). The combined organic layers were dried over Na_2SO_4 and solvent was removed under reduced pressure. The crude products were purified through column chromatography using a gradient solvent system. The detailed preparation for compound **19** is provided below and only amounts used and characterization data are provided for all other compounds. All compounds were synthesized using 75–100 mg (0.23-0.30 mmol) of compound

Synthesis of compound 19: Compound IV (81.0 mg, 0.24 mmol, 1.0 equiv) was dissolved in anhydrous DCM (3 mL) in a 50 mL round bottomed flask. TEA (68 µL, 0.48 mmol, 2.0 equiv) was added to the reaction mixture and the temperature was reduced to 0 °C using an ice bath. Ethyl chloroformate (25 µL, 0.26 mmol, 1.1 equiv) was dissolved in anhydrous DCM (1 mL) and added dropwise to the reaction mixture. The reaction was warmed to room temperature and stirred for 2 hours. The reaction mixture was diluted with DCM (10 mL) and washed with saturated $NaHCO_3$ solution (10 mL) and DI water (10 mL x 2). The aqueous layers were then back extracted with DCM (10 mL x 2). The organic layers were combined, dried over Na_2SO_4, filtered and solvent was removed under reduced pressure. The crude product was purified via column chromatography using 20-50% EtOAc/hexanes to afford a white solid. Yield: 92.1 mg (95%). R_f = 0.50 in 50% EtOAc/hexanes. mp = 181.6–183.2 °C. ^{1}H NMR (400 MHz, $CDCl_3$) δ 8.18 (d, J = 8.4 Hz, 1H), 7.86 (d, J = 8.0 Hz, 2H), 7.76 (d, J = 7.0 Hz, 1H), 7.42–7.56 (m, 3H), 6.11 (s, 1H), 5.04 (d, J = 6.2 Hz, 1H), 4.78 (d, J = 3.4 Hz, 1H), 4.33–4.46 (m, 1H), 4.16 (q, J = 7.1 Hz, 2H), 3.85–4.04 (m, 4H), 3.72 (t, J = 8.9 Hz, 1H), 3.44 (s, 3H), 1.27 (t, J = 7.1 Hz, 3H). ^{13}C NMR (100 MHz, $CDCl_3$) δ 157.0, 133.9, 132.2, 130.5, 129.9, 128.6, 126.4, 125.7, 125.0, 124.6, 124.1, 101.5, 99.4, 82.4,

70.5, 69.2, 62.5, 61.4, 55.5, 14.5. LC-MS m/z calculated for $C_{21}H_{26}NO_7$ $[M+H]^+$ 404.2 found 404.2.

Synthesis of compound 20: Allyl chloroformate (27 µL, 0.24 mmol, 1.0 equiv) was dissolved in anhydrous DCM and added dropwise to a flask containing compound IV (80.2 mg, 0.24 mmol, 1.0 equiv) dissolved anhydrous DCM with K_2CO_3 (70.2 mg, 0.50 mmol, 2.2 equiv) at 0 °C. The reaction warmed to room temperature and stirred for 4 hours. The crude product was purified via column chromatography using 20-50% EtOAc/hexanes to afford a white solid. Yield: 89.3 mg (85%). R_f = 0.34 in 40% EtOAc/hexanes. mp = 169.5–172.6 °C. ^{1}H NMR (400 MHz, $CDCl_3$) δ 8.18 (d, *J* = 8.4 Hz, 1H), 7.85 (d, *J* = 7.9 Hz, 2H), 7.75 (d, *J* = 7.0 Hz, 1H), 7.43–7.56 (m, 3H), 6.10 (s, 1H), 5.86–5.99 (m, 1H), 5.32 (dd, *J* = 17.2, 1.3 Hz, 1H), 5.23 (dd, *J* = 10.4, 1.2 Hz, 1H), 5.13 (d, *J* = 9.2 Hz, 1H), 4.77 (d, *J* = 3.5 Hz, 1H), 4.69–7.75 (m, 2H), 4.60 (d, *J* = 5.4, 1H), 4.34–4.42 (m, 1H), 3.85–4.03 (m, 4H), 3.70 (t, *J* = 8.9 Hz, 1H), 3.43 (s, 3H). ^{13}C NMR (100 MHz, $CDCl_3$) δ 156.6, 133.8, 132.5, 132.2, 130.4, 129.9, 128.6, 126.4, 125.7, 125.0, 124.5, 124.1, 118.1, 101.2, 99.3, 82.4, 70.4, 69.2, 66.1, 62.5, 55.6, 55.5. LC-MS m/z calculated for $C_{22}H_{26}NO_7$ $[M+H]^+$ 416.2 found 416.2.

Synthesis of compound 21: N-butyl chloroformate (30 µL, 0.26 mmol, 1.1 equiv) was dissolved in anhydrous DCM and added dropwise to a flask containing compound IV (78.2 mg, 0.24 mmol, 1.0 equiv) dissolved anhydrous DCM with K_2CO_3 (65.2 mg, 0.48 mmol, 2.0 equiv) at 0 °C. The reaction warmed to room temperature and stirred for 4 hours. The crude product was purified via column chromatography using 20-50% EtOAc/hexanes to afford a white solid. Yield: 85.7 mg (85%). R_f = 0.44 in 40% EtOAc/hexanes. mp = 159.9–162.6 °C. ^{1}H NMR (400 MHz, $CDCl_3$) δ 8.18 (d, *J* = 8.4 Hz, 1H), 7.85 (d, *J* = 8.0 Hz, 2H), 7.76 (d, *J* = 6.9 Hz, 1H), 7.40–7.58 (m, 3H), 6.09 (s, 1H), 5.04 (d, *J* = 7.1 Hz, 1H), 4.76 (d, *J* = 3.3 Hz, 1H), 4.33–4.43 (m, 1H), 4.10

(t, *J* = 6.6 Hz, 2H), 3.83–4.02 (m, 4H), 3.70 (t, *J* = 8.9 Hz, 1H), 3.43 (s, 3H), 1.55–1.71 (m, 2H), 1.32–1.44 (m, 2H), 0.94 (t, *J* = 7.4 Hz, 3H). ^{13}C NMR (100 MHz, $CDCl_3$) δ 157.1, 133.8, 133.2, 130.5, 129.9, 128.6, 126.3, 125.7, 125.0, 124.5, 124.1, 101.2, 99.3, 82.4, 70.5, 69.2, 65.4, 62.4, 55.6, 55.5,31.0, 19.0, 13.7. LC-MS m/z calculated for $C_{23}H_{30}NO_7$ $[M+H]^+$ 432.2 found 432.3.

Synthesis of compound 22: Octyl chloroformate (63 µL, 0.32 mmol, 1.1 equiv) was dissolved in anhydrous DCM and added dropwise to a flask containing compound IV (100.7 mg, 0.30 mmol, 1 equiv) dissolved anhydrous DCM and DIEA (160 µL, 0.90 mmol, 3.0 equiv) at 0 °C. The reaction warmed to room temperature and stirred for 1 hour. The crude product was purified via column chromatography using 20-50% EtOAc/hexanes to afford a white solid. Yield: 124.1 mg (97%). R_f = 0.32 in 25% EtOAc/hexanes. mp = 139.3–140.7 °C. ^{1}H NMR (400 MHz, $CDCl_3$) δ 8.18 (d, *J* = 8.3 Hz, 1H), 7.85 (d, *J* = 8.0 Hz, 2H), 7.76 (d, *J* = 7.1 Hz, 1H), 7.42–7.57 (m, 3H), 6.09 (s, 1H), 5.05 (d, *J* = 8.0 Hz, 1H), 4.76 (d, *J* = 3.0 Hz, 1H), 4.33–4.42 (m, 1H), 4.08 (t, *J* = 6.6 Hz, 2H), 3.82–4.02 (m, 4H), 3.70 (t, *J* = 8.7 Hz, 1H), 3.42 (s, 3H), 1.54–1.70 (m, 2H), 1.18–1.41 (m, 10H), 0.89 (t, *J* = 6.6 Hz, 3H). ^{13}C NMR (100 MHz, $CDCl_3$) δ 157.1, 133.8, 133.2, 130.4, 129.9, 128.6, 126.3, 125.7, 125.0, 124.5, 124.1, 101.2, 99.3, 82.4, 70.4, 69.2, 65.7, 62.4, 55.6, 55.5, 31.8, 29.2, 29.1, 28.9,22.6, 14.0. LC-MS m/z calculated for $C_{27}H_{38}NO_7$ $[M+H]^+$ 488.3 found 488.3.

Synthesis of compound 23: 2.0 M isopropyl chloroformate (160 µL, 0.32 mmol, 1.1 equiv) was dissolved in anhydrous DCM and added dropwise to a flask containing compound IV (100.1 mg, 0.30 mmol, 1 equiv) dissolved in anhydrous DCM and DIEA (160 µL, 0.90 mmol, 3.0 equiv) at 0 °C. The reaction warmed to room temperature and stirred for 1 hour. The crude product was purified via column chromatography using 20-50% EtOAc/hexanes to afford a white solid. Yield: 122.1 mg (98%). R_f = 0.52 in 50% EtOAc/hexanes. mp 234.8–236.4 °C. ^{1}H NMR (400

MHz, $CDCl_3$) δ 8.18 (d, J = 8.3 Hz, 1H), 7.85 (d, J = 8.0 Hz, 2H), 7.76 (d, J = 7.0 Hz, 1H), 7.42–7.56 (m, 3H), 6.10 (s, 1H), 4.84–5.09 (m, 2H), 4.76 (d, J = 3.3 Hz, 1H), 4.30–4.44 (m, 1H), 3.83–4.03 (m, 4H), 3.71 (t, J = 8.9 Hz, 1H), 3.43 (s, 3H), 1.22–1.29 (m, 6H). ^{13}C NMR (100 MHz, $CDCl_3$) δ 156.7, 133.8, 132.3, 130.5, 129.9, 128.6, 126.3, 125.7, 125.0, 124.6, 124.1, 101.2, 99.4, 82.4, 70.6, 69.2, 68.9, 62.4, 55.5, 22.1, 22.0. LC-MS m/z calculated for $C_{22}H_{28}NO_7$ $[M+H]^+$ 418.2 found 418.2.

Synthesis of compound 24: Isobutyl chloroformate (30 µL, 0.23 mmol, 1.0 equiv) was dissolved in anhydrous DCM and added dropwise to a flask containing compound IV (77.1 mg, 0.23 mmol, 1.0 equiv) dissolved anhydrous DCM with K_2CO_3 (69.7 mg, 0.48 mmol, 2.1 equiv) at 0 °C. The reaction warmed to room temperature and stirred for 4 hours. The crude product was purified via column chromatography using 20-60% EtOAc/hexanes to afford a white solid. Yield: 97.4 mg (94%). R_f = 0.54 in 50% EtOAc/hexanes. mp = 175.2–176.8 °C. ^{1}H NMR (400 MHz, $CDCl_3$) δ 8.18 (d, J = 8.3 Hz, 1H), 7.85 (d, J = 8.1 Hz, 2H), 7.76 (d, J = 7.1 Hz, 1H), 7.41–7.57 (m, 3H), 6.09 (s, 1H), 5.06 (d, J = 7.8 Hz, 1H), 4.76 (d, J = 3.2 Hz, 1H), 4.31–4.43 (m, 1H), 3.79–4.06 (m, 6H), 3.69 (t, J = 8.9 Hz, 1H), 3.42 (s, 3H),1.85-2.01 (m, 1H), 0.93 (d, J = 6.7 Hz, 6H). ^{13}C NMR (100 MHz, $CDCl_3$) δ 157.2, 133.8, 132.2, 130.4, 129.9, 128.6, 126.3, 125.7, 125.0, 124.5, 124.1, 101.2, 99.3, 82.4, 71.6, 70.4, 69.2, 62.4, 55.6, 55.4, 27.9, 19.0. LC-MS m/z calculated for $C_{23}H_{30}NO_7$ $[M+H]^+$ 432.2 found 432.2.

Synthesis of compound 25: 2,2,2-trichloroethyl chloroformate (44 µL, 0.32 mmol, 1.1 equiv) was dissolved in anhydrous DCM and added dropwise to a flask containing compound IV (100.0 mg, 0.30 mmol, 1 equiv) dissolved anhydrous DCM and DIEA (160 µL, 0.90 mmol, 3.0 equiv) at 0 °C. The reaction warmed to room temperature and stirred for 1 hour. The crude product was purified via column chromatography using 20-50% EtOAc/hexanes to afford a white solid.

Yield: 141.0 mg (94%). R_f = 0.72 in 50% EtOAc/hexanes. mp = 166.7–168.0 °C. ^{1}H NMR (400 MHz, $CDCl_3$) δ 8.17 (d, J = 8.2 Hz, 1H), 7.86 (d, J = 8.0 Hz, 2H), 7.75 (d, J = 7.0 Hz, 1H), 7.43–7.57 (m, 3H), 6.09 (s, 1H), 5.33 (d, J = 9.1 Hz, 1H), 4.67–4.87 (m, 3H), 4.32–4.44 (m, 1H), 3.84–4.06 (m, 4H), 3.66–3.74 (m, 1H), 3.44 (s, 3H). ^{13}C NMR (100 MHz, $CDCl_3$) δ 154.9, 133.8, 132.2, 130.4, 129.9, 128.6, 126.4, 125.8, 125.0, 124.5, 124.0, 101.2, 99.1, 82.3, 74.8, 70.2, 69.2, 62.4, 55.8, 55.5. LC-MS m/z calculated for $C_{21}H_{23}Cl_3NO_7$ $[M+H]^+$ 506.1 found 506.0.

Synthesis of compound 26: Phenyl chloroformate (40 µL, 0.32 mmol, 1.1 equiv) was dissolved in anhydrous DCM and added dropwise to a flask containing compound IV (100.3 mg, 0.30 mmol, 1 equiv) dissolved anhydrous DCM and DIEA (160 µL, 0.90 mmol, 3.0 equiv) at 0 °C. The reaction warmed to room temperature and stirred for 1 hour. The crude product was purified via column chromatography using 20-50% EtOAc/hexanes to afford a white solid. Yield: 115.0 mg (85%). R_f = 0.23 in 25% EtOAc/hexanes. mp = 201.2–203.4 °C. ^{1}H NMR (400 MHz, $CDCl_3$) δ 8.19 (d, J = 8.4 Hz, 1H), 7.86 (d, J = 8.1 Hz, 2H), 7.77 (d, J = 6.8 Hz, 1H), 7.44–7.59 (m, 3H), 7.32–7.40 (m, 2H), 7.13–7.24 (m, 3H), 6.12 (s, 1H), 5.40 (d, J = 8.0 Hz, 1H), 4.88 (d, J = 3.3, 1H), 4.38–4.43 (m, 1H), 3.87–4.11 (m, 4H), 3.74 (t, J = 8.9 Hz, 1H), 3.49 (s, 3H). ^{13}C NMR (100 MHz, $CDCl_3$) δ 154.9, 150.9, 133.8, 132.2, 130.4, 129.9, 129.3, 128.6, 126.4, 125.8, 125.5, 125.0, 124.6, 124.0, 101.3, 99.1, 82.4, 70.4, 69.2, 62.5, 55.8, 55.6. LC-MS m/z calculated for $C_{25}H_{26}NO_7$ $[M+H]^+$ 452.2 found 452.1.

Synthesis of compound 27: P-tolyl chloroformate (46 µL, 0.32 mmol, 1.1 equiv) was dissolved in anhydrous DCM and added dropwise to a flask containing compound IV (100.0 mg, 0.30 mmol, 1 equiv) dissolved anhydrous DCM and DIEA (160 µL, 0.90 mmol, 3.0 equiv) at 0 °C. The reaction warmed to room temperature and stirred for 1 hour. The crude product was purified via column chromatography using 20-50% EtOAc/hexanes to afford a white solid. Yield:

133.2 mg (95%). R_f = 0.46 in 50% EtOAc/hexanes. mp = 174.8–176.4 °C. ^{1}H NMR (400 MHz, $CDCl_3$) δ 8.19 (d, J = 8.3 Hz, 1H), 7.87 (d, J = 8.2 Hz, 2H), 7.77 (d, J = 7.1 Hz, 1H), 7.40–7.59 (m, 3H), 7.14 (d, J = 8.4 Hz, 2H), 7.04 (d, J = 8.03 Hz, 2H), 6.12 (s, 1H), 5.38 (d, J = 7.5 Hz, 1H), 4.87 (d, J = 2.9, 1H), 4.35–4.47 (m, 1H), 3.85–4.12 (m, 4H), 3.73 (t, J = 8.6 Hz, 1H), 3.48 (s, 3H), 2.33 (s, 3H). ^{13}C NMR (100 MHz, $CDCl_3$) δ 155.2, 148.7, 135.1, 133.8, 132.2, 130.4, 129.9, 129.8, 128.6, 126.4, 125.7, 125.0, 124.6, 124.0, 121.2, 101.3, 99.2, 82.4, 70.4, 69.2, 62.5, 55.8, 55.6, 20.8. LC-MS m/z calculated for $C_{26}H_{28}NO_7$ $[M+H]^+$ 466.2 found 466.1.

Synthesis of compound 28: 4-chlorophenyl chloroformate (45 µL, 0.32 mmol, 1.1 equiv) was dissolved in anhydrous DCM and added dropwise to a flask containing compound IV (101.1 mg, 0.30 mmol, 1 equiv) dissolved anhydrous DCM and DIEA (160 µL, 0.90 mmol, 3.0 equiv) at 0 °C. The reaction warmed to room temperature and stirred for 1 hour. The crude product was purified via column chromatography using 20-50% EtOAc/hexanes to afford a white solid. Yield: 130.3 mg (90%). R_f = 0.22 in 25% EtOAc/hexanes. mp = 183.9–185.6 °C. ^{1}H NMR (400 MHz, $CDCl_3$) δ 8.18 (d, J = 8.3 Hz, 1H), 7.87 (d, J = 8.2 Hz, 2H), 7.77 (d, J = 7.0 Hz, 1H), 7.44–7.58 (m, 3H), 7.31 (d, J = 8.8 Hz, 2H), 7.11 (d, J = 8.8 Hz, 2H), 6.12 (s, 1H), 5.39 (d, J = 8.1 Hz, 1H), 4.87 (d, J = 3.2, 1H), 4.36–4.44 (m, 1H), 3.85–4.10 (m, 4H), 3.74 (t, J = 8.8 Hz, 1H), 3.49 (s, 3H). ^{13}C NMR (100 MHz, $CDCl_3$) δ 154.5, 133.9, 132.2, 130.8, 130.4, 129.3, 128.7, 126.4, 125.8, 125.0, 124.5, 124.0, 122.8, 101.3, 99.1, 82.3, 70.3, 69.2, 62.5, 55.8, 55.6. LC-MS m/z calculated for $C_{25}H_{25}ClNO_7$ $[M+H]^+$ 486.1 found 486.1.

Synthesis of compound 29: Benzyl chloroformate (46 µL, 0.32 mmol, 1.5 equiv) was dissolved in anhydrous DCM and added dropwise to a flask containing compound IV (75.1 mg, 0.23 mmol, 1.0 equiv) dissolved in anhydrous DCM with K_2CO_3 (63.5 mg, 0.46 mmol, 2.0 equiv) at 0 °C. The reaction warmed to room temperature and stirred for 8 hours. The crude product was

purified via column chromatography using 20-50% EtOAc/hexanes to afford a white solid. Yield: 86.6 mg (81%). R_f = 0.44 in 40% EtOAc/hexanes. mp = 208.6–211.0°C. ^{1}H NMR (400 MHz, $CDCl_3$) δ 8.18 (d, J = 8.4 Hz, 1H), 7.86 (d, J = 8.1 Hz, 2H), 7.76 (d, J = 7.0 Hz, 1H), 7.43–7.56 (m, 3H), 7.30–7.40 (m, 5H), 6.10 (s, 1H), 5.06–5.23 (m, 3H), 4.77 (d, J = 3.2, 1H), 4.32–4.46 (m, 1H), 3.84–4.07 (m, 4H), 3.67–3.76 (m, 1H), 3.41 (s, 3H). ^{13}C NMR (100 MHz, $CDCl_3$) δ 156.7, 136.1, 133.8, 132.2, 130.4, 129.9, 128.6, 128.5, 128.3, 126.4, 125.7, 125.0, 124.5, 124.0, 101.2, 99.3, 82.4, 70.6, 69.2, 67.3, 62.4, 55.6, 55.5. LC-MS m/z calculated for $C_{26}H_{28}NO_7$ $[M+H]^+$ 466.2 found 466.2.

CHAPTER 3

SYNTHESIS AND CHARACTERIZATION OF 4,6-(4-CHLOROBENZYLIDENE) ACETAL PROTECTED GLUCOSAMINE DERIVATIVES AS LMWG'S

This chapter is adapted from the following paper: "Bietsch, J.; Olson, M.; Wang, G., Fine-Tuning of Molecular Structures to Generate Carbohydrate Based Super Gelators and Their Applications for Drug Delivery and Dye Absorption. *Gels* **2021**, *7*, 134, 10.3390/gels703013"

3.1 INTRODUCTION

Carbon bound halogen atoms act as electron acceptors, leading to strong non-covalent interactions with various electron donating species.[83] Due to having a similar strength to hydrogen bonding, these strong non-covalent interaction is termed "halogen bonding."[83] While hydrogen bonding is one of the most used widely used forces in supramolecular systems, halogen bonding can also be a powerful tool in driving self-assembly.[83] Like hydrogen bonding, halogen bonding can also play a vital role in stabilizing supramolecular microstructures.[83] Resnati et al. showed that under appropriate conditions, halogen bonding can be a more effective in driving the self-assembly of supramolecular architectures, compared to hydrogen bonding.[83] In their study, mixtures hydrogen bond donating molecules, hydrogen bond accepting molecules and halogen containing molecules were combined in appropriate solvents and allowed to form co-crystals. Single-crystal X-ray diffraction was then used to analyze intermolecular interactions. Competitive experiments were carried out to compare the strength of hydrogen versus halogen bonding, depicted in Figure 59. Molar equivalents of **a**, **b**, and **c** were dissolved in acetone in a sealed vial, which was then

placed in a larger bottle containing a small amount of Vaseline oil in order to grow co-crystals through diffusion. The resulting co-crystal consisted of **a** and **b**, with **c** remaining in the solution. This result indicates that halogen bonding out competed hydrogen bonding in the self-assembly of the supramolecular architecture. Additionally, the co-crystals formed by **a** and **b** melt at a much higher temperature than the co-crystals formed by **a** and **c**, indicating that halogen bonding can provide increased stabilization of supramolecular architecture compared to hydrogen bonding.

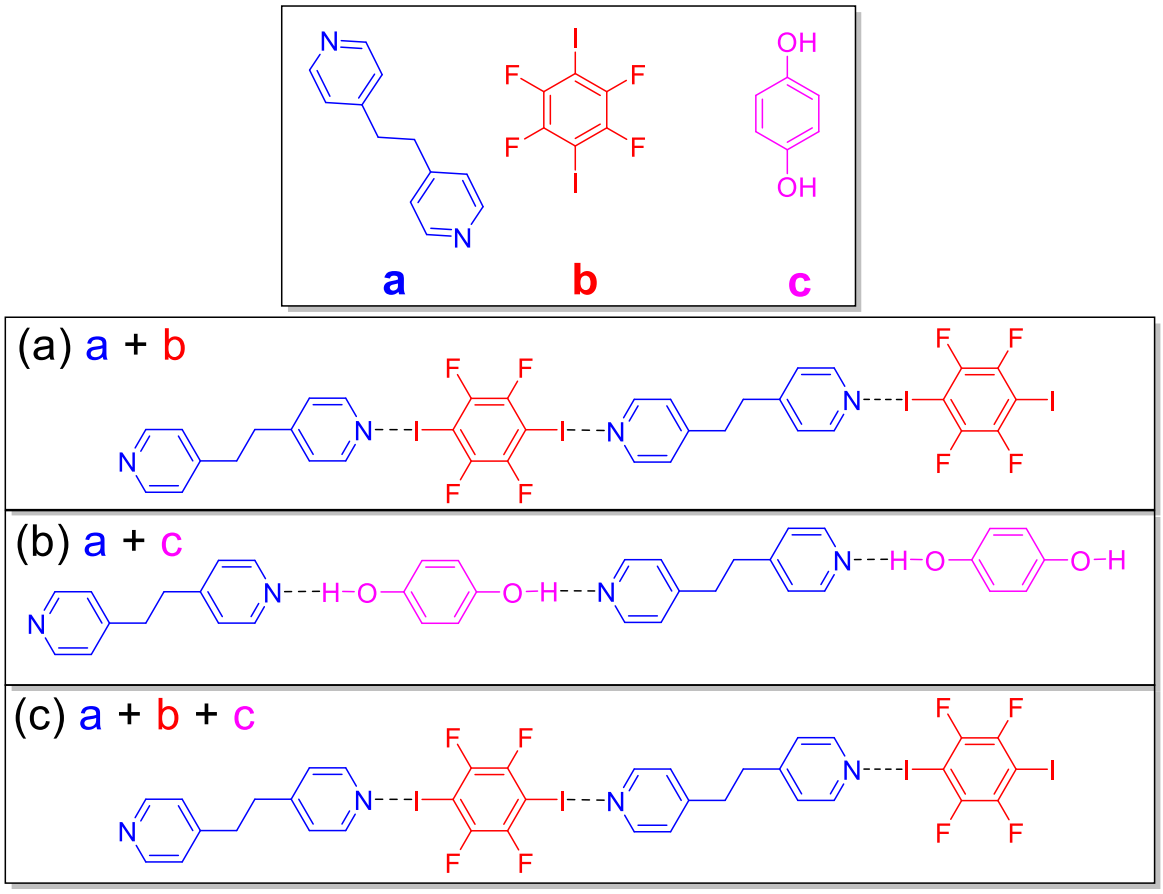

Figure 59. Schematic diagrams representing the intermolecular interactions observed in co-crystals grown in competitive crystallization experiments. (a) a mixture of compounds a and b, (b) a mixture of a and c, and (c) a mixture of a, b, and c.[83]

Various examples of increased self-assembly and gelation properties have been reported from the addition of halogen substituents to either existing gelators or non-gelators. In most of these examples, an aromatic moiety has been halogenated, which not only adds a halogen bonding functional group to the molecule, but also deactivates the aromatic ring, changing the intramolecular interactions caused by aromatic interactions such as π-π stacking. Lin et al. showed that the addition of a bromo group on the naphthyl group of their naphthalene based dipeptide hydrogelator slightly increased the calculated partition coefficient (ClogP) and improved the gelation window with a decrease in the minimum gelation concentration.[84] Yu Feng et al. studied the halogen-substituent effect on gelation properties on a series of dendritic organogelators.[85] They found that the halogen substituents on the periphery of the dendrons have a significant effect on the gelation properties, with several effective gelators being discovered. This study found that the identity of the halogen has a significant effect on the gelation properties of the dendrimer. Dendrons containing chloro and iodo groups were found to be very effective organogelators. Additionally, the identity and placement of the halogen substituent can be used to tune the gelation propensity.

Yi and Xiao et al. worked on fluorescent diphenylimidazole-functionalized anthracene (ADPI), which was found to be an efficient gelator in cyclohexane and cyclohexane mixtures.[86] Later, they replaced the phenyl rings of ADPI with triphenylamine, creating ADPIA, because triphenylamine units are capable of strong aromatic-aromatic interactions and have been utilized in the development of several other organogelators.[87] Unfortunately, ADPIA was not capable of gelation in any of the conventional solvents. They found that the addition of a bromo group to the anthracene of ADPIA, creating Br-ADPIA, led to an efficient low molecular weight organogelator.[87] Molecular modeling carried out in this study suggests that the bromine moiety

plays an important role in balancing the intermolecular π-π interactions between the triphenylamine units in Br-ADIPA. Another example of a non-gelator small molecule being converted to an efficient gelator via the introduction of a halogen on an aromatic ring was seen in the work carried out by Srivastava et al. in designing aryl-triazolyl amino acid benzyl ester gelators.[88] All three of the halogenated derivatives were found to be "super gelators" in several organic solvents with MGC's as low as 0.067 wt%. Another example of a "super gelator" containing halogenated aromatic rings was designed by Guan et al.[76] In this study, a series of 3,4-chlorobenzylidene protected gluconic amide derivatives were designed and synthesized. From this series, the derivative with the eight-carbon aliphatic chain was found to be a "super gelator" in various solvents.

Building off of our previous success in designing LMWGs from 4,6-benzylidene acetal protected glucosamide derivatives, we set out to synthesize a series of glucosamide derivatives containing a chloro substituent in the para position of the benzylidene acetal protection, depicted in Figure 60. We hypothesized that halogen bonding from the chloro substituent would increase the intermolecular interactions and lead to enhanced gelation properties.

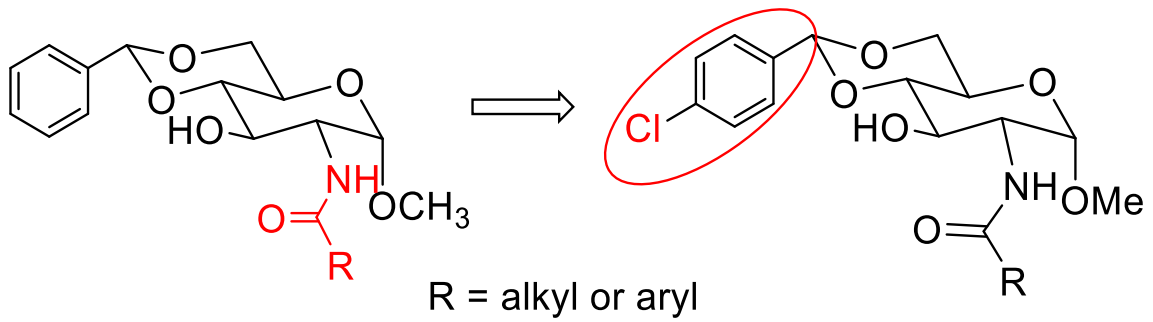

Figure 60. Rational design for the synthesis of 4-chlorobenzylidene acetal protected glucosamine derivatives.

3.2 RESULTS AND DISSCUSSIONS

Scheme 5 depicts the synthesis of the 4,6-(4-chlorobenzylidene) acetal protected glucosamine headgroup **IV.** Starting with N-acetyl glucosamine, an *O*-methoxy group was installed in the anomeric position via a glycosylation reaction utilizing amberlite IR120 acidic resin in methanol, producing compound **II**. Compound **II** then underwent a 4,6-acetal protection using 4-chlorobenzaldehyde dimethyl acetal, producing compound **III**. Compound **III** then underwent a deacetylation reaction by refluxing with a 1.0 M sodium hydroxide in ethanol solution for 24 hours, producing the final 4,6-(4-chlorobenzylidene) acetal protected glucosamine headgroup, compound **IV**.

Scheme 5. Synthesis of the 4,6-(4-chlorobenzylidene) acetal protected glucosamine headgroup

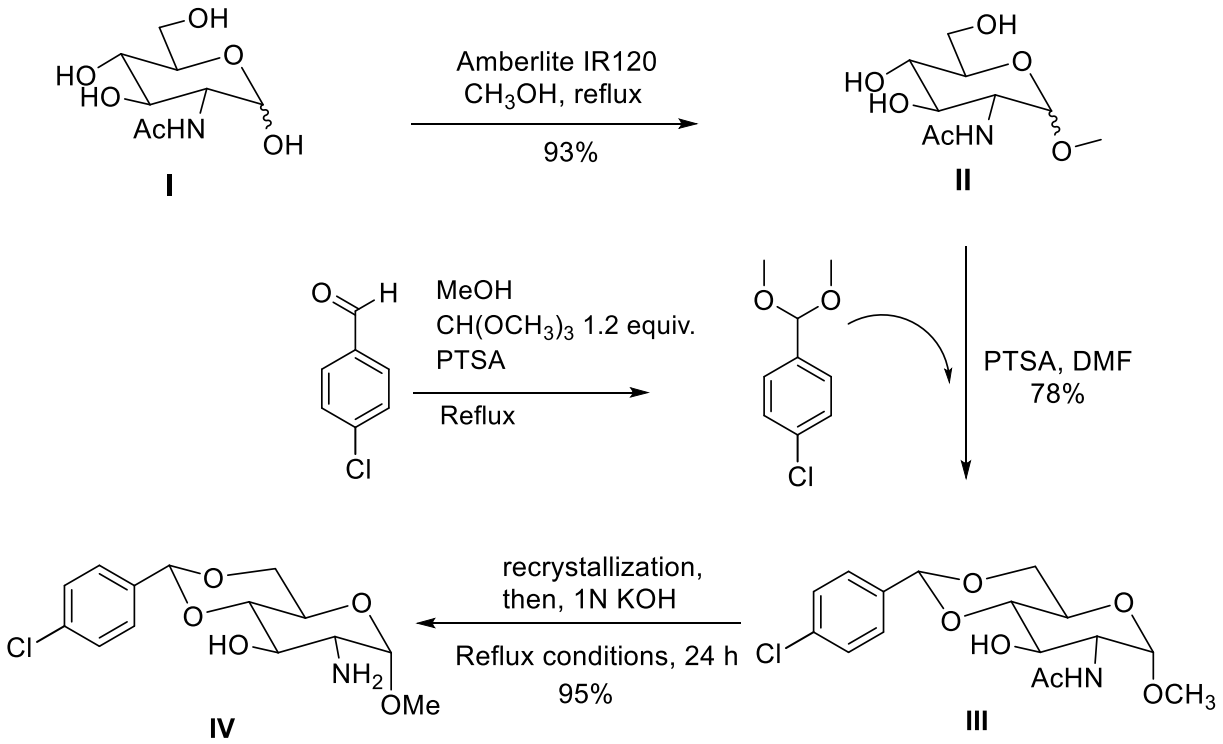

Preliminary gel tests carried out on the acetamide derivative, compound **III**, produced very promising results. Compound **III** was found to be a very versatile gelator, forming gels in ten of the tested solvents, shown in Table 5. Additionally, compound **III** was very effective at gelating toluene, *n*-propanol, ethylene glycol, glycerol, and DMSO-water 1:1 at concentrations under 5 mg/mL. These results suggested that further functionalizing the second position of the headgroup through an amide linkage could allow for tuning the balance of intermolecular forces that lead to supramolecular gelation and lead to very effective carbohydrate based LMWGs.

Table 5. Gelation test results of 4,6-(4-chlorobenzylidene) acetal protected headgroup **III**

No.	Tol.	n-BuOH	n-PrOH	i-PrOH	EtOH	EG	Gly	EtOH: H_2O 1:1	DMSO: H_2O 1:1	DMSO: H_2O 1:2
III	2.9_O	10.0_T	3.3_O	20.0_O	20.0_O	3.3_C	4.0_C	6.7_O	20.0_O	5.0_O

Numbers are the MGCs in mg/mL. C = clear, T = translucent, O = opaque.

Considering the versatility and effectiveness of compound **III** as a supramolecular gelator, we decided to further functionalize the second position of compound **IV** with various aliphatic and aromatic amide groups. Scheme 6 shows the synthesis of amide derivatives with the general structure **V**. Derivative **1**-**6** and **9**-**14** were synthesized by reacting compound **IV** with respective acid chlorides in a solution of anhydrous DCM with pyridine. Derivatives **7**-**8** were synthesized using the respective anhydrides in a solution of DCM with triethylamine. A total of eight aliphatic derivatives, compounds **1**-**8**, and six aromatic derivatives, compounds **9**-**14**, were synthesized. The aliphatic derivatives include four primary derivatives, compounds **1**-**4**, one secondary derivative,

compounds **5**, and three tertiary derivatives, compounds **6-8**. The aromatic derivatives include three benzamide derivatives, compounds **9-10** and three naphthalene containing amide derivatives, compounds **12-14**. The various R groups were chosen to probe the structural requirements for developing versatile and efficient LMWGs from the 4,6-(4-chlorobenzylidene) acetal protected glucosamine scaffold.

Scheme 6. Synthesis of the 4,6-(4-chlorobenzylidene) acetal protected amide derivatives

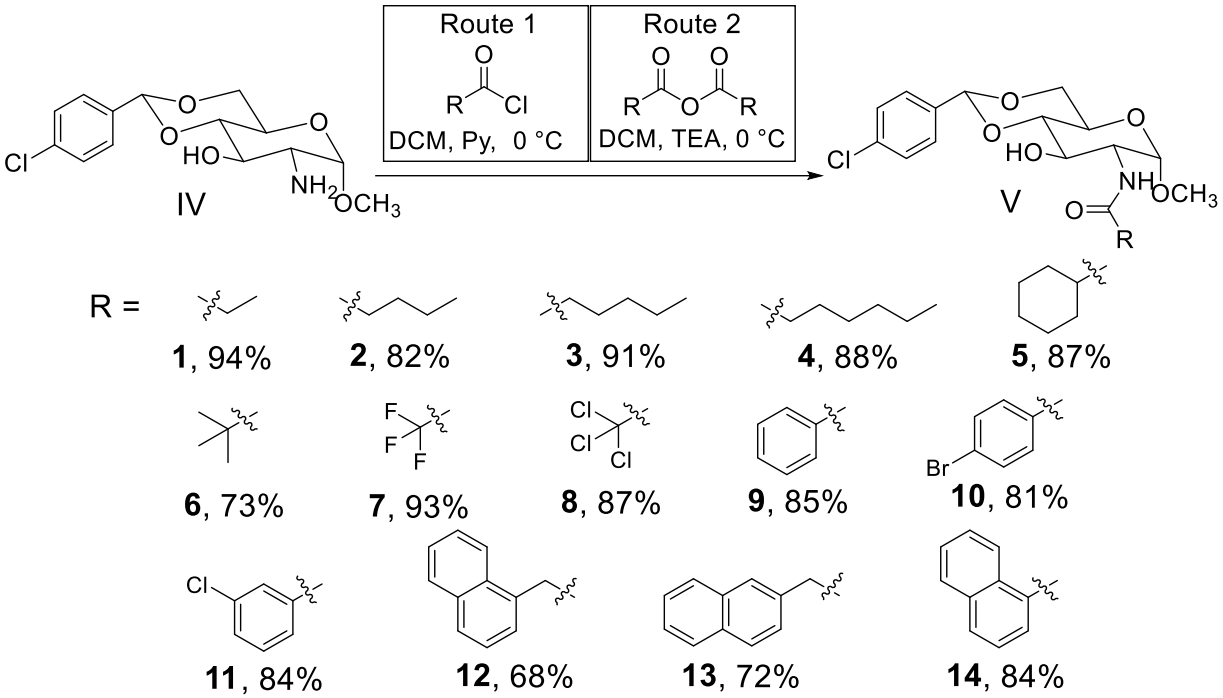

Gelation tests were carried out with a variety of protic and aprotic organic solvents, water and aqueous solutions of DMSO and ethanol. Table 6 shows the results of gelation testing. As predicted, several of the 4,6-(4-chlorobenzylidene) acetal protected amide derivatives were both

versatile and effective LMWGs. Every amide derivative was found to be a supramolecular gelator in at least one of the fourteen solvents tested. The primary aliphatic amide derivatives **1-4** typically performed well in alcohols. The least effective of these compounds is the ethyl amide derivative **1**, which only formed gels in n-propanol, n-butanol, ethanol, and ethylene glycol at higher concentrations. Increasing the length of the aliphatic tail to five carbons to produce valeryl amide **2** significantly increased the gelation properties of the molecule. In addition to performing well in the tested alcohols, derivative **2** formed gels in both aqueous solutions of DMSO and ethanol. Derivative **2** particularly performed exceptionally in both ethanol-water solutions, the DMSO-water 1:1 solution, and in *n*-butanol, with MGCs of 1.0 mg/mL or lower. The aliphatic derivatives **3** and **4** also performed exceptionally in both DMSO-water solutions with MGCs as low at 0.8 mg/mL. The cyclohexyl derivative **5** was found to be the most versatile gelator in this series, forming gels in eleven solvent systems tested. Like the primary aliphatic derivatives, compound **5** also performed well in both DMSO-water and ethanol-water solutions with MGCs between 1.3-2.5 mg/mL. Increasing the steric hindrance further, with the tertiary *t*-butyl derivative **6**, caused a reduction in gelation properties, forming gels in ethylene glycol, glycerol, ethanol-water 1:1, and DMSO-water 1:1 at the high concentration of 20 mg/mL. The *t*-butyl amide derivative **6** did form a gel at 5.0 mg/mL in hexanes and was the only compound in this series to form a gel in hexanes. Substituting the methyl groups on the amide of derivative **6** with fluoro and chloro groups caused a significant increase in gelation properties. The trifluoro amide derivative **7** was a very versatile gelator, forming gels in nine of the tested solvents. Fairly low MGCs were achieved in both ethanol-water solutions and DMSO-water solutions. The trichloro amide derivative **8** was much less versatile, only forming gels in five solvents; however, it was very efficient in gelating both ethanol-water solutions and DMSO-water solutions. The benzamide derivative **9** was the most

effective gelator found in this series and performed extremely well in all of the aqueous mixtures of DMSO and ethanol with MGCs between 0.54 mg/mL and 0.36 mg/mL. Additionally, compound **9** formed a hydrogel at 0.036 mg/mL and was the only derivative that was not insoluble in water during testing. Adding a bulky bromo group to the para position of the benzamide derivative to produce the 4-bromobenamide derivative **10**, caused a significant reduction in the gelation properties of the molecule. Adding a less bulky chloro group at the meta position of the benzamide derivative to produce the 3-chlorobenzamide derivative **11**, increased the number of solvents the compound formed gels in, while retaining the ability to gel the aqueous solutions of DMSO and ethanol at fairly low concentration. Increasing the aromatic interactions in the naphthylamide derivative **12** reduced the overall gelation effectiveness; however, the gelator was still fairly versatile, forming gels in eight of the tested solvents. The bulkier 2-naphthylacetamide derivative **13** and 1-naphthylacetamide derivative **14** both saw a significant decrease in gelation properties, indicating that steric hindrance and/or very strong aromatic interactions can cause a massive reduction in the gelation abilities of a molecule. Overall, the results of the gelation tests support our initial hypothesis that adding a chloro substituent to the benzylidene acetal protection would lead to very effective and versatile LMWGs. Compounds **2-4** and **8-9** are such efficient gelators that they fall into a class of supramolecular gelators termed “super gelator,” which are compounds that can form gels at very low concentrations, under 0.1 wt% (typically under 1.0 mg/mL). Several of these amide derivatives were found to be “super gelators” in multiple solvent systems. LMWGs that can produce gels at low concentrations are sought after due to the reduction in the amount of material required for various applications.

Table 6. Gelation test results of the 4,6-(4-chlorobenzylidene) acetal protected amide derivatives

No.	Tol.	n-BuOH	n-PrOH	i-PrOH	EtOH	EG	Gly	EtOH: H_2O 1:1	EtOH: H_2O 1:2	DMSO: H_2O 1:1	DMSO: H_2O 1:2
1	P	P	20.0_O	20.0_O	10.0_O	6.7_c	I	P	P	P	P
2	P	1.0_O	20.0_O	6.7_T	20.0_T	6.7_T	I	0.74_T	10.0_O	0.74_T	1.0_T
3	10.0_O	20.0_T	P	20.0_T	20.0_T	20.0_T	I	P	P	0.91_T	6.7_T
4	10.0_T	10.0_O	20.0_O	10.0_O	P	I	I	P	P	1.3_T	0.80_T
5	20.0_C	6.7_O	6.7_O	3.3_C	6.7_T	6.7_T	3.3_C	1.3_T	2.5_T	1.5_T	2.2_T
6	S	S	S	S	S	20.0_O	20.0_O	20.0_O	P	20.0_O	P
7	P	20.0_O	10.0_O	20.0_O	10.0_C	10.0_C	I	2.0_C	1.4_T	2.2_C	1.5_C
8	S	S	S	S	S	S	10.0_O	0.67_C	0.91_T	2.0_T	3.3_T
9	10.0_T	P	P	P	5.0_O	10.0_O	5.0_O	0.54_C	0.36_T	0.54_C	0.46_C
10	I	20.0_O	P	I	P	10.0_O	I	I	I	20.0_O	20.0_O
11	10.0_O	10.0_O	10.0_O	6.7_O	P	10.0_O	6.7_O	1.3_O	10.0_O	0.71_O	1.3_O
12	P	10.0_O	10.0_C	10.0_O	20.0_C	10.0_O	6.7_T	I	I	5.0_O	2.9_O
13	P	P	10.0_T	I	I	5.0_T	6.7_T	P	I	P	I
14	P	I	I	I	I	10.0_T	I	I	I	P	I

Numbers are the minimum gelation concentration in mg/mL. P = precipitation; S = soluble; I = insoluble (all at 20 mg/mL). C = clear, T = translucent, O = opaque. All compounds are insoluble in water, except compound **9** which formed gels with a MGC of 0.036 mg/mL. All compounds were found to be insoluble in hexanes, except for compound **6**, which formed gels with a MGC of 5.0 mg/mL. All compounds were found to be soluble in triethylene glycol, except compound **7,** which formed gels at 20.0 mg/mL.

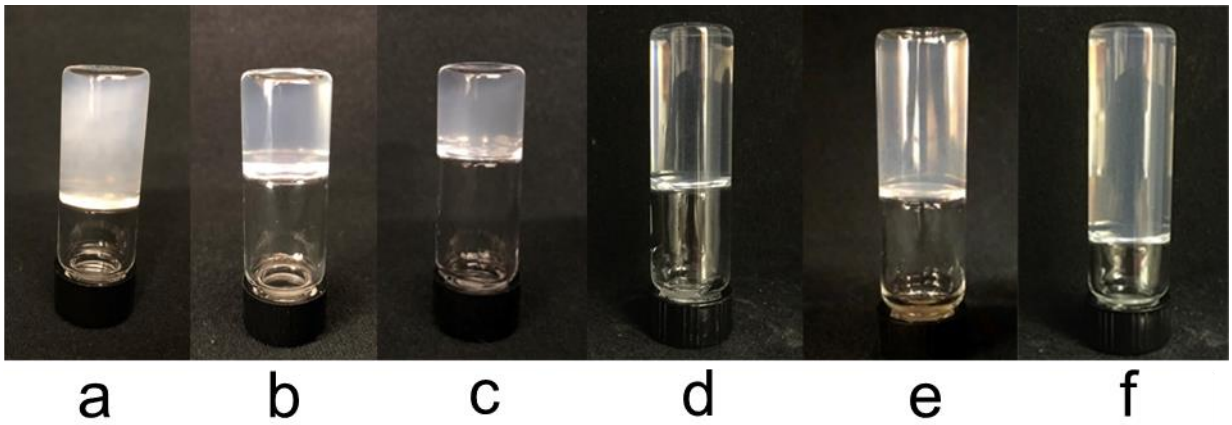

Figure 61. Gel photos of gels formed from compounds **2**, **3**, **8**, and **9**. (a) an opaque gel formed by compound **2** in EtOH/H_2O (1:1 v/v) at 0.74 mg/mL, (b) a translucent gel formed by compound **3** in DMSO/H_2O (1:1 v/v) at 0.91 mg/mL, (c) a translucent gel formed by compound **8** in DMSO/H_2O (1:2 v/v) at 0.91 mg/mL, (d) a clear gel formed by compound **9** in DMSO/H_2O (1:2 v/v) at 0.46 mg/mL, (e) a translucent gel formed by compound **9** in water at 0.40 mg/mL, (f) a translucent gel formed by compound **9** in EtOH/H_2O (1:2 v/v) at 0.36 mg/mL.

Several images of gels in vials at the MGCs are shown in Figure 61. Optical microscopy was used to analyze the morphology of the gel networks of several selected gels. Several optical micrographs (OMs) can be seen in Figure 62. Various morphologies were observed from the optical imaging of the gels formed by the 4,6-(4-chlorobenzylidene) acetal protected amide derivatives in different solvents. An ethanol-water 1:1 gel formed by compound **2** at 0.74 mg/mL was imaged in Figure 62a. This image shows very fine hair-like fibers that twist and curl around each other to make the supramolecular architecture of the gel. Concentrated areas of this gel resemble a solid sheet; however, when observing the edges of the bulk gel, the tiny hair-like fibers become apparent. Figure 62b shows an image of a DMSO-water 1:1 gel formed by compound **3**

at 0.91 mg/mL. This gel is composed of long straight fibers that overlap and intercept to form the gels architecture. Figure 62c shows an image of a DMSO-water 1:1 gel formed by compound **7** at 2 mg/mL. This image shows long windy fibers protruding from one central point to make a star shaped cluster of fibers. It is unclear if a central aggregation point gave rise to multiple fibers growing in various directions to produce this type of morphology, or if multiple long fibers just ended up wrapping around each other at a central point. In concentrated areas, it is difficult to observe these individual star clusters; however, if you look near the edge of the bulk gel, these star clusters are apparent. Figure 62d shows an image of a DMSO-water 1:1 gel formed by compound **9** at 1 mg/mL. The fibers observed in this image are small, curly and densely intertwined. Figure 62e shows an image of the hydrogel formed by compound **9** at a concentration of 4.0 mg/mL. The image shows very tiny hair like fibers that are very densely packed. Towards the center of the bulk gel, the fibers are too small and densely packed to see under an optical microscope. Very small fibers can be identified towards the edge of the bulk gel.

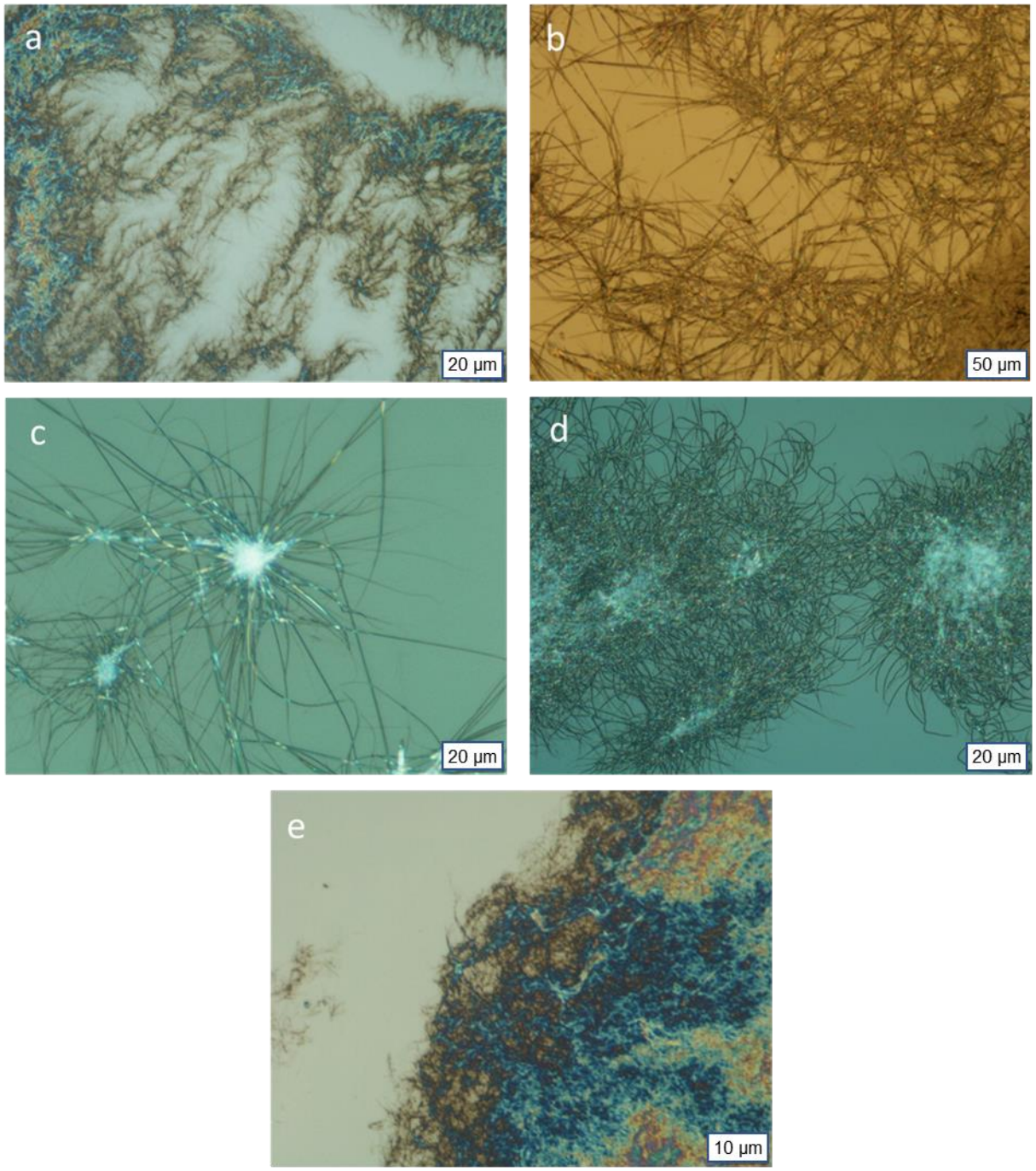

Figure 62. Optical micrographs of gels formed from compounds **2**, **3**, **7**, and **9**. (a) compound **2** in EtOH/H_2O (1:1 v/v) at 0.74 mg/mL; (b) compound **3** in DMSO/H_2O (1:1 v/v) at 0.91 mg/mL; (c) compound **7** in DMSO/H_2O (1:1 v/v) at 2.0 mg/mL; (d) compound **9** in DMSO/H_2O (1:1 v/v) at 1.0 mg/mL; (e) compound **9** in H_2O at 0.40 mg/mL.

Atomic force microscopy was also used to analyze the morphology of the gel networks. Figure 63 shows the height and amplitude images acquired through AFM. Figure 63a-b was captured from a gel formed by compound **7** in DMSO-water 1:1 at 2.0 mg/mL. This image shows long straight continuous fibers, which appear as tubules that interact to form a 3D network. These images give insight into the three-dimensional space available with the self-assembled gel network. Figure 63c-d was captured from a gel formed by compound **9** in EtOH-water 1:1 at 1.0 mg/mL. This image shows a very different self-assembly pattern. In this image, fibrous assemblies are observed, which bundle to form feather type morphology that overlap to form the gel network. Figure 63e-f was captured from a gel formed by compound **9** in DMSO-water 1:1 at 1.0 mg/mL. The morphology in these images appear to be bundles of fibers that twist around each other to form larger rope like fibers, which further overlap to form the gel matrix. The difference in morphology between the AFM images in Figures 63c-d and 63e-f shows how different solvent systems can direct self-assembly in very different directions.

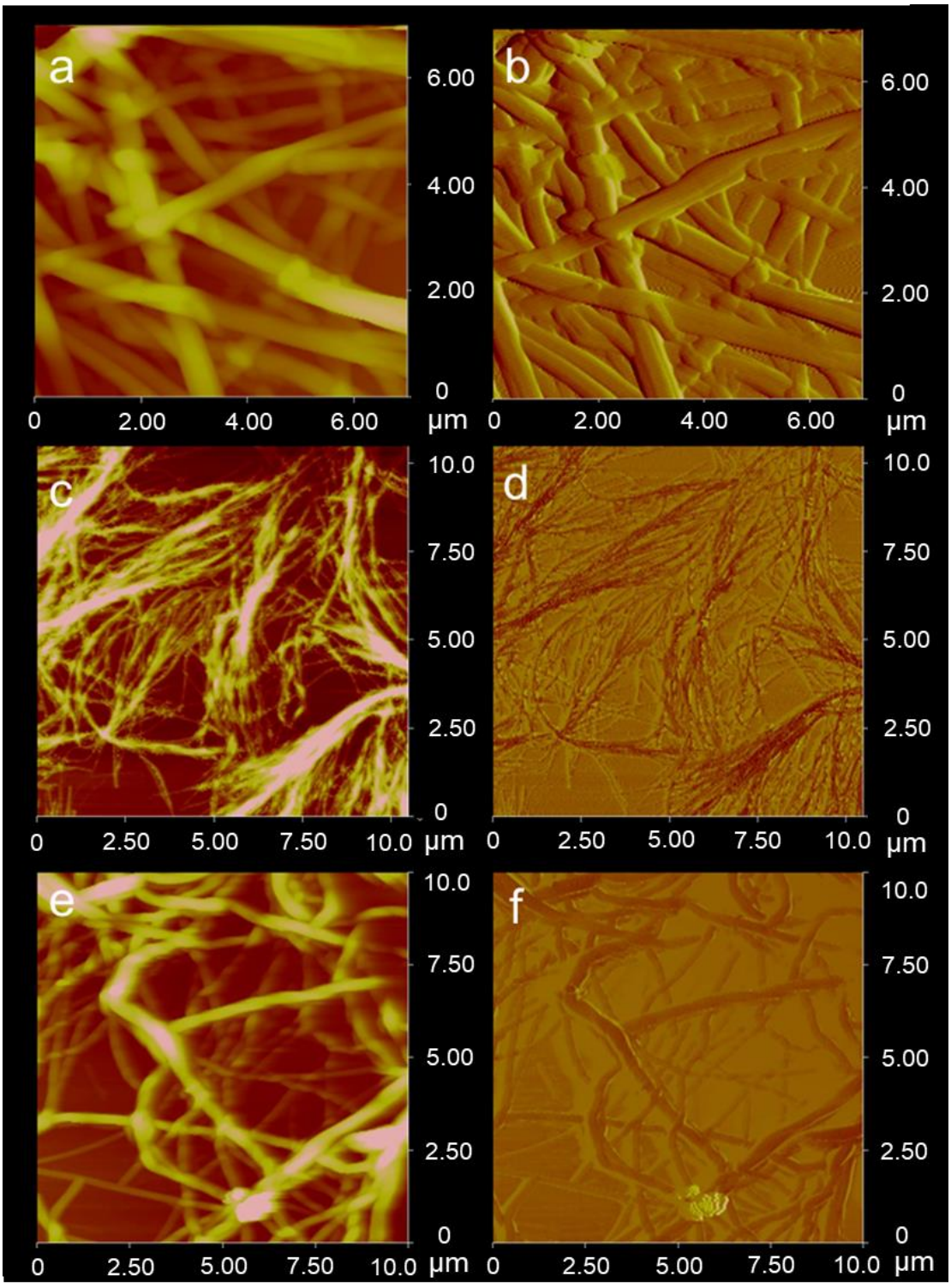

Figure 63. AFM images of gels formed from compounds **7** and **9**. (a-b) DMSO/H_2O (v/v 1:1) gel formed by compound **7** at 2.0 mg/mL; (c-d) EtOH/H_2O (v/v 1:1) gel formed by compound **9** at 1.0 mg/mL; (e-f) DMSO/H_2O (v/v 1:1) gel formed by compound **9** at 1.0 mg/mL.

Variable temperature ^{1}H NMR studies were carried out on several amide derivatives to probe the self-assembly mechanisms. Figure 64 shows the overlaid ^{1}H NMR spectra of compound **III** from 30-60 °C. Upfield changes in chemical shift were observed for both the amide NH signal and 3-hydroxyl signal of 0.19 ppm and 0.16 ppm respectively. This indicates that these functional groups are readily capable of partaking in intermolecular hydrogen bonding. An interesting phenomenon that was first observed in this ^{1}H NMR study was a change chemical shift in the aromatic region. The ortho and meta protons on the 4-chlorobenzylidene protection seem to be moving away from each other from a central point, indicating this group is partaking in some sort of interactions which are reduced or increased at higher temperatures. This could be caused by typical aromatic interactions; however, it could also be caused by halogen bonding. Figure 65 shows the overlaid ^{1}H NMR spectra of the benzamide derivative **9** from 30-60 °C. Like the acetamide compound **III**, a similar change in chemical shift of 0.22 ppm was observed for the amide NH signal. Significant changes in the shape of the aromatic signals were also observed; however, due to the overlapping aromatic groups, analysis is difficult. The ortho proton signal from the benzamide functional group was observed to have a slight upfield shift of 0.07 ppm with evaluated temperature, indicating that this group may be partaking in intermolecular interactions during the act of self-assembly. Since self-assembled structures cannot always be seen with the naked eye, after the NMR sample cooled back down to room temperature, the sample was poured onto a microscope slide. The sample was immediately imaged, and fibrous structures were observed. Figure 66 shows optical micrographs of the NMR sample that was imaged after the temperature study.

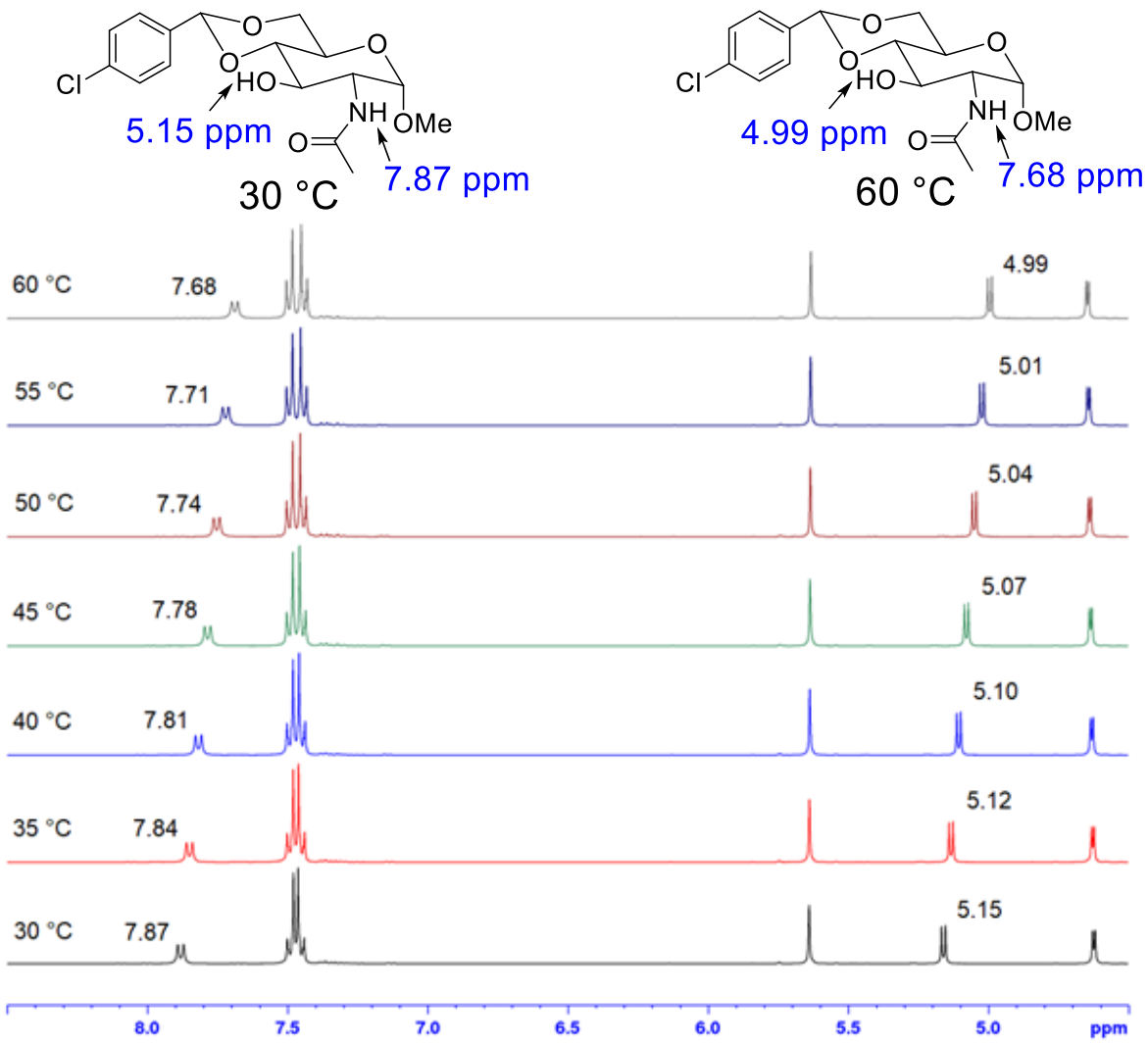

Figure 64. Overlaid ^{1}H NMR (400 MHz) spectra of compound **III** from 30–60 °C. The sample was prepared at 12.5 mg/mL in DMSO-d_6.

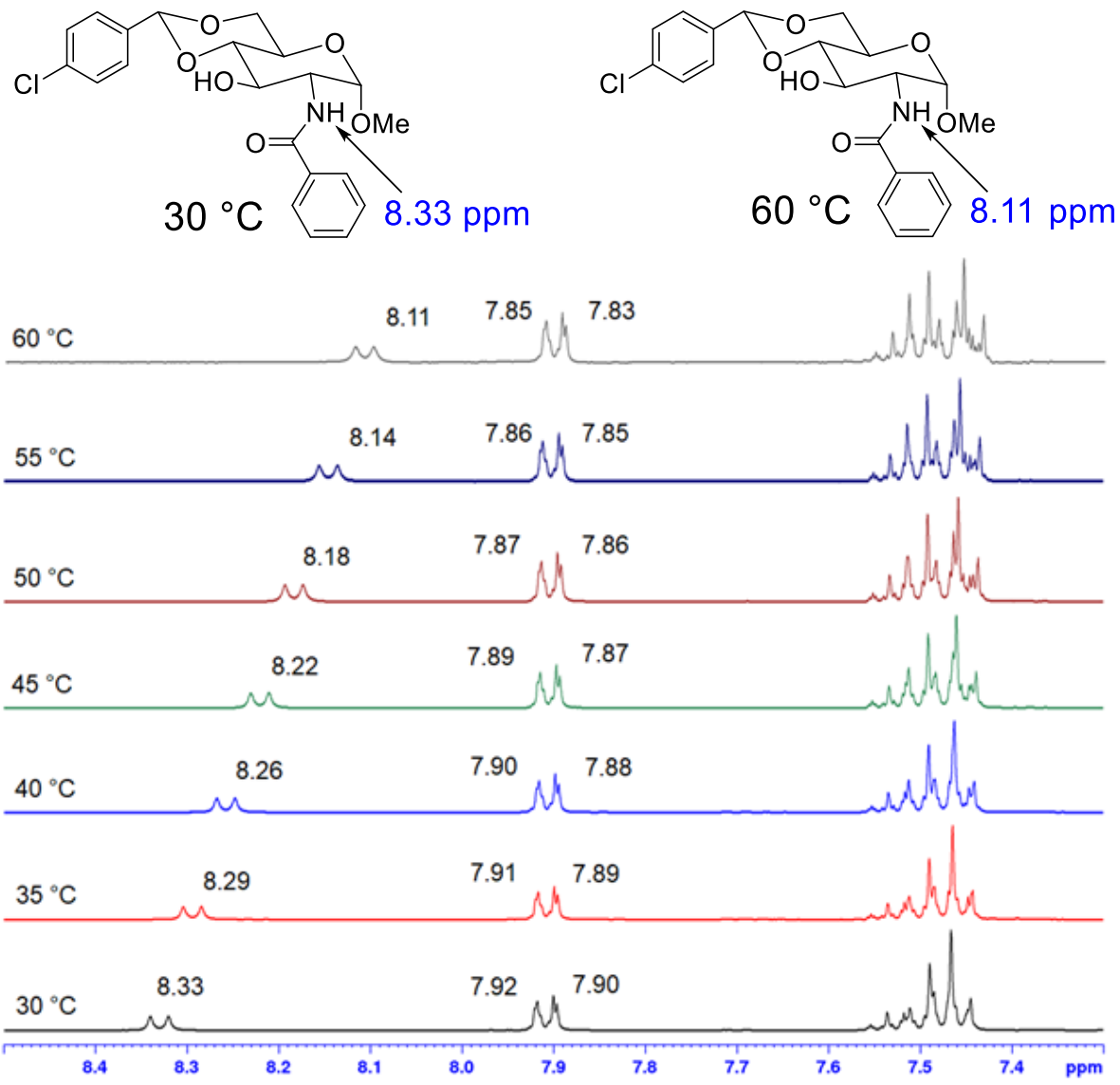

Figure 65. Overlaid ^{1}H NMR spectra of compound **9** from 30–60 °C. Sample was prepared at 10.0 mg/mL in DMSO-d_6.

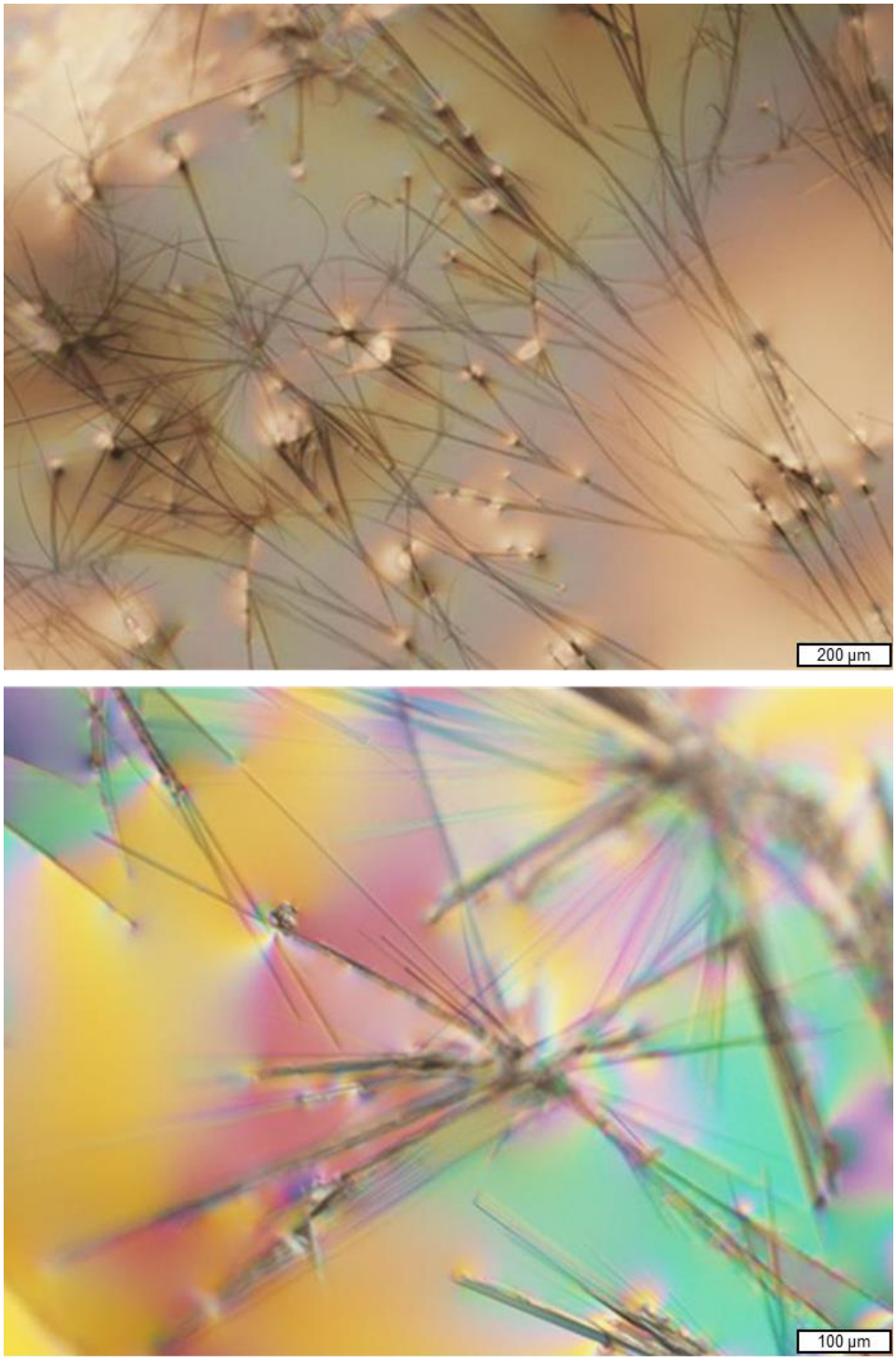

Figure 66. Optical microscope images of the NMR sample from the variable temperature study. Top: 5 X magnifications; Bottom: 10 X magnification. The sample was made with compound **9** at 10 mg/mL in d_6-DMSO.

After analyzing the morphology of several gels, we next analyzed the viscoelastic properties of several of the gel that were formed at very low concentrations. Figures 67-68 show frequency sweep overlays for several of the gels formed by super gelators at their MGCs. For all gels tested, the storage modulus (G′) is greater that the loss modulus (G″) throughout the full angular frequency ω range. This indicates that the gels have viscoelastic properties and are stable. Surprisingly, most of these low concentration gels had very similar storage moduli. The loss moduli, on the other hand, were fairly different.

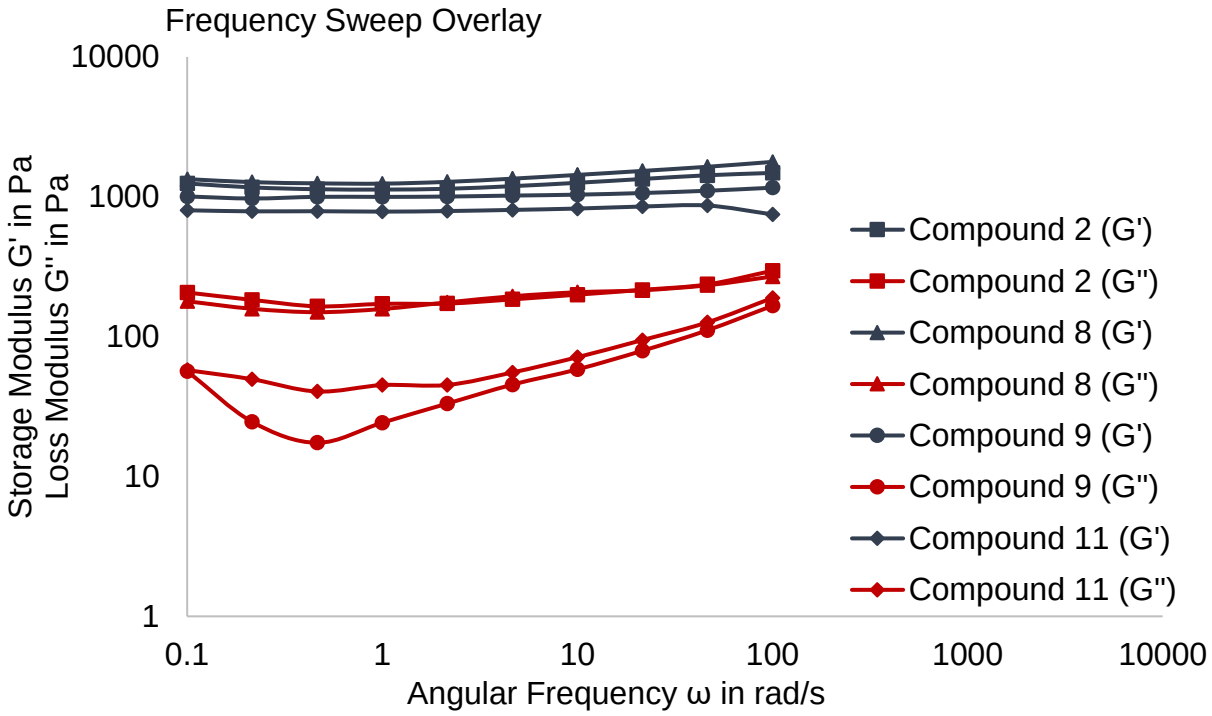

Figure 67. Overlaid rheology spectra of gels formed by compounds **2**, **8**, **9** and **11**. Gels were formed by compound **2** in EtOH/H_2O 1:1 v/v at 0.74 mg/mL, compound **8** in EtOH/H_2O 1:1 v/v at 0.67 mg/mL, compound **9** in H_2O at 0.36 mg/mL, and compound **11** in DMSO/H_2O 1:1 v/v at 0.71 mg/mL. The applied strain was 0.1%.

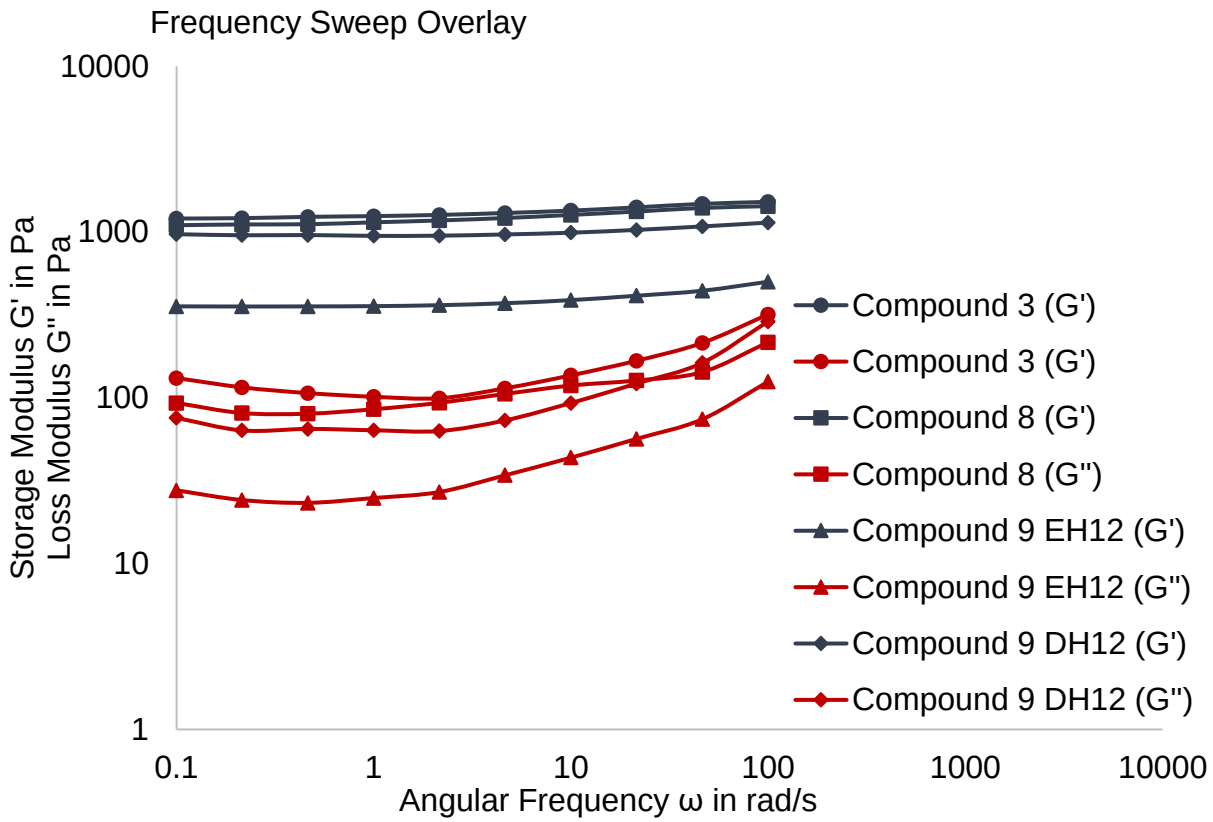

Figure 68. Overlaid rheology spectra of gels formed by compounds **3**, **8**, and **9**. Gels formed by compound **3** in DMSO/H_2O 1:1 v/v at 0.91 mg/mL, compound **8** in EtOH/H_2O 1:2 v/v at 0.91 mg/mL, compound **9** in EtOH/H_2O 1:2 v/v at 0.36 mg/mL, compound **9** in DMSO/H_2O 1:2 v/v at 0.46 mg/mL. The applied strain was 0.1%.

Since the gel network of a supramolecular gel is held together through weak non-covalent forces, shaping these gels through any method other than forming them within a mold is a very difficult task.[89] Applying too much force to these gels will usually destroy the supramolecular architecture or at a minimum significantly weaken them. For this reason, extrusion-based printing methods for shaping supramolecular gels has received very little exploration. In this study, we analyzed the possibility of using the gels for extrusion-based printing. The extrusion set-up is

shown in Figure 69. An inverted syringe pump was used to control the extrusion rate. Gels were formed within 1 mL syringes equipped with a 14-gauge blunt tipped needle, which acts as a nozzle. A microscope slide, which acts as a print bed, was set on a laminate board with 4 cm graduation marks, which acted as a guide during the extrusion process. Forming the gels within the syringe was a difficult task. Gels were prepared at the desired concentrations and then heated until the gel to solution transition occurred. Then, while still hot, the solution was pulled into the syringe. The syringes were then allowed to sit upright for up to 24 hours. Out of this study, many limitations were recognized. One major limitation was forming the gels within the syringes. Upon heating the gelator/solvent solution in a sealed vial, pressure builds up within the vial. When removing the cap of the vial to pull up the hot solution in the syringe, we found that the sudden pressure change caused rapid gelation or precipitation for most of the samples, especially samples containing more volatile solvents and the hydrogel of compound **9**. Aqueous DMSO solutions were found to be the most successful solvent systems for the preparation of gels in the 1 mL syringes. While a variety of gels were tested in the preliminary extrusion studies, the most successful trials were carried out using gels formed from compounds **7** and **9** in DMSO/H_2O 1:1. For this reason, further optimization was carried out using DMSO/H_2O gels of compounds **7** and **9**. From here, the extrusion rate and gel concentration needed to be optimized. The extrusion rate of the syringe pump was limited to 3.0 ml/min due to the size of the syringe that was being used. Using a larger syringe allowed for a higher extrusion rate; however, all testing using 3 mL and 10 mL syringes failed. The most successful prints were carried out using a 1 mL syringe at the maximum extrusion rate of 3.0 mL/min. The concentration of the gelators was found to be a significant parameter, as the trials using gels formed above 10 mg/mL mainly extruded clumps of solid and puddles of liquid. The trials using concentrations under 5 mg/mL mainly extruded puddles of liquid. Extrusion

studies using gels formed by compounds **7** and **9** in DMSO/H_2O 1:1 at both 5 mg/mL and 10 mg/mL were successfully printed lines of gels, seen in Figure 69. To analyze the viscoelastic properties of the printed lines of gel, as well as the gels recovery over time, rheometric studies were carried out. Gels were analyzed via rheometry before, immediately after, and 24 hours after extrusion. The overlay of the frequency sweeps for the extrusion studies carried out using the 5 mg/mL gels can be seen in Figures 70. In all cases, the storage modus (G′) was found to be higher than the loss modus (G″) across the full angular frequency range ω, indicating both stability and viscoelasticity. While the results of these studies are promising, much more extensive studies are required to analyze the ability of these gels to be used as soft materials for 3-D printing. Studies carried out on fully automated systems would be required to further analyze these gels for 3-D printing applications.

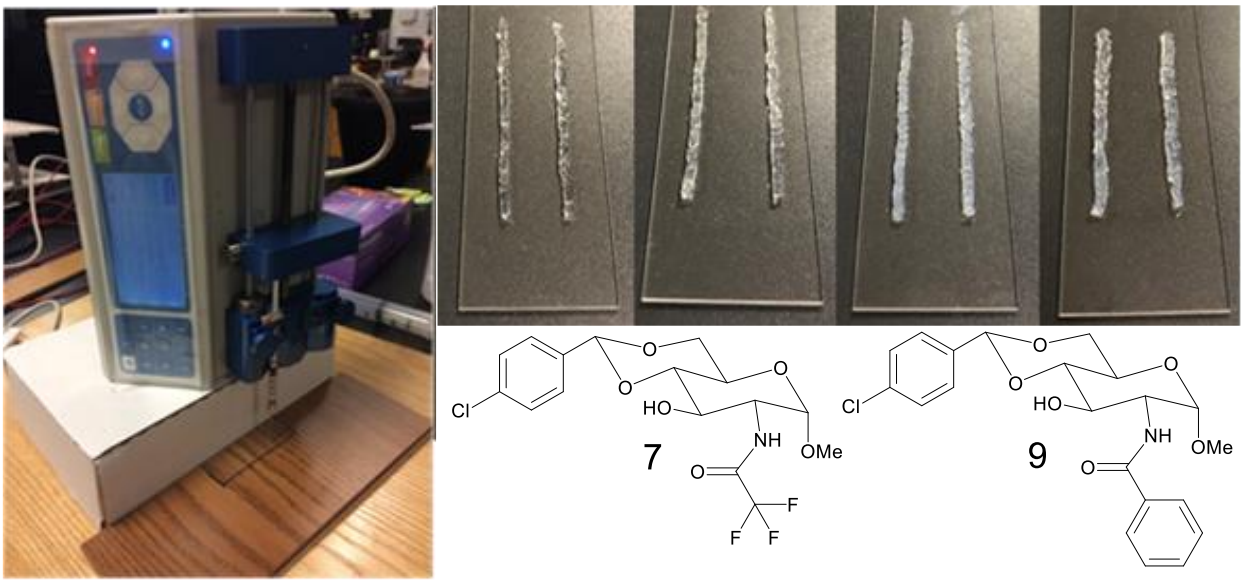

Figure 69. Extrusion study-set up and successfully printed gel lines of gel. Gels were formed from compound **7** and **9** in DMSO/H_2O 1:1 at 5 mg/mL and 10 mg/mL.

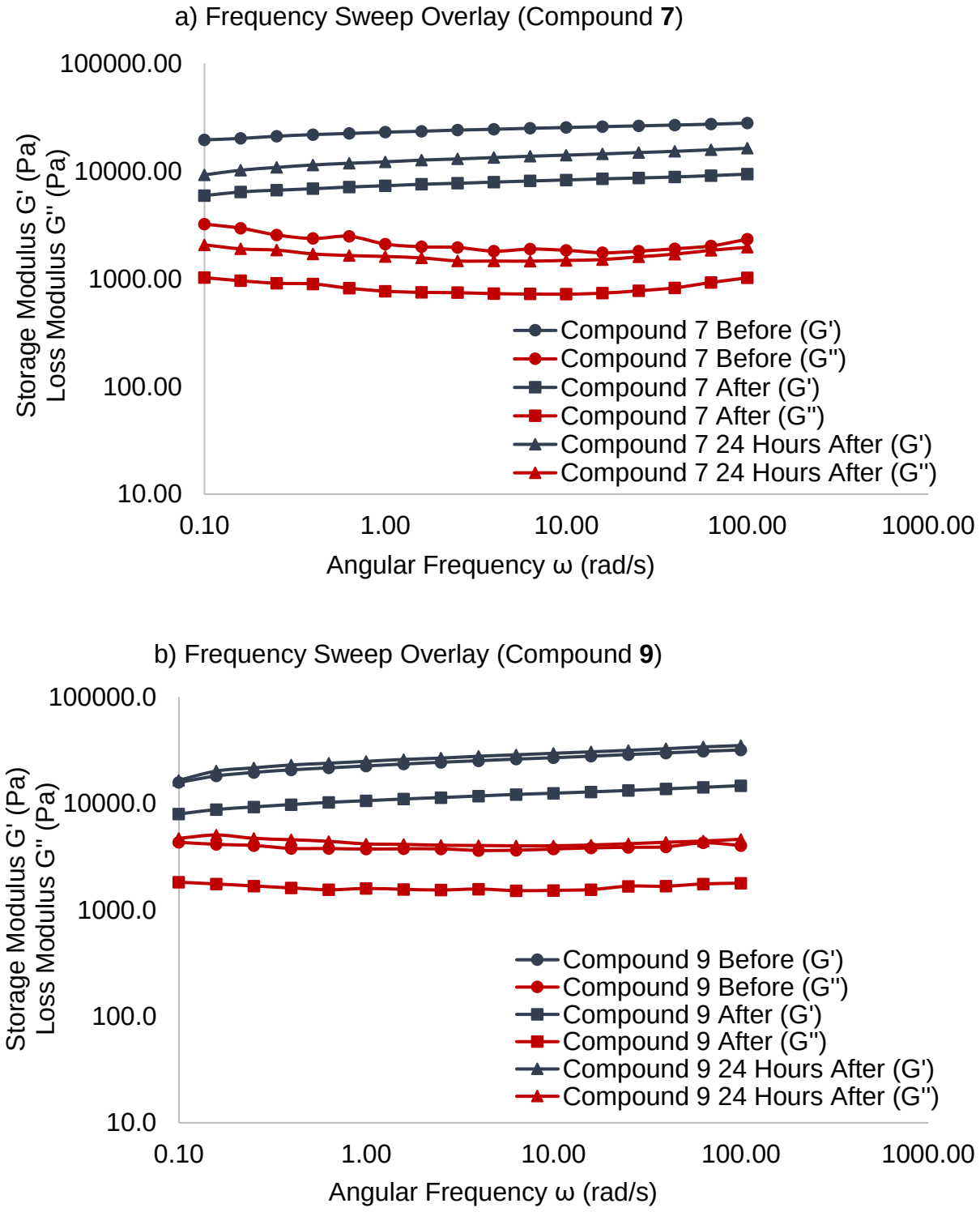

Figure 70. Frequency sweep overlay before, after extrusion, and 24 h after extrusion. (a) a gel of compound **7** and (b) a gel of compound **9**, both in DMSO/H_2O 1:1 at 5 mg/mL.

Drug entrapment and release studies were carried out using naproxen sodium as a model drug. Since the benzamide derivative **9** formed a hydrogel at the very low concentration of 0.36 mg/mL, it was utilized for this study. A 0.25 mg/mL stock solution of naproxen sodium in 5% DMSO in water was used to prepare a 2 mL gel at a concentration of 1 mg/mL. DI water was then carefully added on top of the gel to begin the experiment. At various times, the aqueous layer was removed and analyzed via UV-vis spectroscopy. The UV-vis spectra of the naproxen release at various time points and the percent release over time are shown in Figure 71. By forty hours, an estimated 97% of the naproxen sodium had diffused to the aqueous layer. Additional studies utilizing a gel with a lower concentration of gelator resulted in very similar results. Images of the gel over the course of the study are shown in Figure 72. UV-vis spectra of compound **9** in 5% DMSO in water solution, shown in Figure 73, show that there is no overlap between the UV-vis absorption of naproxen sodium and compound **9**. A calibration curve of naproxen sodium is provided in Figure 74 to show the linear relationship between absorption and concentration in the concentration range that was being investigated in this study. Additional studies were carried out in a similar fashion using chloramphenicol as a model drug with similar results. This study demonstrates that aqueous gels formed by compound **9** are capable of sustained drug release.

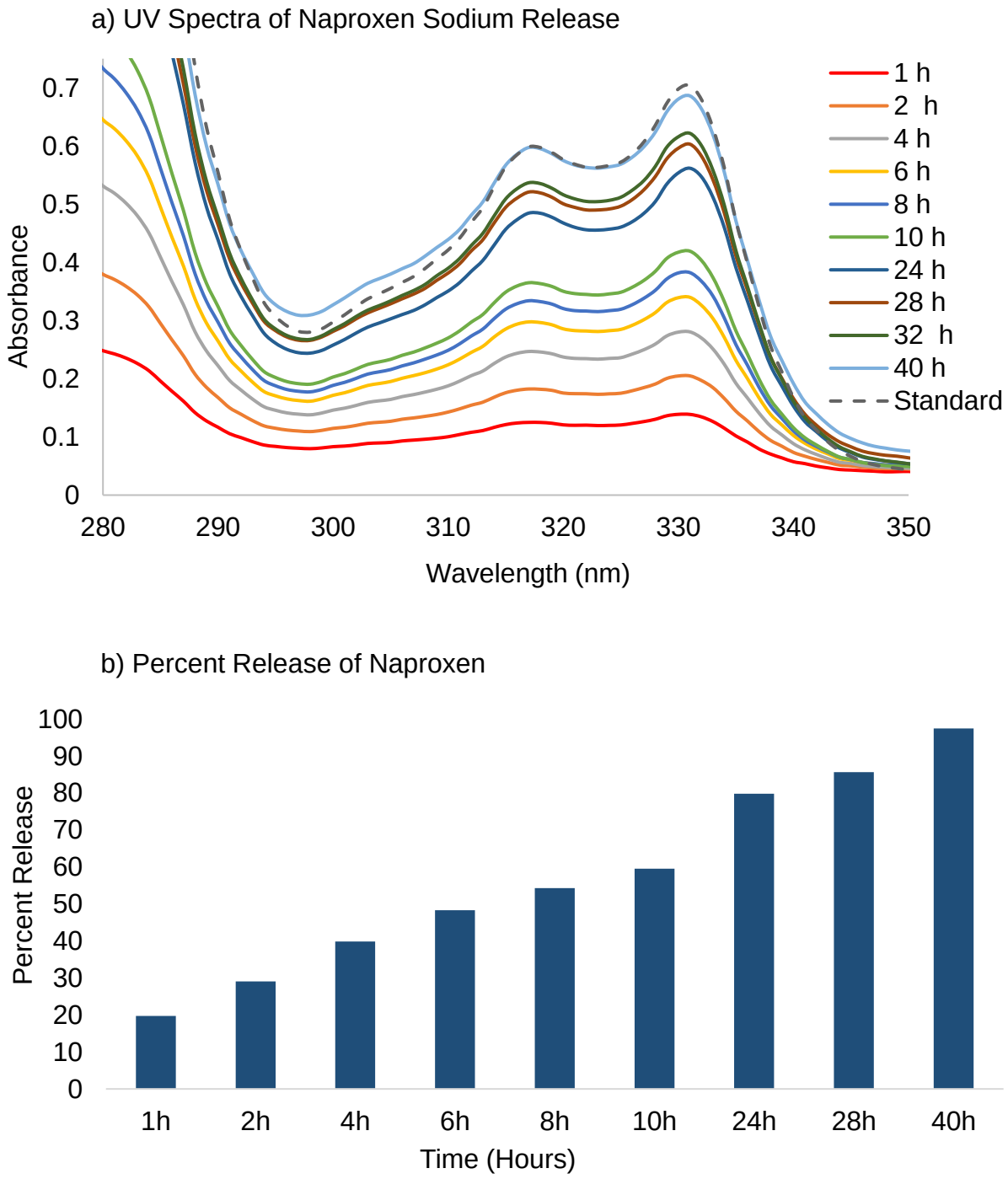

Figure 71. UV-vis spectra of naproxen sodium release from the gel into the aqueous phase and percent release of naproxen sodium over time.

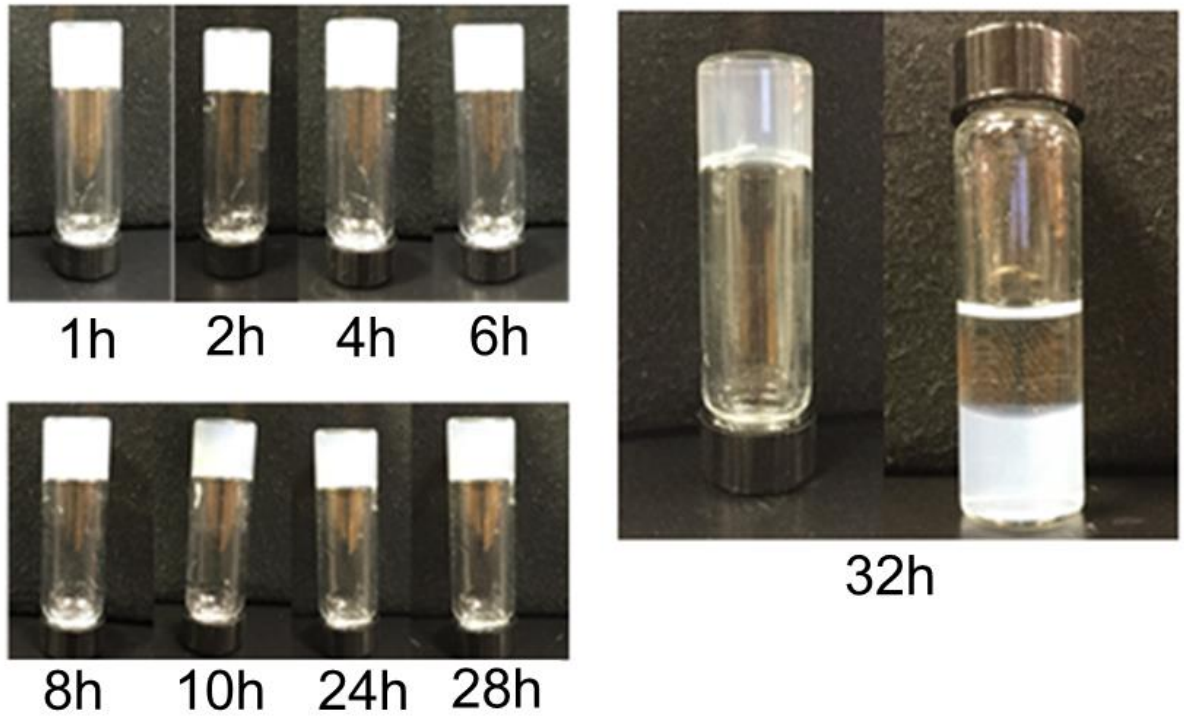

Figure 72. Gel images over the duration of the naproxen release study.

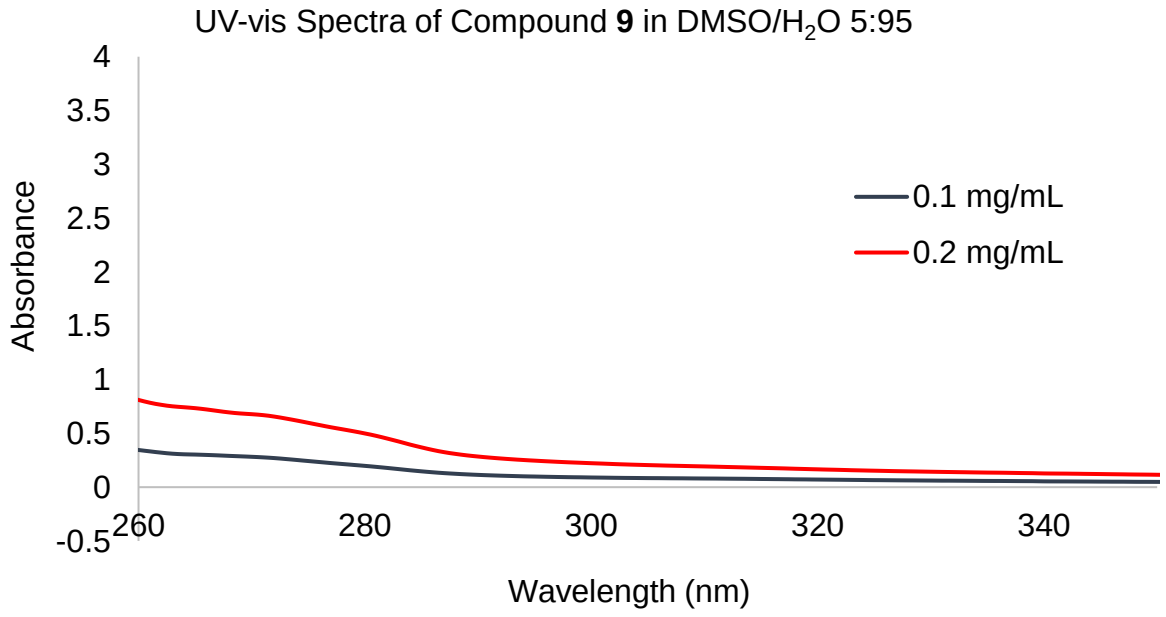

Figure 73. UV-vis spectra of compound **9** in a 5% DMSO-water solution.

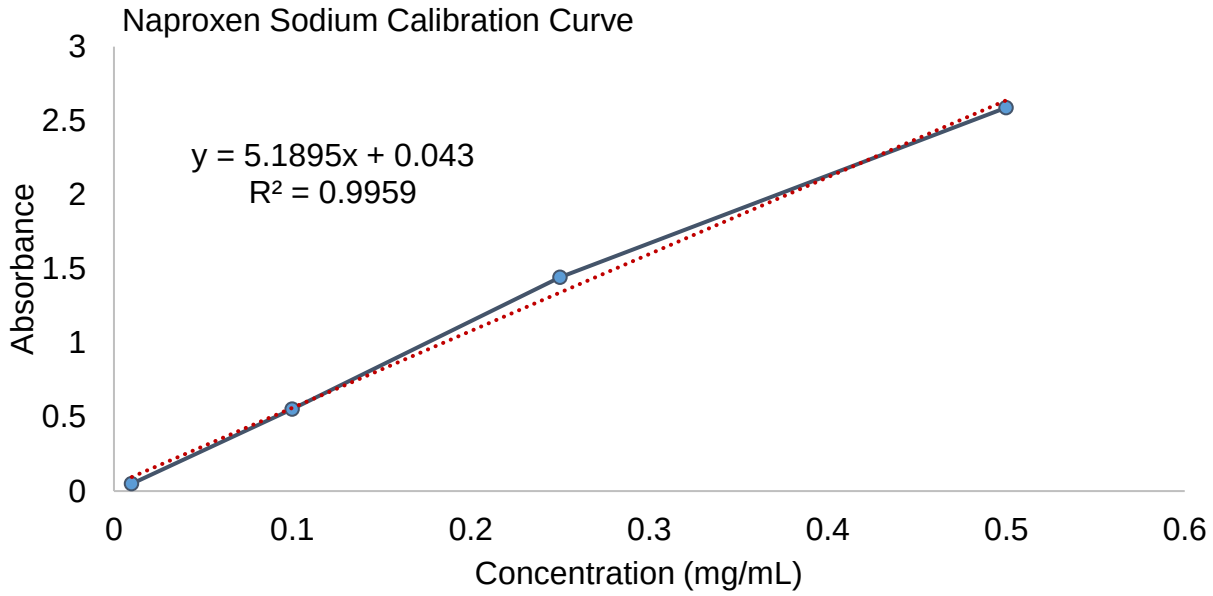

Figure 74. Calibration curve of naproxen sodium.

Supramolecular gels have been investigated for their ability to act as supramolecular sponges for a variety of water purification purposes. One popular application is the removal of toxic dyes from wastewater. We investigated gels formed by compound **9** for applications in removing toluidine blue for aqueous solution. To do this, a 2 mL gel formed by compound **9** in DMSO/H_2O 1:1 at a concentration of 0.5 mg/mL was prepared in a plugged glass syringe. Then, 1 mL of a 32.7 µM toluidine blue solution was added to the top of the gel column and the plug was removed to allow the solution to elute. DI water was then used to flush the gel column and ensure that the toluidine blue dye was adsorbed onto the gel. A total of 3.2 mL of a very light blue solution was collected from the column in total. Figure 75 shows images of each step in the gel column experiment. Analysis of the collected aqueous solution was carried out via UV-vis spectroscopy. UV-vis spectra of the collected aqueous phase and the original toluidine blue stock soltuion are shown in Figure 76. Using the calibration curve in Figure 77, the concentration of

toluidine blue in the collected solution was calculated to be 1.119 µM. Accounting for the dilution caused by the DI water flushes, the amount of toluidine blue remaining in solution was calculated to be 0.001095 mg. With this, the estimated amount of toluidine blue removed from the initial stock solution was 89%. In an attempt to use a more environmentally friendly solvent system to form the gel, this study was repeated with a 4 mL gel formed by compound **9** in EtOH/H_2O 1:2; however, it was found to be less efficient, indicating that gel morphology plays an important role in the gels ability to adsorb pollutants.

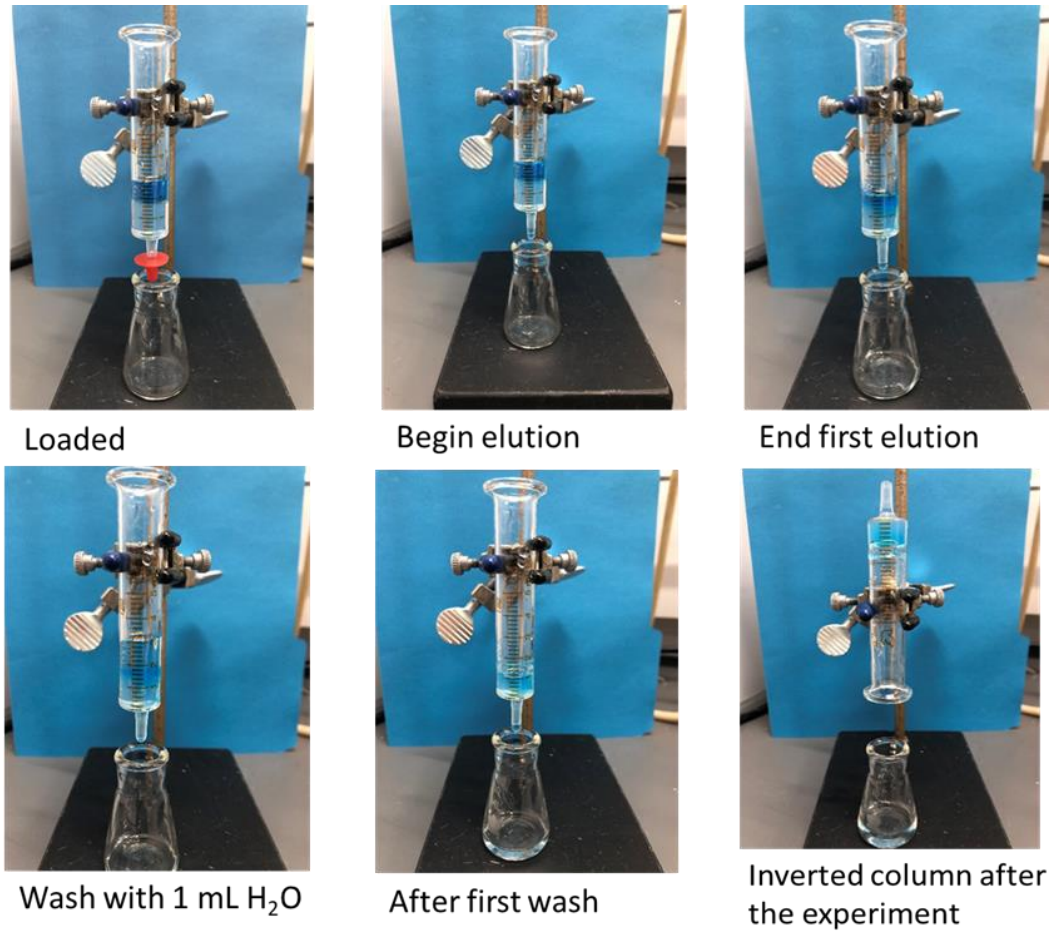

Figure 75. Images from various points during the dye removal study.

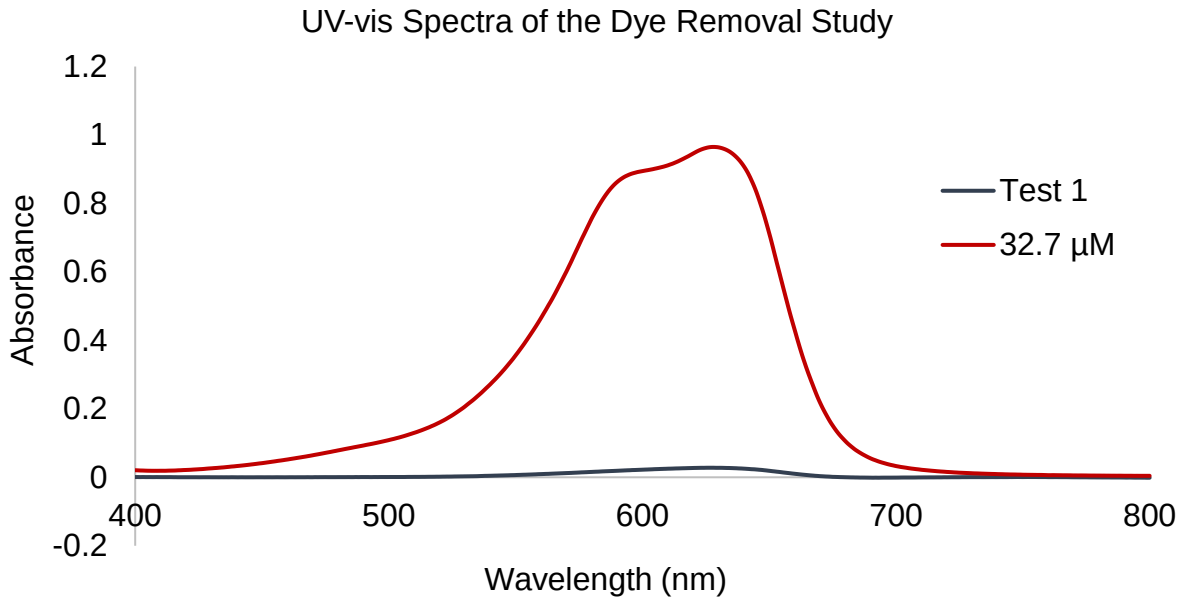

Figure 76. UV-vis spectra of the aqueous solution collected from the gel column and the toluidine blue stock solution.

Characterization of the head group and the final amide derivatives were carried out through 1D ^{1}H NMR and ^{13}C NMR spectroscopy, 2D HSQC and COSY NMR spectroscopy, and LC-MS. Figures 78-83 show the 1D and 2D NMR spectra obtained from compounds **III**, **5**, and **12**. These spectra are included as representative spectra that are obtained during the characterization of each of the final derivatives after purification.

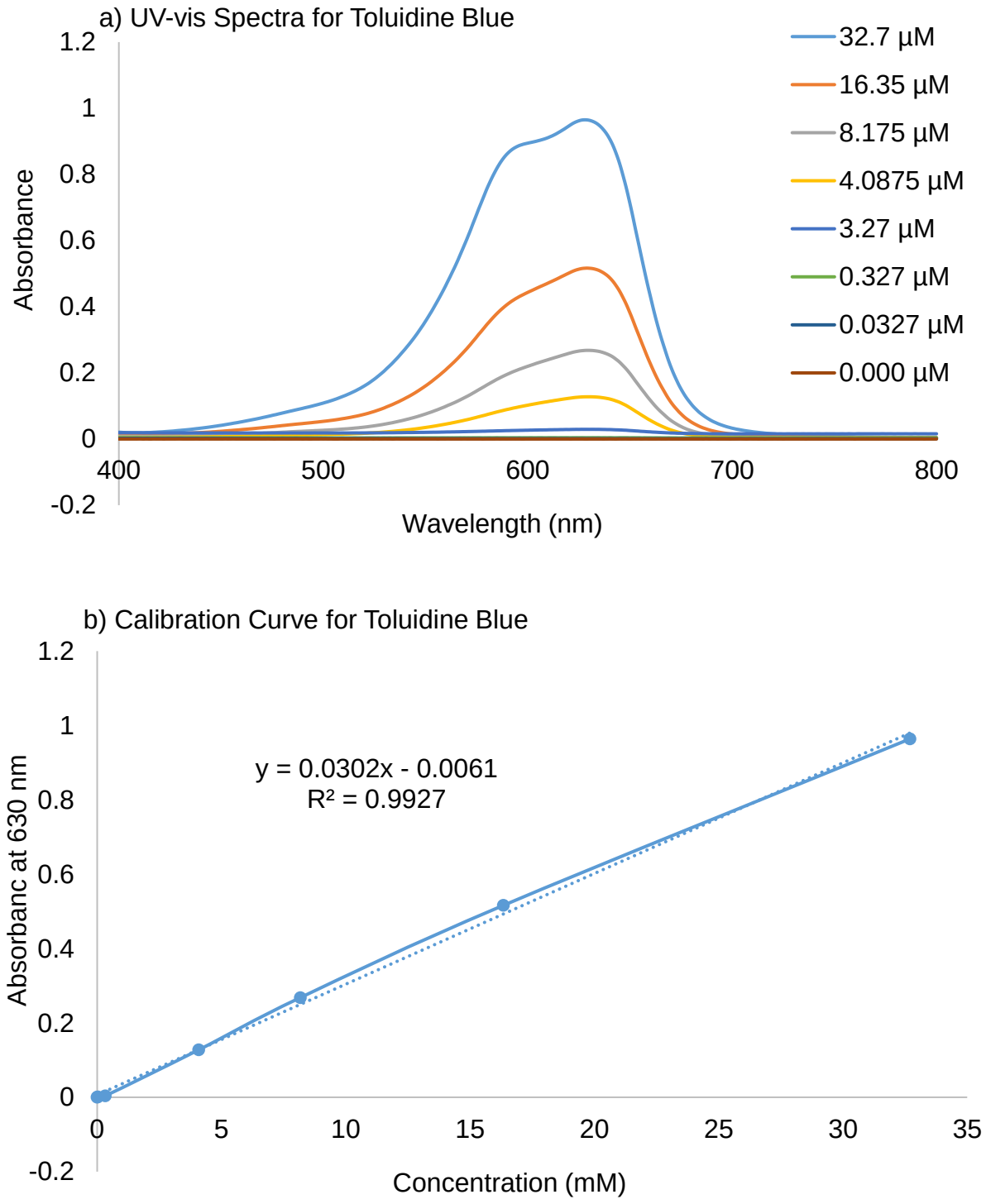

Figure 77. UV-vis spectra and calibration curve of toluidine blue. (a) UV-vis spectra of toluidine blue obtained through a serial dilution; (b) Calibration curve of toluidine blue.

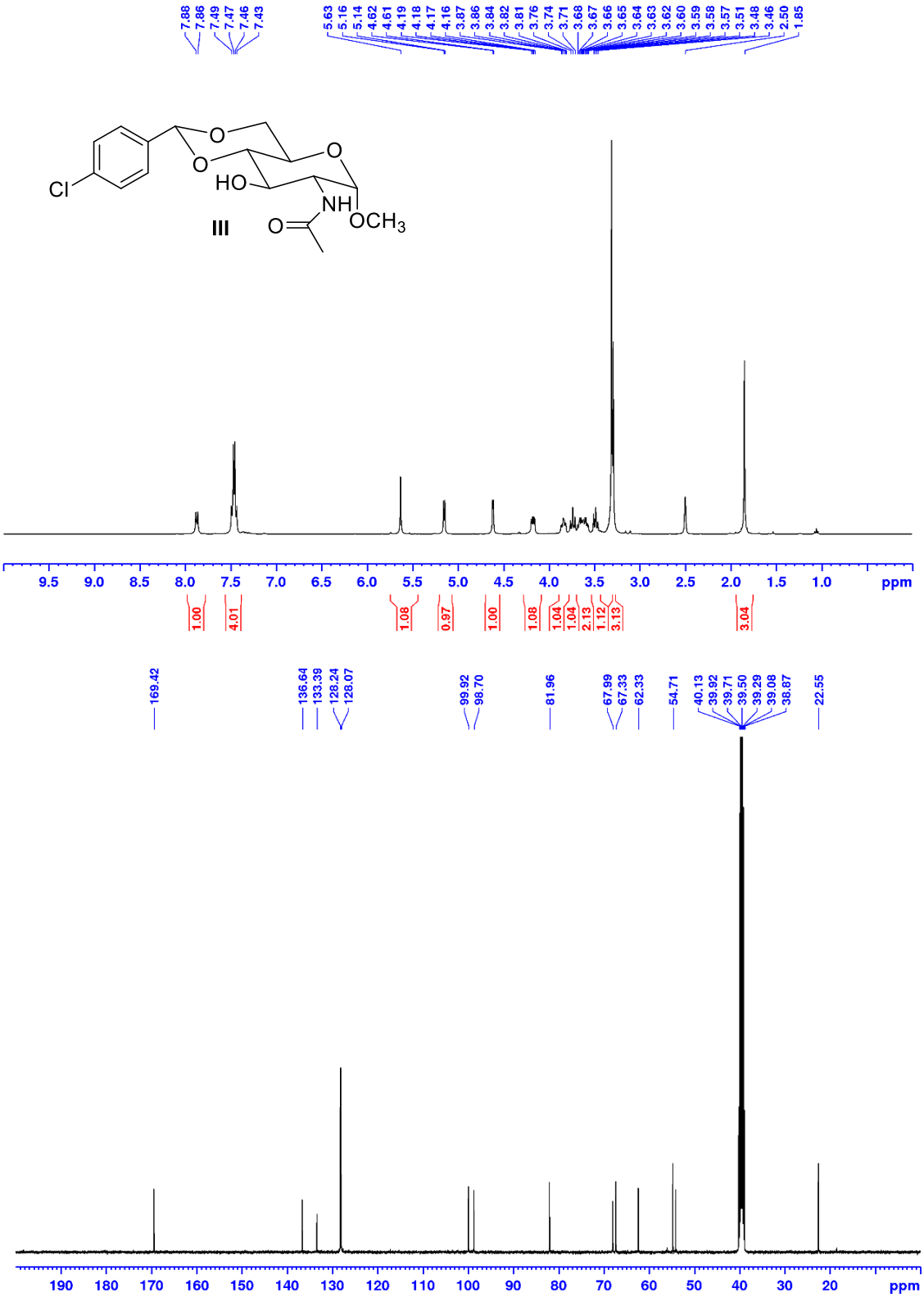

Figure 78. ^{1}H NMR and ^{13}C NMR spectra of compound **III** in d_6-DMSO.

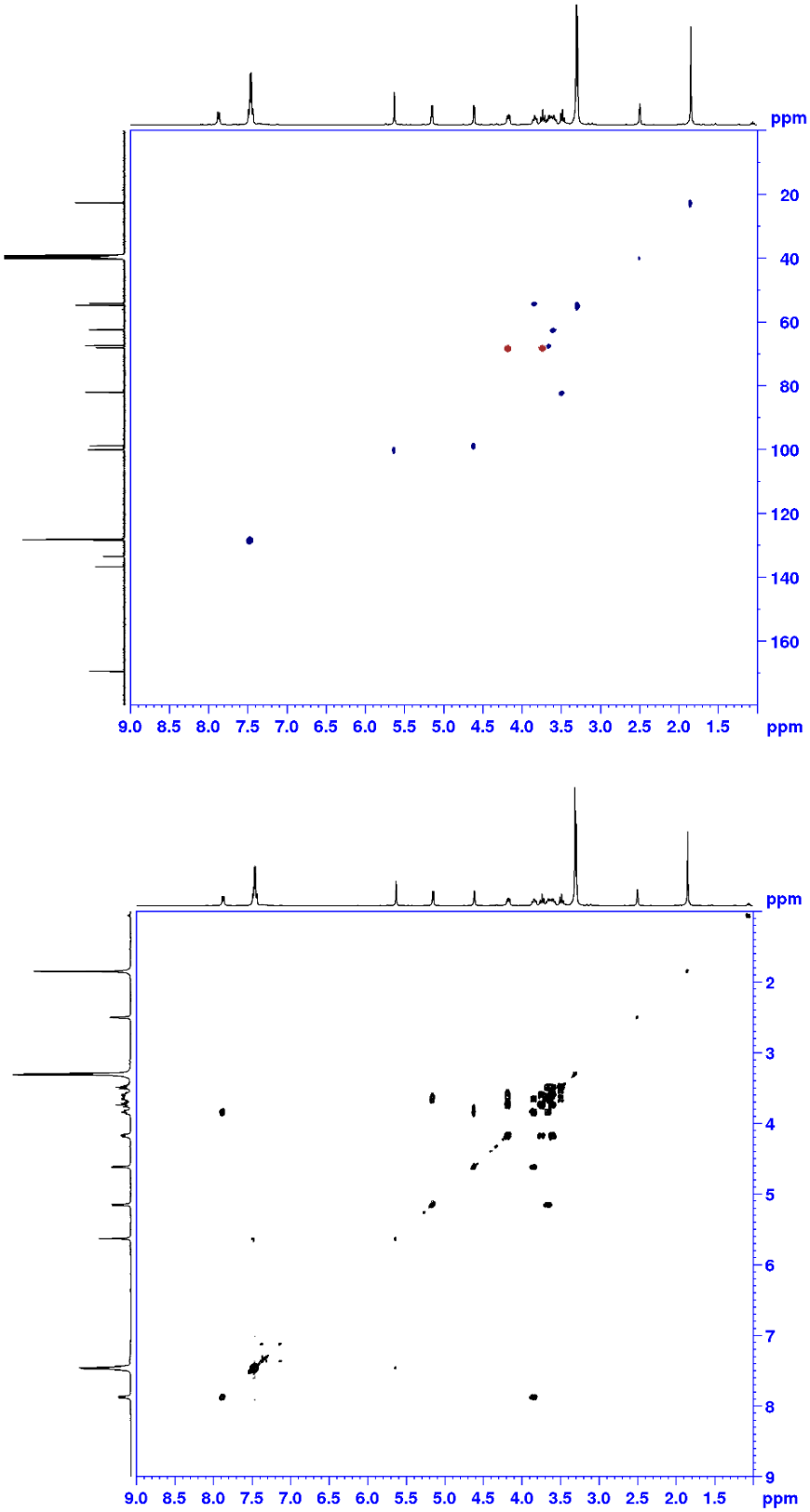

Figure 79. HSQC and COSY spectra of compound **III** in d_6-DMSO.

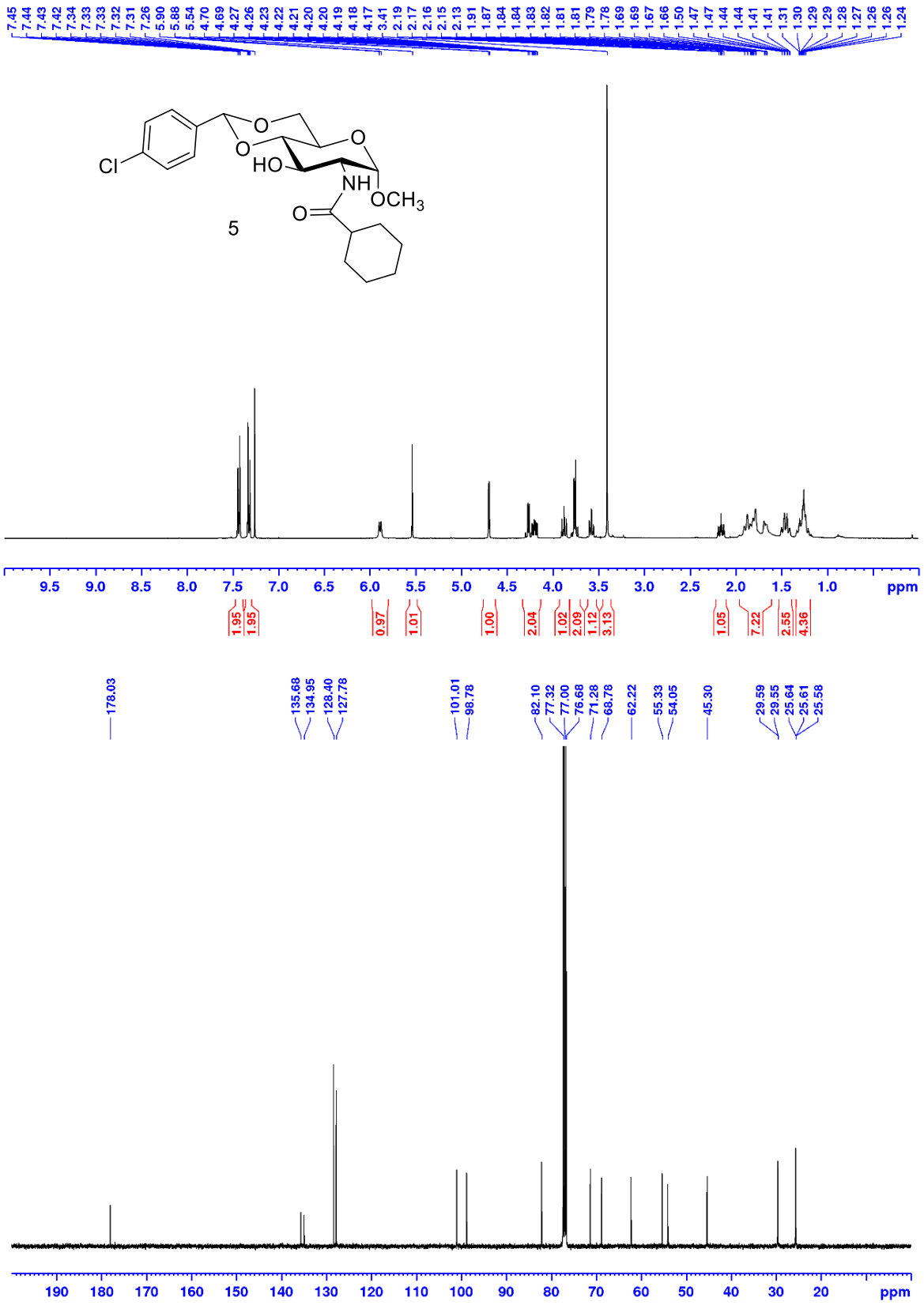

Figure 80. ^{1}H NMR and ^{13}C NMR spectra for compound **5** in $CDCl_3$.

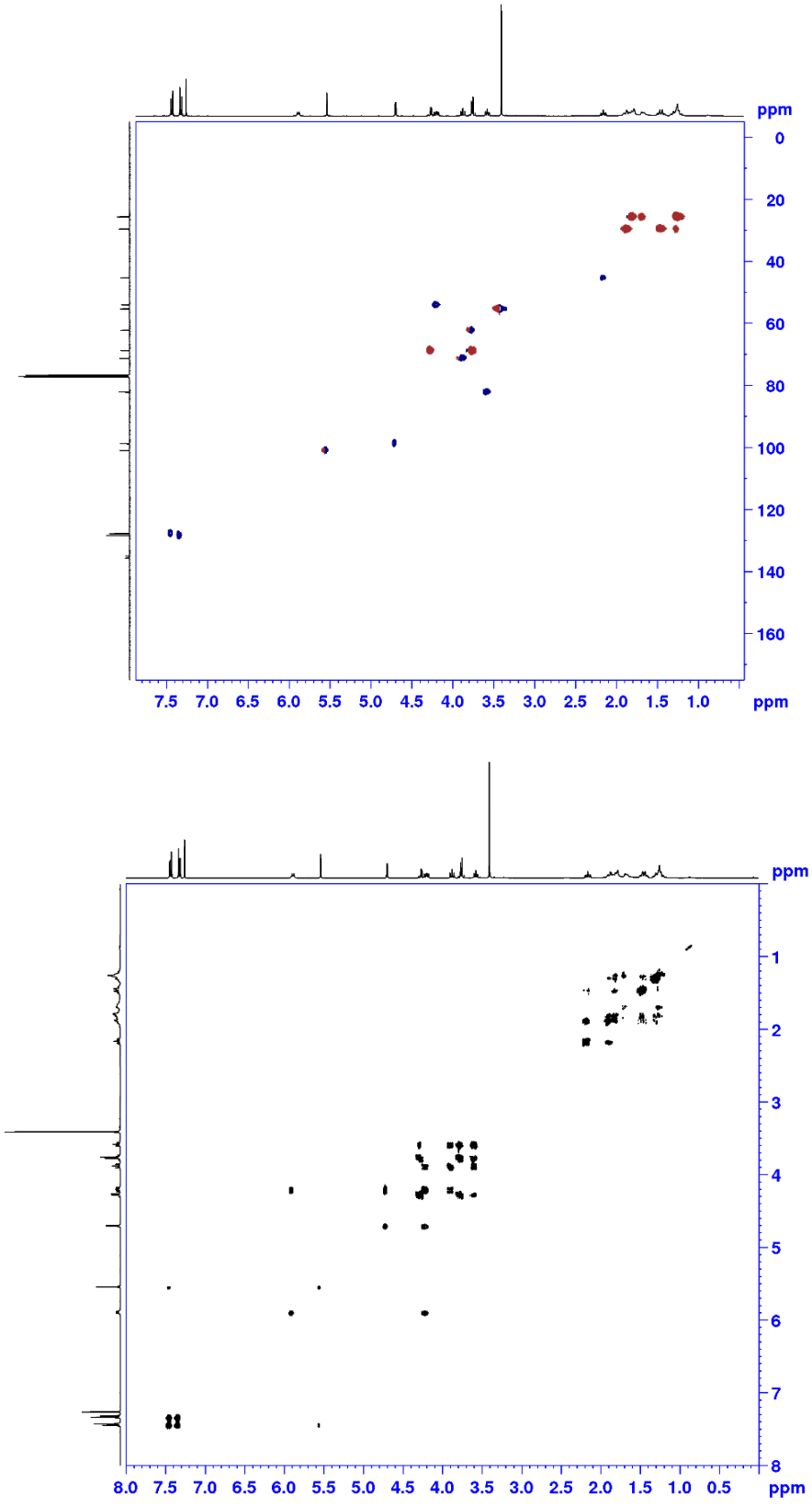

Figure 81. HSQC and COSY spectra for compound 5 in $CDCl_3$.

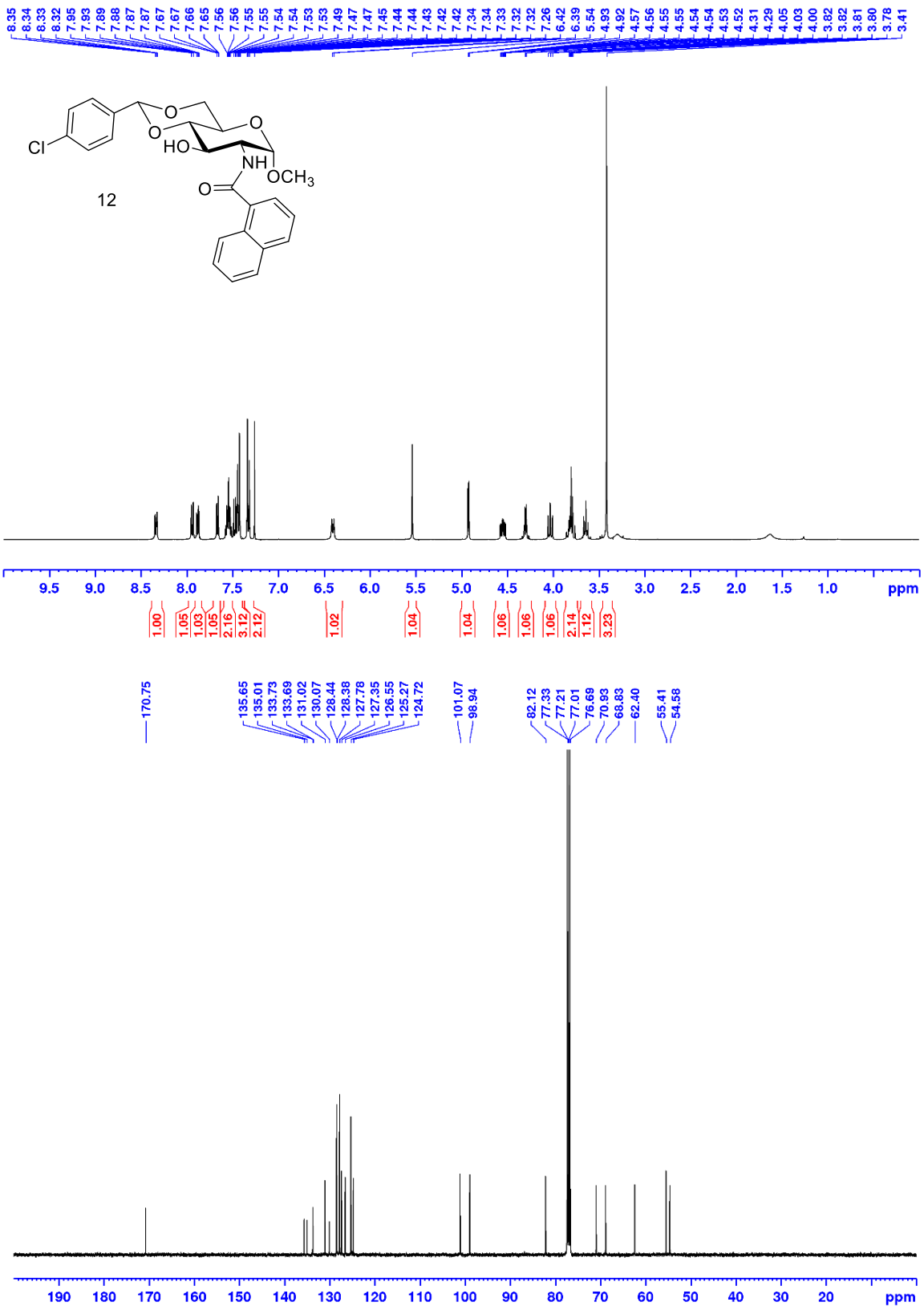

Figure 82. ^{1}H NMR and ^{13}C NMR spectra for compound **12** in $CDCl_3$.

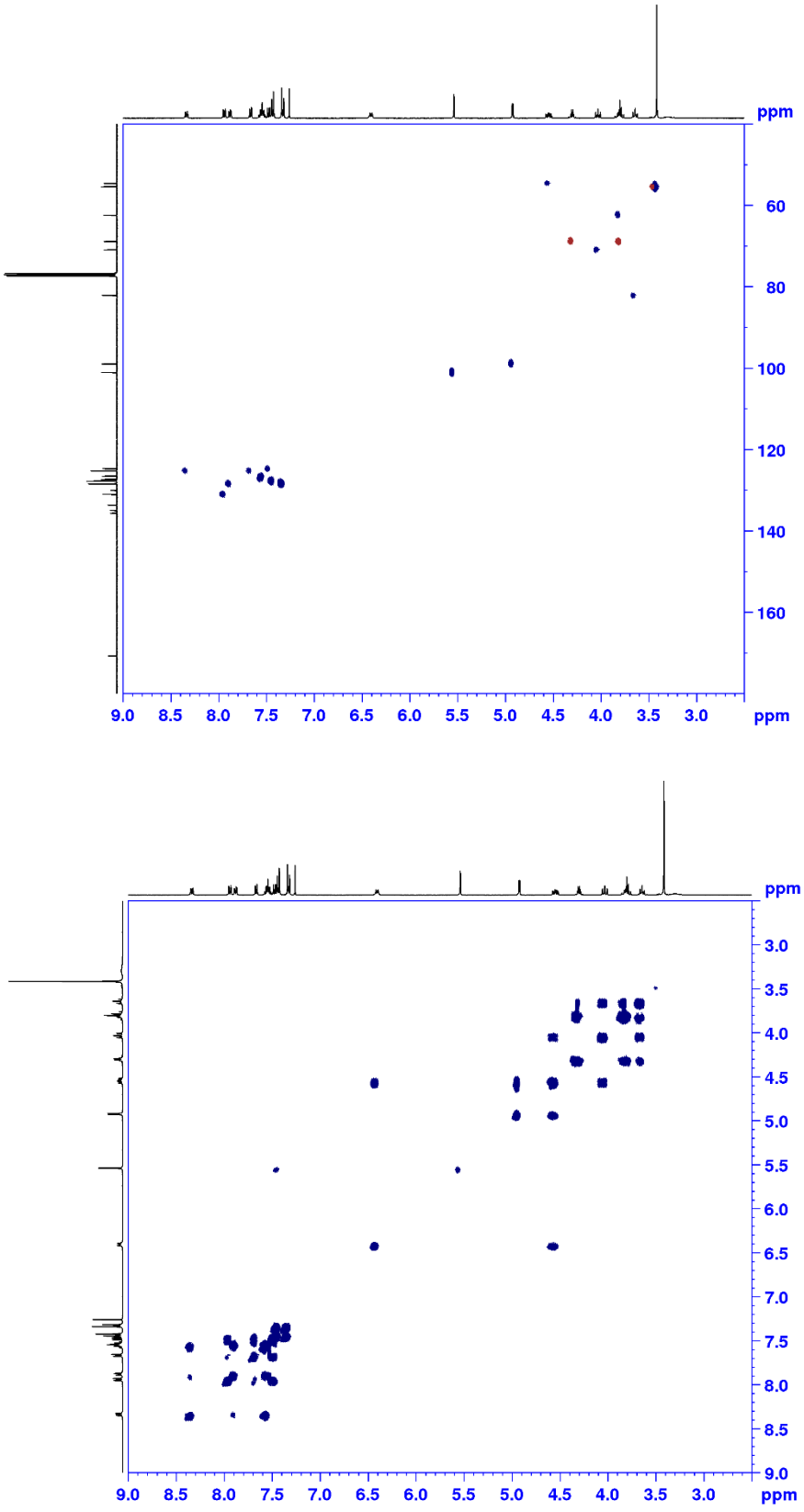

Figure 83. HSQC and COSY spectra for compound **12** in $CDCl_3$.

3.3 CONCLUSION

Introducing the chloro substituent to the para position of the 4,6-benzylidene acetal protected *N*-acetyl glucosamine resulted in enhanced gelation properties. This enticed us to design and synthesize a series of fourteen amide derivatives using the 4,6-O-(p-chlorobenzylidene) acetal protected D-glucosamine head group. From this series, a majority of the derivatives were found to be effective and versatile gelators. Five derivatives were found to form gels at concentrations under 0.1 wt%, classifying them at super gelators. The benzamide derivative **9** was a remarkable gelator, forming hydrogels at 0.36 mg/mL, as well as forming gels in several other solvents at concentrations under 1 mg/mL. The morphologies of the gel networks were investigated through optical microscopy and atomic force microscopy. The intermolecular interactions that promote self-assembly were analyzed via variable temperature ^{1}H NMR studies. Significant upfield changes in chemical shift were observed for all exchangeable proton signals as temperature increased, indicating these molecules are partaking in intermolecular hydrogen bonding. Interestingly, the aromatic proton signals changed with increased temperature, indicating that aromatic interactions and/or halogen bonding may be playing a role in the self-assembly process. The viscoelastic properties of several gels at concentrations less than 1 mg/mL were studied via rheology. In all instances, the storage modulus G′ remained higher than the loss modulus across the full range of angular frequency ω, indicating these low concentration gels are stable and have viscoelastic properties. Preliminary extrusion studies successfully printed lines of gel formed by compound **7** and **9** in DMSO/H_2O 1:1. Drug release studies demonstrated that aqueous gels formed by compound **9** are capable of sustained drug release. Dye absorption studies utilizing a gel column also found that low concentration DMSO/H_2O gels formed by compound **9** can also act as supramolecular sponges and removed dye from aqueous media. The gelators discovered in this

study have been found to be quite remarkable. The structure to gelation property relationships analyzed over the course of this study will provide valuable insight into using structure-based design to fine-tune supramolecular gelators.

3.4 EXPERIMENTAL SECTION

General method and materials: All reagents and solvents were purchased from chemical suppliers and uses as they were received. Purifications were carried out through recrystallization, trituration, or column chromatography using 230-400 mesh silica gel using gradient solvent systems. A Bruker 400 MHz spectrometer was utilized to obtain ^{1}H NMR, proton-decoupled ^{13}C NMR, HSQC, and COSY in either $CDCl_3$ or DMSO-d_6. The chemical shifts reported are based off of using $CDCl_3$/DMSO-d_6 as internal standards at 7.26/2.50 ppm (^{1}H NMR) and at 77.00/39.50 ppm (^{13}C NMR), respectively. Carbon and proton assignment was determined with the assistance of 2D NMR experiments (HSQC, COSY). Melting point analysis was carried out using a Fisher Jones melting point apparatus. Rheological experiments were carried out using a HR-2 Discovery Hybrid Rheometer from TA instrument, equipped with a 25 mm Peltier Plate. Mass spectroscopy was carried out using a LC-MS on an Agilent 6120B Single Quad Mass Spectrometer.

Optical Microscopy: A BX60M optical microscope using an Olympus DP73-1-51 high-performance 17MP digital camera with pixel shifting and Peltier cooling was used to image the morphology of the gel's microstructures. CellSens Dimension 1.11 software was used to acquire and process images. Samples were prepared by transferring small gel samples to microscope slides with either a pipette or spatula and allowing the ample to air dry for at least 24 hours before imaging. An alternative method for sample preparation utilized cellulose frits and vacuum

filtration to remove excess solvent from the gel's microstructures, which were then carefully transferred to a microscope slide using a razor blade.

Atomic Force Microscopy: A Dimension 3100 atomic force microscope was used to acquire AFM images of various gel samples. All imaging was carried out in tapping mode, using Tap300-G silicon AFM probes with a resonant frequency of 300 KHz and a force constant of 40 N/m. Sample preparation for AFM is identical to the methods used for preparing samples for optical microscopy imaging.

Gel Testing: All testing began at a concentration of 20.0 mg/mL, where 2 mg of the compound was added to a 1-dram vial and 0.1 mL of the respective solvent was added. The vial was then sealed and gently heated until a homogenous solution was acquired. In several cases, cycles of sonication followed by heating were required to achieve full dissolution of the gelator in solution. Samples were allowed to sit undisturbed and cool to room temperature for about 30 minutes before examination. The vials were then inverted and gently tapped to analyze whether a gel was formed. Upon inverting the vial, if no solvent flow was observed, a stable gel was formed. If solvent flow was observed upon inversion of the vial, the gel was recorded as unstable. For all samples that formed gels, 0.1 mL of the respective was added to the vial and the vial was heated until the sample transitioned into solution phase and the process was repeated. This process was repeated until the gel became unstable, at which point the minimum gelation concentration (MGC) was recorded. At lower concentrations, several gelators would not fully dissolve. Up to 0.6 mL of solvent was required to fully dissolve some of the gelators, with several cycles of heating and sonication. The gelators with very low MGCs also required the use of 2-dram vials to complete gelation testing. The appearance of each gel was recorded as either clear (transparent), translucent

(semi-transparent and allows some light to pass through it), or opaque (typically white in color and does not allow light to pass through it).

Rheological Analyses: Rheological experiments carried out on selected gels at concentrations under 1.0 mg/mL were done using a MCR 302 rheometer equipped with RheoCompass software. The cone geometry utilized was a 25-mm Peltier plate, with a 100 μm gap. Amplitude sweeps were obtained using an angular frequency (ω) of 10.0 radians per second to identify the linear viscosity range and frequency sweeps were carried out at a strain of 0.1%. In each study ≈500 μL gel samples were centered under the Peltier plate and any excess was trimmed before analysis.

Rheological experiments carried out in the gel extrusion studies were done on a Discovery HR2 Hybrid Rheometer from TA Instruments equipped with the TRIOS software. This instrument also utilized a 25-mm Peltier plate and with a 100 μm gap. Amplitude sweeps were also carried out using an angular frequency (ω) of 10.0 radians per second to identify the linear viscosity range. Frequency sweeps were then carried out using 0.5% strain. In each study, 200 μL samples were centered under the Peltier plate and any excess was trimmed before analysis. In each study, entire lines of extruded gel (200 μL) were scraped off of the glass slides immediately after extrusion and 24 hours after extrusion. Extruded gel lines were stored in airtight containers to prevent solvent evaporation until the second experiment 24 hours later. The non-extruded gel samples in each study were made by leaving 200 μL of the hot gel solution in the original vial and carefully transferring the entire sample for analysis.

Gel extrusion studies: Each gel was prepared in a 1-dram vial using a DMSO/H_2O solution. The vial was then gently heated until the gel to solution transition occurred and then the hot gelator solution was drawn up into a 1 mL syringe. The solution then cooled within the syringe,

forming a gel. The syringe was then stored upright for 24 hours. A Fusion 100 Touch syringe pump was utilized to control the extrusion rate. The syringe pump was set upright to hold the syringe vertically. A 14-gauge blunt tipped needle was utilized as a nozzle and a glass microscope slide was utilized as a print bed. A guide with graduation marks was used to slide the print bed underneath the extrusion apparatus during extrusion. The clearance between the nozzle and the print bed was measured to be ≈2.2 mm, measured via a micrometer. In each extrusion study, 200 µL of gel was extruder over a distance of ≈4 cm at an extrusion rate of 3 mL/min.

Liquid chromatography-mass spectrometer (LC-MS) conditions: An Agilent 1260 Infinity LC system coupled to a G6120B single quadrupole mass spectrometer, utilizing an atmospheric pressure ionization electrospray (API-ES) ionization source was used for molecular mass acquisition. Agilent poroshell 120 EC-C18 4.6 mm x 50 mm columns with 2.7 µm particle size were used for chromatographic separation. The system was linked to a diode array detector (DAD), which analyzes at 254 nm. The injection volume for each run was 5 µL. The flow rate for each experiment was 0.40 mL/min and each experiment's run time was 8 minutes. Agilent OpenLAB CDS ChemStation (Version C.01.05) was used to process data. The mass spectrometer's range was set from 0-2000.

Naproxen trapping and release studies: A naproxen sodium stock solution was made by dissolving 25.0 mg of naproxen sodium in 100 mL of DMSO/H_2O 5:95 solution. 2 mL gels were then prepared using this solution and allowed to rest at room temperature for at least 12 hours. 2 mL of DI water (pH 7) was then carefully added to the top of the gel to start the experiment. The aqueous layer was carefully removed and transferred to a quartz cuvette for UV-vis analysis at specific time intervals. After UV-vis analysis, the aqueous layer was carefully transferred back on top of the gel. Compound **13** was used in two diffusion studies to analyze the effect that gelator

concentration has on diffusion rate. The gelator concentrations in the two studies were 1.0 mg/mL and 0.5 mg/mL.

Chloramphenicol trapping and release: A chloramphenicol stock solution was made by dissolving 20 mg of chloramphenicol in 100 mL of DMSO/H_2O 5:95 solution2 mL gels were then prepared using this solution and allowed to rest at room temperature for at least 12 hours. 2 mL of DI water (pH 7) was then carefully added to the top of the gel to start the experiment. The aqueous layer was carefully removed and transferred to a quartz cuvette for UV-vis analysis at specific time intervals. After UV-vis analysis, the aqueous layer was carefully transferred back on top of the gel. Compound **13** was used in two diffusion studies to analyze the effect that gelator concentration has on diffusion rate. The gelator concentrations in the two studies were 1.0 mg/mL and 0.5 mg/mL.

Dye absorption studies: Gel columns were prepared in 5 mL glass syringes. Compound **13** was used to prepare a 2 mL gel at a concentration of 0.5 mg/mL in DMSO/H_2O 1:1. To prepare the column, 1.0 mg (2.4 µmol) of compound **13** was carefully weighed out in a 2-dram vial and 2 mL of DMSO/H_2O was added. The vial was then heated until a homogeneous solution was achieved. While hot and still in the solution phase, the solution was poured into glass syringe equipped with a plug. The solution was then allowed to cool within the syringe and a clear gel formed. A toluidine blue solution (32.7 µM) was then added on top of the gel column and the plug was removed. Once the toluidine blue solution finished eluting, 2 mL of DI water was added to flush the column and ensure that the toluidine blue dye was adsorbed to the gel's supramolecular architecture. After the column flush, a total of 3.2 mL of a light blue solution was acquired. UV-vis spectroscopy of the collected aqueous phase and a toluidine blue calibration curve was utilized to determine the concentration of residual toluidine blue in the collected aqueous phase. Using the

calibration curve, the concentration of toluidine blue was calculated to be 1.119 µM. The total amount of toluidine blue in the 3.2 mL collected aqueous phase was calculated to be 0.001095 mg. The original concentration of the toluidine blue solution was 0.01 mg/mL, so the initial amount of toluidine blue placed on top of the gel column was 0.01 mg. This indicates that 89.05% of the toluidine blue had been removed from the stock solution. A second dye absorption study was carried out using a larger volume EtOH/H_2O (1:2) gel, using the same method previously stated. Compound **13** was also used to prepare a 4 mL EtOH/H_2O (1:2) gel at a concentration of 0.5 mg/mL in a plugged glass syringe. The same volume of toluidine blue solution (32.7 µM) was then added on top of the gel column and the plug was removed. Once the toluidine blue solution finished eluting, 3 mL of DI water was added to flush the column and ensure that the toluidine blue dye was adsorbed to the gel's supramolecular architecture. After the column flush, a total of 5.2 mL of a light blue solution was collected. The concentration of toluidine blue in the collected solution was determined to be 1.344 µM and the amount of residual toluidine blue was calculated to be 0.00214 mg. These results indicate that 78.6% of the toluidine blue in the stock solution adsorbed onto the gel column.

Synthesis of compound III: 4-Chlorobenzaldehyde (5.60 g, 25.6 mmol, 1.2 equiv), trimethyl orthoformate (5.2 mL, 47.9 mmol, 2.25 equiv) and PTSA (0.418 g, 2.2 mmol, 1.0 equiv) were added to a 100 mL nitrogen flushed round bottom flask containing anhydrous MeOH (5 mL). The reaction mixture was refluxed for 3 h. The solvent was then removed under reduced pressure and the crude product was dissolved in anhydrous DMF (10 mL). Compound 2 (5.00 g, 21.3 mmol, 1 equiv) was then added and the reaction mixture was heated to 70 °C. The reaction was stirred at 70 °C for 6 h. Upon cooling the reaction mixture, a white solid precipitated. The reaction mixture was diluted with DCM (30 mL) and the precipitate was filtered. The filtrate was quenched with

$NaHCO_3$, followed by an aqueous workup using DI water (× 3) and DCM (× 2). Organic layers were dried with Na_2SO_4 and the solvent was removed under reduced pressure leaving an off white solid. The precipitate and crude product were combined and recrystallized in ethanol. The mother liquor was then purified via column chromatography (SiO_2) using 0–5% MeOH/DCM affording a white solid (5.974 g, 78%). R_f = 0.36 in 3% MeOH/DCM, mp 273.2–275.2 °C. ^{1}H-NMR (400 MHz, d_6-DMSO) δ 7.88 (d, J = 8.3 Hz, 1H); 7.51–7.42 (m, 4H); 5.63 (s, 1H); 5.15 (d, J = 5.7 Hz, 1H); 4.62 (d, J = 3.4 Hz, 1H); 4.22–4.14 (m, 1H); 3.89–3.80 (m, 1H); 3.74 (t, J = 10.1, 1H,); 3.70–3.55 (m, 2H), 3.53–3.45 (m, 1H), 3.29 (s, 3H); 1.85 (s, 3H,). ^{13}C-NMR (100 MHz, d_6-DMSO) δ 169.5; 136.6, 133.4, 128.2, 128.1; 99.9; 98.7; 82.0; 68.0; 67.3; 62.3; 54.7; 54.1; 22.5. MS m/z calculated for $C_{16}H_{20}ClNO_6Na$ $[M+Na]^+$ 380.1 found 380.1.

Synthesis of compound IV: Compound **3** (5.974 g, 16.7 mmol, 1 equiv.) was added to a 250 mL round bottomed flask containing a 1N NaOH ethanol solution. The reaction mixture was heated to refluxing temperature for 48 h. The reaction was monitored via ^{1}H-NMR and thin layer chromatography (TLC). Ethanol was removed under reduced pressure leaving an off white solid. An aqueous workup was carried out using EtOAc (× 3) and DI water (× 3). Organic layers were dried with Na_2SO_4 and the solvent was removed under reduced pressure. The crude product was purified via column chromatography (SiO_2) using 0–15% MeOH/DCM to afford a white solid (5.0126 g, 95%). R_f = 0.18 in 3% MeOH/DCM, mp 207.9–209.1 °C. ^{1}H-NMR (400 MHz, $CDCl_3$) δ 7.46–7.40 (m, 2H); 7.36–7.31 (m, 2H); 5.50 (s, 1H); 4.67 (d, J = 3.6 Hz, 1H); 4.29–4.22 (m, 1H); 3.82–3.66 (m, 3H); 3.45 (t, J = 9.1 Hz, 1H); 3.40 (s, 3H,); 2.81–2.74 (m, 1H). ^{13}C-NMR (100 MHz, $CDCl_3$) δ 135.8; 135.0; 128.5; 127.8; 101.2; 101.0; 82.0; 71.5; 69.1; 62.5; 56.7; 55.5. LC-MS m/z calculated for $C_{14}H_{19}ClNO_5$ $[M+H]^+$ 316.1 found 316.1.

General procedure for the synthesis of amide derivatives 1-14: The amides were synthesized using the corresponding acid chlorides (for compounds **1-6** and **9-14**) or anhydrides (for compounds **7-8**). In general, the headgroup amine **IV** (1 equiv.) was added to a round bottom flask with a drying tube under nitrogen atmosphere, followed by anhydrous DCM and either pyridine (5 equiv) or triethylamine (3 equiv), the flask was cooled to 0 °C, and the acid chloride or anhydride (1.1 equiv) diluted in anhydrous DCM, was added dropwise. Reaction mixture was typically stirred at 0 °C for 1–2 h. Reactions were monitored via ^{1}H-NMR spectroscopy and TLC. After completion, the reaction mixture was then quenched with 5% $NaHCO_3$ and stirred for an additional 30 min. Reaction mixture then underwent an aqueous workup with saturated $NaHCO_3$, saturated NH_4Cl, DI water, and DCM (× 3). The combined organic phase was dried with Na_2SO_4 and solvent was removed under reduced pressure. The crude product was purified via flash column chromatography on silica gel using a gradient solvent system. The detailed preparation for compound **1** is provided below and only amount used and characterization data are provided for all other compounds. All compounds were synthesized using 75 mg (0.24 mmol) of compound **IV** and 0.1 mL of either pyridine or trimethylamine unless otherwise mentioned.

Synthesis of compound 1: Compound **IV** (75 mg, 0.24 mmol, 1 equiv) dissolved in 3 mL of anhydrous DCM and anhydrous pyridine (0.1 mL, 1.2 mmol) was added to a dried 50 mL round bottomed flask. The reaction mixture was cooled in an ice bath. The propionyl chloride, prepared from propionic acid (37 µL, 0.27 mmol, 1.1 equiv) in situ, was dissolved in 2 mL anhydrous DCM and added dropwise to the flask over 10 min. The reaction mixture was stirred at 0 °C for 1 h. Reaction conversion was monitored via ^{1}H-NMR and TLC. The crude product was purified via column chromatography using DCM to 5% MeOH/DCM to afford a white solid (84 mg, 94%) as the desired product. R_f = 0.11 in 1% MeOH/DCM, mp 258.9–261.3 °C. ^{1}H-NMR (400 MHz,

$CDCl_3$) δ 7.47–7.41 (m, 2 H); 7.36–7.30 (m, 2 H); 5.85 (d, J = 8.6, 1 H); 5.54 (s, 1 H); 4.71 (d, J = 3.8 Hz, 1 H); 4.33–4.17 (m, 2 H); 3.89 (t, J = 9.6 Hz, 1 H); 3.81–3.72 (m, 2 H); 3.58 (t, J = 8.8, 1 H); 3.41 (s, 3 H); 2.30 (q, J = 7.5, 2 H); 1.18 (t, J =7.6, 3 H). ^{13}C-NMR (100 MHz, $CDCl_3$) δ 175.5; 135.7; 135.0; 128.4; 127.8; 101.1; 98.8; 82.1; 71.1; 68.8; 62.2; 55.3; 54.1; 29.6; 9.6. LC-MS *m*/*z* calculated for $C_{17}H_{23}ClNO_6$ $[M+H]^+$ 372.1 found 372.2.

Synthesis of compound 2: Valeryl chloride (0.27 mmol, 1.1 equiv) was synthesized from valeric acid (30 µL, 0.27 mmol) and oxalyl chloride (25 µL, 0.29 mmol). The crude acid chloride was added dropwise to a flask containing compound **IV** dissolved in anhydrous DCM with pyridine at 0 °C. The reaction mixture was stirred at 0 °C for 2 h. Crude product was purified via trituration using 50% EtOAc/hexanes, which afforded a white solid (89 mg, 82%). R_f = 0.17 in 1% MeOH/DCM, mp 238.7–240.0 °C. ^{1}H-NMR (400 MHz, $CDCl_3$) δ 7.47–7.40 (m, 2 H); 7.36–7.30 (m, 2 H); 5.87 (d, J = 8.4); 5.53 (s, 1 H); 4.71 (d, J = 3.9 Hz, 1 H); 4.34–4.15 (m, 2 H); 3.87 (t, J = 9.6 Hz, 1 H); 3.81–3.71 (m, 2 H); 3.62–3.54 (m, 1 H); 3.40 (s, 3 H); 2.26 (t, J = 7.6, 2 H); 1.69–1.58 (m, 2 H); 1.43–1.30 (m, 2 H); 0.92 (t, J = 7.3, 3 H). ^{13}C- NMR (100 MHz, $CDCl_3$) δ 174.9; 135.7; 135.0; 128.4; 127.8; 101.1; 98.8; 82.1; 71.0; 68.8; 62.2; 55.3; 54.1; 36.4; 27.6; 22.3; 13.7. LC-MS *m*/*z* calculated for $C_{19}H_{26}ClNO_6Na$ $[M+Na]^+$ 422.1 found 422.1.

Synthesis of compound 3: Hexanoyl chloride (38 µL, 0.27 mmol, 1.1 equiv) was dissolved in anhydrous DCM and added dropwise to a flask containing compound **IV** dissolved in anhydrous DCM with pyridine at 0 °C. The reaction mixture was stirred at 0 °C for 2 h. The crude product was purified via chromatography using 0–5% MeOH/DCM, affording a white solid (90 mg, 91%). R_f = 0.17 in 1% MeOH/DCM, mp 228.3–229.8 °C. ^{1}H-NMR (400 MHz, $CDCl_3$) δ 7.47–7.40 (m, 2 H); 7.37–7.30 (m, 2 H); 5.85 (d, J = 8.1, 1 H); 5.54 (s, 1 H); 4.71 (d, J = 3.7 Hz, 1 H); 4.36–4.16 (m, 2 H); 3.89 (t, J = 9.5 Hz, 1 H); 3.82–3.71 (m, 2 H); 3.63–3.54 (m, 1 H); 3.41 (s, 3 H); 2.25 (t,

J = 7.5, 2 H); 1.71–1.59 (m, 2 H); 1.41–1.24 (m, 4 H,); 0.90 (t, *J* = 6.9, 3 H. ^{13}C-NMR (100 MHz, $CDCl_3$) δ 174.9; 135.7; 135.0; 128.4; 127.8; 101.1; 98.8; 82.1; 71.1; 68.8; 62.2; 55.3; 54.1; 36.1; 31.3; 25.3; 22.3; 13.9.LC-MS *m*/*z* calculated for $C_{20}H_{29}ClNO_6$ $[M+H]^+$ 414.2 found 414.3 and $[M+Na]^+$ 436.2 found 436.3.

Synthesis of compound 4: Heptanoyl chloride (42 µL, 0.27 mmol, 1.1 equiv) was dissolved in anhydrous DCM and added dropwise to a flask containing compound **IV** dissolved in anhydrous DCM with pyridine at 0 °C. The reaction mixture was stirred at 0 °C for 2 h. The crude product was purified via column chromatography using 0–5% MeOH/DCM, affording a slightly yellow solid (91 mg, 88%). R_f = 0.29 in 1% MeOH/DCM, mp 223.9–225.8 °C, ^{1}H-NMR (400 MHz, $CDCl_3$) δ 7.48–7.40 (m, 2 H); 7.37–7.30 (m, 2 H); 5.85 (d, *J* = 8.2, 1 H); 5.54 (s, 1 H); 4.71 (d, *J* = 3.8 Hz, 1 H); 4.35–4.15 (m, 2 H); 3.88 (t, *J* = 9.6 Hz, 1 H); 3.82–3.70 (m, 2 H); 3.58 (t, *J* = 8.7, 1 H); 3.40 (s, 3 H); 2.25 (t, *J* = 7.5, 2 H); 1.73–1.56 (m, 2 H); 1.42–1.15 (m, 4 H); 0.98–0.79 (m, 3 H). ^{13}C-NMR (100 MHz, $CDCl_3$) δ 174.9; 135.7; 135.0; 128.4; 127.8; 101.1; 98.8; 82.1; 71.1; 68.8; 62.2; 55.3; 54.1; 36.6; 31.5; 29.7; 28.8; 25.5; 22.5; 14.0. LC-MS *m*/*z* calculated for $C_{21}H_{31}ClNO_6$ $[M+H]^+$ 428.2 found 428.2.

Synthesis of compound 5: Cyclohexanecarbonoyl chloride (0.27 mmol, 1.1 equiv) was synthesized using cyclohexanecarboxylic acid (34 mg, 0.27 mmol, 1.1 equiv) and oxalyl chloride (25 µL, 0.29 mmol, 1.2 equiv). The crude acid chloride was added dropwise to a flask containing compound **IV** dissolved in anhydrous DCM with pyridine at 0 °C. The reaction mixture was stirred at 0 °C for 1 h. The crude product was purified via column chromatography using 0–5% MeOH/DCM, affording an off white solid (88 mg, 87%). R_f = 0.23 in 1% MeOH/DCM, mp 250.3–253.2 °C. ^{1}H-NMR (400 MHz, $CDCl_3$) δ 7.47–7.40 (m, 2 H); 7.36–7.30 (m, 2 H); 5.89 (d, *J* = 8.4, 1 H); 5.54 (s, 1 H); 4.70 (d, *J* = 3.9 Hz, 1 H); 4.32–4.16 (m, 2 H); 3.88 (t, *J* = 9.6 Hz, 1 H); 3.81–

3.72 (m, 2 H); 3.58 (t, *J* = 9.1, 1 H); 3.41 (s, 3 H); *δ* 2.16 (tt, *J* = 11.6, *J* = 3.5, 1 H); 1.98–1.73 (m, 4 H); 1.72–1.61 (m, 1 H,); 1.53–1.39 (m, 2 H); 1.35–1.16 (m, 3 H). ^{13}C-NMR 100 MHz, $CDCl_3$) *δ* 178.0; 135.7; 135.0; 128.4; 127.8; 101.0; 98.8; 82.1; 71.3; 68.8; 62.2; 55.3; 54.1; 45.3; 29.6; 29.5; 25.65; 25.62; 25.60. LC-MS *m/z* calculated for $C_{21}H_{29}ClNO_6$ $[M+H]^+$ 426.1 found 426.1.

Synthesis of compound 6: Pivaloyl chloride (33 μL, 0.27 mmol, 1.1 equiv) was dissolved in anhydrous DCM and added dropwise to a flask containing compound **IV** dissolved in anhydrous DCM with pyridine at 0 °C. The reaction mixture was stirred at 0 °C for 2 h. The crude product was purified via column chromatography using 0–3% MeOH/DCM, affording a white solid (70 mg, 73%). R_f = 0.23 in 1% MeOH/DCM, mp 162.4–164.3 °C. ^{1}H-NMR (400 MHz, $CDCl_3$) *δ* 7.47–7.41 (m, 2 H); 7.36–7.30 (m, 2 H); 6.08 (d, *J* = 8.1, 1 H); 5.54 (s, 1 H); 4.70 (d, *J* = 3.9 Hz, 1 H); 4.35–4.14 (m, 2 H); 3.89 (t, *J* = 9.5 Hz, 1 H); 3.83–3.70 (m, 2 H); 3.62–3.55 (m, 1 H); 3.41 (s, 3 H,); 1.23 (s, 9 H). ^{13}C-NMR (100 MHz, $CDCl_3$) *δ* 180.7; 135.7; 134.9; 128.4; 127.8; 101.0; 98.8; 82.1; 71.5; 68.8; 62.2; 55.4; 54.2; 38.8; 27.5. LC-MS *m/z* calculated for $C_{19}H_{27}ClNO_6$ $[M+H]^+$ 400.1 found 400.1 and $[M+Na]^+$ 422.1 found 422.1.

Synthesis of compound 7: Trifluoroacetic anhydride (100 μL, 0.71 mmol, 1.1 equiv) was dissolved in anhydrous DCM and added dropwise to a flask containing compound **IV** (200 mg, 0.64 mmol, 1 equiv) dissolved in anhydrous DCM and triethylamine (0.450 mL, 3.2 mmol) at 0 °C. The reaction mixture was stirred at 0 °C for 1.5 h. The crude product was purified via column chromatography using 0–3% MeOH/DCM, affording a white solid (244 mg, 93%). R_f = 0.31 in 1% MeOH/DCM, mp 291.3–292.7 °C, sample turned brown at 285.2 °C ^{1}H-NMR (400 MHz, d_6-DMSO) *δ* 9.56 (d, *J* = 7.1 Hz, 1 H); 7.51–7.40 (m, 4 H); 5.65 (s, 1 H); 5.37 (d, *J* = 5.5 Hz, 1 H; 4.74 (d, *J* = 3.1 Hz, 1 H); 4.24–4.16 (m, 1 H); 3.96–3.83 (m, 2 H); 3.76 (t, *J* = 10.1, 1 H); 3.68–

3.59 (m, 1 H), 3.57–3.49 (m, 1 H), 3.32 (s, 3 H,). ^{13}C-NMR (100 MHz, d_6-DMSO) δ 157.2; 156.8; 156.5; 156.1; 136.6; 134.5; 128.2; 128.1; 120.1; 117.3; 114.4; 111.7; 99.9; 97.7; 81.7; 67.8; 66.4; 62.3; 55.1; δ 54.9. LC-MS *m*/*z* calculated for $C_{16}H_{17}ClF_3NO_6Na$ $[M+Na]^+$ 434.1 found 434.1.

Synthesis of compound 8: Trichloroacetic anhydride (59 μL, 0.32 mmol, 1.3 equiv) was dissolved anhydrous DCM and added to a flask containing compound **IV** dissolved in anhydrous DCM and triethylamine (0.100 mL, 0.72 mmol) at 0 °C. The reaction mixture was stirred at 0 °C for 7.5 h. The crude product was purified via column chromatography using 0–3% MeOH/DCM, affording a white solid (86 mg, 87%). R_f = 0.40 in 1% MeOH/DCM. mp 181.7–182.8 °C. ^{1}H-NMR (400 MHz, $CDCl_3$) δ 7.46–7.40 (m, 2 H); 7.38–7.32 (m, 2 H); 6.91 (d, *J* = 8.7, 1 H); 5.55 (s, 1 H); 4.83 (d, *J* = 3.7 Hz, 1 H); 4.34–4.26 (m, 1 H); 4.22–4.14 (m, 1 H); 4.02 (t, *J* = 9.6, 1 H); 3.86–3.74 (m, 2 H); 3.60 (t, *J* = 9.1, 1 H); 3.45 (s, 3 H). ^{13}C-NMR (100 MHz, $CDCl_3$) δ 162.5; 135.5; 135.2; 128.5; 127.7; 101.1; 98.3; 92.4, 81.6; 70.0; 68.7; 62.4; 55.6; 55.5. LC-MS *m*/*z* calculated for $C_{16}H_{17}Cl_4NO_6Na$ $[M+Na]^+$ 482.1 and 482.1.

Synthesis of compound 9: Benzoyl chloride (38 μL, 0.27 mmol, 1.1 equiv) was dissolved in anhydrous DCM and added dropwise to a flask containing compound **IV** dissolved in anhydrous DCM with pyridine at 0 °C. The reaction mixture was stirred at 0 °C for 1 h. The crude product was purified via column chromatography using 0–3% MeOH/DCM, affording a white solid (86 mg, 85%). R_f = 0.31 in 1% MeOH/DCM. mp 202.3–203.5 °C ^{1}H-NMR (400 MHz, $CDCl_3$) δ 7.85–7.75 (m, 2 H); 7.57–7.50 (m, 1 H); 7.49–7.40 (m, 4 H); 7.37–7.31 (m, 2 H); 6.54 (d, *J* = 8.5, 1 H); 5.56 (s, 1 H); 4.83 (d, *J* = 3.8 Hz, 1 H); 4.48–4.40 (m, 1 H); 4.32–4.27 (m, 1 H); 4.01 (t, *J* = 9.6 Hz, 1 H); 3.87–3.75 (m, 2 H); 3.65 (t, *J* = 9.1, 1 H); 3.43 (s, 3 H,). ^{13}C-NMR (100 MHz, $CDCl_3$) δ 168.6; 135.6; 135.0; 133.6; 132.0; 128.7; 128.4; 127.8; 127.2; 101.1; 98.9; 82.1; 71.0; 68.8; 62.3;

55.4; 54.6.LC-MS *m*/*z* calculated for $C_{21}H_{23}ClNO_6$ $[M+H]^+$ 420.1 found 420.2 and $[M+Na]^+$ 442.1 found 442.1.

Synthesis of compound 10: 4-Bromobenzoyl chloride (59 mg, 0.27 mmol, 1.1 equiv) was dissolved in anhydrous DCM and added dropwise to a flask containing compound **IV** dissolved in anhydrous DCM with pyridine at 0 °C. The reaction mixture was stirred at 0 °C for 1.5 h. The crude product was purified via trituration using 5% MeOH/DCM, affording a white solid (88 mg, 74%). R_f = 0.31 in 1% MeOH/DCM. mp 308.0–309.0 °C. ^{1}H-NMR (400 MHz, d_6-DMSO) δ 8.27 (d, J = 7.8, 1 H); 7.91–7.80 (m, 2 H); 7.72–7.63 (m, 2 H); 7.53–7.40 (m, 4 H); 5.66 (s, 1 H); 5.06 (d, J = 5.6, 1 H); 4.78 (d, J = 3.6 Hz, 1 H); 4.25–4.18 (m, 1 H); 4.12–4.03 (m, 1 H); 3.98–3.89 (m, 1 H); 3.83–3.74 (m, 1 H); 3.72–3.64 (m, 1 H); 3.61–3.54 (m, 1 H); 3.16 (s, 3 H). ^{13}C-NMR (100 MHz, d_6-DMSO) δ 166.5; 136.5; 133.2; 130.9; 129.4; 128.0; 127.8; 124.6; 99.8; 98.4; 81.7; 67.8; 66.9; 62.2; 55.0; 54.7. LC-MS *m*/*z* calculated for $C_{21}H_{22}BrClNO_6$ $[M+H]^+$ 498.0 and 500.0 found 497.9 and 499.9.

Synthesis of compound 11: 3-Chlorobenzoyl chloride (0.27 mmol, 1.1 equiv) was synthesized using 3-chlorobenzoic acid (41 mg, 0.27 mmol, 1.1 equiv) and oxalyl chloride (25 µL, 0.29 mmol, 1.2 equiv). The crude acid chloride was added dropwise to a flask containing compound **IV** dissolved in anhydrous DCM with pyridine at 0 °C. The reaction mixture was stirred at 0 °C for 12 h. Crude product was purified via recrystallization in ethanol and the mother liquor was purified via column chromatography using 20–80% EtOAc/hexanes, affording a white solid (91 mg, 84%). R_f = 0.26 in 1% MeOH/DCM. mp 225.2–227.0 °C. ^{1}H-NMR (400 MHz, $CDCl_3$) δ 7.83 (t, J = 3.4 Hz, 1 H); 7.72 (d, J = 7.8, 1 H); 7.55–7.32 (m, 7 H); 6.53 (d, J = 8.7 Hz, 1 H); 5.59 (s, 1 H); 4.87 (d, J = 3.8, 1 H); 4.50–4.41 (m, 1 H); 4.39–4.27 (m, 1 H); 4.06 (t, J = 9.6 Hz, 1 H); 3.91–3.76 (m, 2 H); 3.67 (t, J = 9.1 Hz); 3.47 (s, 3 H). ^{13}C NMR (100 MHz, $CDCl_3$) δ 167.1;

135.6; 135.5; 135.1; 134.9; 132.0; 130.0; 128.5; 127.8; 127.6; 125.3; 101.2; 98.8; 82.0; 70.6; 68.8; 62.4; 55.4; 54.6. LC-MS *m*/*z* calculated for $C_{21}H_{22}Cl_2NO_6$ $[M+H]^+$ 454.1 found 454.0.

Synthesis of compound 12: 1-Naphthoyl chloride (41 µL, 0.27 mmol, 1.1 equiv) was dissolved in anhydrous DCM and added to a flask containing compound **IV** dissolved in anhydrous DCM with pyridine at 0 °C. The reaction mixture was stirred at 0 °C for 3 h. Crude reaction mixture was purified via column chromatography using 0–3% MeOH/DCM and trituration with ethanol (94 mg, 84%). R_f = 0.26 in 1% MeOH/DCM. mp 227.7–229.0 °C. ^{1}H-NMR (400 MHz, $CDCl_3$) δ 8.38–8.30 (m, 1 H); 7.94 (d, *J* = 8.3, 1 H); 7.91–7.85 (m, 1 H); 7.70–7.64 (m, 1 H); 7.59–7.50 (m, 2 H); 7.50–7.40 (m, 3 H); 7.36–7.30 (m, 2 H); 6.40 (d, *J* = 8.8, 1 H); 5.54 (s, 1 H); 4.92 (d, *J* = 3.8, 1 H); 4.59–4.51 (m, 1 H); 4.35–4.26 (m, 1 H); 4.03 (t, *J* = 9.6 MHz, 1 H); 3.86–3.75 (m, 2 H); 3.64 (t, *J* = 9.1 Hz, 1 H); 3.41 (s, 3 H). ^{13}C-NMR (100 MHz, $CDCl_3$) δ 170.7; 135.7; 135.0; 133.73; 133.69; 131.0; 130.1; 128.44; 128.38; 127.8; 127.4; 126.6; 125.3; 124.7; 101.1; 98.9; 82.1; 70.9; 68.8; 62.4; 55.4; 54.6. LC-MS *m*/*z* calculated for $C_{25}H_{25}ClNO_6$ $[M+H]^+$ 470.1 found 470.1.

Synthesis of compound 13: 1-Naphthylacetyl chloride (0.27 mmol, 1.1 equiv) was synthesized using 1-naphthaleneacetic acid (50 mg, 0.27 mmol, 1.1 equiv) and oxalyl chloride (25 µL, 0.29 mmol, 1.2 equiv). The crude acid chloride was added dropwise to a flask containing compound **IV** dissolved in anhydrous DCM with pyridine at 0 °C. The reaction mixture was stirred at 0 °C for 3 h. Crude reaction mixture was purified via trituration using 5% MeOH/DCM (79 mg, 71%). R_f = 0.14 in 1% MeOH/DCM. mp 258.4–260.9 °C. ^{1}H-NMR (400 MHz, DMSO-d_6) δ 8.33 (d, *J* = 8.2 Hz, 1 H); 8.15–8.06 (m, 1 H), 7.95–7.87 (m, 1 H); 7.85–7.76 (m, 1 H); 7.57–7.39 (m, 8H); 5.64 (s, 1 H); 5.27 (d, *J* = 5.9, 1 H); 4.60 (d, *J* = 3.5, 1 H); 4.22–4.14 (m, 1 H); 4.08–3.81 (m, 3 H); 3.80–3.70 (m, 2 H); 3.63 (tt, *J* = 9.8 Hz, *J* = 4.7 Hz, 1 H); 3.55–3.47 (m, 1 H); 3.30 (s, 3 H). ^{13}C-NMR (100 MHz, DMSO-d_6) δ 170.4; 136.6; 133.4; 133.3; 132.9; 132.0; 128.2; 128.1; 127.7;

126.9; 125.8; 125.5; 125.4; 124.2; 99.9; 98.6; 81.9; 68.0; 67.3; 62.4; 54.9; 54.3; 39.6. LC-MS *m*/*z* calculated for $C_{26}H_{27}ClNO_6$ $[M+H]^+$ 484.1 found 484.1.

Synthesis of compound 14: 2-Naphthylacetyl chloride (0.27 mmol, 1.1 equiv) was synthesized using 2-naphthaleneacetic acid (50 mg, 0.27 mmol, 1.1 equiv) and oxalyl chloride (25 µL, 0.29 mmol, 1.2 equiv). The crude acid chloride was added dropwise to a flask containing compound **IV** dissolved in anhydrous DCM with pyridine at 0 °C. The reaction mixture was stirred at 0 °C for 3 h. Crude reaction mixture was purified via trituration using 5% MeOH/DCM (79 mg, 71%). R_f = 0.14 in 1% MeOH/DCM. mp 262.2–264.2 °C. ^{1}H-NMR (400 MHz, DMSO-d_6) δ 8.29 (d, *J* = 8.2 Hz); 7.91–7.80 (m, 3 H); 7.77 (s, 1 H); 7.53–7.41 (m, 7 H); 5.64 (s, 1 H); 5.30 (d, *J* = 5.9, 1 H); 4.65 (d, *J* = 3.6); 4.23–4.15 (m, 1 H); 3.91–3.83 (m, 1 H); 3.79–3.58 (m, 5 H); 3.55–3.47 (m, 1 H); 3.29 (s, 3 H). ^{13}C-NMR (100 MHz, DMSO-d_6) δ 170.3; 136.6; 134.2; 133.4; 132.9; 131.7; 128.2, 128.1, 127.6; 127.4; 127.3; 127.1; 125.9; 125.4; 99.9; 98.6; 81.9; 68.0; 67.3; 62.4; 54.9; 54.3; 42.1. LC-MS *m*/*z* calculated for $C_{26}H_{27}ClNO_6$ $[M+H]^+$ 484.1 found 484.1.

CHAPTER 4

DESIGN, SYNTHESIS, CHARACTERIZATION AND SELF-ASSEMBLING PROPERTIES OF JANUS GLYCOCLUSTERS

This chapter is adapted in part from the following paper: "Wang, G.; Wang, D.; Bietsch, J.; Chen, A.; Sharma, P., Synthesis of Dendritic Glycoclusters and Their Applications for Supramolecular Gelation and Catalysis. *The Journal of Organic Chemistry* **2020,** *85* 16136-16156, 100.121/acs.joc.0c01978."

4.1 INTRODUCTION

Multivalent glycoarchitectures, such as glycoclusters and glycodendrimers, are well known for forming well defined self-assemblies and well organized cross-linked lattices.[90] Utilizing multivalency in the design of self-assembling molecules has led to the creation of multiple advanced materials with applications in material science, medicinal chemistry, and bioorganic chemistry.[91-93] Rationally designing dendritic compounds containing appropriate functional groups can lead to the discovery of self-assembling molecules, such as LMWGs.[94] Copper catalyzed azide alkyne cycloaddition (CuAAC), or "Click" chemistry, has been utilized in the synthesis of a variety of glycoconjugates.[95-97] Our previous work investigated the effect that increasing the number of branches in triazole linked glycoclusters had on self-assembly properties.[45] In these studies, we tethered non-gelator sugar derivatives to a central pentaerythritol core and analyzed the effect that the number of branches had on gelation properties. Two main series of glycoclusters were designed and synthesized in this study, a series of ether linked clusters

and a series of ester linked clusters, shown in Figure 84. In general, we found that increasing the number of tethered sugar units increased the overall gelation properties of the molecule, with the trimeric and tetrameric derivatives of both series performing the best in the solvents tested. When comparing the two series, the ether linked derivatives outperformed the ester linked derivatives. Additionally, utilizing a terminal peracetylated glucosamine sugar unit was found to produce more effective gelators.

Janus glycodendrimers, or two faced glycodendrimers, have been found to self-assemble into monodisperse unilamellar and multilamellar vesicles, termed glycodendrimersomes, when bound to sugar-binding proteins such as lectins and galectins.[98] A Janus triazole linked lactose cluster was found to not only bind to lectin, but was also very efficient hydrogelator with a MGC of 0.1 mg/mL.[99] Two faced glycoclusters have been found to have unique self-assembling properties.[98] Having recently achieved success by linking several non-gelator units to a central core unit to create glycocluster derivatives with effective gelation properties, we set out to break one plane of symmetry in our cluster system and synthesize Janus glycoclusters utilizing a combination of ether and ester linkages, depicted in Figure 84.[38] We hypothesize that by breaking one plane of symmetry, the molecule will acquired unique self-assembling properties.

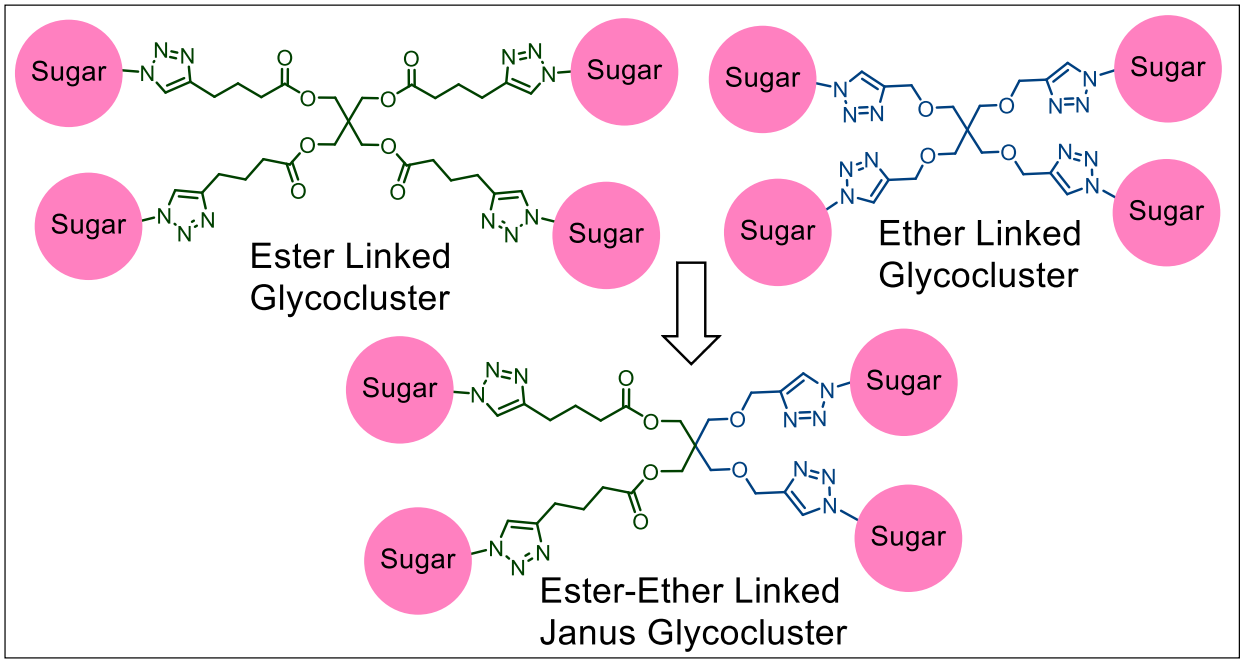

Figure 84. Design rational of Janus Glycoclusters.

4.2 RESULTS AND DISSCUSSIONS

We set out to synthesize the ester-ether linked Janus glycoclusters according to scheme 7. Starting with pentaerythritol, compound **2** was synthesized by protecting two of the hydroxyl groups with a benzylidene acetal protecting group. The two remaining hydroxyl groups on compound **2** then underwent a Williamson ether synthesis using sodium hydride and propargyl chloride to produce compound **3**. The acetal protection was then removed from compound **3** under acidic conditions to produce compound **4**. Compound **4** was then reacted with hexynoyl chloride producing the tetra-alkyne intermediate **5**. The tetra-alkyne intermediate **5** was then used to make the final ester-ether linked Janus glycoclusters $\mathbf{6_{a\text{-}b}}$ by linking either peracetylated glucose or peracetylated glucosamine to the central core through triazole groups using CuAAC chemistry.

Scheme 7. Synthesis of the ether-ester linked Janus glycocluster

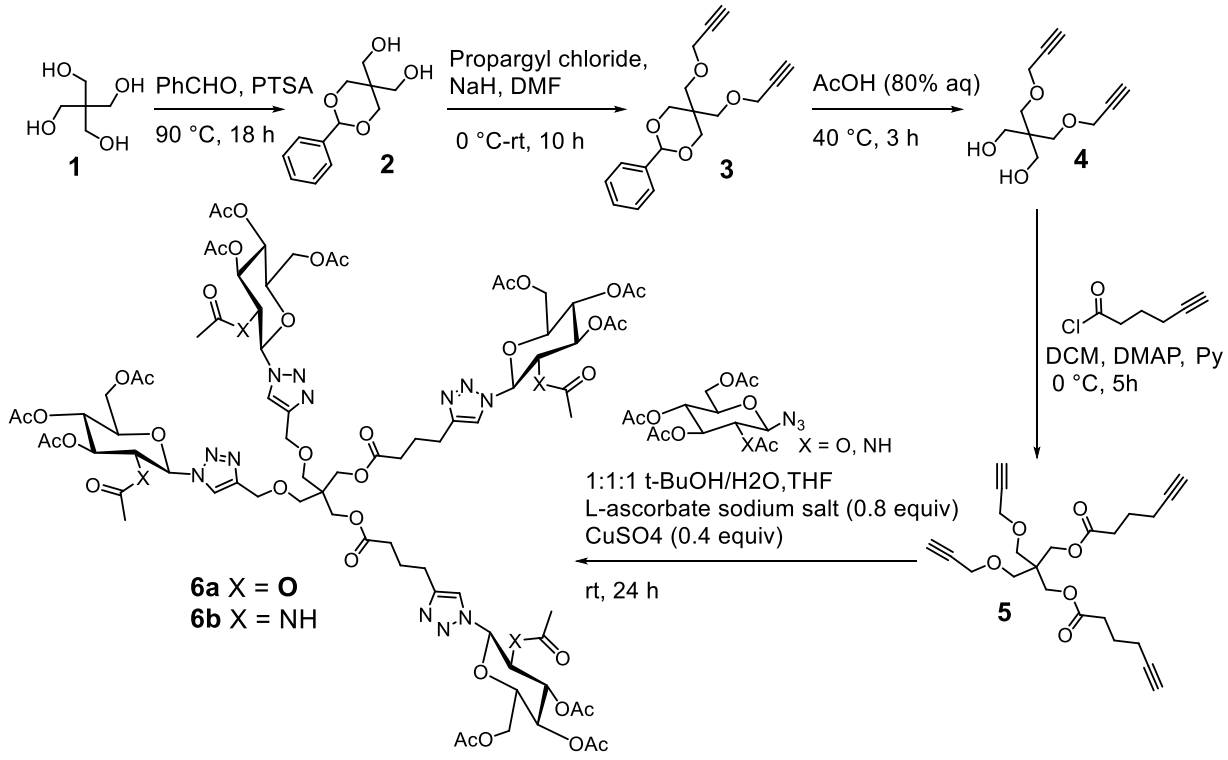

Gelation testing was then carried out on the ester-ether linked Janus glycoclusters, shown in Table 7. Unfortunately, the glucose based glycocluster did not perform well in the tested solvents, only forming a gel in glycerol at 10.0 mg/mL. The glucosamine based glycocluster, on the other hand, did form gels in both DMSO-water solutions, all of the primary alcohols, and glycerol; making it a fairly versatile gelator. The glucosamine derivative significantly outperformed the glucose derivative, which was also observed in our previous work on glycoclusters with pentaerythritol cores.

Table 7. Gelation test results of the ester-ether linked Janus glycoclusters

No.	Tol	EtOH	i-PrOH	n-PrOH	n-BuOH	Gly	EtOH: H_2O (1:2)	EtOH: H_2O (1:1)	DMSO: H_2O (1:2)	DMSO: H_2O (1:1)
6a	P	P	P	P	P	10.0_C	P	P	P	P
6b	I	10.0_T	10.0_T	20.0_T	20.0_T	10.0_C	P	P	20.0_T	20.0_T

Numbers are the minimum gelation concentration in mg/mL. P = precipitation; S = soluble; I = insoluble (all at 20 mg/mL). C = clear, T = translucent, O = opaque. All compounds are insoluble in water and hexanes. All compounds were found to be soluble in triethylene glycol.

In comparison to our previous work on ester and ether linked glycoclusters with pentaerythritol cores, the gelation properties of the Janus ester-ether linked glycocluster containing peripheral glucosamine units seemed to fall right in between the previously reported ether and ester linked tetrameric glycoclusters. As shown in Table 8, the ether linked tetrameric glycocluster **11** was found to be a very versatile gelator, forming gels in a total of nine solvents.[45] The ester linked tetrameric glycocluster **10** was found to be less versatile, forming gels in a total of five solvents.[45] The Janus ester-ether linked cluster **6b** formed gels in seven solvents, falling right in between the two previously reported tetrameric glycoclusters.

Table 8. Comparison of the gelation properties Janus glycocluster **6b** to previous glycoclusters[45]

No.	EtOH	i-PrOH	n-PrOH	n-BuOH	Gly	EtOH: H_2O (1:2)	EtOH: H_2O (1:1)	DMSO: H_2O (1:2)	DMSO: H_2O (1:1)
Ester 10	20.0_T	4.0_T	10.0_T	20.0_T	20.0_C	P	P	P	P
6b	10.0_T	10.0_T	20.0_T	20.0_T	10.0_C	p	P	20.0_T	20.0_T
Ether 11	6.7_T	5.0_T	10.0_T	10.0_T	20.0_C	4.0_T	20.0_T	10.0_T	10.0_T

Numbers are the minimum gelation concentration in mg/mL. P = precipitation; S = soluble; I = insoluble (all at 20 mg/mL). C = clear, T = translucent, O = opaque.

With these results in hand, we attempted to increase the gelation properties of the Janus clusters by replacing the ester linkage with a carbamate linkage. Since carbamate groups are both hydrogen bond donors and acceptors, we were expecting that stronger intermolecular forces would lead to enhanced gelation properties. Scheme 8 shows the synthesis of carbamate-ether linked Janus glycoclusters **9a-b**. This synthesis starts off by reacting the dialkyne diol **4** with 1,1'-carbonyldiimidazole to produce compound **7**. Compound **7** was then reacted with propargyl amine to produce the tetra-alkyne **8**. The tetra-alkyne intermediate **8** was then used to make the final carbamate-ether linked Janus glycoclusters **9a-b** by linking either peracetylated glucose or peracetylated glucosamine to the central core through triazole groups using CuAAC chemistry.

Scheme 8. Synthesis of carbamate-ether linked Janus glycoclusters

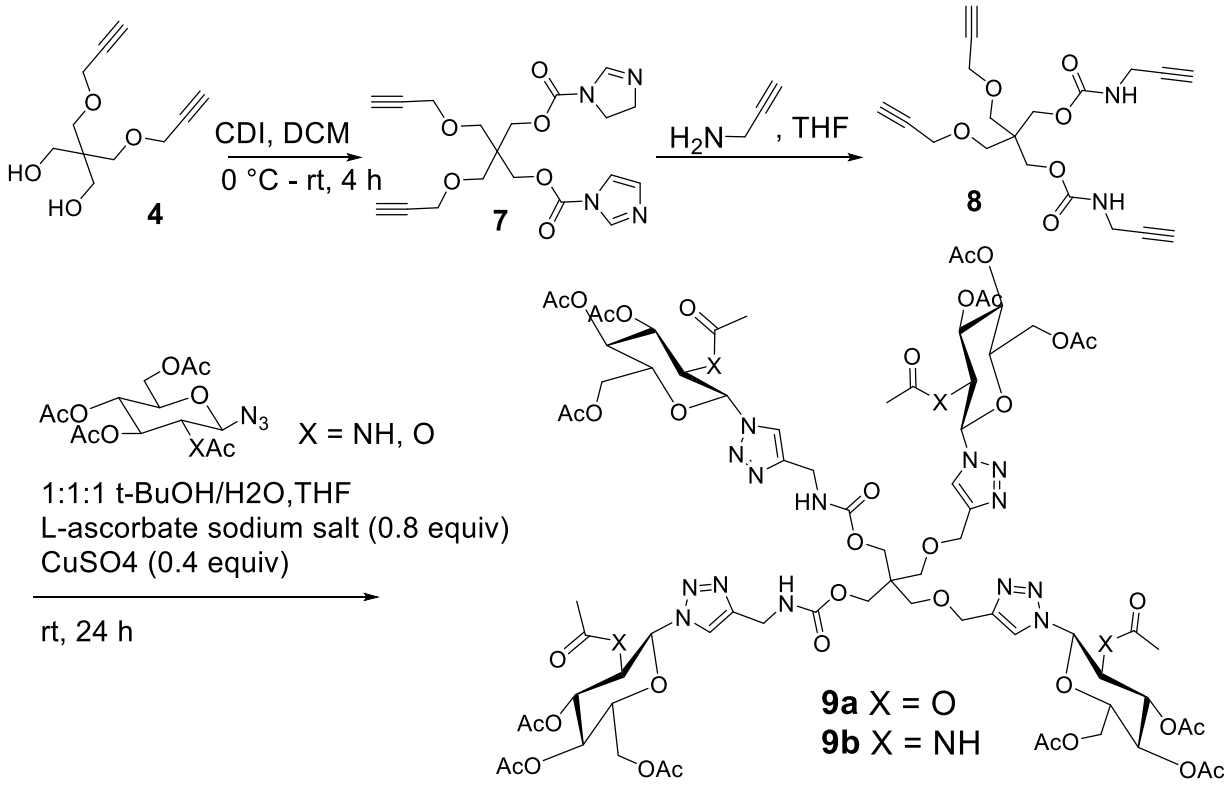

Unfortunately, the replacement of the ester linkage with the carbamate group did not enhance the gelation properties of the Janus glycoclusters, as shown in Table 9. Like the ester-ether linked Janus glycoclusters, the cluster with the peripheral glucose units only formed a gel in glycerol. Once again, the glycoclusters with peripheral glucosamine units were found to have better gelation properties. These results may be due to intramolecular hydrogen bonding holding the molecules in a confirmation that reduces the multivalency effect.

Table 9. Gelation test results of the carbamate-ether linked Janus glycoclusters

No	Tol	EtOH	i-PrOH	n-PrOH	n-BuOH	Gly	EtOH: H_2O (1:2)	EtOH: H_2O (1:1)	DMSO: H_2O (1:2)	DMSO: H_2O (1:1)
9a	I	P	P	P	P	20.0_O	P	P	P	P
9b	I	20.0_T	P	P	5.0_O	20.0_O	P	P	P	P

Numbers are the minimum gelation concentration in mg/mL. P = precipitation; S = soluble; I = insoluble (all at 20 mg/mL). C = clear, T = translucent, O = opaque.

The morphology of the gels formed by compound **6a** in ethanol at a concentration of 10.0 mg/mL was investigated through optical microscopy. Images of the gel morphology can be seen in Figure 85. The gel network appeared to be composed of dense spherical clusters of fibers with thin webs of fibers stretching from cluster to cluster. This morphology is consistent with morphologies previously observed with the ester and ether linked glycoclusters. Optical imaging was attempted on gels formed by compound **8a** in butanol at 10 mg/mL; however**,** only amorphous blobs were observed under the microscope.

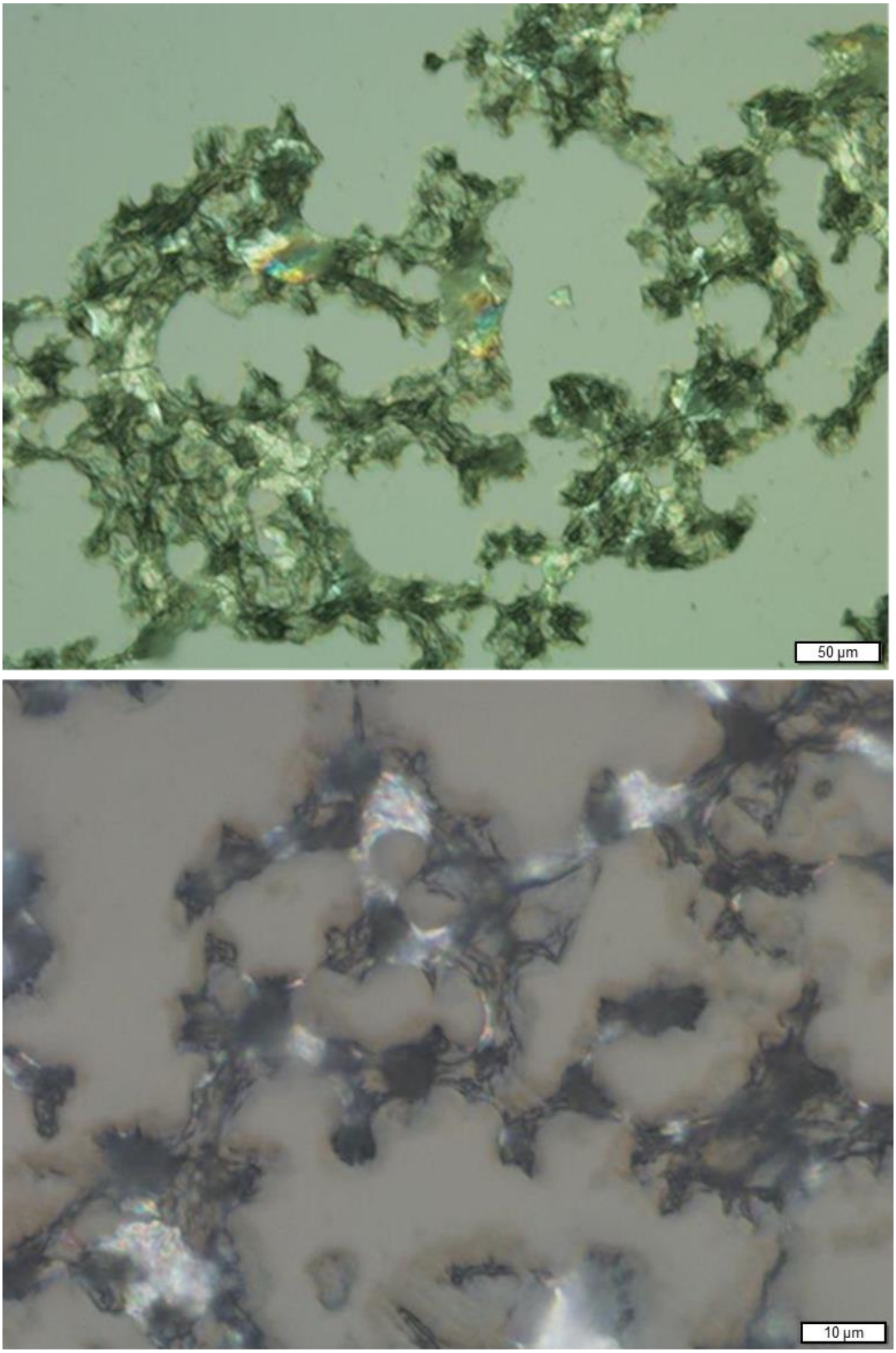

Figure 85. Optical micrographs of a gel formed by compound **6b** in ethanol at 10 mg/mL.

Atomic force microscopy was also utilized to investigate the morphology of the gel networks formed by compound **6b** and **9b**, shown in Figure 86a-h. The gel network formed by compound **6b** in ethanol at a concentration of 10.0 mg/mL appeared as uniform fibrous assembly. AFM imaging shows the fibers twist around each other creating rope like structures which then weave and intertwine very tightly to form the gel network. The gel formed by **9b** in butanol at 10 mg/mL showed very unique morphologies. The AFM imaging showed long thin fibers, small aggregates with thin fibers extruding out of them like a tail, and micelles. Figure 86g-h show AFM images which are zoomed in on structures that resemble micelles. Janus glycoclusters have been reported to form colloidal solutions, which consist of self-assembled micelles.[99]

This study also explored the use of triazole containing glycoclusters in accelerating the rate of CuAAC reactions, with the goal of utilizing these molecules in supramolecular catalysis. The click reaction shown in scheme 9 between peracetylated glucosamine azide and phenylacetylene was used as a model reaction for this study. Without a molecule acting as a ligand for copper, the reaction only reaches 50% at 24 hours. All of Janus glycoclusters were found to significantly increase this reaction rate, with the reactions reaching full conversion within six hours for both carbamate-ether clusters **9a-b** and within 5 hours for the ester-ether derivative **6b**. These results suggest that these Janus glycoclusters may be relevant in supramolecular catalytic applications.

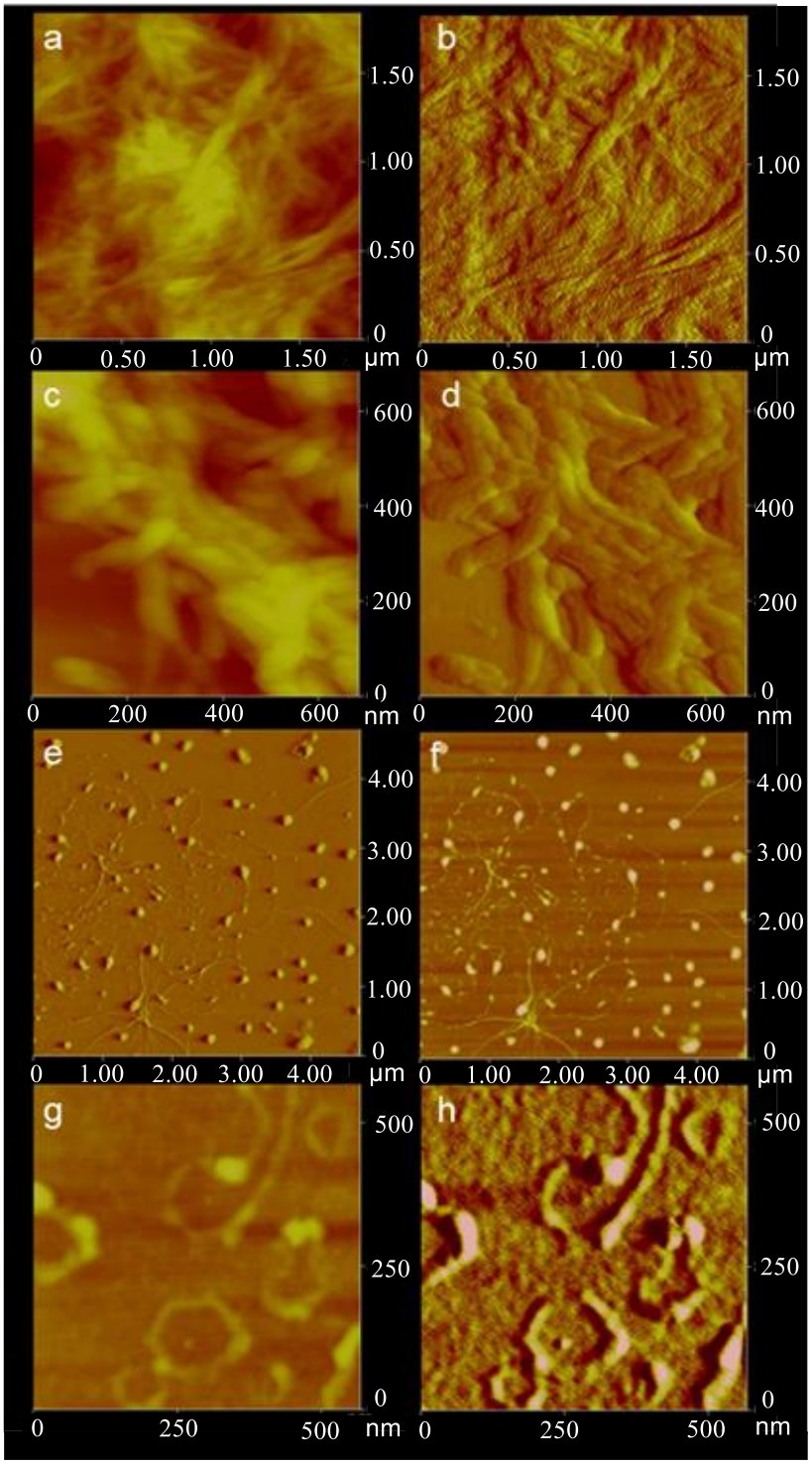

Figure 86. AFM images of gels formed by compound **6b** and **9b**. AFM images of: (a-d) an ethanol gel formed by compound **6b** at 10.0 mg/mL; (e-h) a butanol gel formed by compound **9b** at 10.0 mg/mL.

Scheme 9. Model click reaction used to analyze rate acceleration generated by glycoclusters

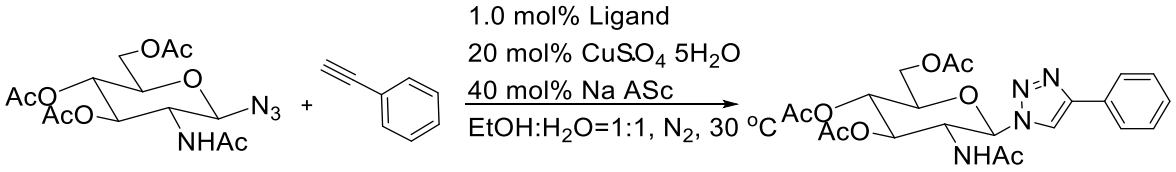

Compound	Conversion, time, %	Conversion, time, %
Control	24h, 50%	
6a	4h, 74%	6h, 82%
6b	1h, 50%	5h, 100%
9a	4h, 73%	6h, 100%
9b	4h, 79%	6h, 100%

Characterization of each intermediate and all of the final Janus glycocluster was carried out through 1 dimensional ^{1}H NMR and ^{13}C NMR spectroscopy, 2-dimensional HSQC and COSY NMR spectroscopy, and LC-MS. High resolution mass spectroscopy was carried out for the tetra-alkyne intermediates and all of the final Janus glycoclusters. Figures 87-92 show both the 1D and 2D NMR spectra and the high-resolution mass spectra obtained from compounds **6b** and **9b**. These spectra are included as representative spectra that are obtained during the characterization of each of the final derivatives after purification.

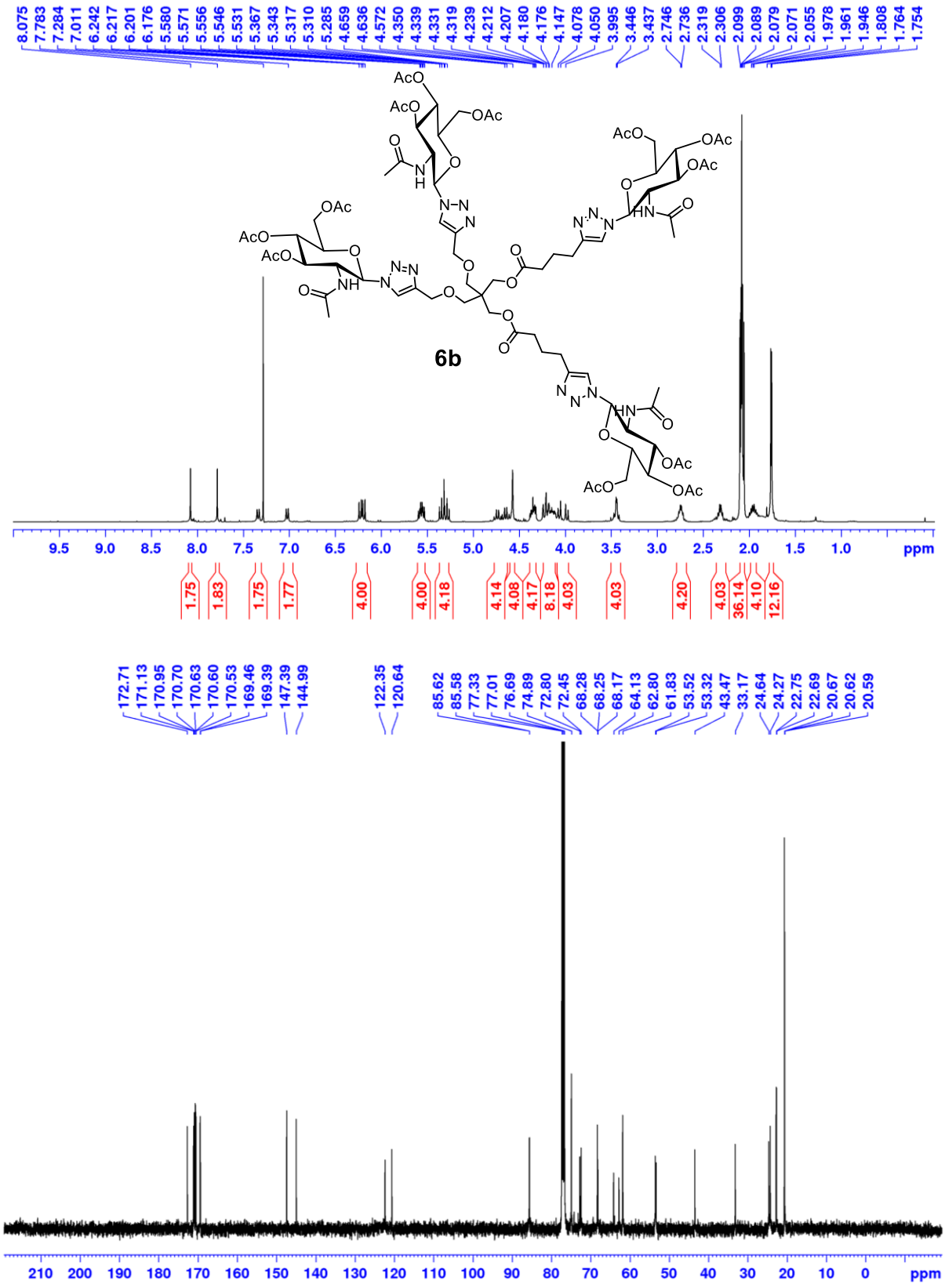

Figure 87. ^{1}H NMR and ^{13}C NMR spectra of compound **6b** in $CDCl_3$.

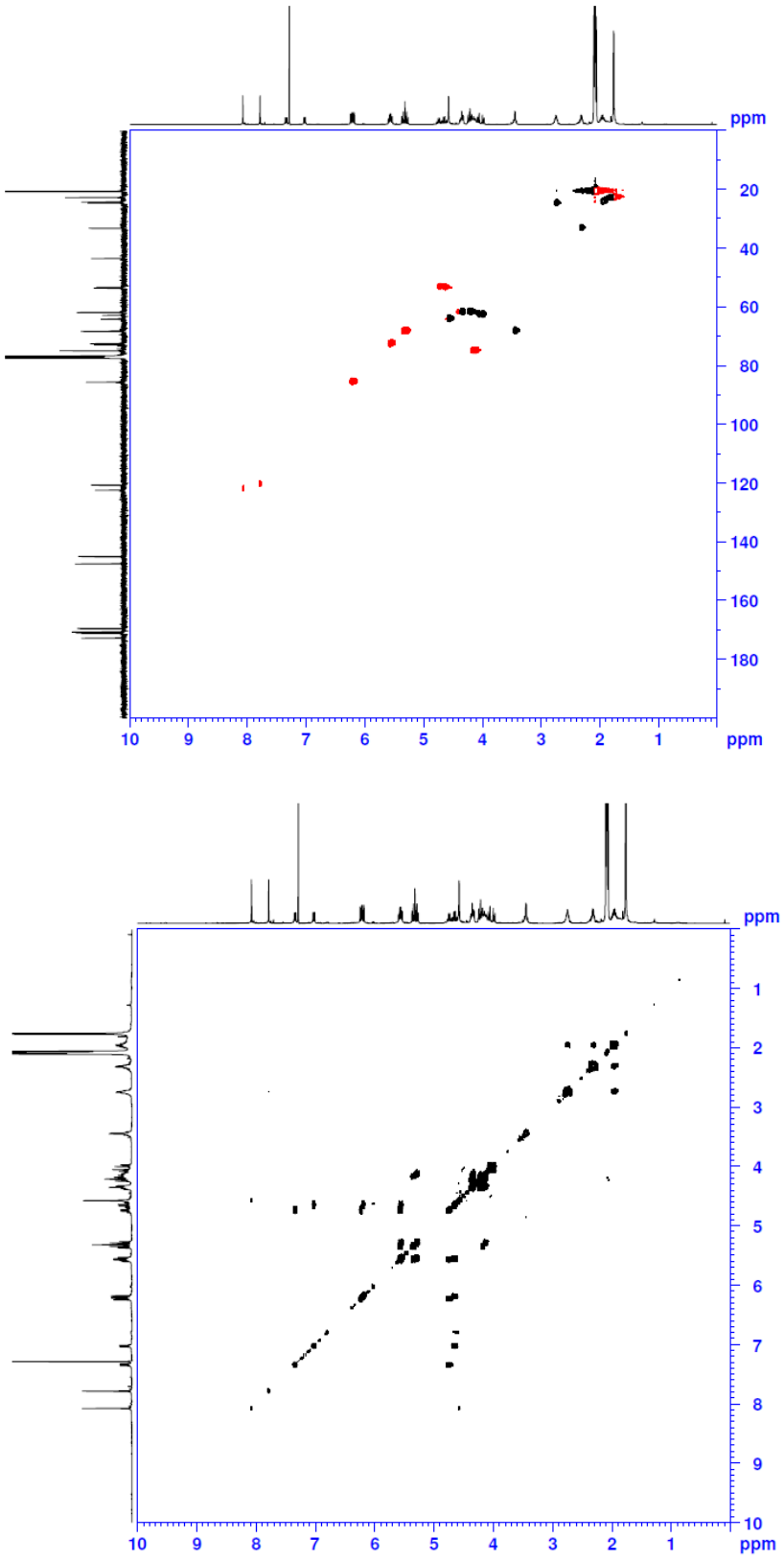

Figure 88. HSQC and COSY spectra of compound **6b** in $CDCl_3$.

Mass Spectrum List Report

Analysis Info

Analysis Name	Z:\FTICR-MS\MS-1\Data\2020\apexdata073120\JB-1031-021_pos_000001.d	Acquisition Date	7/31/2020 1:13:08 PM
Method		Operator	FTMS_USER
Sample Name	1031-021	Instrument	apex-Qe
Comment	1031-021 in MeOH [C79H108N16O38+2Na]2+		

Sample Name	1031-021 in MeOH			
Exact Mass of	[C79H108N16O38+2Na]2+	=	967.339743	m/z
Mass Observed		=	967.340172	m/z

Difference < 1.0 ppm

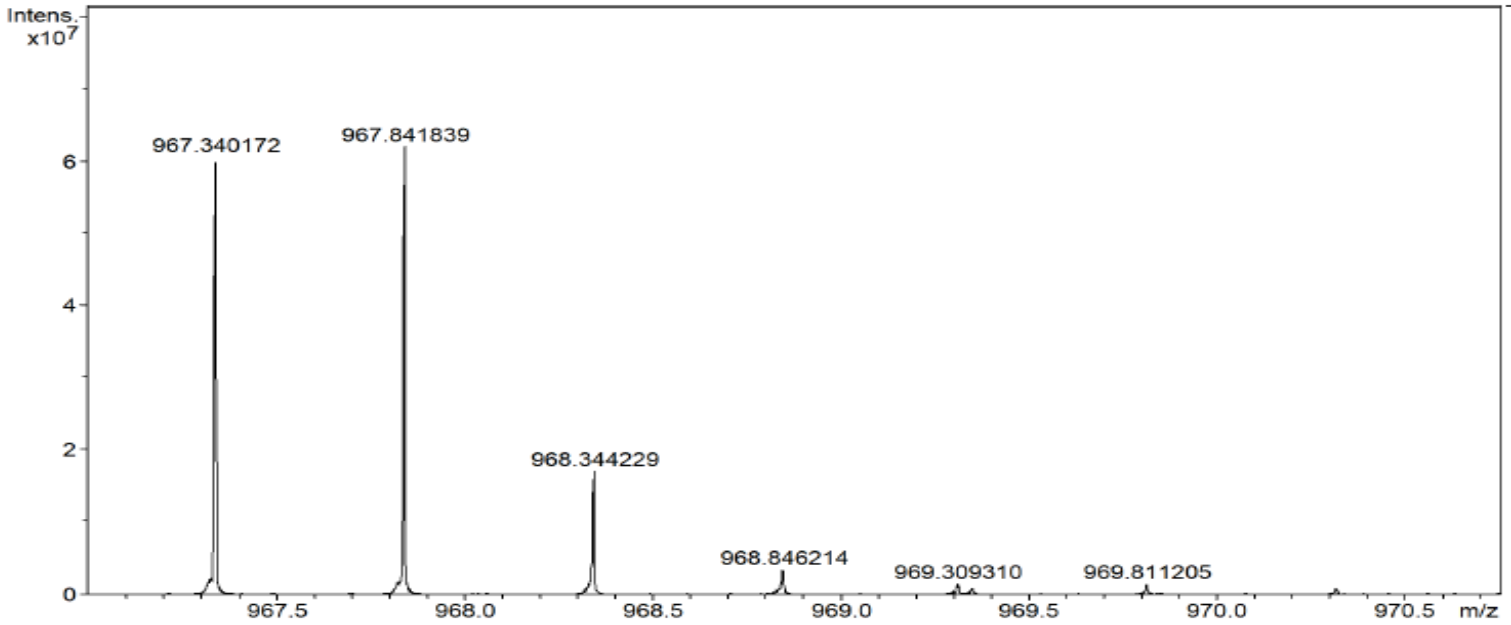

Figure 89. HRMS (ESI/ICR) spectrum for compound **6b**. m/z $[M + 2Na]^{2+}$ calculated for $[C_{79}H_{108}N_{16}O_{38}Na_2]^{2+}/2$ is 967.3397; found 967.340172.

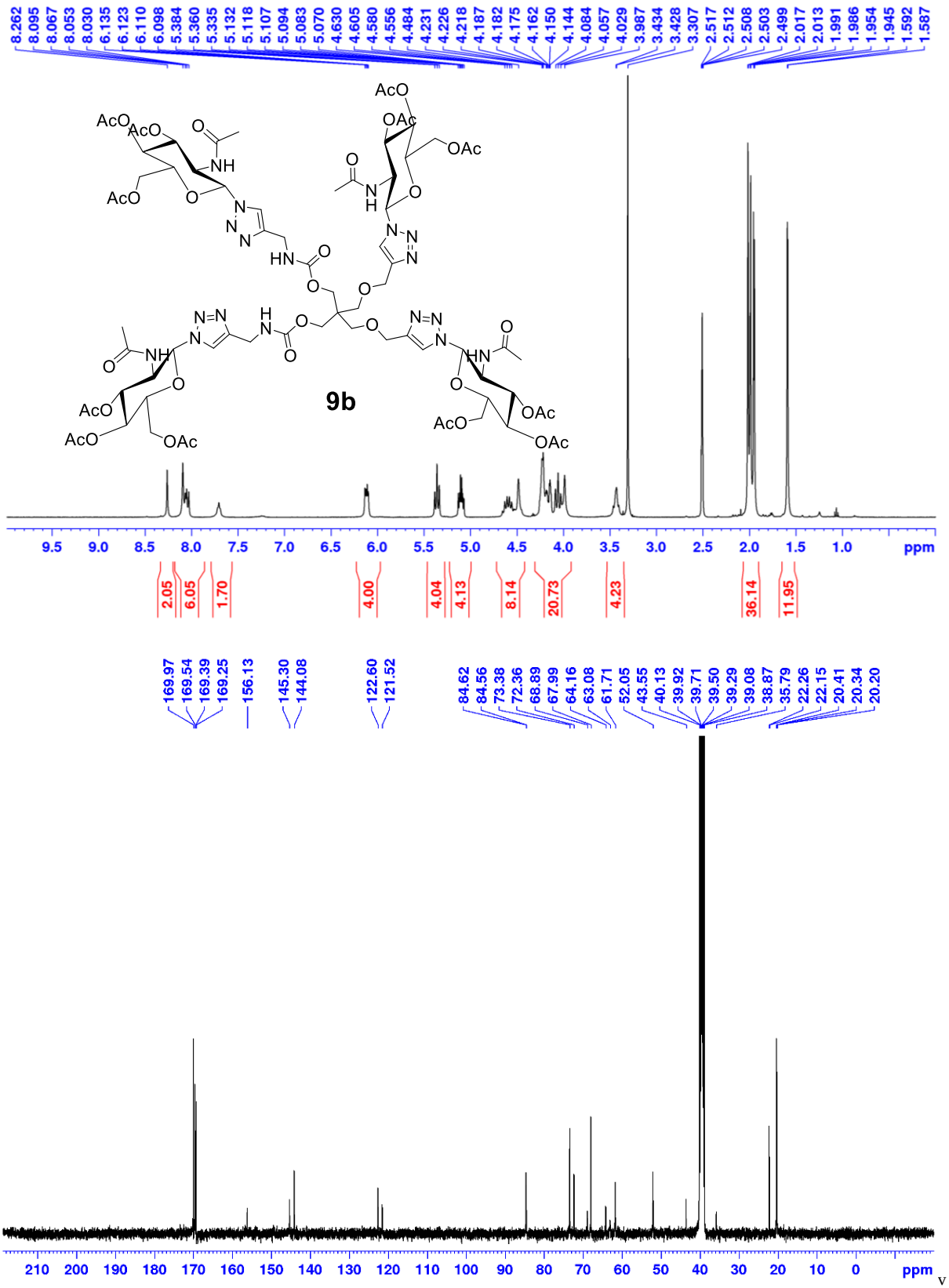

Figure 90. ^{1}H NMR and ^{13}C NMR spectra of compound **9b** in d_6-DMSO.

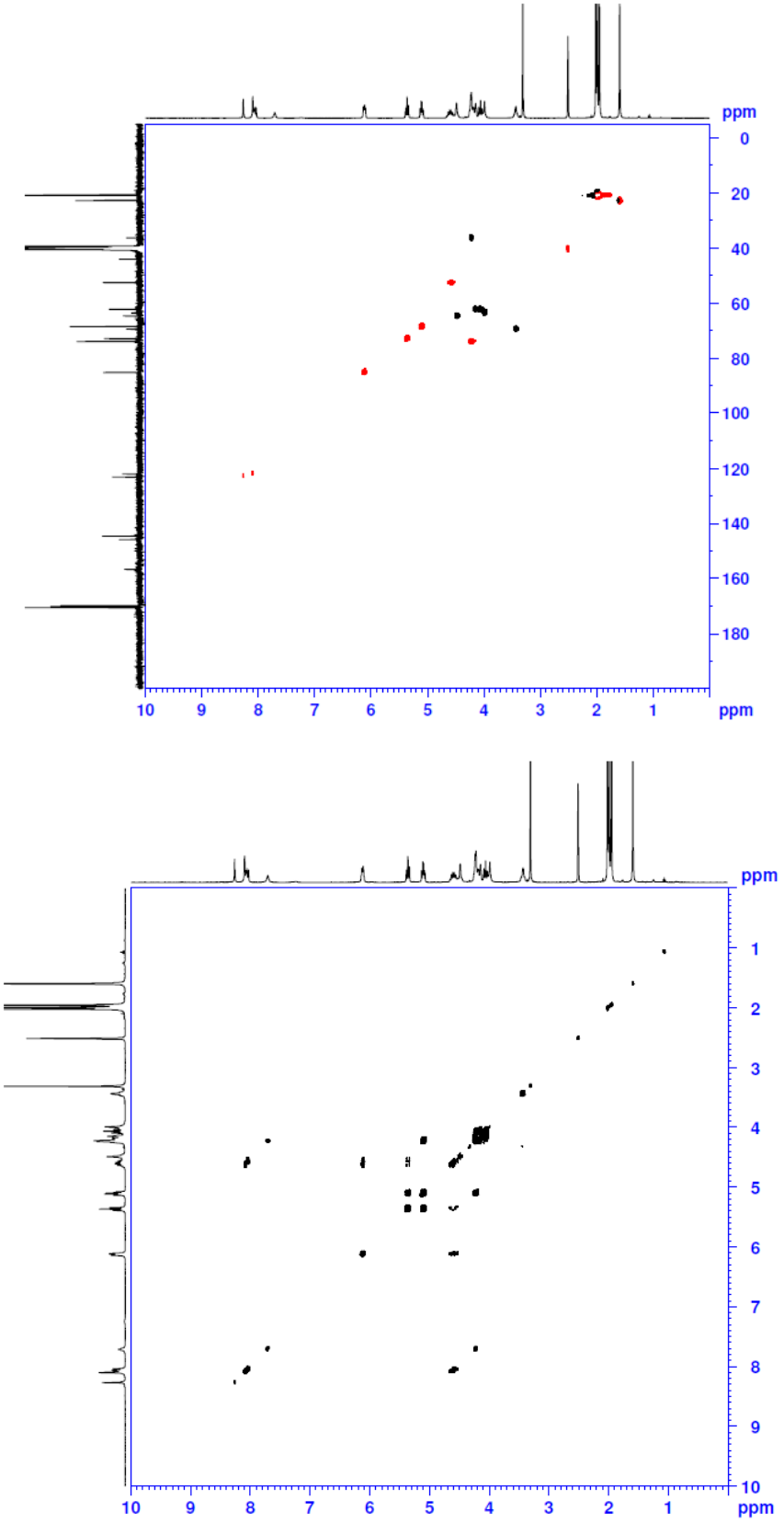

Figure 91. HSQC and COSY spectra of compound **9b** in d_6-DMSO.

Mass Spectrum List Report

Analysis Info

Analysis Name	Z:\FTICR-MS\MS-1\Data\2020\apexdata073120\JB-1031-058_pos_000003.d	Acquisition Date	7/31/2020 12:52:24 PM
Method		Operator	FTMS_USER
Sample Name	1031-058	Instrument	apex-Qe
Comment	1031-058 in MeOH [C75H102N18O38+2Na]2+		

Sample Name	1031-058 in MeOH			
Exact Mass of	[C75H102N18O38+2Na]2+	=	954.319342	m/z
Mass Observed		=	954.319205	m/z

Difference < 1.0 ppm

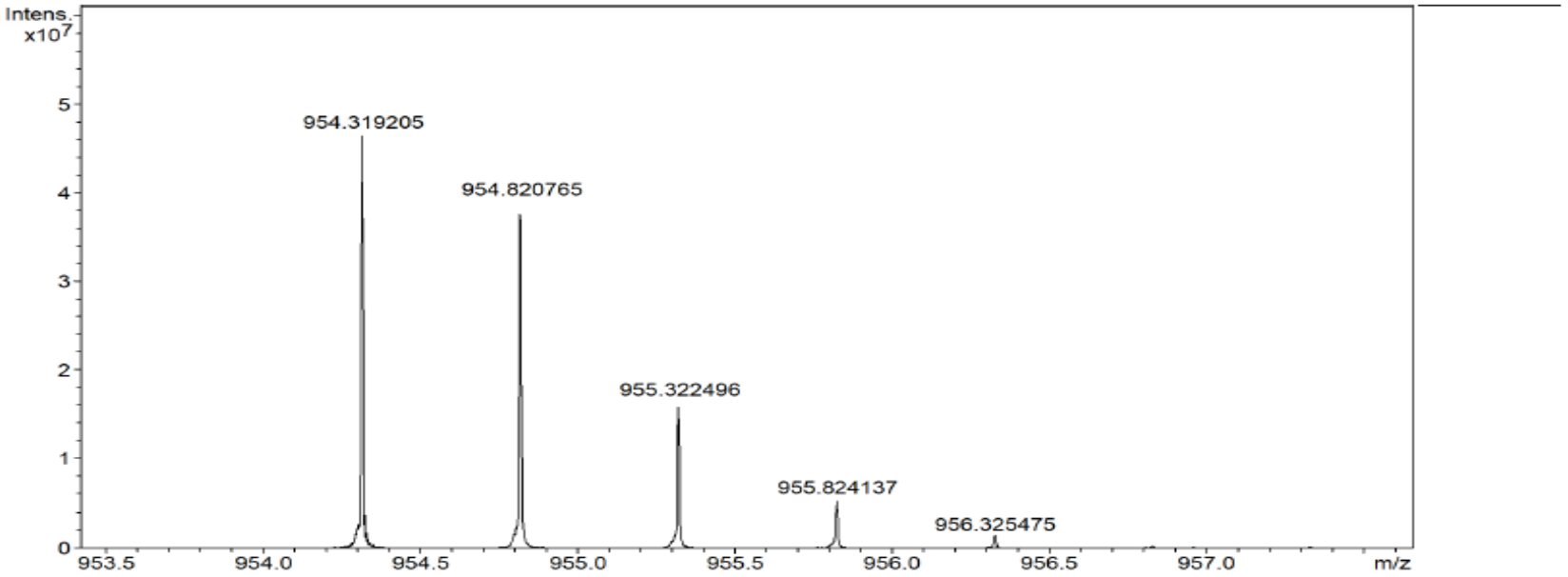

Figure 92. HRMS (ESI/ICR) spectrum for compound **9b**. m/z $[M + 2Na]^{2+}$ calculated for $[C_{75}H_{102}N_{18}O_{38}Na_2]^{2+}/2$ is 954.3193; found 954.319205.

4.3 CONCLUSION

Two series of Janus glycoclusters were designed and synthesized through linking peracetylated glucose or peracetylated glucosamine to a central pentaerythritol core through click chemistry. The first series of glycoclusters were designed by using both ester linkages and ether linkages which were individually explored in previous work. The ester-ether Janus glycocluster containing peripheral glucosamine sugar units were found to be versatile gelators, forming gels in seven of the solvents tested. The gelation properties of this gelator seem to fall in between the tetrameric ester and tetrameric ether derivatives previously reported. In an attempt to increase the gelation properties of the system, a second series of Janus glycoclusters was designed utilizing a carbamate hydrogen bonding group as a replacement for the ester linkage. Unfortunately, a significant reduction in gelation properties was observed. This is thought to be due to strong intramolecular hydrogen bonding causing the cluster to conform to a disadvantageous conformation that negates the multivalent effect, thus reducing the self-assembling properties of the molecule. The morphologies of the gels were analyzed by optical microscopy and atomic force microscopy. Optical micrographs of an ethanol gel of compound **6b** showed dense spherical fibrous clusters with interconnecting fibrous webs. AFM images of this gel showed fibers that entwined to form a rope like morphology that further weaved together to form the bulk gel network. AFM images of compound **9b** showed multiple morphologies such as long tubule fibers and micelles. Studies carried out to analyze the effect these clusters have on the reaction rate of click reactions found that all of the Janus glycoclusters can accelerate reaction rate significantly. Further studies will be carried out to explore the uses of these molecules in supramolecular catalysis utilizing copper metallogels for copper catalyzed reactions such as copper catalyzed azide alkyne cycloadditions.

4.4 EXPERIMENTAL SECTION

General method and materials: A Bruker 400 MHz spectrometer was utilized to obtain ^{1}H NMR, proton-decoupled ^{13}C NMR, HSQC, and COSY in either $CDCl_3$ or DMSO-d_6. The chemical shifts reported are based off using $CDCl_3$/DMSO-d_6 as internal standards at 7.26/2.50 ppm (^{1}H NMR) and at 77.00/39.50 ppm (^{13}C NMR), respectively. Carbon and proton assignment was determined with the assistance of 2D NMR experiments (HSQC, COSY). Melting point analysis was carried out using a Fisher Jones melting point apparatus. Agilent 6120B Single Quad mass spectrometer and LC1260 system was used for mass analysis. A Bruker 10 Telsa APEX-Qe Fourier-transform ion cyclotron resonance mass spectrometer (FTICR-MS) with an Apollo II ion source using positive electrospray ionization was used for high resolution mass analysis.

Optical Microscopy: A BX60M optical microscope using an Olympus DP73-1-51 high-performance 17MP digital camera with pixel shifting and Peltier cooling was used to image the morphology of the gel's microstructures. CellSens Dimension 1.11 software was used to acquire and process images. Samples were prepared by transferring small gel samples to microscope slides with either a pipette or spatula and allowing the ample to air dry for at least 24 hours before imaging

Atomic Force Microscopy: A Dimension 3100 atomic force microscope was used to acquire AFM images of various gel samples. All imaging was carried out in tapping mode, using Tap300-G silicon AFM probes with a resonant frequency of 300 KHz and a force constant of 40 N/m. Sample preparation for AFM is identical to the methods used for preparing samples for optical microscopy imaging.

Gel Testing: testing began at a concentration of 20.0 mg/mL, where 2 mg of the compound was added to a 1-dram vial and 0.1 mL of the respective solvent was added. The vial was then sealed and gently heated until a homogenous solution was acquired. In several cases, cycles of

sonication followed by heating were required to achieve full dissolution of the gelator in solution. Samples were allowed to sit undisturbed and cool to room temperature for about 30 minutes before examination. The vials were then inverted and gently tapped to analyze whether a gel was formed. Upon inverting the vial, if no solvent flow was observed, a stable gel was formed. If solvent flow was observed upon inversion of the vial, the gel was recorded as unstable. For all samples that formed gels, 0.1 mL of the respective was added to the vial and the vial was heated until the sample transitioned into solution phase and the process was repeated. This process was repeated until the gel became unstable, at which point the minimum gelation concentration (MGC) was recorded. The appearance of each gel was recorded as either clear (transparent), translucent (semi-transparent and allows some light to pass through it), or opaque (typically white in color and does not allow light to pass through it).

Liquid chromatography-mass spectrometer (LC-MS) conditions: An Agilent 6120B Single Quad mass spectrometer and LC1260 system were used for the mass analysis of intermediates. A Bruker 10 Telsa APEX-Qe Fourier-transform ion cyclotron resonance mass spectrometer (FTICR-MS) with an Apollo II ion source using positive electrospray ionization was used for high resolution mass analysis of the final compounds.

Synthesis of compound 2: Pentaerythritol (5.780 g, 42.5 mmol, 1.5 equiv) was dissolved in anhydrous DMF (5 mL) in a dried 100 mL round bottomed flask. PTSA monohydrate (266 mg, 1.4 mmol, 0.05 equiv) and benzaldehyde (3.000 g, 28.3 mmol, 1 equiv) were added to the flask. The reaction mixture was then heated to 90 °C and stirred for 30 hours. The reaction mixture was the diluted with DCM (50 mL) and washed with DI water (50 mL x 2). The aqueous layers were then back extracted with DCM (50 mL). The organic layers were then dried over Na_2SO_4 and solvent was removed under reduced pressure. The crude product was recrystallized in toluene,

affording a fluffy white solid (4.8431 g, 76.3%). ^{1}H NMR (400 MHz, CDCl3) δ 7.45–7.51 (m, 2H), 7.32–7.41 (m, 3H), 5.44 (s, 1H), 4.09–4.23 (m, 4H), 3.73–3.83 (m, 2H), 3.56 (s, 2H); ^{13}C NMR (100 MHz, CDCl3) δ 138.1, 129.1, 128.3, 126.0, 102.1, 70.0, 65.6, 64.1, 38.9.

Synthesis of compound 3: Compound **2** (1.500 g, 6.7 mmol, 1 equiv) was dissolved in anhydrous DMF (5 mL) in a dried nitrogen flushed 250 mL round bottomed flask. The temperature was reduced to 0 °C via an ice bath. NaH 60% in mineral oil (352.8 mg, 14.7 mmol, 2.2 equiv) was added to the reaction mixture and reaction stirred at 0 °C for 30 minutes. Propargyl chloride (70% in toluene) (1.4 mL, 16.7 mmol, 2.5 equiv) was the added to the reaction mixture. After 10 minutes, the ice bath was removed, and reaction mixture warmed to rt and stirred for 2 hours. The reaction mixture was dropped into 30 mL of DCM and 30 mL of saturated NH_4Cl solution with vigorous stirring. The aqueous layer was then extracted with DCM (30 mL x 2). The organic layers were then combined, washed with DI water (30 mL x 2), dried over Na_2SO_4, and the solvent was removed under reduced pressure. The crude product was purified via column chromatography using pure hexanes to 5% EtOAc/hexanes to afford a light-yellow oil (1.634 g, 81.3%). R_f = 0.46 in 10% EtOAc/hexanes. ^{1}H NMR (400 MHz, CDCl3) δ 7.53–7.46 (m, 2H), 7.41–7.33 (m, 3H), 5.44 (s, 1H), 4.21 (d, *J* = 2.4 Hz, 2H), 4.15–4.09 (m, 4H), 3.93–3.86 (m, 4H), 3.38 (s, 2H), 2.44, 2.43 (2 overlapping triplets, *J* = 2.4 Hz, 2H); ^{13}C NMR (100 MHz, CDCl3) δ 138.3, 128.9, 128.3, 126.1, 101.8, 79.9, 79.5, 74.5, 74.2, 69.9, 69.8, 68.7, 58.77, 58.75, 38.5. LC-MS *m/z* calculated for $C_{18}H_{21}O_4$ $[M+H]^+$ 301.1 found 301.1.

Synthesis of compound 4: Compound **3** (1.634 g, 5.4 mmol, 1 equiv) was dissolved in an 80% acetic acid solution (10 mL) in a 100 mL round bottomed flask. Reaction mixture was heated to 40 °C for 2 hours. The reaction mixture was poured into a stirring mixture of DCM (30 mL) and DI water (30 mL). Solid $NaHCO_3$ was added until effervescence ceased. The aqueous layer was

then extracted with DCM (30 mL x 2). The organic layers were combined, washed with DI water (30 mL x 2), dried over Na_2SO_4, and the solvent was removed under reduced pressure. The crude product was purified via column chromatography (SiO_2) using pure hexanes to 60% EtOAc/hexanes to afford a light-yellow oil (978.6 mg, 85.4%). R_f = 0.42 in 50% EtOAc/hexanes. 1H NMR (400 MHz, CDCl3) δ 4.15 (d, *J* = 2.4 Hz, 4H), 3.69 (s, 4H), 3.60 (s, 4H), 2.45 (t, *J* = 2.4 Hz, 2H), 2.29 (s, 2H); 13C NMR (100 MHz, CDCl3) δ 79.4, 74.8, 71.0, 64.4, 58.8, 44.9. LC-MS *m/z* calculated for $C_{11}H_{17}O_4$ 213.2, found 213.2.

Synthesis of ester linked tetra-alkyne 5: *5*-hexynoic acid (0.172 mL, 1.56 mmol, 2.2 equiv) was dissolved in anhydrous DCM (2 mL) with a catalytic amount of DMF in a dried and nitrogen flushed 50 mL round bottomed flask. The temperature was decreased to 0 °C via an ice bath. Oxalyl chloride (0.146 mL, 1.70 mmol, 2.4 equiv) was then added to the reaction mixture. The reaction stirred at 0 °C for 10 minutes and then the ice bath was removed, and the reaction mixture warmed to room temperature. The reaction stirred for an additional 3 hours. Compound **4** (150 mg, 0.71 mmol, 1 equiv), K_2CO_3 (294 mg, 2.14 mmol, 3 equiv), and DMAP (8.7 mg, 0.071 mmol, 0.1 equiv) were dissolved in 3 mL of anhydrous DCM in a dried and nitrogen flushed round bottomed flask. The temperature was reduced to 0 °C via an ice bath. The crude acid chloride solution was then added dropwise. After 10 minutes, the ice bath was removed, and the reaction mixture warmed to rt. The reaction stirred for an additional 5 hours. The reaction was quenched with 0.5 mL of a 5% $NaHCO_3$ solution. The reaction mixture was the diluted with DCM (20 mL) and washed with DI water (20 mL x 2). The aqueous layers were then back extracted with DCM (20 mL). The organic layers were then dried over Na_2SO_4 and solvent was removed under reduced pressure. The crude product was purified via column chromatography (SiO_2) using pure hexanes to 25% EtOAc/hexanes affording a clear liquid (231.7 mg, 82%). R_f = 0.5 in 20% EtOAc/hexanes.

^{1}H NMR (400 MHz, $CDCl_3$) δ 4.11 (d, J = 2.4 Hz, 6H), 3.39 (s, 6H), 2.39 (t, J = 2.4 Hz, 3H), 0.96 (s, 3H); ^{13}C NMR (100 MHz, $CDCl_3$) δ 80.1, 74.0, 72.7, 58.6, 40.3, 17.3; HRMS (ESI/ICR) m/z: $[M + Na]^+$ calcd for $C_{23}H_{28}O_6Na$ 423.1778; found 423.1778.

Synthesis of ester linked Janus glycocluster 6a: Tetra-Alkyne **5** (50 mg, 0.13 mmol, 1 equiv), peracetylated glucose azide (213 mg, 0.57 mmol, 4.4 equiv), $CuSO_4$ pentahydrate (26 mg, 0.10 mmol, 0.8 equiv), and 3 mL of *t*-BuOH/H_2O/THF (v/v/v = 1/1/1) were added to a 50 mL round bottomed flask. L-ascorbate sodium salt (42 mg, 0.20 mmol, 1.6 equiv) was added to start the reaction The reaction mixture stirred at 30 °C for 20 hours. The solvent was then removed under reduced pressure. Crude product was purified via column chromatography using pure DCM to 5% MeOH/DCM to afford a white solid (190.5 mg, 77%). R_f = 0.55 in 5 % MeOH/DCM. mp 104.2–106.5 °C. ^{1}H NMR (400 MHz, $CDCl_3$) δ 8.02 (s, 2H), 7.69 (s, 2H), 6.02 (d, J = 9.3 Hz, 2H), 5.92 (d, J = 9.1 Hz, 2H), 5.56 (t, J = 9.4 Hz, 2H), 5.50–5.27 (m, 10H), 4.67–4.57 (m, 4H), 4.36–4.28 (m, 4H), 4.21–4.14 (m, 4H), 4.13–4.08 (m, 6H), 4.07–4.02 (m, 2H), 3.54–3.46 (m, 4H), 2.77 (dt, J = 7.5, 1.6 Hz, 4H), 2.37 (t, J = 7.4 Hz, 4H), 2.10–2.05 (m, 18H), 2.05–2.02 (m, 18H), 2.02–1.97 (m, 4H), 1.86 (s, 6H), 1.82 (s, 6H); ^{13}C NMR (100 MHz, $CDCl_3$) δ 172.7, 170.5, 170.5, 169.94, 169.88, 169.43, 169.38, 168.82, 168.75, 147.8, 145.5, 121.6, 119.5, 85.62, 85.56, 77.2, 75.0, 72.8, 72.7, 70.31, 70.27, 68.6, 67.8, 64.8, 62.7, 61.6, 43.6, 33.2, 24.8, 24.3, 20.60, 20.58, 20.55, 20.51, 20.50, 20.47, 20.1, 20.0. HRMS (ESI/ICR) m/z $[M + 2Na]^{2+}$ calcd for $[C_{79}H_{104}N_{12}O_{42}Na_2]^{2+}$/2 calcd for 969.3078; found 969.3078.

Synthesis of ester linked Janus glycocluster 6b: Tetra-Alkyne **5** (50 mg, 0.13 mmol, 1 equiv), peracetylated glucosamine azide (213 mg, 0.57 mmol, 4.4 equiv), $CuSO_4$ pentahydrate (26 mg, 0.10 mmol, 0.8 equiv), and 3 mL of *t*-BuOH/H_2O/THF (v/v/v = 1/1/1) were added to a 50 mL round bottomed flask. L-ascorbate sodium salt (42 mg, 0.20 mmol, 1.6 equiv) was added to start

the reaction The reaction mixture stirred at 30 °C for 24 hours. The solvent was then removed under reduced pressure. Crude product was purified via column chromatography using 5 % MeOH/DCM to 7.5% MeOH/DCM to afford a white solid (198.6 mg, 81%). R_f = 0.45 in 7.5 % MeOH/DCM. mp 142.6–145.1°C. ^{1}H NMR (400 MHz, $CDCl_3$) δ 8.08 (s, 2H), 7.78 (s, 2H), 7.34 (d, J = 9.2 Hz, 2H), 7.02 (d, J = 9.2 Hz, 2H), 6.28–6.16 (m, 4H), 5.62–5.56 (m, 4H), 5.39–5.24 (m, 4H), 4.79–4.62 (m, 4H), 4.57 (s, 4H), 4.39–4.31 (m, 4H), 4.25–4.10 (m, 8H), 4.09–3.96 (m, 4H), 3.50–3.39 (m, 4H), 2.81–2.68 (m, 4H), 2.37–2.25 (m, 4H), 2.12–2.04 (m, 36H), 2.01–1.90 (m, 4H), 1.78–1.72 (m, 12H). ^{13}C NMR (100 MHz, $CDCl_3$) δ 172.7, 171.1, 170.9, 170.7, 170.6, 170.6, 170.53, 169.5, 169.4, 147.4, 145.0, 122.4, 120.6, 85.6, 85.6, 74.9, 72.8, 72.4, 68.3, 68.3, 68.2, 64.1, 62.8, 61.8, 53.5, 53.3, 43.5, 33.2, 24.6, 24.3, 22.8, 22.7, 20.7, 20.6, 20.6. HRMS (ESI/ICR) m/z $[M + 2Na]^{2+}$ calcd for $[C_{79}H_{108}N_{16}O_{38}Na_2]^{2+}/2$ calcd for 967.3397; found 967.3402.

Synthesis of compound 7: 1,1'-Carbonyldiimidazole (2.292 g, 14.1 mmol, 3 equiv) was dissolved in 8 mL of anhydrous THF in a dried nitrogen flushed 50 mL round bottomed flask. The temperature was reduced to 0 °C via an ice bath. Compound **4** (1.00 g, 4.7 mmol, 1 equiv) was dissolved in 8 mL of anhydrous THF and added dropwise over 5 minutes. The ice bath was then removed and the reaction warmed to room temperature and continued to stir for an additional 16 hours. Solvent was removed from the reaction mixture under reduced pressure. The crude product underwent an aqueous workup by dissolving it in DCM (60 mL) and washing it with DI water (30 mL x 2). The organic layer was dried over Na_2SO_4 and solvent was removed under reduced pressure. The crude product was purified via column chromatography using 20-80% EtOAc/hexanes, affording a white solid (1.763 g, 94%). R_f = 0.25 in 60% EtOAc/hexanes. mp 113.0–115.0 °C. ^{1}H NMR (400 MHz, $CDCl_3$) δ 8.15–8.11 (m, 2H), 7.42–7.38 (m, 2H), 7.09–7.05 (m, 2H), 4.56 (s, 4H), 4.13 (d, J = 2.4 Hz, 4H), 3.65 (s, 4H), 2.34 (t, J = 2.4 Hz, 2H); ^{13}C NMR

(100 MHz, $CDCl_3$) δ 148.3, 137.0, 130.9, 117.0, 78.7, 77.2, 75.2, 67.9, 66.4, 58.7, 43.9; HRMS (ESI/ICR) m/z: $[M + Na]^+$ calcd for $C_{19}H_{20}N_4O_6Na$ 423.1275; found 423.1274.

Synthesis of carbamate linked tetra-alkyne 8: Compound **6** (100 mg, 0.25 mmol, 1 equiv) was dissolved in THF (2 mL) in a dried and nitrogen-flushed 50 mL round bottomed flask. The reaction mixture was cooled to 0 °C via an ice bath. Propargyl amine (40 μL, 0.625 mmol, 2.5 equiv) was dissolved in THF and added dropwise to the reaction mixture. The reaction was warmed to room temperature and stirred for 18 hours. THF was removed under reduced pressure. The crude product was then dissolved in EtOAc (10 mL) and washed with DI water (10 mL x 2). The aqueous layers were back extracted with EtOAc (10 mL). The organic layers were then dried over Na_2SO_4 and solvent was removed under reduced pressure. The crude product was purified via column chromatography using pure hexanes to 60% EtOAc/hexanes to afford a clear liquid (88.4 mg, 95%). R_f = 0.45 in 45% EtOAc/hexanes. ^{1}H NMR (400 MHz, $CDCl_3$) δ 4.99 (s, 2H), 4.15 (s, 4H), 4.11 (d, J = 2.3 Hz, 4H), 3.96 (d, J = 2.6 Hz, 4H), 3.51 (s, 4H), 2.41 (t, J =2.3 Hz, 2H), 2.25 (t, J = 2.6 Hz, 2H); ^{13}C NMR (100 MHz, $CDCl_3$) δ 155.7, 79.7, 79.6, 74.5, 71.6, 68.5, 64.1, 58.7, 43.6, 30.8. HRMS (ESI/ICR) m/z: $[M + Na]^+$ calcd for $C_{19}H_{22}N_2O_6Na$ 397.1370; found 397.1367.

Synthesis of carbamate linked Janus glycocluster 9a. Tetra-Alkyne **8** (45 mg, 0.12 mmol, 1 equiv), peracetylated glucose azide (197 mg, 0.53 mmol, 4.4 equiv), $CuSO_4$ pentahydrate (24 mg, 0.10 mmol, 0.8 equiv), and 3 mL of *t*-BuOH/H_2O/THF (v/v/v = 1/1/1) were added to a dried 50 mL round bottomed flask. L-ascorbate sodium salt (38 mg, 0.19 mmol, 1.6 equiv) was added to start the reaction. The reaction mixture was stirred at 30 °C for 24 hours. Solvent was removed under reduced pressure. The crude product was purified via column chromatography using pure DCM to 15% MeOH/DCM and the product was further purified via recrystallization in reagent alcohol affording a white solid (161 mg, 72%). R_f = 0.45 in 5 % MeOH/DCM. mp 134.3–

135.8 °C. ^{1}H NMR (400 MHz, $CDCl_3$) δ 7.90 (s, 4H), 6.01 (d, J = 9.0 Hz, 2H), 5.92 (d, J = 8.8 Hz, 2H), 5.86–5.67 (s, 2H), 5.24–5.61 (m, 12H), 4.67–4.54 (m, 4H), 4.52–4.27 (m, 8H), 4.25–3.99 (m, 12H), 3.42 (s, 4H), 2.12–2.00 (m, 36H), 1.92–1.80 (m, 12H); ^{13}C NMR (100 MHz, $CDCl_3$) δ 170.52, 170.50, 170.0, 169.9, 169.4, 169.1, 168.9, 156.3, 145.9, 145.7, 121.4, 120.9, 85.7, 85.6, 75.1, 75.0, 72.80, 72.75, 70.4, 70.3, 68.7, 67.9, 67.8, 64.7, 63.9, 61.7, 44.0, 36.5, 20.64, 20.61, 20.55, 20.52, 20.49, 20.13, 20.07; HRMS (ESI/ICR) m/z $[M + 2Na]^{2+}$ calcd for $[C_{75}H_{98}N_{14}O_{42}Na_2]^{2+}$/2 calcd for 956.2873; found 956.2881.

Synthesis of carbamate linked Janus glycocluster 9b: Tetra-Alkyne **8** (45 mg, 0.12 mmol, 1 equiv), peracetylated glucosamine azide (197 mg, 0.53 mmol, 4.4 equiv), $CuSO_4$ pentahydrate (24 mg, 0.10 mmol, 0.8 equiv), and 3 mL of *t*-BuOH/H_2O/THF (v/v/v = 1/1/1) were added to a dried 50 mL round bottomed flask. L-ascorbate sodium salt (38 mg, 0.19 mmol, 1.6 equiv) was added to start the reaction. The reaction mixture was stirred at 30 °C for 24 hours. Solvent was removed under reduced pressure. The crude product was purified via column chromatography using pure DCM to 8% MeOH/DCM to afford a white solid (191 mg, 85%). R_f = 0.5 in 7.5 % MeOH/DCM. mp 235.0–238.0°C. ^{1}H NMR (400 MHz, d_6-DMSO) δ 8.26 (s, 2H), 8.16–7.97 (m, 6H), 7.79–7.62 (m, 2H), 6.16–6.07 (m, 4H), 5.36 (t, J = 9.7 Hz, 4H), 5.10 (dt, J = 9.7, 5.4 Hz, 4H), 4.72–4.41 (m, 8H), 4.30–3.92 (m, 20H), 3.48–3.37 (m, 4H), 2.06–1.91 (m, 36H), 1.62–1.55 (m, 12H); ^{13}C NMR (100 MHz, d_6-DMSO) δ 170.0, 169.5, 169.4, 169.3, 156.1, 145.3, 144.1, 122.6, 121.5, 84.62, 84.56, 73.4, 72.4, 68.9, 68.0, 64.2, 63.1, 61.7, 52.1, 43.6, 35.8, 22.3, 22.2, 20.4, 20.3, 20.3. HRMS (ESI/ICR) m/z $[M + 2Na]^{2+}$ calcd for $[C_{75}H_{102}N_{18}O_{38}Na_2]^{2+}$/2 calcd for 954.3193; found 954.3192.

CHAPTER 5

FINAL CONCLUSION AND FUTURE PERSPECTIVE

Supramolecular gels are interesting and useful soft materials that are finding applications in various fields such as tissue engineering, drug delivery, environmental remediation, and supramolecular catalysis. Using the bottom-up approach, we are expanding our knowledge of the structural requirements for designing low molecular weight gelators. Carbohydrates are an ideal material for designing LMWGs and probing the structure to gelation properties relationships due to their structural diversity and various points of functionalization. In this study, several series of novel carbohydrate-based molecules were designed and synthesized with the goal of obtaining effective and versatile supramolecular gelators. The research carried out in chapters 2, 3, and 4 explore the structure to gelation properties relationships of functionalized carbohydrate-based derivatives. Figure 93 depicts representative molecules from each series that were successful LMWGs.

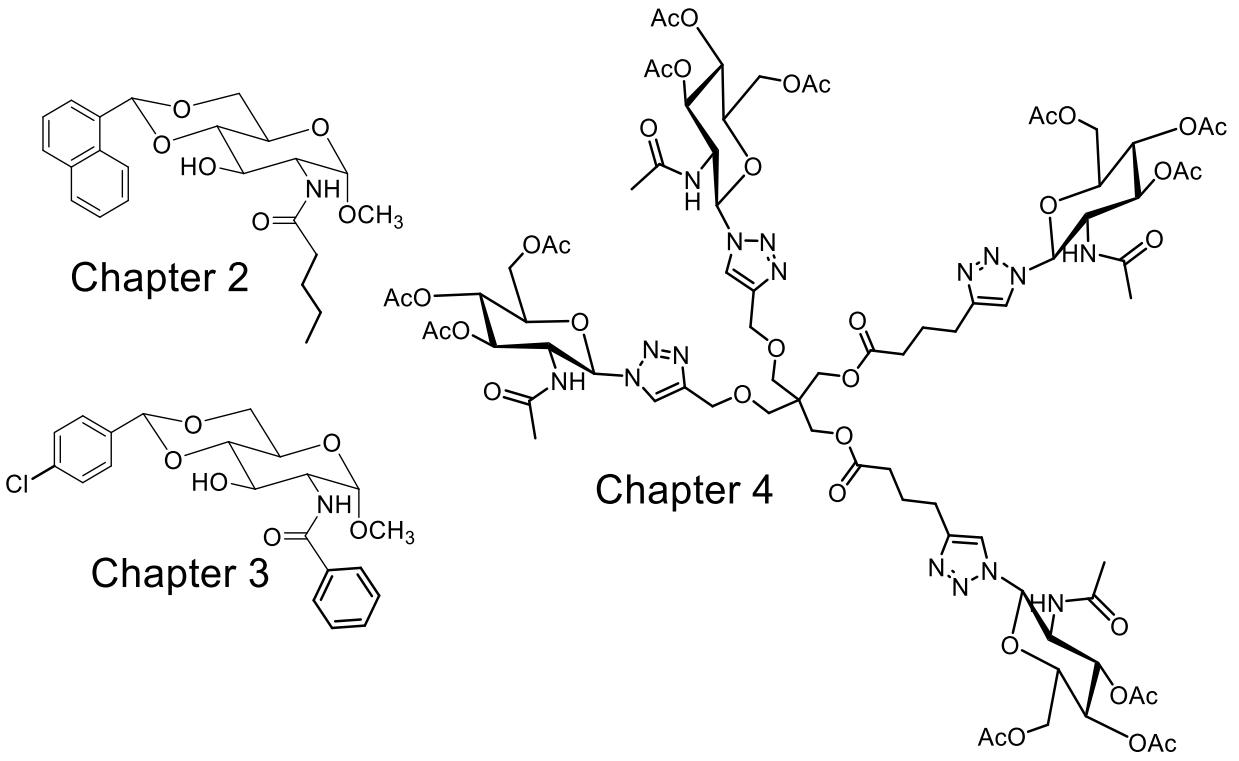

Figure 93. Representative carbohydrate derived LMWGs from chapters 2, 3, and 4.

Chapter 2 explored both the use of a strong aromatic 4,6-protecting group and the effectiveness of various hydrogen bonding groups at the second position of glucosamine. We systematically studied the 1-naphthybenzylidene acetal protected glucosamine system by designing and synthesizing a series of amide, urea, and carbamate derivatives. Several amide and carbamate derivatives were found to be versatile and effective supramolecular gelators. The urea derivatives were typically not very versatile; however, several derivatives were found to be very effective gelators in specific solvent systems. Variable temperature ^{1}H NMR was utilized to probe the ability of the different hydrogen bonding groups to intermolecularly hydrogen bond. Increasing the temperature reduces the concentration of intermolecular hydrogen bonding, so if large upfield changes in chemical shift are observed, that functional group is most likely partaking in hydrogen

bonding. Both the amide and carbamate NH signals were observed to have a significant upfield shift at elevated temperatures. The urea NH signals, on the other hand, saw very small upfield changes in chemical shift. To further probe this observation, deuterium exchange studies were carried out using ^{1}H NMR. A fast exchange of exchangeable protons with deuterium indicates a functional group is very capable hydrogen bonding interactions with other molecules and solvent. The amide and carbamate derivatives both had fairly fast exchange rates with a half-life of 29.1 minutes and 38.5 minutes respectively. The urea derivatives' exchange rates were much slower, with the inner and outer NH protons exchanging at 165.0 minutes and 58.2 minutes respectively. These two studies indicate that the urea functional group, which is supposed to be a strong hydrogen bonding group, is not partaking in intermolecular hydrogen bonding. Computational modeling using Chem3D to run MM2 energy minimization was then carried out to further explore this phenomenon. After energy minimization, the urea molecule was in a conformation that suggest that the outer NH is hydrogen bonding with the hydroxyl group at the third position of the sugar ring, which not only prevent the outer NH from interacting with other molecules and solvent, but also creates a pocket that entombs the inner NH proton, preventing it from the same interactions. The results from computational modeling validate the variable temperature studies and deuterium exchange studies. Further validation could possibly be obtained through X-ray crystallography. The gelators that have been discovered over the course of this study perform well in organic solvents and aqueous mixtures of organic solvents. Further studies into their uses as environmental remediation remedies as oil gelators and dye removal media will be explored in due time.

Chapter 3 probed the effect of a halogen substituent added to the para position of a 4,6-benzylidene protecting group on glucosamine and utilized various aliphatic and aromatic amides at the second position to fine tune gelation properties. This method was incredibly successful in

obtaining effective and versatile gelators. From this series of glucosamine derivatives, six compounds were found to be supergelators in at least one of the solvents they were tested in. The benzamide derivative **9** was found to be a hydrogelator at 0.36 mg/mL, which means over 58,000 molecules of water are entrapped for every gelator molecule at the minimum gelation concentration. Variable temperature studies on several derivatives showed a significant shift in the amides NH signal and an interesting change in peak shape was observed in the aromatic region. This change in peak shape could either indicate that the 4-chlorobenzylidene protection is partaking in strong aromatic interactions or the chloro substituent is partaking in halogen bonding. Gels formed by compound **7** and **9** in DMSO-water 1:1 were utilized in extrusions studies, which resulted in the successful printing of gel lines. Gels formed from benzamide derivative **9** in 5% DMSO in water solution were utilized for drug entrapment and diffusion studies. Naproxen sodium and chloramphenicol were used as model drugs in these studies. The results suggest that these gels are capable sustained drug release. Additionally, these studies were carried out at two different concentrations, with very little difference in delivery rate. This indicates that very low concentration gels will also be capable of sustained release, which would reduce possible negative side effect the gelator could possibly have. Benzamide derivative **9** was also used in dye absorption studies. In these studies, gel columns were prepared using a DMSO-water (v/v 1:1) gel formed by benzamide derivative **9** at 0.5 mg/mL. A toluene blue solution was then eluted through the column and UV-vis was used to analyze the eluent. This study found that an estimated 89% of the toluene blue dye had been adsorbed onto the gel column, meaning these gels can act as supramolecular sponges for organic dyes and have plausible applications in water purification.

Chapter 4 used the design rational of covalently linking multiple carbohydrate units to a central core to promote self-assembly through multivalency. We set out to design Janus, or two

faced, glycocluster by using an ester linkage on one side of the cluster and an ether linkage on the other. The glucosamine derivative performed much better than the glucose derivative in gelation testing, which coincides with results from previous studies on branched glycoclusters. The ester-ether glycocluster utilizing peripheral glucosamine units had gelation properties in between the gelation properties of the ether and ester glycoclusters previously report. We decided to make a second set of Janus clusters with carbamate linkages instead of the ester linkages, hypothesizing that additional hydrogen bonding would increase intermolecular interactions and thus enhance the gelation properties of the cluster. Unfortunately, the carbamate group caused a significant reduction in gelation properties. This is thought to be due to the carbamate group hydrogen bonding with other branches of the cluster and causing the molecule to adopt a disadvantageous conformation that negates the multivalent effect. Optical imaging and AFM imaging were carried out to analyze the morphology of the gel's microstructures. Gels formed by the ester-ether linked glycocluster with peripheral glucosamine units have very interesting spherical bundles of fibers that interconnected through a web of fibers. Several morphologies were observed for the gels formed by the carbamate-ether linked glycocluster with peripheral glucosamine including long intertwined fibers, aggregates with tails, and micelles. Preliminary testing was carried out to analyze the catalytic effect these clusters have as copper ligands in a copper catalyzed alkyne azide cycloaddition reaction. Every cluster in the series was found to increase the rate of the reaction, indicating they may be useful for supramolecular catalysis.

Future studies for each of these series of carbohydrate derivatives include exploring applications and some structural modification. Several derivatives in the 1-naphthylidine acetal protected glucosamine series performed very well in nonpolar solvents, so there are potential applications in the solidification of oil distillates that need to be explored. Additionally, due to the

extra aromatic group, these gels most likely also behave as supramolecular sponges for removing aromatic organic waste from waste. The 4-chlorobenzylidene system produced remarkable gelators with excellent viscoelastic properties. Gels formed by these gelators should be analyzed for plausible uses in tissue engineering. Further optimization for printing using automated 3D printer would make them a valuable soft material as a shapeable scaffold. Since the preliminary studies into drug diffusion showed that these gels are capable of sustained release, future studies should include analytical methods to determine diffusion rates and rate constants for development of drug diffusion devices. For the Janus glycocluster project, supramolecular catalysis experiments will be carried out, analyzing rate acceleration for various copper catalyzed reactions. In addition, other analogs with more branches that are similar to dendritic systems may produce functional gels with greater stability and utilities.

REFERENCES

(1) Draper, E. R.; Adams, D. J. Low-Molecular-Weight Gels: The State of the Art. *Chem* **2017**, *3*, 390-410.

(2) Dastidar, P. Supramolecular gelling agents: can they be designed? *Chem. Soc. Rev.* **2008**, *37*, 2699-2715.

(3) Dastidar, P. Designing Supramolecular Gelators: Challenges, Frustrations, and Hopes. *Gels* **2019**, *5*, 15.

(4) Okesola, B. O.; Vieira, V. M. P.; Cornwell, D. J.; Whitelaw, N. K.; Smith, D. K. 1,3:2,4-Dibenzylidene-d-sorbitol (DBS) and its derivatives – efficient, versatile and industrially-relevant low-molecular-weight gelators with over 100 years of history and a bright future. *Soft Matter* **2015**, *11*, 4768-4787.

(5) Jadhav, S. R.; Chiou, B.-S.; Wood, D. F.; DeGrande-Hoffman, G.; Glenn, G. M.; John, G. Molecular gels-based controlled release devices for pheromones. *Soft Matter* **2011**, *7*, 864-867.

(6) Nolan, M. C.; Fuentes Caparros, A. M.; Dietrich, B.; Barrow, M.; Cross, E. R.; Bleuel, M.; King, S. M.; Adams, D. J. Optimising low molecular weight hydrogels for automated 3D printing. *Soft Matter* **2017**, *13*, 8426-8432.

(7) Zhang, X.; Yang, C.; Li, J.; Meng, Q.; Raza, H.; Zhang, L. Enzymatic synthesis of mannitol dioctanoate and its utilisation in the preparation of structured edible oil. *Int. J. Food Sci* **2015**, *51*, n/a-n/a.

(8) Lim, J. Y. C.; Lin, Q.; Xue, K.; Loh, X. J. Recent advances in supramolecular hydrogels for biomedical applications. *Mater. Today Adv.* **2019**, *3*, 100021.

(9) Du, X.; Zhou, J.; Shi, J.; Xu, B. Supramolecular Hydrogelators and Hydrogels: From Soft Matter to Molecular Biomaterials. *Chem. Rev.* **2015**, *115*, 13165-13307.

(10) Skilling, K. J.; Citossi, F.; Bradshaw, T. D.; Ashford, M.; Kellam, B.; Marlow, M. Insights into low molecular mass organic gelators: a focus on drug delivery and tissue engineering applications. *Soft Matter* **2014**, *10*, 237-256.

(11) George, M.; Weiss, R. G. Molecular Organogels. Soft Matter Comprised of Low-Molecular-Mass Organic Gelators and Organic Liquids. *Acc. Chem. Res.* **2006**, *39*, 489-497.

(12) Cheuk, S.; Stevens, E. D.; Wang, G. Synthesis and structural analysis of a series of d-glucose derivatives as low molecular weight gelators. *Carbohydr. Res.* **2009**, *344*, 417-425.

(13) Lin, Y. C.; Weiss, R. G. Liquid-crystalline solvents as mechanistic probes. 24. A novel gelator of organic liquids and the properties of its gels. *Macromolecules* **1987**, *20*, 414-417.

(14) Morris, J.; Bietsch, J.; Bashaw, K.; Wang, G. Recently Developed Carbohydrate Based Gelators and Their Applications. *Gels* **2021**, *7*, 24.

(15) Wang, G.; Cheuk, S.; Yang, H.; Goyal, N.; Reddy, P. V. N.; Hopkinson, B. Synthesis and Characterization of Monosaccharide-Derived Carbamates as Low-Molecular-Weight Gelators. *Langmuir* **2009**, *25*, 8696-8705.

(16) Goyal, N.; Cheuk, S.; Wang, G. Synthesis and characterization of d-glucosamine-derived low molecular weight gelators. *Tetrahedron* **2010**, *66*, 5962-5971.

(17) Goyal, N.; Mangunuru, H. P. R.; Parikh, B.; Shrestha, S.; Wang, G. Synthesis and characterization of pH responsive D-glucosamine based molecular gelators. *J. Org. Chem.* **2014**, *10*, 3111-3121.

(18) Schön, E.-M.; Marqués-López, E.; Herrera, R. P.; Alemán, C.; Díaz, D. D. Exploiting Molecular Self-Assembly: From Urea-Based Organocatalysts to Multifunctional Supramolecular Gels. *Chem. Eur. J.* **2014**, *20*, 10720-10731.

(19) Gim, S.; Zhu, Y.; Seeberger, P. H.; Delbianco, M. Carbohydrate-based nanomaterials for biomedical applications. *Wiley Interdiscip. Rev. Nanomed. Nanobiotechnol.*, *0*, e1558.
(20) Hunter, C. A.; Lawson, K. R.; Perkins, J.; Urch, C. J. Aromatic interactions. *J. Chem. Soc.* **2001**, 651-669.
(21) Wang, G.; Chen, A.; Mangunuru, H. P. R.; Yerabolu, J. R. Synthesis and characterization of amide linked triazolyl glycolipids as molecular hydrogelators and organogelators. *RSC Adv.* **2017**, *7*, 40887-40895.
(22) Wang, G.; Cheuk, S.; Yang, H.; Goyal, N.; Reddy, P. V. N.; Hopkinson, B. Synthesis and Characterization of Monosaccharide-Derived Carbamates as Low-Molecular-Weight Gelators. *Langmuir* **2009**, *25*, 8696-8705.
(23) Chen, A.; Adhikari, S. B.; Mays, K.; Wang, G. Synthesis and Study of Molecular Assemblies Formed by 4,6-O-(2-Phenylethylidene)-Functionalized d-Glucosamine Derivatives. *Langmuir* **2017**, *33*, 8076-8089.
(24) Bietsch, J.; Olson, M.; Wang, G. Fine-Tuning of Molecular Structures to Generate Carbohydrate Based Super Gelators and Their Applications for Drug Delivery and Dye Absorption. *Gels* **2021**, *7*, 134.
(25) Kumar, D. K.; Jose, D. A.; Das, A.; Dastidar, P. First snapshot of a nonpolymeric hydrogelator interacting with its gelling solvents. *Chem. Commun.* **2005**, 4059-4061.
(26) Zhang, Y.; Kuang, Y.; Gao, Y.; Xu, B. Versatile Small-Molecule Motifs for Self-Assembly in Water and the Formation of Biofunctional Supramolecular Hydrogels. *Langmuir* **2011**, *27*, 529-537.
(27) Bredikhin, A. A.; Gubaidullin, A. T.; Bredikhina, Z. A.; Fayzullin, R. R.; Lodochnikova, O. A. Chirality, Gelation Ability and Crystal Structure: Together or Apart? Alkyl Phenyl Ethers of Glycerol as Simple LMWGs. *Symmetry* **2021**, *13*, 732.
(28) Draper, E. R.; Adams, D. J. How should multicomponent supramolecular gels be characterised? *Chem. Soc. Rev.* **2018**, *47*, 3395-3405.
(29) Hashemnejad, S. M.; Huda, M. M.; Rai, N.; Kundu, S. Molecular Insights into Gelation of Di-Fmoc-l-Lysine in Organic Solvent–Water Mixtures. *ACS Omega* **2017**, *2*, 1864-1874.
(30) Sánchez-Ferrer, A.; Adamcik, J.; Mezzenga, R. Edible supramolecular chiral nanostructures by self-assembly of an amphiphilic phytosterol conjugate. *Soft Matter* **2012**, *8*, 149-155.
(31) Skilling, K. J.; Kellam, B.; Ashford, M.; Bradshaw, T. D.; Marlow, M. Developing a self-healing supramolecular nucleoside hydrogel. *Soft Matter* **2016**, *12*, 8950-8957.
(32) Angelerou, M. G. F.; Frederix, P. W. J. M.; Wallace, M.; Yang, B.; Rodger, A.; Adams, D. J.; Marlow, M.; Zelzer, M. Supramolecular Nucleoside-Based Gel: Molecular Dynamics Simulation and Characterization of Its Nanoarchitecture and Self-Assembly Mechanism. *Langmuir* **2018**, *34*, 6912-6921.
(33) Ghosh, K.; Panja, S. Naphthalene-cholesterol conjugate as simple gelator for selective sensing of CN ion. *Supramol. Chem.* **2017**, *29*, 350-359.
(34) Mangunuru, H. P. R.; Yerabolu, J. R.; Wang, G. Synthesis and study of N-acetyl D-glucosamine triazole derivatives as effective low molecular weight gelators. *Tetrahedron Lett.* **2015**, *56*, 3361-3364.
(35) Mangunuru, H. P. R.; Yerabolu, J. R.; Liu, D.; Wang, G. Synthesis of a series of glucosyl triazole derivatives and their self-assembling properties. *Tetrahedron Lett.* **2015**, *56*, 82-85.
(36) Sharma, P.; Chen, A.; Wang, D.; Wang, G. Synthesis and Self-Assembling Properties of Peracetylated β-1-Triazolyl Alkyl D-Glucosides and D-Galactosides. *Chemistry* **2021**, *3*, 935-958.

(37) Wang, D.; Chen, A.; Morris, J.; Wang, G. Stimuli-responsive gelators from carbamoyl sugar derivatives and their responses to metal ions and tetrabutylammonium salts. *RSC Adv.* **2020**, *10*, 40068-40083.

(38) Wang, G.; Wang, D.; Bietsch, J.; Chen, A.; Sharma, P. Synthesis of Dendritic Glycoclusters and Their Applications for Supramolecular Gelation and Catalysis. *J. Org. Chem.* **2020**, *85*, 16136-16156.

(39) Morris, J.; Kozlowski, P.; Wang, G. Synthesis and Characterization of Hybrid Glycolipids as Functional Organogelators and Hydrogelators. *Langmuir* **2019**, *35*, 14639-14650.

(40) Chen, A.; Samankumara, L. P.; Garcia, C.; Bashaw, K.; Wang, G. Synthesis and characterization of 3-O-esters of N-acetyl-D-glucosamine derivatives as organogelators. *New J. Chem.* **2019**, *43*, 7950-7961.

(41) Chen, A.; Okafor, I. S.; Garcia, C.; Wang, G. Synthesis and self-assembling properties of 4,6-O-benzylidene acetal protected D-glucose and D-glucosamine β-1,2,3-triazole derivatives. *Carbohydr. Res.* **2018**, *461*, 60-75.

(42) Okafor, I. S.; Wang, G. Synthesis and gelation property of a series of disaccharide triazole derivatives. *Carbohydr. Res.* **2017**, *451*, 81-94.

(43) Hein, J. E.; Fokin, V. V. Copper-catalyzed azide–alkyne cycloaddition (CuAAC) and beyond: new reactivity of copper(i) acetylides. *Chem. Soc. Rev.* **2010**, *39*, 1302-1315.

(44) Bachl, J.; Mayr, J.; Sayago, F. J.; Cativiela, C.; Díaz Díaz, D. Amide–triazole isosteric substitution for tuning self-assembly and incorporating new functions into soft supramolecular materials. *Chem. Commun.* **2015**, *51*, 5294-5297.

(45) Chen, A.; Wang, D.; Bietsch, J.; Wang, G. Synthesis and characterization of pentaerythritol derived glycoconjugates as supramolecular gelators. *Org. Biomol. Chem.* **2019**, *17*, 6043-6056.

(46) Yang, Z. M.; Xu, K. M.; Guo, Z. F.; Guo, Z. H.; Xu, B. Intracellular Enzymatic Formation of Nanofibers Results in Hydrogelation and Regulated Cell Death. *Adv. Mater.* **2007**, *19*, 3152-3156.

(47) Huaimin, W.; Chunhua, R.; Zhijian, S.; Ling, W.; Xuemei, C.; Zhimou, Y. Enzyme-triggered self-assembly of a small molecule: a supramolecular hydrogel with leaf-like structures and an ultra-low minimum gelation concentration. *Nanotechnology* **2010**, *21*, 225606.

(48) Gao, Y.; Kuang, Y.; Guo, Z.-F.; Guo, Z.; Krauss, I. J.; Xu, B. Enzyme-Instructed Molecular Self-assembly Confers Nanofibers and a Supramolecular Hydrogel of Taxol Derivative. *J. Am. Chem. Soc.* **2009**, *131*, 13576-13577.

(49) Li, J.; Gao, Y.; Kuang, Y.; Shi, J.; Du, X.; Zhou, J.; Wang, H.; Yang, Z.; Xu, B. Dephosphorylation of d-Peptide Derivatives to Form Biofunctional, Supramolecular Nanofibers/Hydrogels and Their Potential Applications for Intracellular Imaging and Intratumoral Chemotherapy. *J. Am. Chem. Soc.* **2013**, *135*, 9907-9914.

(50) Pires, R. A.; Abul-Haija, Y. M.; Costa, D. S.; Novoa-Carballal, R.; Reis, R. L.; Ulijn, R. V.; Pashkuleva, I. Controlling Cancer Cell Fate Using Localized Biocatalytic Self-Assembly of an Aromatic Carbohydrate Amphiphile. *J. Am. Chem. Soc.* **2015**, *137*, 576-579.

(51) Brito, A.; Pereira, P. M. R.; Soares da Costa, D.; Reis, R. L.; Ulijn, R. V.; Lewis, J. S.; Pires, R. A.; Pashkuleva, I. Inhibiting cancer metabolism by aromatic carbohydrate amphiphiles that act as antagonists of the glucose transporter GLUT1. *Chem. Sci.* **2020**, *11*, 3737-3744.

(52) Tao, M.; Liu, J.; He, S.; Xu, K.; Zhong, W. In situ hydrogelation of forky peptides in prostate tissue for drug delivery. *Soft Matter* **2019**, *15*, 4200-4207.

(53) Yang, Z.; Liang, G.; Ma, M.; Abbah, A. S.; Lu, W. W.; Xu, B. d-Glucosamine-based supramolecular hydrogels to improve wound healing. *Chem. Commun.* **2007**, 843-845.

(54) Shaunak, S.; Thomas, S.; Gianasi, E.; Godwin, A.; Jones, E.; Teo, I.; Mireskandari, K.; Luthert, P.; Duncan, R.; Patterson, S.; Khaw, P.; Brocchini, S. Polyvalent dendrimer glucosamine conjugates prevent scar tissue formation. *Nat. Biotenol.* **2004**, *22*, 977-984.

(55) Siva Prasad, Y.; Manikandan, S.; Lalitha, K.; Sandeep, M.; Vara Prasad, R.; Arun Kumar, R.; Srinandan, C. S.; Uma Maheswari, C.; Sridharan, V.; Nagarajan, S. Supramolecular gels of gluconamides derived from renewable resources: Antibacterial and anti-biofilm applications. *Nano Select* **2020**, *1*, 510-524.

(56) Brito, A.; Abul-Haija, Y. M.; da Costa, D. S.; Novoa-Carballal, R.; Reis, R. L.; Ulijn, R. V.; Pires, R. A.; Pashkuleva, I. Minimalistic supramolecular proteoglycan mimics by co-assembly of aromatic peptide and carbohydrate amphiphiles. *Chem. Sci.* **2019**, *10*, 2385-2390.

(57) Chalard, A.; Vaysse, L.; Joseph, P.; Malaquin, L.; Souleille, S.; Lonetti, B.; Sol, J.-C.; Loubinoux, I.; Fitremann, J. Simple Synthetic Molecular Hydrogels from Self-Assembling Alkylgalactonamides as Scaffold for 3D Neuronal Cell Growth. *ACS Appl. Mater. Interfaces* **2018**, *10*, 17004-17017.

(58) Godbe, J. M.; Freeman, R.; Burbulla, L. F.; Lewis, J.; Krainc, D.; Stupp, S. I. Gelator Length Precisely Tunes Supramolecular Hydrogel Stiffness and Neuronal Phenotype in 3D Culture. *ACS Biomat. Sci. Eng.* **2020**, *6*, 1196-1207.

(59) Hu, Y.; Gao, W.; Wu, F.; Wu, H.; He, B.; He, J. Low molecular weight gels induced differentiation of mesenchymal stem cells. *J. Mater. Chem. B* **2016**, *4*, 3504-3508.

(60) Rizzo, C.; Andrews, J. L.; Steed, J. W.; D'Anna, F. Carbohydrate-supramolecular gels: Adsorbents for chromium(VI) removal from wastewater. *J. Colloid Interface Sci.* **2019**, *548*, 184-196.

(61) Sekhar, K. P. C.; Swain, D. K.; Holey, S. A.; Bojja, S.; Nayak, R. R. Unsaturation and Polar Head Effect on Gelation, Bioactive Release, and Cr/Cu Removal Ability of Glycolipids. *Langmuir* **2020**, *36*, 3080-3088.

(62) Basak, S.; Nandi, N.; Paul, S.; Hamley, I. W.; Banerjee, A. A tripeptide-based self-shrinking hydrogel for waste-water treatment: removal of toxic organic dyes and lead (Pb2+) ions. *Chem. Commun.* **2017**, *53*, 5910-5913.

(63) Srivastava, B. K.; Manheri, M. K. Aryl-triazolyl peptides for efficient phase selective gelation and easy removal of dyes from water. *RSC Adv.* **2016**, *6*, 29197-29201.

(64) Pathak, N. P.; Rajkamal; Yadav, S. A gelator–starch blend for dry powder based instant solidification of crude oil at room temperature. *Chem. Commun.* **2020**, *56*, 2999-3002.

(65) Zhang, B.; Chen, S.; Luo, H.; Zhang, B.; Wang, F.; Song, J. Porous amorphous powder form phase-selective organogelator for rapid recovery of leaked aromatics and spilled oils. *J. Hazard. Mater.* **2020**, *384*, 121460.

(66) Pal, K. B.; Mukhopadhyay, B. Carbohydrate-BasedSafe Fuel Gel with Significant Self–healing Property. *ChemistrySelect* **2017**, *2*, 967-974.

(67) Chalard, A.; Joseph, P.; Souleille, S.; Lonetti, B.; Saffon-Merceron, N.; Loubinoux, I.; Vaysse, L.; Malaquin, L.; Fitremann, J. Wet spinning and radial self-assembly of a carbohydrate low molecular weight gelator into well organized hydrogel filaments. *Nanoscale* **2019**, *11*, 15043-15056.

(68) Chalard, A.; Mauduit, M.; Souleille, S.; Joseph, P.; Malaquin, L.; Fitremann, J. 3D printing of a biocompatible low molecular weight supramolecular hydrogel by dimethylsulfoxide water solvent exchange. *Addit. Manuf.* **2020**, *33*, 101162.

(69) Okesola, B. O.; Smith, D. K. Applying low-molecular weight supramolecular gelators in an environmental setting – self-assembled gels as smart materials for pollutant removal. *Chem. Soc. Rev.* **2016**, *45*, 4226-4251.

(70) Slavík, P.; Kurka, D. W.; Smith, D. K. Palladium-scavenging self-assembled hybrid hydrogels – reusable highly-active green catalysts for Suzuki–Miyaura cross-coupling reactions. *Chem. Sci.* **2018**, *9*, 8673-8681.

(71) Piras, C. C.; Slavik, P.; Smith, D. K. Self-Assembling Supramolecular Hybrid Hydrogel Beads. *Angew. Chem. Int. Ed.* **2020**, *59*, 853-859.

(72) Hawkins, K.; Patterson, A. K.; Clarke, P. A.; Smith, D. K. Catalytic Gels for a Prebiotically Relevant Asymmetric Aldol Reaction in Water: From Organocatalyst Design to Hydrogel Discovery and Back Again. *J. Am. Chem. Soc.* **2020**, *142*, 4379-4389.

(73) Zhang, Y.; Gu, H.; Yang, Z.; Xu, B. Supramolecular Hydrogels Respond to Ligand−Receptor Interaction. *J. Am. Chem. Soc.* **2003**, *125*, 13680-13681.

(74) Pozzo, J.-L.; Michel Clavier, G.; Desvergne, J.-P. Rational design of new acid-sensitive organogelators. *J. Mater. Chem.* **1998**, *8*, 2575-2577.

(75) Zhou, J.; Du, X.; Gao, Y.; Shi, J.; Xu, B. Aromatic–Aromatic Interactions Enhance Interfiber Contacts for Enzymatic Formation of a Spontaneously Aligned Supramolecular Hydrogel. *J. Am. Chem. Soc.* **2014**, *136*, 2970-2973.

(76) Guan, X.; Fan, K.; Gao, T.; Ma, A.; Zhang, B.; Song, J. A novel multi-stimuli responsive gelator based on d-gluconic acetal and its potential applications. *Chem. Commun* **2016**, *52*, 962-965.

(77) Fan, K.; Wang, X.; Wang, X.; Yang, H.; Han, G.; Zhou, L.; Fang, S. One-step-synthesized d-gluconic acetal-based supramolecular organogelators with effective phase-selective gelation. *RSC Adv.* **2020**, *10*, 37080-37085.

(78) Kesava Raju, C. S.; Pramanik, B.; Ravishankar, R.; Chalapathi Rao, P. V.; Sriganesh, G. Xylitol based phase selective organogelators for potential oil spillage recovery. *RSC Adv.* **2017**, *7*, 37175-37180.

(79) Dizon, G. C.; Atkinson, G.; Argent, S. P.; Santu, L. T.; Amabilino, D. B. Sustainable sorbitol-derived compounds for gelation of the full range of ethanol–water mixtures. *Soft Matter* **2020**, *16*, 4640-4654.

(80) Wang, G.; Yang, H.; Cheuk, S.; Coleman, S. Synthesis and self-assembly of 1-deoxyglucose derivatives as low molecular weight organogelators. *Beilstein J. Org. Chem.* **2011**, *7*, 234-242, No. 231.

(81) Ono, F.; Ichimaru, K.; Hirata, O.; Shinkai, S.; Watanabe, H. Universal Glucose-based Low-molecular-weight Gelators for Both Organic and Aqueous Solvents. *Chem. Lett.* **2020**, *49*, 156-159.

(82) Williams, K. A. Synthesis and Characterization of Monosaccharide-derived Low Molecular Weight Gelators. University of New Orleans 2011.

(83) Corradi, E.; Meille, S. V.; Messina, M. T.; Metrangolo, P.; Resnati, G. Halogen Bonding versus Hydrogen Bonding in Driving Self-Assembly Processes. *Angew. Chem. Int. Ed.* **2000**, *39*, 1782-1786.

(84) Chen, L.; Revel, S.; Morris, K.; C. Serpell, L.; Adams, D. J. Effect of Molecular Structure on the Properties of Naphthalene−Dipeptide Hydrogelators. *Langmuir* **2010**, *26*, 13466-13471.

(85) Feng, Y.; Chen, H.; Liu, Z.-X.; He, Y.-M.; Fan, Q.-H. A Pronounced Halogen Effect on the Organogelation Properties of Peripherally Halogen Functionalized Poly(benzyl ether) Dendrons. *Chem. Eur. J.* **2016**, *22*, 4980-4990.

(86) Li, R.; Wang, S.; Li, Q.; Lan, H.; Xiao, S.; Li, Y.; Tan, R.; Yi, T. A fluorescent non-conventional organogelator with gelation-assisted piezochromic and fluoride-sensing properties. *Dyes Pigm.* **2017**, *137*, 111-116.

(87) Li, Q.; Li, R.; Lan, H.; Lu, Y.; Li, Y.; Xiao, S.; Yi, T. Halogen Effect on Non-Conventional Organogel Assisted by Balanced π-π Interaction. *ChemistrySelect* **2017**, *2*, 5421-5426.

(88) Srivastava, B. K.; Manheri, M. K. Towards a fragment-based approach in gelator design: halogen effects leading to thixotropic, mouldable and self-healing systems in aryl-triazolyl amino acid-based gelators! *Chem. Commun.* **2017**, *53*, 4485-4488.

(89) Morris, J.; Bietsch, J.; Bashaw, K.; Wang, G. Recently Developed Carbohydrate Based Gelators and Their Applications. *Gels-Basel* **2021**, *7*.

(90) Chabre, Y. M.; Roy, R. Multivalent glycoconjugate syntheses and applications using aromatic scaffolds. *Chem. Soc. Rev.* **2013**, *42*, 4657-4708.

(91) Bojarová, P.; Křen, V. Sugared biomaterial binding lectins: achievements and perspectives. *Biomater. Sci.* **2016**, *4*, 1142-1160.

(92) Tyagi, M.; Kartha, K. P. R. Synthesis of glycotriazololipids and observations on their self-assembly properties. *Carbohydr. Res.* **2015**, *413*, 85-92.

(93) Ligeour, C.; Vidal, O.; Dupin, L.; Casoni, F.; Gillon, E.; Meyer, A.; Vidal, S.; Vergoten, G.; Lacroix, J.-M.; Souteyrand, E.; Imberty, A.; Vasseur, J.-J.; Chevolot, Y.; Morvan, F. Mannose-centered aromatic galactoclusters inhibit the biofilm formation of Pseudomonas aeruginosa. *Org. Biomol. Chem.* **2015**, *13*, 8433-8444.

(94) Feng, Y.; He, Y.-M.; Fan, Q.-H. Supramolecular Organogels Based on Dendrons and Dendrimers. *Chem. Asian J.* **2014**, *9*, 1724-1750.

(95) Tiwari, V. K.; Mishra, B. B.; Mishra, K. B.; Mishra, N.; Singh, A. S.; Chen, X. Cu-Catalyzed Click Reaction in Carbohydrate Chemistry. *Chem. Rev.* **2016**, *116*, 3086-3240.

(96) Kushwaha, D.; Dwivedi, P.; Kuanar, S. K.; Tiwari, V. K. Click reaction in carbohydrate chemistry: recent developments and future perspective. *Curr. Org. Synth.* **2013**, *10*, 90-135.

(97) Percec, V.; Leowanawat, P.; Sun, H.-J.; Kulikov, O.; Nusbaum, C. D.; Tran, T. M.; Bertin, A.; Wilson, D. A.; Peterca, M.; Zhang, S.; Kamat, N. P.; Vargo, K.; Moock, D.; Johnston, E. D.; Hammer, D. A.; Pochan, D. J.; Chen, Y.; Chabre, Y. M.; Shiao, T. C.; Bergeron-Brlek, M.; Andre, S.; Roy, R.; Gabius, H.-J.; Heiney, P. A. Modular Synthesis of Amphiphilic Janus Glycodendrimers and Their Self-Assembly into Glycodendrimersomes and Other Complex Architectures with Bioactivity to Biomedically Relevant Lectins. *J. Am. Chem. Soc.* **2013**, *135*, 9055-9077.

(98) Buzzacchera, I.; Xiao, Q.; Han, H.; Rahimi, K.; Li, S.; Kostina, N. Y.; Toebes, B. J.; Wilner, S. E.; Möller, M.; Rodriguez-Emmenegger, C.; Baumgart, T.; Wilson, D. A.; Wilson, C. J.; Klein, M. L.; Percec, V. Screening Libraries of Amphiphilic Janus Dendrimers Based on Natural Phenolic Acids to Discover Monodisperse Unilamellar Dendrimersomes. *Biomacromolecules* **2019**, *20*, 712-727.

(99) Cano, M. E.; Di Chenna, P. H.; Lesur, D.; Wolosiuk, A.; Kovensky, J.; Uhrig, M. L. Chirality inversion, supramolecular hydrogelation and lectin binding of two thiolactose amphiphiles constructed on a di-lauroyl-l-tartaric acid scaffold. *New J. Chem.* **2017**, *41*, 14754-14765.

APPENDIX

LIST OF SCHEMES Page

VITA

Jonathan Bietsch
Department of Chemistry and Biochemistry
Old Dominion University
Norfolk, VA 23529

Education:

August 2015-expected December 2021: Ph.D. Chemistry, Old Dominion University, Virginia
August 2015-December 2020: M.S. Chemistry, Old Dominion University, Virginia
January 2013-May 2015: B.S. Chemistry, Longwood University, Virginia

List of publications:

1. Chen, A.; Wang, D.; **Bietsch, J.**; Wang, G., Synthesis and characterization of pentaerythritol derived glycoconjugates as supramolecular gelators. *Organic & Biomolecular Chemistry* **2019**, *17* (24), 6043-6056.
2. Wang, G.; Wang, D.; **Bietsch, J**.; Chen, A.; Sharma, P., Synthesis of Dendritic Glycoclusters and Their Applications for Supramolecular Gelation and Catalysis. *The Journal of Organic Chemistry* **2020**, *85* (24), 16136-16156.
3. Morris, J.; **Bietsch, J.**; Bashaw, K.; Wang, G., Recently Developed Carbohydrate Based Gelators and Their Applications. *Gels* **2021**, *7* (1), 24.
4. **Bietsch, J.**; Olson, M.; Wang, G., Fine-Tuning of Molecular Structures to Generate Carbohydrate Based Super Gelators and Their Applications for Drug Delivery and Dye Absorption. *Gels* **2021**, *7* (3), 134, DOI: 10.3390/gels703013.
5. Yoon, L. U.; Adihikari, S.; Sarabamoun, E.; **Bietsch, J.**; Tsai, E. H. R.; Wang, G. and Choi, J. J., Exciton Dissociation in Quantum Dots Connected with Photochromic Molecule Bridges *Journal of Material Chemistry* C **2021**, *9* (44), 16006-16013, DOI: 10.1039/D1TC04451F.
6. Strausser, S.; **Bietsch, J**; Hodges, H.; McCoy, T.; Stewart, B.; Kintz, H.; Yeagley, A, An Organic Laboratory Experience: Synthesis and Antimicrobial Screening of Brominated Parabens. *Journal of Chemical Education* **2021**, *98* (11), 3524-3532.